

Doctoral thesis

Doctoral theses at NTNU, 2022:224

Sergio Miguel Castañeda Zegarra

Impact of DNA double-strand break response factors on B and T lymphocyte development

NTNU
Norwegian University of Science and Technology
Thesis for the Degree of
Philosophiae Doctor
Faculty of Medicine and Health Sciences
Department of Clinical and Molecular Medicine



Norwegian University of
Science and Technology

Sergio Miguel Castañeda Zegarra

Impact of DNA double-strand break response factors on B and T lymphocyte development

Thesis for the Degree of Philosophiae Doctor

Trondheim, August 2022

Norwegian University of Science and Technology
Faculty of Medicine and Health Sciences
Department of Clinical and Molecular Medicine



Norwegian University of
Science and Technology

NTNU

Norwegian University of Science and Technology

Thesis for the Degree of Philosophiae Doctor

Faculty of Medicine and Health Sciences
Department of Clinical and Molecular Medicine

© Sergio Miguel Castañeda Zegarra

ISBN 978-82-326-5493-2 (printed ver.)
ISBN 978-82-326-6461-0 (electronic ver.)
ISSN 1503-8181 (printed ver.)
ISSN 2703-8084 (online ver.)

Doctoral theses at NTNU, 2022:224

Printed by NTNU Grafisk senter

NORGES TEKNISK-NATURVITENSKAPELIGE UNIVERSITET FAKULTET FOR MEDISIN OG HELSEVITENSKAP

“Virkningen av DNA-dobbeltråddbrudd responsfaktorer på B- og T-lymfocyt utvikling”

Sammendrag

De mest cytotoksiske DNA-skadene i en celle er forårsaket av brudd på dobbeltrådet DNA (DSB). NHEJ er en essensiell DNA-reparasjonsmekanisme som detekterer, prosesserer, og ligerer dobbeltrådet DNA brudd. NHEJ er også nødvendig for V(D)J-rekombinasjon i utviklingen av B- og T-lymfocytter og for klasse bytte rekombinasjon (CSR) i utviklede B-celler. Gjennom NHEJ danner Ku70 og Ku80 en heterodimer som gjenkjenner brudd i dobbeltrådet DNA og fremmer rekruttering av nedstrøms faktorer som DNA-PKcs, Artemis, XRCC4, LIG4, PAXX, XLF og MRI. Mangel på NHEJ-faktorer, slik som Ku, DNA-pkcs, Xlf eller Paxe, fører til varierende mengder DNA-reparasjonsdefekter i mus, mens mangel på Xrcc4 eller Lig4 fører til embryonal død. Kombinert inaktivering av XLF og DNA-PKcs, XLF og PAXX, eller XLF og MRI fører til embryonal død hos mus, samt økt genetisk ustabilitet i cellene.

Inntil nylig var det uklart om MRI virkelig var en NHEJ-faktor, og om den var nødvendig for embryonal utvikling og utvikling av lymfocytter. Derfor, i artikkel I, genererte vi *Mri*^{-/-} mus for å belyse hvordan B- og T-celleutvikling ble påvirket. Her viste vi at mus uten MRI hadde normal kroppsstørrelse og antall B- og T-lymfocytter sammenlignet med WT-mus. Likevel ble det detektert at MRI var nødvendig for effektiv CSR i utviklede B-celler. I likhet med NHEJ fungerer DNA-skade reparasjonsveier (DDR) som respons på V(D)J-rekombinasjon under utvikling av B- og T-lymfocytter. DDR-faktoren MDC1 og NHEJ-faktoren XLF er foreslått å ha funksjoner før DNA ligeringen. Derfor, i artikkel II, undersøkte vi påvirkningen av kombinert inaktivering av *Mdc1* og *Xlf* på V(D)J rekombinasjon i både *in vivo* og *in vitro* studier. Vi fant at en kombinert inaktivering av *Mdc1* og *Xlf* resulterte i embryonal dødelighet. MDC1 stimulerer V(D)J rekombinasjon i celler uten XLF. I artikkel III undersøkte vi om inaktivering av en eller to alleler av *Trp53* kunne redde dødeligheten til *Xlf*^{-/-}*Mri*^{-/-} mus, og om kombinert mangel på XLF og MRI eller XLF og PAXX *in vivo* avbryter B- og T-celleutvikling. Her viste vi at ved å fjerne *Trp53* unngår en embryonal dødelighet i *Xlf*^{-/-}*Mri*^{-/-} og *Xlf*^{-/-}*Paxe*^{-/-} mus. Vi demonstrerte at disse musene hadde redusert kroppsvekt og størrelse på milt, thymi, mangel på modne B-celler i milten, og dramatisk redusert antall T-celler i både milt og thymus. I disse tre studiene har vi vist at det er komplekse genetiske interaksjoner mellom NHEJ gener og mellom NHEJ og DDR faktorer. Videre, genetisk modifiserte musemodeller og murine cellelinjer har bidratt til forståelsen av spesifikke funksjoner i DNA reparasjons faktorer som tidligere var ukjent grunnet funksjonell redundans.

Navn kandidat: Sergio Miguel Castañeda Zegarra

Institutt: Institutt for klinisk og molekylær medisin (IKOM)

Veileder(e): Valentyn Oksenysh (hovedveileder), Denis Kainov (biveileder), og Richard Kumaran Kandasamy (biveileder)

Finansieringskilde: NTNU Aktiveringsteknologiprogram om bioteknologi (NTNU Enabling Technology Programme on Biotechnology)

Ovennevnte avhandling er funnet verdig til å forsvares offentlig
for graden PhD i Medisin og helsevitenskap
Disputas finner sted i digitalt forsvar via Zoom
mandag 22. august, kl. 12.15

TABLE OF CONTENTS

SAMMENDRAG	I
TABLE OF CONTENTS	II
ACKNOWLEDGMENTS	IV
LIST OF PUBLICATIONS	V
ADDITIONAL CONTRIBUTIONS DURING AND RELATED TO PHD STUDIES	VI
ABBREVIATIONS	VII
1. INTRODUCTION	1
1.1 DNA DAMAGE	1
1.1.1 Endogenous DNA damage	1
1.1.1.1 Oxidative DNA damage	1
1.1.1.2 Replication errors	1
1.1.1.3 Spontaneous base deamination	1
1.1.1.4 Abasic sites	2
1.1.1.5 Physiological DSBs	2
1.1.2 Exogenous DNA damage	2
1.1.2.1 Ionizing Radiation (IR)	2
1.1.2.2 Ultraviolet (UV) radiation	3
1.1.2.3 Chemical agents	3
1.1.2.4 Chemical therapies and strategies based on DNA damage	4
1.2 DNA DAMAGE RESPONSE (DDR)	7
1.2.1 ATM-dependent DNA damage sensing and promoting of DSBs repair by NHEJ	7
1.3 DNA REPAIR	11
1.3.1 Direct reversal	11
1.3.2 Base excision repair (BER)	13
1.3.3 Nucleotide excision repair (NER)	15
1.3.4 Mismatch repair (MMR)	17
1.3.5 DNA double-strand break repair	19
1.3.5.1 Homologous recombination (HR)	19
1.3.5.2 Alternative pathways to repair DSBs	21
1.4 NON-HOMOLOGOUS END-JOINING (NHEJ)	23

1.5	LYMPHOCYTE DEVELOPMENT AND NHEJ	27
1.5.1	<i>V(D)J recombination</i>	27
1.5.1.1	<i>V(D)J recombination associated to B and T cell development</i>	30
1.5.2	<i>Class switch recombination (CSR)</i>	33
1.5.3	<i>Similarities between V(D)J and CSR processes</i>	36
1.6	HUMAN DISEASES ASSOCIATED WITH DEFECTS IN DSB REPAIR	37
1.7	GENETIC INTERACTION OF DNA DSB REPAIR FACTORS DURING LYMPHOCYTE DEVELOPMENT	42
1.7.1	<i>Single NHEJ factor-deficient mouse models</i>	42
1.7.2	<i>Synthetic lethal NHEJ mouse models</i>	47
1.7.3	<i>Complex viable NHEJ mouse models</i>	48
1.7.4	<i>DDR mouse models</i>	50
1.7.5	<i>Genetic interaction between ATM-DDR and NHEJ factors</i>	53
1.7.6	<i>Shieldin-deficient mouse models and CSR</i>	54
2.	AIMS OF THE STUDY	55
3.	SUMMARY OF PAPERS	56
3.1	PAPER I	56
3.2	PAPER II	58
3.3	PAPER III	60
4.	GENERAL DISCUSSION AND FUTURE PERSPECTIVES	63
5.	CONCLUDING REMARKS	69
6.	REFERENCES	70
7.	PAPERS I-III	98

ACKNOWLEDGMENTS

Mainly, I would like to thank my main supervisor, Dr. Valentyn Oksenysh, who gave me the opportunity of being guided during all this time, which involved my MSc and Ph.D. thesis at the Department of Clinical and Molecular Medicine (IKOM), Norwegian University of Science and Technology (NTNU), Norway. I sincerely appreciate his excellent supervision and advice, which made me improve every day as a scientist and as a person, especially during this challenging time that included COVID-time and, sadly, the war against Ukraine, the country where Valentyn was born.

Then, I want to thank my co-supervisors, Prof. Denis Kainov and Prof. Richard Kumaran Kandasamy, who supported my Ph.D. training. Especially Prof. Denis Kainov, who shared with me good moments during fishing as well as his fantastic gift, a couple of beautiful rabbits, my pets Croissant and Napoleon, who contributed to my mental health during quarantine until now.

Furthermore, I would like to thank all my colleagues that I met at Oksenysh's lab, especially Amin Alirezaylavasani. In addition, to Prof. Thomas Helleday at Karolinska Institutet (KI), who gave me the opportunity to collaborate with his scientific team in Sweden. Especially Dr. Carlos Benitez Buelga, Dr. Kumar Sanjiv, and Dr. Maurice Michel, members of Helleday's lab, who helped me during my research visit both scientifically and socially.

To my beautiful family for the strength and love. Thanks for all his support to my parents, my cousin-brother Italo, to my siblings, Alex, Maria, and especially Giancarlo. They taught me to work hard to achieve each one of my dreams.

Finally, thanks to my wife Silvana for sharing all these years with me and giving me her support in moments of frustration and in situations where I felt lost. For being by my side in the development of the thesis and thus living adventures, trips, etc., what will be unforgettable. Also, who more than a scientist to understand another scientist. For all that, thanks, my love.

Sergio Miguel Castañeda Zegarra
Trondheim, 2022

LIST OF PUBLICATIONS

Paper I

Castañeda-Zegarra S, Huse C, Røsand Ø, Sarno A, Xing M, Gago-Fuentes R, Zhang Q, Alirezaylavasani A, Werner J, Ji P, Liabakk N, Wang W, Bjørnas M, Oksenych V. (2019). Generation of a Mouse Model Lacking the Non-Homologous End-Joining Factor Mri/Cyren. *Biomolecules*, 9(12), 798. DOI:10.3390/biom9120798

Paper II

Beck C, **Castañeda-Zegarra S**, Huse C, Xing M, Oksenych V. (2020). Mediator of DNA Damage Checkpoint Protein 1 Facilitates V(D)J Recombination in Cells Lacking DNA Repair Factor XLF. *Biomolecules*, 10(1), 60. DOI:10.3390/biom10010060

Paper III

Castañeda-Zegarra S, Zhang Q, Alirezaylavasani A, Fernandez-Berrocal M, Yao R, Oksenych V. (2020). Leaky severe combined immunodeficiency in mice lacking non-homologous end joining factors XLF and MRI. *Aging*, 12(23), 23578-23597. DOI: 10.18632/aging.202346

ADDITIONAL CONTRIBUTIONS DURING AND RELATED TO PHD STUDIES

Castañeda-Zegarra S, Fernandez-Berrocal M, Tkachov M, Yao R, Esnardo-Upfold N, Oksenych V. (2020). Genetic interaction between the non-homologous end joining factors during B and T lymphocyte development: *in vivo* mouse models. *Scandinavian Journal of Immunology*, 92, e12936. DOI: 10.1111/sji.12936

Castañeda-Zegarra S, Xing, M., Gago-Fuentes, R., Sæterstad, S., & Oksenych, V. (2019). Synthetic lethality between DNA repair factors *Xlf* and *Paxx* is rescued by inactivation of *Trp53*. *DNA repair*, 73, 164-169. DOI: 10.1016/j.dnarep.2018.12.002

ABBREVIATIONS

A	Adenine
Ab	Antibody
Ag	Antigen
AGT	Alkylguanine DNA alkyltransferases
AID	Activation-induced deaminase
AP	Apurinic/aprimidinic
APC	Antigen-presenting cell
APE	AP endonuclease
APLF	Aprataxin and PNK-like factor
ATLD	Ataxia telangiectasia like disorder
ATM	Ataxia-telangiectasia mutated
ATR	ATM and Rad3-related
A-EJ	Alternative end-joining
A-T	Ataxia–telangiectasia syndrome
BCR	B cell receptor
BD	Behçet’s disease
BER	Base excision repair
bp	Base pair
BRCA	Breast cancer susceptibility protein
BRCT	BRCA1 C terminus
C	Cytosine
CAK	Cdk-activating kinase complex
CDK	Cyclin-dependent kinase
CE	Coding end
CETN2	Centrin 2
CHK	Checkpoint kinase
CID	Combined immunodeficiency
CJ	Coding joint
CLP	Common lymphoid progenitor
CPD	Cyclobutane pyrimidine dimers
CS	Cockayne syndrome
CSP	Close synapsis

CSR	Class switch recombination
CST	CTC1–STN1–TEN1 complex
CtIP	(C-terminal binding protein)-interacting protein
CYREN	Cell cycle regulator of NHEJ
C-NHEJ	Classical non-homologous end-joining
D	Diversity
DCLRE1C	DNA cross-link repair 1C
DDB	DNA-damage binding
DDR	DNA damage response
DN	Double-negative T cell
DNA	Deoxyribonucleic acid
DNA-PK	DNA-dependent protein kinase
DNA-PKcs	DNA-dependent protein kinase, catalytic subunit
DNET	Dysembryoplastic neuroepithelial tumor
DP	Double-positive T cell
DSB	Double-strand break
D-loop	Displacement loop
ERCC1	Excision repair protein cross-complementation 1
ETP	Early thymic progenitor
EXO1	Exonuclease 1
FAD	Flavin adenine dinucleotide
FADH	Reduced form of flavin adenine dinucleotide
FEN1	Flap endonuclease 1
FSP	Flexible synaptic
G	Guanine
GCN5	General control non-depressible 5
GG-NER	global genome NER
GLT	Germline transcript
Gy	Gray
G0	Resting phase cell cycle
G1	First gap phase cell cycle
G2	Second gap phase cell cycle
HAP	Haploid
HAP1	A near-haploid cell line derived from KBM-7 cell line

HIV	Human immunodeficiency virus
HR	Homologous recombination
H2AX	H2A histone family member X
Ig	Immunoglobulin
IgH	Immunoglobulin heavy chain
IgL	Immunoglobulin light chain
IR	Ionizing radiation
J	Joining
KBM	Ku-binding motif
kDa	Kilodalton
Ku	Ku70/80 heterodimer
LIG1	DNA ligase
LMPP	Lymphoid-primed multipotent progenitor
L3MBTL2	Lethal (3) malignant brain tumor-like protein 2
M	Mitosis
MDC1	Modulator of DNA damage checkpoint 1
MEF	Mouse embryonic fibroblast
MHC	Major histocompatibility complex
MLV	Murine leukemia virus
MMR	Mismatch repair
MRI	Modulator of retrovirus infection
MRN	MRE11-RAD50-NBS1 complex
NBS	Nijmegen breakage syndrome
NEIL1	Endonuclease VII-like 1
NER	Nucleotide excision repair
NHEJ	Non-homologous end-joining
NK	Natural killer
NSPC	Neuronal stem progenitor cells
OGG1	8-oxoG DNA glycosylase
OS	Omenn syndrome
PALB2	Partner and localizer of BRCA2
PARP	Poly (ADP-ribose) polymerase
PAXX	Paralog of XRCC4 and XLF
PCAF	p300/CBP-associated factor

PCNA	Proliferating cell nuclear antigen
PIKK	Phosphoinositide 3-kinase (PI3K)-related kinase
PNKP	Polynucleotide kinase phosphatase
Pre-B	Precursor B cell
Pro-B	Progenitor B cell
Pol	Polymerase
PUA	Phosphor- α,β -unsaturated aldehyde
PTIP	PAX-interacting protein 1
RAD23B	UV excision repair protein radiation sensitive 23B
RAG	Recombination-activating gene
RIF1	Rap1 interacting factor 1
RNF	Really Interesting New Gene (RING) Finger Protein
ROS	Reactive oxygen species
RPA	Replication protein A
RSS	Recombination signal sequence
RS-SCID	Radiosensitive SCID
S	DNA synthesis phase
SCID	Severe combined immunodeficiency
SE	Signal end
SEC	Signal end complex
SHM	Somatic hypermutation
SJ	Signal joint
SP	Single-positive T cell
SS	Single-stranded DNA
SSA	Single-strand annealing
SSB	Single-strand break
TC-NER	Transcription-coupled NER
TCR	T cell receptor
TdT	Terminal deoxynucleotidyl transferase
TFIIH	Transcription initiation factor II H
TLS	Translesion synthesis
U	Uracil
UNG	Uracil-DNA glycosylase
UV	Ultraviolet

V	Variable
vAbl	Abelson murine leukemia virus-transformed
V(D)J	Variable (Diversity) Joining
XLF	XRCC4-Like Factor
XP	Xeroderma pigmentosum
XRCC	X-ray cross-complementing protein
WT	Wild-type
WRN	Werner syndrome helicase protein
5mC	5-methyl cytosine
53BP1	p53- binding protein
5'-dRP	5'-deoxyribose phosphate
6-4 PPs	Pyrimidine pyrimidones photoproducts
8-oxoG	8-oxoguanine
γH2AX	H2AX phosphorylated at serine 139

1. INTRODUCTION

1.1 DNA DAMAGE

Each human cell receives tens of thousands of DNA lesions per day (Lindahl & Barnes, 2000). These lesions can produce injuries at different DNA structure levels, for example, in a single DNA base, or even more severe, causing breaks in one or both DNA chains (Jackson & Bartek, 2009; Jackson & Helleday, 2016; Lindahl & Barnes, 2000). DNA damage agents can be commonly classified into two categories, endogenous and exogenous, according to the source of origin (Tubbs & Nussenzweig, 2017).

Endogenous DNA damage occurs at a higher frequency compared to exogenous damage (Tubbs & Nussenzweig, 2017). Interestingly, many of the consequences in the DNA structure caused by endogenous agents are similar to those caused by some exogenous agents (Friedberg, 2008; Lindahl, 1993; Tubbs & Nussenzweig, 2017).

1.1.1 Endogenous DNA damage

1.1.1.1 Oxidative DNA damage

Reactive oxygen species (ROS) are continuously formed during metabolic processes (Cadet & Davies, 2017). ROS possesses the potential to oxidize the DNA, and at high levels, ROS might induce several types of DNA damage, including DNA single-strand breaks (SSBs) and DNA double-strand breaks (DSBs) (Hegde *et al*, 2012; Srinivas *et al*, 2019). Moreover, ROS's overabundance might lead to cellular damage and human diseases, such as cancer, atherosclerosis, diabetes, and heart failure (Aggarwal *et al*, 2019; Kaneto *et al*, 2010; Tsutsui *et al*, 2011).

1.1.1.2 Replication errors

During DNA replication, each human cell copies thousands of millions of DNA bases per time. DNA polymerases (Pol) carry the insertion of a correct complementary deoxynucleotide opposite the template base which safeguards a high accuracy during this process. Errors during DNA replication involve insertions, deletions, and mismatches of nucleotide bases into the DNA strands (Cortez, 2019).

1.1.1.3 Spontaneous base deamination

A deamination is a primary form of spontaneous DNA damage where adenine (A), cytosine (C), guanine (G), and 5-methyl cytosine (5mC) can be deaminated resulting in mutagenic lesions, such as uracil (U), xanthine, and hypoxanthine (Chatterjee & Walker, 2017;

Krokan *et al*, 2002). From an immunological perspective, the activation-induced deaminase (AID) enzyme deaminates C to turn into U during the immunoglobulin (Ig) gene class switch recombination (CSR) and somatic hypermutation (SHM) in mature B cells (Castaneda-Zegarra *et al*, 2020a; Chi *et al*, 2020; Daniel & Nussenzweig, 2013; Muramatsu *et al*, 2000).

1.1.1.4 Abasic sites

Daily, thousands of abasic sites (apurinic/aprimidinic (AP) sites), are generated in a human cell (Lindahl, 1993; Thompson & Cortez, 2020). AP sites are characterized as unstable and become quickly SSBs. Mainly, the base excision repair (BER) pathway repairs the damage caused by abasic sites after APs are removed by AP endonucleases (Grundy & Parsons, 2020).

1.1.1.5 Physiological DSBs

DSBs are one of the most deleterious forms of DNA damage. They can be originated in response by both exogenous and endogenous agents. DSBs in either condition require effective processes of repair that cause minimal to no changes (Pannunzio *et al*, 2018). Programmed DSBs are generated during physiological processes, such as B and T lymphocyte development, meiosis, transcription, and replication (Oster & Aqeilan, 2020). For instance, physiological DSBs trigger the recombination of the *variable (V)*, *joining (J)*, and *diversity (D)* gene segments (V(D)J recombination) in developing B and T cells and the Ig heavy chain (IgH) CSR in mature B cells (Castaneda-Zegarra *et al.*, 2020a; Wang *et al*, 2020b).

1.1.2 Exogenous DNA damage

1.1.2.1 Ionizing Radiation (IR)

Ionizing radiation (IR) is high-energy radiation that consists of X-rays, neutrons, alpha, beta, and gamma particles. IR has the potential to release electrons from atoms and molecules, generating ions that break covalent bonds. IR can trigger harmful effects to people, depending on the levels of exposure. A biological factor of radiosensitivity is whether a cell possesses a high proliferation or not; for instance, cells of the epithelium and bone marrow are more radiosensitive than cells in the nervous system (Borrego-Soto *et al*, 2015; McBride & Schae, 2020).

Furthermore, IR can directly alter the DNA structure by causing SSBs and DSBs (Lomax *et al*, 2013; Rangunathan *et al*, 2020; Zhao *et al*, 2020). For example, in mammalian cells, 1 Gy produces approximately 850 pyrimidine lesions, 450 purine lesions, 1000 SSBs, and 20 to 40 DSBs (Cadet *et al*, 2008; Hutchinson *et al*, 2020; Lomax *et al.*, 2013).

1.1.2.2 Ultraviolet (UV) radiation

Ultraviolet (UV) radiation is one of the most common environmental hazards that affect living organisms. The UV radiation directly disturbs the DNA and induces ROS's high production (Sung-Lim & Sung-Keun, 2017). UV radiation possesses shorter wavelengths than visible light (700-400nm), and it can be classified into three classes depending on the wavelength range: UV-A (320-400nm), UV-B (290-320 nm), and UV-C (100-290 nm) (Ikehata & Ono, 2011; Roy, 2017). Both UV-B and UV-C radiation mainly damages the DNA by causing pyrimidine dimers, unlike UV-A, which can cause this type of damage but with less efficiency (Ikehata & Ono, 2011; Oksenysh & Coin, 2010; Roy, 2017; Zhovmer *et al*, 2010).

Highly conserved DNA repair mechanisms, such as direct reversal of DNA-damaged bases, nucleotide excision repair (NER) (Coin *et al*, 2007; Oksenysh *et al*, 2009), base excision repair (BER) (Jang *et al*, 2019), mismatch repair (MMR) (Tanaka *et al*, 2017), homologous recombination (HR) (Covo *et al*, 2012), and also non-homologous end-joining (NHEJ) (Huang *et al*, 2017) repairs the DNA when it is damaged by UV (Oksenysh *et al*, 2013b; Rastogi *et al*, 2010).

1.1.2.3 Chemical agents

The alkylating agents are chemical compounds with the capacity to react biologically. Two of the most common alkylating agents are nitrogen mustards and sulfur mustards. On the one side, nitrogen mustards act directly with biological molecules and are one of the most commonly used alkylating agents in medicine since their use for lymphoma treatment (Rhoads, 1946; Singh *et al*, 2018). On the other side, sulfur mustards produce intra- and interstrand crosslinks and DNA-protein crosslinks, giving rise to DNA-blocking activity. The latter was used as a military weapon during World War I due to its potential to cause severe burns to the eyes, skin, and respiratory tract (Jiang & Maibach, 2018). DNA damage induced by sulfur mustards involves several DNA repair pathways, such as BER, NER, HR, and NHEJ (Panahi *et al*, 2018). On 29 April 1997, the Chemical Weapons Convention (CWC) entered in force. CWC has a working relationship with the United Nations (UN), and it is accepted by the Conference of the States Parties (COSP), which is formed by 193 countries. CWC mainly forbids the development, production, stockpiling, and use of any chemical weapon (OPCW, 2021; UN, 2021).

Alkylating agents are also present in some people's daily activities, being found in tobacco smoke and dietary ingredients. Moreover, many chemical therapies for treating cancers are based on alkylating-chemical compounds due to their potential for DNA damage and killing

of fast-proliferating tumor cells due to the transfer of alkyl-groups to the DNA (DeVita & Chu, 2008; Gutierrez & O'Connor, 2021).

1.1.2.4 Chemical therapies and strategies based on DNA damage

Several DNA damaging agents are used therapeutically against different types of cancers. Each cancer drug possesses its own mechanism of action and damage in the DNA. Therefore, not all the different DNA repair pathways respond against all the induced damage by chemotherapeutic drugs. Some of the most popular DNA damaging agents used for treatment in cancer will be listed below.

The alkylating agents were the first non-hormonal drugs used efficiently for cancer treatment, including bendamustine and melphalan. Bendamustine is a white, water-soluble microcrystalline powder and a nitrogen mustard derivative used for the treatment of chronic lymphocytic leukemia (CLL). This chemotherapeutic drug forms monoadducts of purine bases leading to DNA damage, which is repaired by the BER pathway (Leoni *et al*, 2008; Visani *et al*, 2020). Melphalan, another nitrogen mustard drug, is taken as a tablet (orally) or intravenously, and it is used against a variety of neoplastic conditions mainly multiple myeloma treatment (Barlogie *et al*, 2004; Esma *et al*, 2017). This drug induces the formation of interstrand DNA crosslinks via alkylation, leading to base deletions and interfering during the DNA replication and transcription (Balcome *et al*, 2004; Esma *et al.*, 2017). The NER pathway is engaged in repairing induced DNA damage by melphalan (Episkopou *et al*, 2009; van Kan *et al*, 2021).

Cisplatin is a platinum-based chemotherapeutic drug used widely to treat several cancers, including lung, ovarian, testicular, breast, bladder, head and neck, and cervical cancers (Ghosh, 2019). Cisplatin induces bulky DNA adducts, blocking the DNA transcription and replication. The DNA damage induced by cisplatin is mainly repaired by the NER, and MMR mechanisms (Coin *et al*, 2008; Ghosh, 2019; Oksenysh *et al.*, 2009).

Another strategy is to block DNA replication, which is very active in cancer cells, by using etoposide and doxorubicin. Various cancers are treated with etoposide, such as lung and testicular cancers, whereas doxorubicin is frequently used to treat leukemia, bladder, breast, lung, and ovarian cancers (Reyhanoglu & Tadi, 2021; Woods & Turchi, 2013). Both drugs induce DSBs by inhibiting DNA topoisomerase II but with independent mechanisms. Etoposide stabilizes covalently DNA-protein complexes leading to replication stress, unlike doxorubicin that intercalates into DNA, leading to inhibition of the topoisomerase II. DSBs

induced by etoposide and doxorubicin are repaired by both HR and NHEJ (Montecucco *et al*, 2015; Woods & Turchi, 2013).

Bleomycin is a radiomimetic agent that is used to treat lymphomas and other cancers, including ovarian and testicular cancer (Brandt & Gerriets, 2021; Lavoie & Kollmannsberger, 2019; Murray *et al*, 2018). This drug is involved in the inhibition of DNA synthesis, although its precise mechanism is unknown. Bleomycin causes DSBs as a consequence of accumulation and lack of SSB repair. Both HR and NHEJ repair DSBs induced by bleomycin (Letavayova *et al*, 2006; Reid *et al*, 2015; Woods & Turchi, 2013).

Besides the chemotherapies listed above, during this century, DNA repair inhibitors have attracted researchers' and clinicians' attention for their potential as a cancer therapy treatment (Helleday, 2011; Pilger *et al*, 2021; Yap *et al*, 2019). Ideally, DNA repair inhibition might be exclusively toxic to cancer cells with reduced side effects in patients. An example of this therapy is based on the synthetic lethality between poly (ADP-ribose) polymerase (PARP) and breast cancer susceptibility protein (BRCA) (Bryant *et al*, 2005; Cong *et al*, 2021; Farmer *et al*, 2005). Theodore Dobzhansky coined the term "synthetic lethality" when a combined mutation in two genes leads to cell death, whereas mutation of either gene alone does not (Dobzhansky, 1946). PARP inhibitors are used to treat inherited breast and ovarian cancer patients with defective *BRCA1* or *BRCA2* genes. In general, these patients have either mutations in the *BRCA1* or *BRCA2* genes, though a few cases have been reported with both mutations (*BRCA1* and *BRCA2*), for example among Ashkenazi populations (Leegte *et al*, 2005; Meynard *et al*, 2017; Vietri *et al*, 2013). *BRCA1*- or *BRCA2*-defective cancer cells have shown 100 to 1000-fold more sensitivity to PARP inhibitors than *BRCA* proficient cells (Bryant *et al.*, 2005; Farmer *et al.*, 2005). Biologically, PARP is involved in the SSB repair while *BRCA1* and *BRCA2* in DSB repair by HR. In this case, PARP inhibitors cause an increase of SSBs and DSBs accumulation, which are toxically irreparable in *BRCA1* and/or *BRCA2* defective cells, inducing cell death, as illustrated in Figure 1. Nevertheless, not all patients with *BRCA1* and/or *BRCA2* deficiency respond positively to the therapy with PARP inhibitors (PARPi) and some patients develop tumor resistance (LaFargue *et al*, 2019). Patients with PARPi resistance show HR restoration due to secondary mutations, NHEJ suppression, and increased drug efflux, among others (Rose *et al*, 2020).

Furthermore, during the last years, it has emerged a great interest in the target of proteins involved in the DNA damage response (DDR), such as ataxia-telangiectasia mutated (ATM), ATM and Rad3-related (ATR), including DNA-dependent protein kinase (DNA-PK), with the latter involved in the NHEJ pathway (Yap *et al.*, 2019). Notably, a clinical trial has

shown positive effects in treating patients with solid tumors using an inhibitor of DNA-PK combined with radiotherapy (Triest *et al*, 2017).

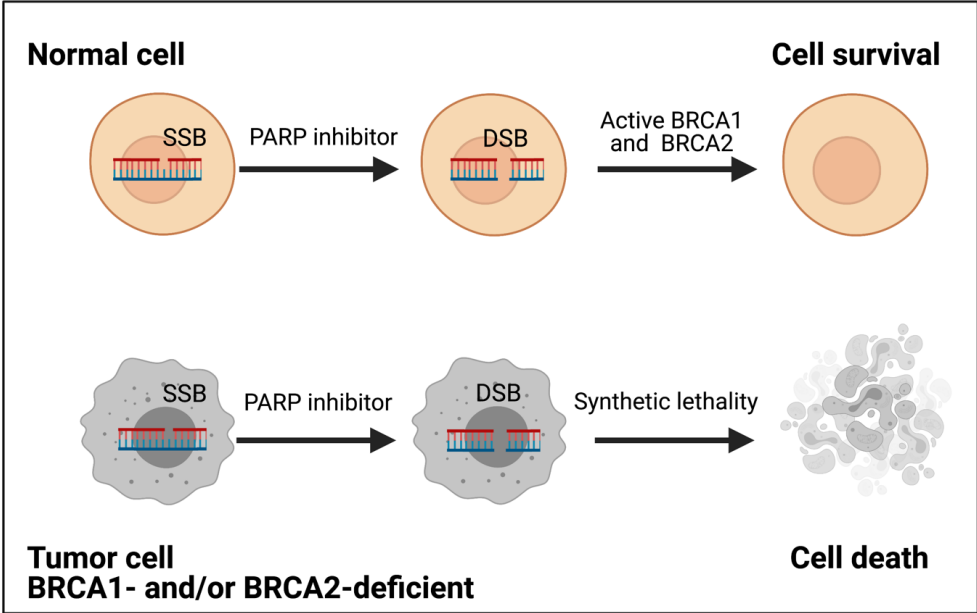


Figure 1. Synthetic lethality in BRCA1- and/or BRCA2-deficient cancer. SSBs are naturally originated in WT and BRCA1- and/or BRCA2-deficient cells. When PARP action is inhibited, SSBs are converted to DSBs. DSBs are repaired in cells with functional BRCA1 and BRCA2, in contrast to BRCA1- and/or BRCA2-deficient, which cannot efficiently repair DSBs, leading to cell death. BRCA, breast cancer susceptibility gene; DSB, double-strand break; PARP, poly (ADP-ribose) polymerase; SSB, single-strand break. This Figure was made in BioRender platform and inspired by (Polyak & Garber, 2011).

1.2 DNA DAMAGE RESPONSE (DDR)

In order to respond against endogenous and exogenous agents and maintain genomic integrity, cells have developed an intricate signaling cascade called DNA damage response (DDR). DDR provides enough time either for arresting cell-cycle progression, or activating specified DNA repair pathways, or to lead the cells with unreparable genomes to apoptosis. DDR is mainly regulated by DNA damage sensors from the family of the phosphoinositide 3-kinase (PI3K)-related kinases (PIKKs), such as ATR, ATM, and DNA-PK, which phosphorylate different substrates to activate DDR. ATM and DNA-PK are implicated during DSBs repair, while ATR activation occurs mainly during DNA replication (Blackford & Jackson, 2017). The following section briefly describes the ATM-dependent DDR due to its relevance in the DNA DSBs repair.

1.2.1 ATM-dependent DNA damage sensing and promoting of DSBs repair by NHEJ.

ATM is recruited to the DSBs through the stimulation and activation by the MRE11-RAD50-NBS1 (MRN) complex. Activated ATM can phosphorylate a diversity of downstream mediators to amplify the damage signals involved in DNA repair as well as the activation of other protein kinases that phosphorylate even more substrates, such as checkpoint kinase 2 (CHK2) and the tumor suppressor p53 (Blackford & Jackson, 2017; Shiloh & Ziv, 2013). Upon DSBs, ATM phosphorylates the H2A histone family member X (H2AX) at serine 139, a variant of histone H2A (Burma *et al*, 2001; Celeste *et al*, 2002; Gonzalez-Gutierrez *et al*, 2019; Rogakou *et al*, 1998). The phosphorylated H2AX (γ H2AX) facilitates the recruitment of modulator of DNA damage checkpoint 1 (MDC1) (Stucki *et al*, 2005). Subsequently, ATM phosphorylates the recruited MDC1, which contributes to the recruitment of the ubiquitin E3 ligase, Really Interesting New Gene (RING) Finger Protein 8 (RNF8) (Kolas *et al*, 2007; Mailand *et al*, 2007). The relevance to recruit ubiquitin ligases relies on their functions to regulate the assembly and disassembly of DDR proteins as well as mediate the protein stability and activity (Tang *et al*, 2021; Yu *et al*, 2020). Afterward, MDC1 recruits a protein involved in transcriptional repression activity and chromatin compaction called lethal (3) malignant brain tumor-like protein 2 (L3MBTL2), which is phosphorylated by ATM and ubiquitinated by RNF8 (Nowsheen *et al*, 2018). Consequently, ubiquitinated L3MBTL2 facilitates the recruitment of the ubiquitin kinase RNF168 to the DNA lesion (Nowsheen *et al.*, 2018). RNF168 ubiquitinates γ H2AX, wherewith the phosphorylated and ubiquitinated H2AX promotes the recruitment of different DDR factors, such as p53-binding protein (53BP1),

RNF169, RAP80, and RAD18 to the DSB depending on DNA end resection (Bohgaki *et al*, 2013; Mattioli *et al*, 2012; Nowsheen *et al.*, 2018). For instance, RNF169 limits the recruitment of DDR factors working as a negative regulator of the DNA damage signaling cascade by competing with RNF168 (Chen *et al*, 2012). RAP80 and RAD18 facilitate HR repair by recruiting HR factors, such as BRCA1 (Huang *et al*, 2009; Kim *et al*, 2007). In contrast, 53BP1 is recruited to DSBs to engage NHEJ and suppress HR. When 53BP1 is phosphorylated, it binds PAX-interacting protein 1 (PTIP) and Rap1 interacting factor 1 (RIF1) proteins (Callen *et al*, 2013; Chapman *et al*, 2013; Escribano-Díaz *et al*, 2013). On the one side, PTIP binds Artemis to trim DNA ends, promoting NHEJ and preventing DNA end resection (Wang *et al*, 2014). On the other side, RIF1 recruits the shieldin complex (C20orf196 (SHLD1), FAM35A (SHLD2), CTC-534A2.2 (SHLD3) and REV7) (Boersma *et al*, 2015; Dev *et al*, 2018; Findlay *et al*, 2018; Ghezraoui *et al*, 2018; Gupta *et al*, 2018; Noordermeer *et al*, 2018). In addition, RIF1 recruits the CTC1–STN1–TEN1 (CST) complex, which interacts with shieldin and localizes with polymerase α -primase (Pol α -prim) in a 53BP1- and shieldin-dependent manner (Mirman *et al*, 2018; Schimmel *et al*, 2021), as illustrated in Figure 2. The relevance of SHLD1, SHLD2, SHLD3, and REV7 as a 53BP1 downstream and effector complex lies in their functionality during the DNA ends protection and enhancing DSB repair by NHEJ (Setiaputra & Durocher, 2019).

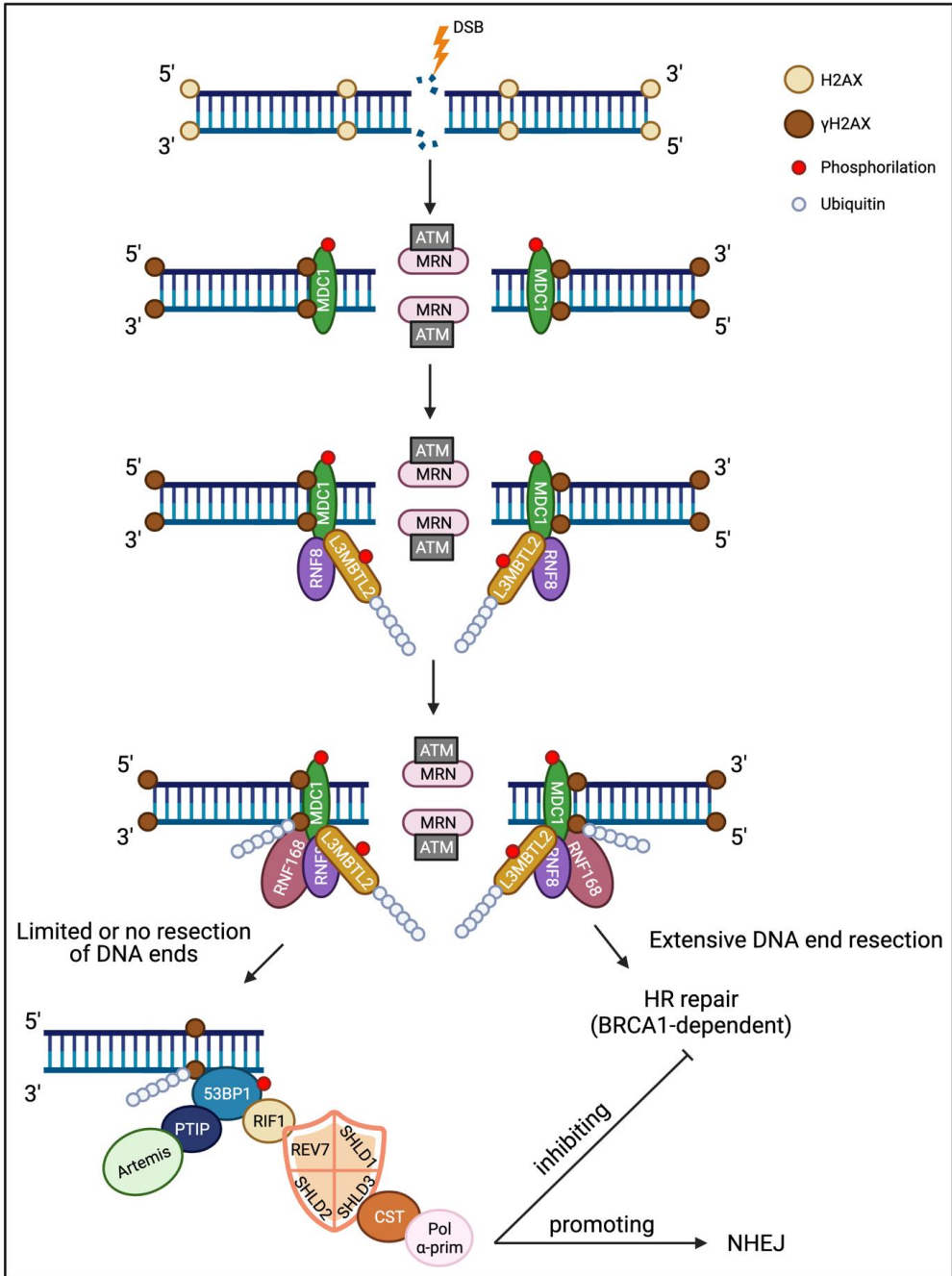


Figure 2. Schematic illustration of DDR signaling pathway mediated by ATM. DSBs are sensed by the MRN complex, which recruits ATM. Later, ATM phosphorylates H2AX; the phosphorylated H2AX (γ H2AX) promotes the recruitment of MDC1 for further phosphorylation by ATM. Then, activated MDC1 facilitates the recruitment of the ubiquitin E3 ligase RNF8 and L3MBTL2 protein. The latter is phosphorylated and ubiquitinated by ATM and RNF8, respectively. Consequently, phosphorylated and ubiquitinated L3MBTL2

contributes to the recruitment of the ubiquitin RNF168, which ubiquitinates γ H2AX. Afterward, phosphorylated and ubiquitinated H2AX promotes the recruitment of 53BP1 to the DSBs to antagonize BRCA1-dependent end resection. 53BP1 binds PTIP and RIF1. PTIP promotes NHEJ repair by recruitment of Artemis. While RIF1 recruits the Shieldin complex (formed by REV7, SHLD1, SHLD2, and SHLD3 subunits), CST complex and, polymerase α -primase, promoting NHEJ and countering HR. DDR, DNA damage response; HR, homologous recombination; NHEJ, non-homologous end-joining. This Figure was made in BioRender platform.

1.3 DNA REPAIR

A mammalian cell suffers thousands of DNA lesions per day, among which the majority are SSBs (Jackson & Helleday, 2016; Lindahl & Barnes, 2000). For instance, using a method called aldehyde reactive probe (ARP)-slot-blot, which reacts with the aldehydic group of ring-opened AP sites, Nakamura and colleagues found that under physiological conditions, around 9000 AP sites are generated every day in a mammalian cell (Nakamura *et al.*, 1998). Moreover, DNA SSBs might also be converted to DSBs, which are less frequent but more deleterious. Cells have developed intricate molecular mechanisms to cope with the different DNA lesions caused by endogenous and exogenous agents to face genomic instability and restore genome integrity protecting cells from different injuries (Friedberg, 2008; Lindahl & Barnes, 2000; Tubbs & Nussenzweig, 2017).

1.3.1 Direct reversal

DNA repair by reversal of DNA damage involves repairing the DNA without an incision in the backbone. Notwithstanding this mechanism resolves only a tiny group of DNA lesions, it repairs the DNA directly and often only uses a single repair protein with error-free properties, making it attractive for cells. Direct reversal of DNA damage might be classified into three central mechanisms: (1) photolyases related to UV light-induced photolesions. (2) O⁶-alkylguanine-DNA alkyltransferases (AGTs) that reverse a set of O-alkylated DNA damage, and (3) AlkB family dioxygenases that reverse N-alkylated base adducts (Kavakli *et al.*, 2019; Yi & He, 2013). Below, one example is described to illustrate the event.

DNA repair by photolyases is interesting for its simplicity. Photolyases repair UV-light-induced DNA damage, such as cyclobutane pyrimidine dimers (CPDs) and pyrimidine pyrimidones photoproducts (6-4 PPs) using blue and near-UV light. Initially, photolyases transfer an electron from the reduced form of the cofactor flavin adenine dinucleotide (FADH⁻) to the UV-lesions. Subsequently, photolyases split pyrimidine dimers into monomers, utilizing the light energy at 300-500 nm. Finally, there is an electron transfer from the pyrimidine monomer radical back to FADH, hence reestablishing FADH⁻, as illustrated in Figure 3 (Brettel & Byrdin, 2010; Kavakli *et al.*, 2019; Yi & He, 2013).

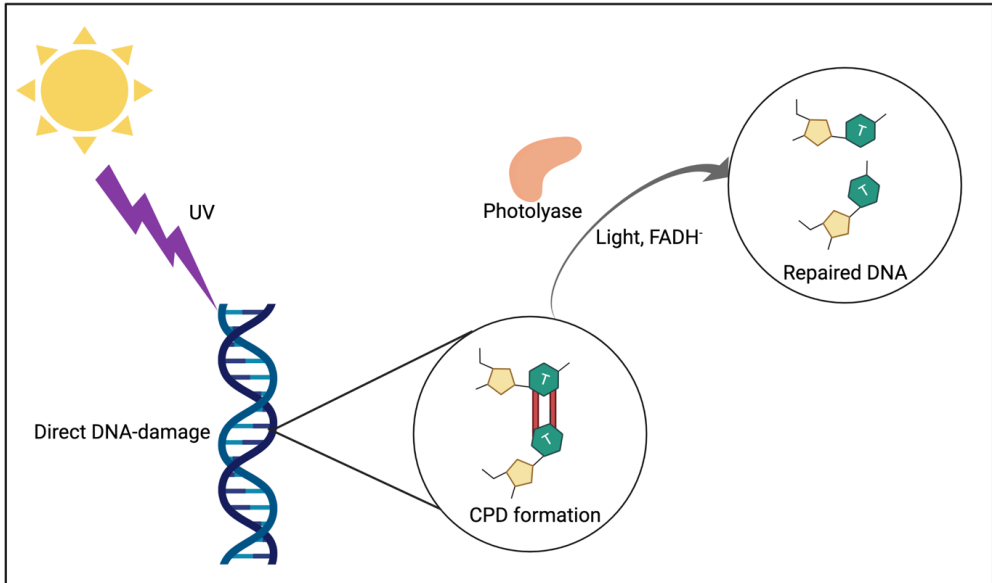


Figure 3. Schematic illustration of CPDs repair by direct reversal of DNA damage. UV induces the formation of covalent linkages between consecutive bases, e.g., between two thymines, forming CPDs. The photo reactivating enzyme (photolyase) recognizes CPDs induced by UV and splits it into two monomers, utilizing the electron transfer capacity by the reduced form of the cofactor flavin adenine dinucleotide (FADH) and the energy of light (>300 nm). CPD, cyclobutane pyrimidine dimers; UV, Ultraviolet light. This Figure was made in BioRender platform.

1.3.2 Base excision repair (BER)

BER pathway corrects damaged DNA bases originated from different sources, such as oxidative damage generated by respiration, alkylation reactions, and natural hydrolysis (Lindahl, 1993; Thompson & Cortez, 2020).

DNA glycosylases take part in the initial step of the BER pathway; according to functionality, they can be either monofunctional or bifunctional. Monofunctional glycosylases have only glycosylase activity, whereas bifunctional glycosylases possess additional DNA strand cleavage activity (Carter & Parsons, 2016). During BER, monofunctional DNA glycosylases, e.g., uracil-DNA glycosylase (UNG), recognize and dissociate the N-glycosidic bond between the damaged base and the phosphodiester DNA backbone, leaving an AP site. Nevertheless, bifunctional DNA glycosylases remove the damaged base and additionally cut the DNA backbone to originate a single-nucleotide gap flanked by either a 5' phosphate and a 3' phosphor- α,β -unsaturated aldehyde (PUA) by β -elimination or 5'-phosphate and 3'-phosphate residues by β,δ -elimination. For instance, 8-oxoguanine (8-oxoG) DNA glycosylase (OGG1) catalyzes the β -elimination while the endonuclease VIII-like 1 (NEIL1) catalyzes β,δ -elimination with the participation of the polynucleotide kinase phosphatase (PNKP) (Carter & Parsons, 2016; Grundy & Parsons, 2020; Hegde *et al.*, 2008).

After AP sites are generated, AP endonucleases, such as AP endonuclease 1 (APE1), the major AP endonuclease in mammalian cells, create a gap flanked by 3'-hydroxyl and 5'-deoxyribose phosphate (5'-dRP) ends. The 5'-dRP end is afterward removed and filled with the correct nucleotide into the gap by the DNA polymerase β (Pol β). Subsequently, the complex formed by X-ray cross-complementing protein 1 (XRCC1) and DNA ligase III (LIG3) seals the nicks in the DNA during short-patch BER. However, in some circumstances, a long-patch BER is required. In this case, a polymerase switch from Pol β to DNA polymerases δ or ϵ (Pol δ/ϵ) occurs after the addition of the first nucleotide, incorporating from 2 to 12 nucleotides and generating a 5'-flap structure with dRP end. Finally, proliferating cell nuclear antigen (PCNA) stimulates flap endonuclease 1 (FEN1); and together with the DNA ligase I (LIG1), complete the pathway by sealing the remaining nick in the DNA backbone (Carter & Parsons, 2016; Grundy & Parsons, 2020; Hegde *et al.*, 2008), as illustrated in Figure 4. Commonly, bifunctional DNA glycosylases participate during short-patch BER, whereas monofunctional DNA glycosylases are involved in either pathway (Dizdaroglu, 2017).

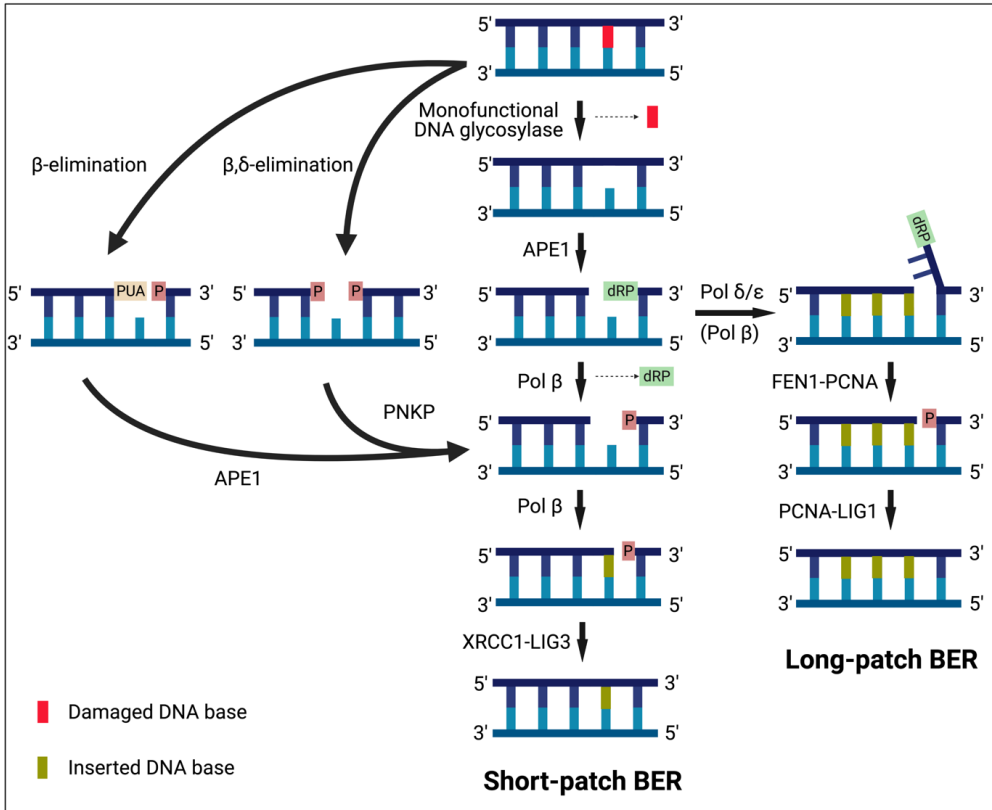


Figure 4. Schematic illustration of a DNA base repair by the human BER pathway. Monofunctional DNA glycosylases (e.g., UNG) recognize and excise the damaged base, leaving an AP site. APE1 incises abasic sites creating a single-strand break containing a 5'-deoxyribose phosphate (5'-dRP), which might be processed by either short-patch BER or long-patch BER. During short-patch BER, Pol β removes the 5'-dRP end and fills the gap with a new nucleotide. In contrast to monofunctional glycosylases, bifunctional glycosylases initiate BER by β -elimination (e.g., OGG1) or β,δ -elimination (e.g., NEIL1). β -elimination creates a nucleotide gap flanked by 3' phosphor- α,β -unsaturated aldehyde (PUA), and 5' phosphate. APE1 removes PUA, and Pol β extends the DNA by one nucleotide. β,δ -elimination creates a single-nucleotide gap containing 3'- and 5'-phosphate ends. PNKP removes the 3'-phosphate, and subsequently, Pol β adds a nucleotide. XRCC1-LIG3 complex ligates the remaining nick after polymerase activity during BER initiated by bifunctional glycosylases and monofunctional glycosylases dependent on short-patch BER. However, if the 5'-dRP end is resistant to Pol β activity, a long-patch BER is required. Long-patch BER adds 2 to 12 more nucleotides into the gap by polymerase switch to Pol δ/ϵ generating a 5'-flap structure with dRP end. The latter is recognized and removed by FEN1 and PCNA, and finally, the remaining nick is sealed by the interaction of PCNA and LIG1. AP, apurinic/aprimidinic; BER, base excision repair. This Figure was made in BioRender platform and inspired by (Carter & Parsons, 2016).

1.3.3 Nucleotide excision repair (NER)

NER eliminates bulky lesions caused by UV radiation, such as 6–4PPs and CPDs and chemical adducts caused by chemotherapeutic drugs (Lee & Kang, 2019). NER can be divided into two sub-pathways, according to whether the lesions' elimination occurs throughout the whole genome or during the gene transcription. The first sub-pathway is called the global genome NER (GG-NER), while the second is the transcription-coupled NER (TC-NER). GG-NER and TC-NER differ only in the initial steps of DNA damage recognition. Recognition of DNA damage during GG-NER is carried out by the complex formed by xeroderma pigmentosum (XP) group C (XPC), UV excision repair protein radiation sensitive 23B (RAD23B) and CETN2 (Centrin 2), as well as by UV-DDB (UV-damaged DNA binding protein; a heterodimeric complex with DNA-damage binding (DDB)-1 and 2). Meanwhile, in TC-NER, the lesions cause the stalling of the RNA polymerase II (RNA Pol II) during transcript elongation, which is subsequently recognized by Cockayne syndrome (CS)-A and B proteins (Duan *et al.*, 2020; Lee & Kang, 2019).

After damage recognition, the DNA repair and transcription initiation factor II H (TFIIH) core complex (XPB, XPD, p62, p52, p44, p34 and TTDA/p8) links the cdk-activating kinase (CAK) complex (cdk7, MAT1, and cyclin H) via XPD in order to process NER (Coin *et al.*, 2007; Greber *et al.*, 2019). XPB and XPD helicases are recruited to the lesion in both GG-NER and TC-NER for opening a repair bubble around damaged nucleotides and performing the helix unwinding, followed by recruitment of XPA and release of CAK (Coin *et al.*, 2007; Coin *et al.*, 2008; Oksenyich *et al.*, 2009; Oksenyich & Coin, 2010; Zhovmer *et al.*, 2010). Then, XPA with XPD perform the damage verification, and simultaneously the DNA binding protein replication protein A (RPA) is recruited into the undamaged strand. XPG and the excision repair protein cross-complementation 1 (ERCC1)-XPF complex catalyzes the lesion excision, promoting the removal of a DNA single-strand gap of 22-32 nucleotides. Finally, PCNA recruits DNA polymerases (δ , ϵ and/or κ) for DNA synthesis while LIG1 or the LIG3-XRCC1 complex seal the nicks to complete NER, as illustrated in Figure 5 (Duan *et al.*, 2020; Lee & Kang, 2019).

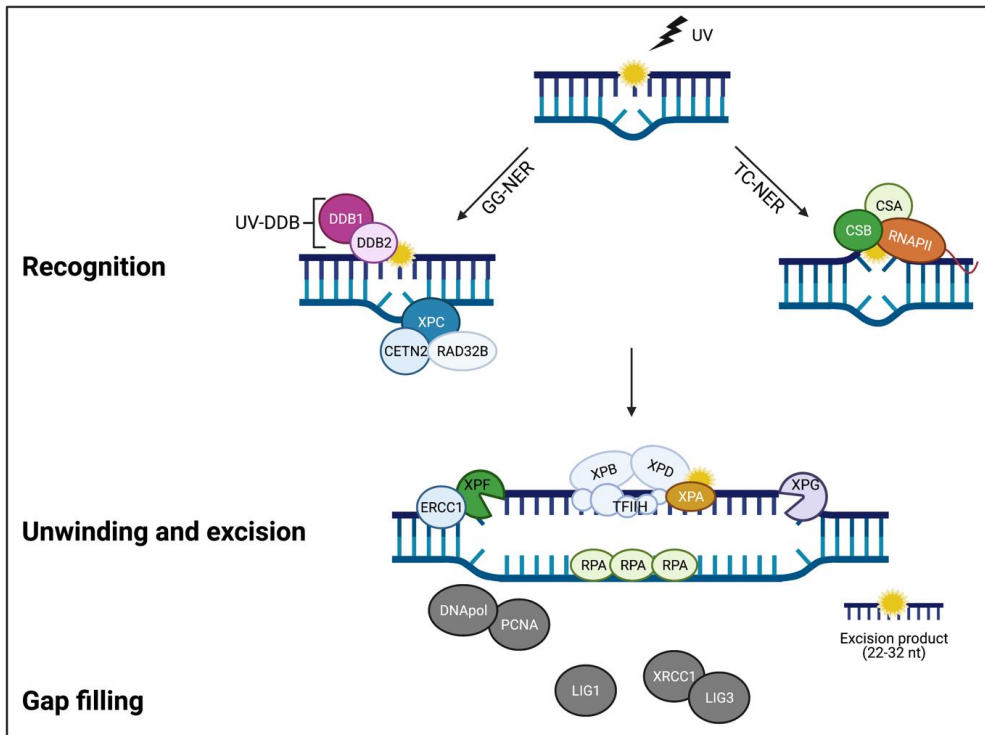


Figure 5. Repair of UV-induced DNA damage by NER. UV-damage can be recognized either by the XPC complexed with RAD23B, CETN2, and UV-DDB or by the elongating RNA Pol II with CSA and CSB proteins to initiate GG-NER or TC-NER, respectively. After damage recognition, both sub-pathways share the same set of repair enzymes to perform DNA unwinding, 22-32 nucleotides excision, repair synthesis, and ligation. GG-NER, global genome-NER; NER, nucleotide excision repair; TC-NER, transcription-coupled NER; UV, ultraviolet light. This Figure was made in BioRender platform and inspired by (Lee & Kang, 2019).

1.3.4 Mismatch repair (MMR)

MMR is an evolutionary safeguard of genomic stability due to preserving DNA homeostasis during DNA replication (Huang & Li, 2018; Liu *et al.*, 2017a). The mismatch repair system was first discovered in *Escherichia coli* (Su & Modrich, 1986). Although MMR is highly conserved, MMR is markedly more complex in eukaryotic cells than in prokaryotic cells. Research on *E. coli* has revealed a number of MMR genes that are hypermutable when mutationally inactivated. These genes were called “*Mut*” (short for “mutagenic”), such as *MutS*, *MutL*, *MutH*. Humans possess MMR homolog proteins to *E. coli*, such as MSH and MLH, which are homologs to MutS and MutL, respectively (Modrich, 2016; Pecina-Slaus *et al.*, 2020). MMR involves three main steps: lesion recognition, lesion excision, and DNA resynthesis and ligation. Initially, MutS participates at the early stages of mismatch recognition, followed by recruitment of MutL. The latter acts as an endonuclease, and together with exonuclease 1 (Exo1) recognize and excise the mismatch. Subsequently, DNA polymerases (δ , ϵ) fill the gap during the resynthesis, and LIG1 seals the remaining nick, as illustrated in Figure 6 (Kunkel & Erie, 2015; Prindle & Loeb, 2012). In addition, PCNA accomplishes roles in every MMR step (Guillotin & Martin, 2014; Pecina-Slaus *et al.*, 2020). It has been found that patients with genetic MMR mutations possess a high risk of having Lynch syndrome, also known as hereditary non-polyposis colorectal cancer (HNPCC). These patients are more likely to develop colon and ovarian cancers (Duraturo *et al.*, 2019; Sekine *et al.*, 2017).

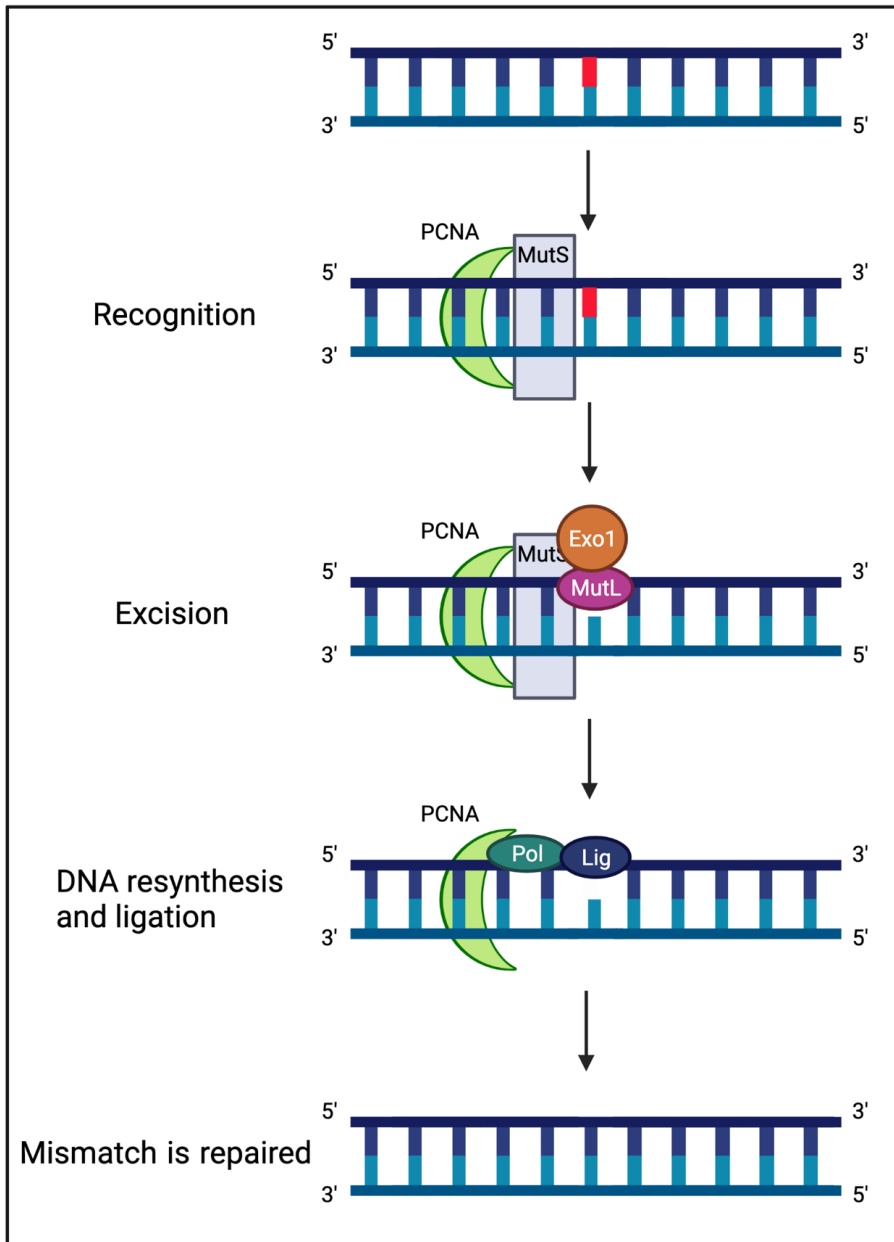


Figure 6. Schematic illustration of mismatch repair by the human MMR pathway. MutS recognizes and binds the misincorporated nucleotide together with PCN during the mismatch recognition. Then, an endonuclease subunit of MutL together with the exonuclease Exo1 are recruited by MutS to excise the mismatch. Finally, DNA polymerases and ligases perform DNA resynthesis and ligation. MMR, mismatch repair. This Figure was made in BioRender platform.

1.3.5 DNA double-strand break repair

DSBs are the most deleterious and toxic type of DNA breaks that may occur in a cell. Commonly, cells employ two major pathways to repair DSBs, the homologous recombination (HR) and the classical non-homologous end-joining (C-NHEJ), or simply NHEJ. On the one side, HR is usually restricted to the S/G2 phases (DNA synthesis phase/second gap phase) due to the requirement for a sister chromatid as a template (Zhao *et al.*, 2017). For instance, it was found that HR is almost non-existent in G1 (first gap phase) (Mao *et al.*, 2008) with 24 times higher DSB repair by HR in S-phase than in G1/G0 (first gap phase/resting phase) (Saleh-Gohari & Helleday, 2004). On the other side, NHEJ is active throughout the whole cell cycle but predominantly during the G1 phase because cells spend longer times during G0/G1 added to the almost null participation of HR during G1 (Mao *et al.*, 2008; Zhao *et al.*, 2017). However, NHEJ efficiency in G2/M is almost five-fold higher than in the G1 phase (Mao *et al.*, 2008). Therefore, the cell cycle phase and DNA repair protein abundance determine whether the HR or NHEJ pathway is going to repair a DSB. In addition, other DNA repair pathways, such as alternative end-joining (A-EJ) or single-strand annealing (SSA), occur when HR and NHEJ are not accessible or molecular alterations occur during them. The A-EJ and SSA mechanisms are both more error-prone than HR and NHEJ, often causing chromosomal translocations, and deletions, leading to genome instability (Betermier *et al.*, 2014; Ceccaldi *et al.*, 2016; Oster & Aqeilan, 2020).

In the present study, we have focused our efforts on researching NHEJ factors and their participation during a mechanism called V(D)J recombination, which is needed during B and T cell development (Castaneda-Zegarra *et al.*, 2020a; Wang *et al.*, 2020b). We mainly used mouse models to elucidate the genetic interactions between NHEJ factors and DNA repair during our research. Further details are discussed in the following sections.

1.3.5.1 Homologous recombination (HR)

HR is initiated with the DNA end resection at the 5' ends of the DSB, generating 3' single-stranded DNA (ssDNA) intermediates by the proteins that conform the MRN complex (MRE11–RAD50–NBS1) and the endonuclease (C-terminal binding protein)-interacting protein (CtIP) (Makharashvili & Paull, 2015). The 3'-ssDNA ends are coated and stabilized by replication protein A (RPA). BRCA2, together with BRCA1 and partner and localizer of BRCA2 (PALB2), bind and load RAD51 onto the 3'-ssDNA end, which promotes the assembly of an ordered RAD51–ssDNA filament. The RAD51–ssDNA filament induces the formation of a displacement loop (D-loop) through the invasion of the duplex homologous DNA, as

illustrated in Figure 7. Subsequently, different polymerases participate during the DNA synthesis, followed by a ligation and substrate resolution by different HR sub-pathways (Hosoya & Miyagawa, 2014; Ranjha *et al*, 2018; San Filippo *et al*, 2008).

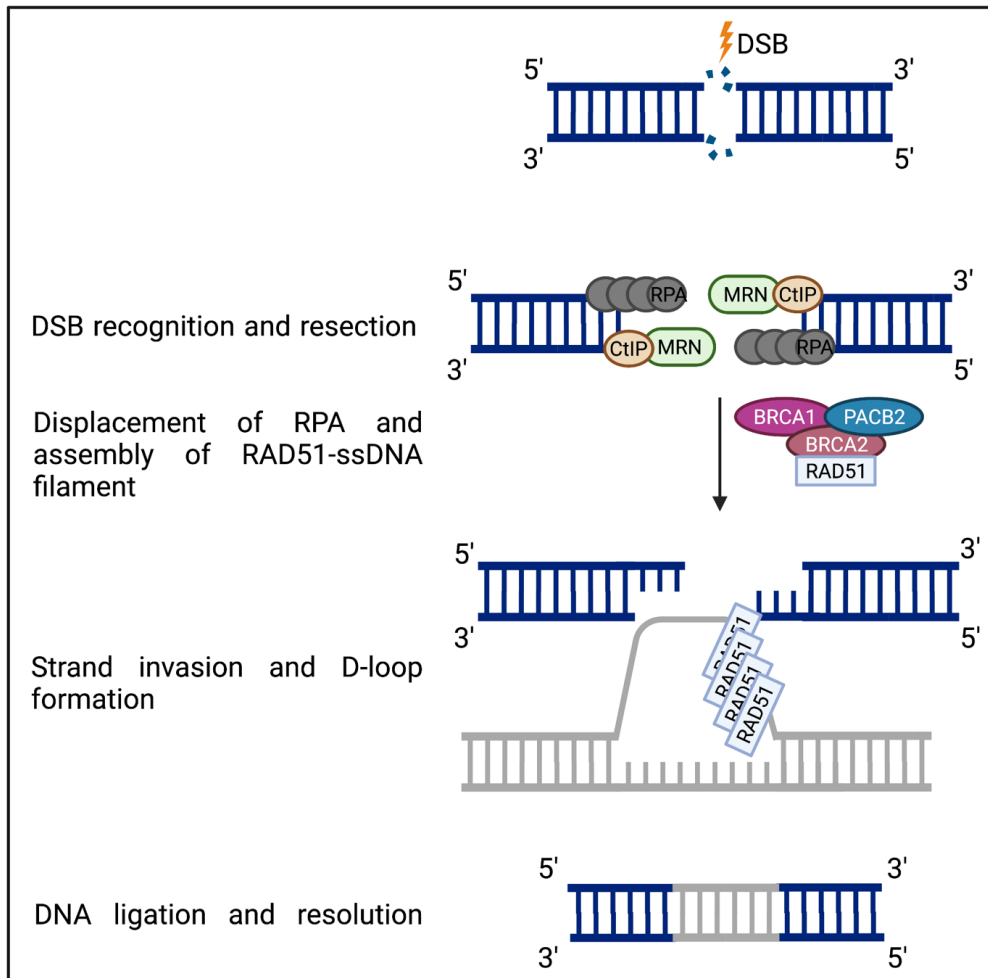


Figure 7. Schematic illustration of DSB repair by HR pathway. After the DSB sensing, the MRN complex and CtIP resect at 5' to 3' of the DSB, while the resulting 3'-ssDNA ends are coated and stabilized by RPA. A complex formed by BRCA2, BRCA1, and PALB2 recruits RAD51 and load it onto ssDNA, when simultaneously RPA is displaced. Next, the RAD51-ssDNA filament invades the homologous duplex and induces the formation of a D-loop. Finally, the invading strand primes the DNA synthesis, followed by DNA ligation and resolution. D-loop, displacement loop; HR, homologous recombination. This Figure was made in BioRender platform.

1.3.5.2 Alternative pathways to repair DSBs

In addition to the HR, the resected DSBs originated by MRN and CtIP might also be repaired by mutagenic repair pathways named alternative end-joining (A-EJ) and single-strand annealing (SSA) (Sallmyr & Tomkinson, 2018; Scully *et al*, 2019). A-EJ uses microhomology usually ranging from 2 to 20 base pairs (bp). In contrast, SSA demands even longer microhomology, generally more than 20bp (Blasiak, 2021; Chang *et al*, 2017).

On the one side, A-EJ causes genomic instability, and it is known to generate mutagenic rearrangements and translocations by joining DSBs between different chromosomes. Molecularly, A-EJ relies on the XRCC1/LIG3 complex or LIG1, Pol θ , and the competitor of Ku (an essential NHEJ factor), PARP1, to repair DSBs (Boboila *et al*, 2012; Caracciolo *et al*, 2019; Liang *et al*, 2021; Sallmyr & Tomkinson, 2018). On the other side, RAD52 anneals homologous repeat sequences during the SSA pathway, followed by excision of the non-homologous 3' ssDNA tails by ERCC1 and XPF. Following that, DNA polymerases are used to fill any gaps to generate the substrate for a DNA ligase to complete SSA, giving rise to a deletion rearrangement between the repeats, as illustrated in Figure 8 (Bai *et al*, 2021; Bhargava *et al*, 2016; Blasiak, 2021; Ceccaldi *et al.*, 2016; Sallmyr & Tomkinson, 2018).

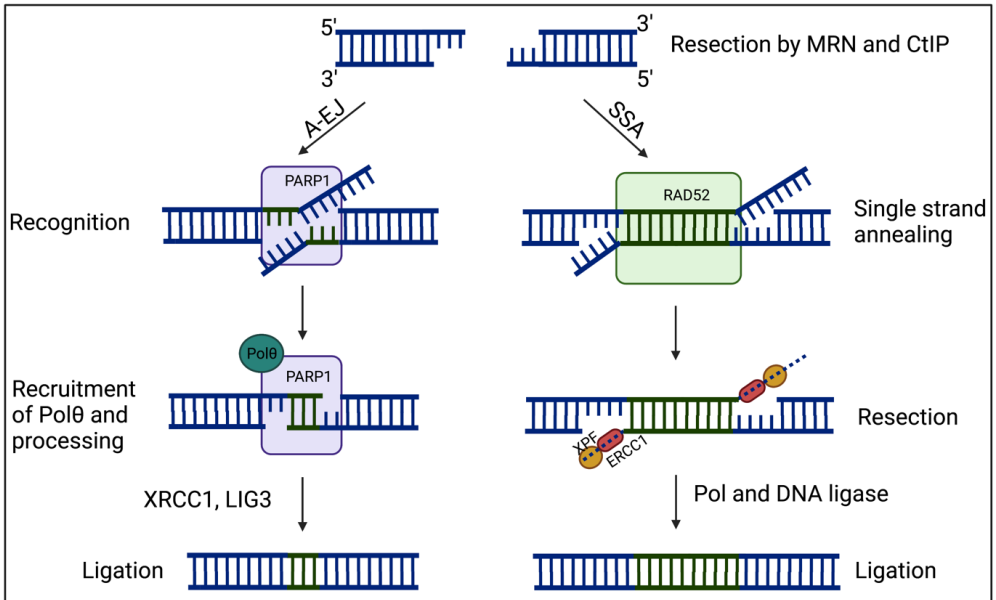


Figure 8. Schematic illustration of two alternative pathways to repair DSBs. Two additional mechanisms, A-EJ and SSA, compete to repair DSBs when DNA resection occurs by MRN and CtIP. On the one hand, PARP1 detects and binds the broken ends during A-EJ repair, followed by Polθ and other unknown factors. Subsequently, LIG3, in conjunction with XRCC1, or LIG1, performs the ligation step. On the other hand, during SSA, RAD52 facilitates strand annealing while ERCC1-XPF removes the 3'-ssDNA between the two direct repeats. Then, the two DSB ends are re-joined by polymerases and DNA ligases. A-EJ, alternative end-joining; SSA, single-strand annealing. This Figure was made in BioRender platform.

1.4 NON-HOMOLOGOUS END-JOINING (NHEJ)

NHEJ is the major system to repair DSBs in eukaryotes, and this pathway operates throughout the cell cycle, and it is of particular note in G1-phase cell (Castaneda-Zegarra *et al.*, 2020a; Frock *et al.*, 2021; Wang *et al.*, 2020b). In addition, some bacteria species, such as *Streptomyces coelicolor* and *Pseudomonas putida* have also been found to use it (Aravind & Koonin, 2001; Paris *et al.*, 2015; Sharda *et al.*, 2020).

NHEJ factors are involved in DSB repair depending on the complexity of the damage. In consequence, more complex DSBs will require a larger subset of NHEJ proteins than simpler DSBs (Reynolds *et al.*, 2012). However, if a DSB is going to be repaired by NHEJ, this is consistently recognized by the ring-shaped Ku heterodimer formed by the Ku70 and Ku80 proteins (Frit *et al.*, 2019; Walker *et al.*, 2001). Ku possesses a high affinity for DNA ends and is highly abundant in the nucleus, which may explain why Ku70/80 recruitment on DSBs does not require the presence of any other NHEJ factors and starts within seconds after DNA damage induction (Blier *et al.*, 1993; Mari *et al.*, 2006; Walker *et al.*, 2001; Zahid *et al.*, 2021). The Ku binding to the broken ends inhibits other DSB repair mechanisms, such as HR and A-EJ by blocking associated resection to MRN and CtIP (Chang *et al.*, 2017; Chanut *et al.*, 2016). Ku recruits a broad range of proteins, such as the DNA-dependent protein kinase catalytic subunit (DNA-PKcs) to form the DNA-PK holoenzyme (Gao *et al.*, 1998a; Gell & Jackson, 1999; Sharif *et al.*, 2017), and NHEJ factors containing motifs called Ku-binding motifs (KBMs) (Grundy *et al.*, 2013; Shirodkar *et al.*, 2013), e.g., XRCC4-like factor (XLF) (Ahnesorg *et al.*, 2006b; Buck *et al.*, 2006a; Grundy *et al.*, 2016; Li *et al.*, 2008; Yano *et al.*, 2008; Zha *et al.*, 2007), paralog of XRCC4 and XLF (PAXX) (Grundy *et al.*, 2016; Ochi *et al.*, 2015; Xing *et al.*, 2015) and modulator of retrovirus infection (MRI, or CYREN) (Grundy *et al.*, 2016; Slavoff *et al.*, 2014) either directly or indirectly (Frit *et al.*, 2019).

Different models have been proposed to explain how the two free DNA ends are brought back together through synapsis. For instance, Lieber's group proposed a model (Zhao *et al.*, 2019) based on the NHEJ factors conserved in all eukaryotes; it includes Ku70, Ku80, XLF, XRCC4, and LIG4 (Sharda *et al.*, 2020; Zhao *et al.*, 2019). This model suggests that two sequential complexes, flexible synaptic (FSP) and close synapsis (CSP), are formed during the NHEJ synapsis. Ku70, Ku80, XRCC4, and LIG4 form the FSP, while XLF and PAXX promote the transition from FSP to CSP to increase the stability of the synaptic complex. Nevertheless, XLF stabilizes CSP to a greater extent compared to PAXX. In the mentioned model, DNA-PKcs is not required to form either FS or CS (Castaneda-Zegarra *et al.*, 2020a; Zhao *et al.*,

2019). Unlike the first model, Loparo's group (Graham *et al.*, 2016) suggested a two-stage model that includes DNA-PKcs. Based on this model, the holoenzyme formed by Ku70, Ku80, and DNA-PKcs forms a long-range complex. Subsequently, a second stage called short-range complex is formed by the previous DNA-PK holoenzyme and the NHEJ factors, XLF, LIG4 and XRCC4, to bring together the distant DNA ends and contribute to the DNA ligation (Castaneda-Zegarra *et al.*, 2020a; Graham *et al.*, 2016). Both models do not include MRI participation because its functions have not been well identified. Although, during the last years, it has been evidenced that MRI is an adaptor for DDR factors, promoting NHEJ during G1 phase cell, and is required to mediate NHEJ in XLF-deficient lymphocytes (Castaneda-Zegarra *et al.*, 2020b; Hung *et al.*, 2018). Moreover, the association of MRI with DNA-PKcs, XLF, PAXX, and XRCC4 is dependent of the association of Ku with the N-terminus of MRI (Hung *et al.*, 2018).

A simplified model is presented based on three main phases: DSB recognition, stabilization-processing, and end ligation. During the first stage, Ku recognizes and binds DSBs ends, followed by DNA-PKcs recruitment to form the DNA-PK holoenzyme to activate the kinase activity of DNA-PKcs. Auto-phosphorylated DNA-PK provides a platform to recruit and activate downstream components, for example, Artemis endonuclease, to open the DNA hairpin structure (Jiang *et al.*, 2015; Ma *et al.*, 2002; Rooney *et al.*, 2002; Wang *et al.*, 2020b). Subsequently, the NHEJ complex is stabilized and processed by PAXX (Abramowski *et al.*, 2018; Balmus *et al.*, 2016; Gago-Fuentes *et al.*, 2018; Xing *et al.*, 2015), MRI (Castaneda-Zegarra *et al.*, 2019a; Hung *et al.*, 2018) and XLF (Li *et al.*, 2008; Vera *et al.*, 2013). Furthermore, XLF physically interacts with the components of the NHEJ ligation complex, XRCC4 and LIG4, as illustrated in Figure 9 (Ahnesorg *et al.*, 2006a; Buck *et al.*, 2006a; Gu *et al.*, 2007; Kumar *et al.*, 2014; Tsai *et al.*, 2007).

Furthermore, other factors are also involved in NHEJ throughout the interaction with Ku via KBM. For example, nuclease aprataxin and PNK-like factor (APLF) endonuclease is recruited to perform scaffold functions and binds XRCC4 to promote recruitment and/or retention of XRCC4-LIG4 and XLF, stabilizing the DNA end ligation (Grundy *et al.*, 2013; Shirodkar *et al.*, 2013). DNA polymerases of the Pol X family (μ , λ , and TdT) are involved in NHEJ in humans through interaction with Ku through their N-terminal BRCA1 C terminus (BRCT) domain, which contains KBM (Bebenek *et al.*, 2014; Lieber, 2006; Ma *et al.*, 2004; Moon *et al.*, 2014). However, the terminal deoxynucleotidyl transferase (TdT) is only expressed in early B lymphocytes and T lymphocytes during V(D)J recombination (further details are introduced in 1.5.1.1 section) (Desiderio *et al.*, 1984; Komori *et al.*, 1993; Lieber, 2006).

Additionally, the Werner syndrome helicase protein (WRN) interacts directly with Ku80 (Li & Comai, 2000) and is phosphorylated by DNA-PK to regulate its catalytic activities (Karmakar *et al*, 2002).

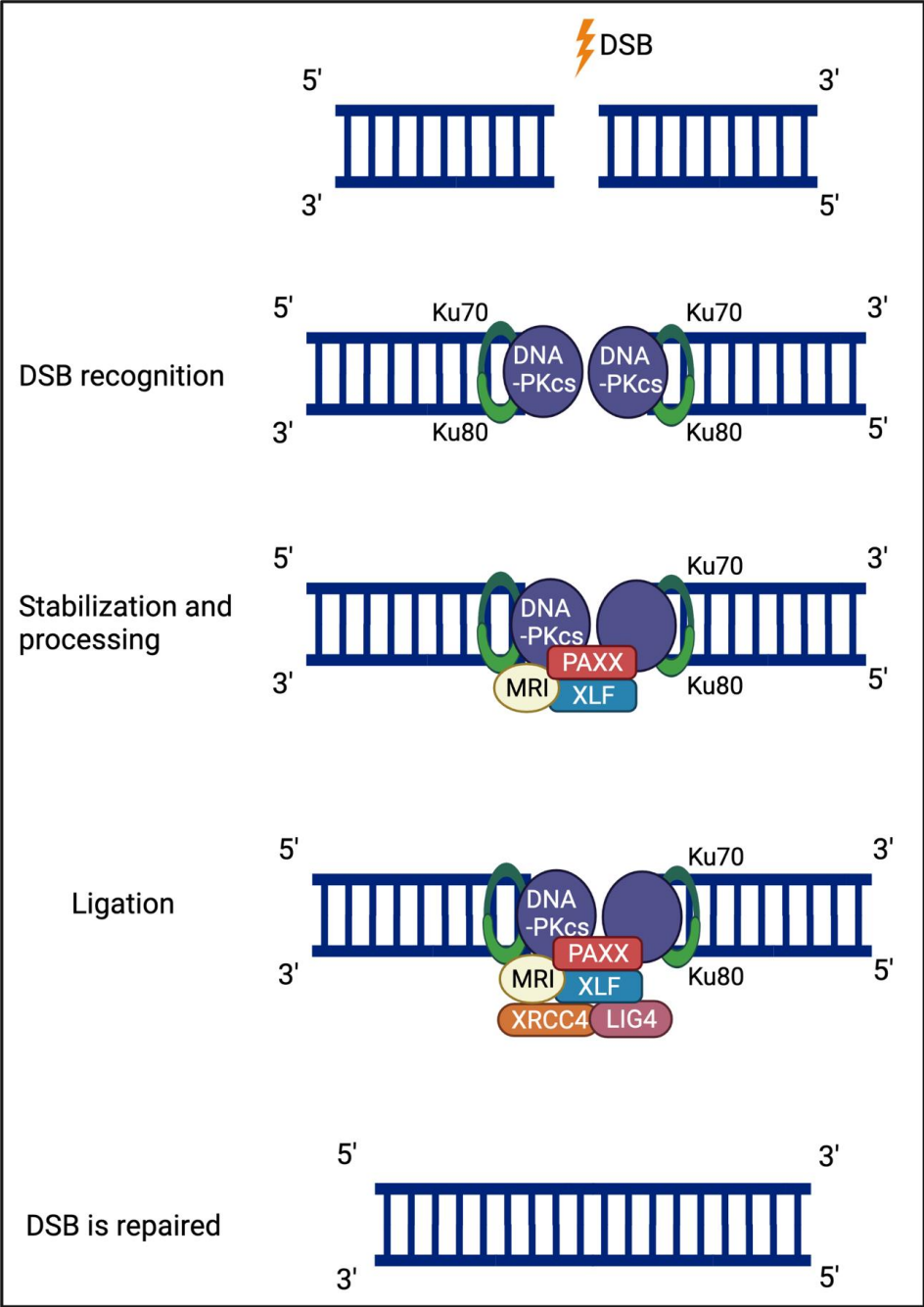


Figure 9. Schematic illustration of NHEJ in humans. DSBs induced either by exogenous or endogenous sources are actively repaired by NHEJ during the whole cell cycle. NHEJ starts with recognition of the DNA ends by the Ku (Ku70 and Ku80) heterodimer, which recruits DNA-PKcs to form the DNA-PK holoenzyme. Subsequently, different NHEJ factors, including MRI, PAXX, XLF, XRCC4, and LIG4 are recruited and activated to stabilize, process, and ligate the DNA ends. DSB, double-strand break; NHEJ, Non-homologous end-joining. This Figure was made in BioRender platform.

1.5 LYMPHOCYTE DEVELOPMENT AND NHEJ

Depending on the specificity and speed of the required reaction, the immune system activates two types of responses, innate and adaptive responses. The innate immune system provides immediate host defense and is highly conserved evolutionarily, while the adaptive immune system is characterized to be present in vertebrates (Yatim & Lakkis, 2015). Particularly, the adaptive immunity is composed of highly specific responses to pathogens, providing additional long-term protection where B and T lymphocytes carry out the main activities (Boehm & Swann, 2014; Cooper & Alder, 2006; Flajnik & Kasahara, 2010). On the one side, B cells can differentiate into plasma cells to produce antibodies or act as antigen-presenting cells (APCs). On the other side, T cells play a central role in cell-mediated immunity by recognizing diverse antigens from APCs with antigen specificity (Marshall *et al*, 2018). Different lymphoid organs are involved in the process of development and maturation of B and T cells. Moreover, lymphoid organs can be divided into two groups, primary and secondary. Primary lymphoid organs, also called central lymphoid organs, are sites where lymphocytes are generated; they include the bone marrow and thymus. While secondary lymphoid organs, also termed peripheral lymphoid organs, are responsible sites for promoting adaptive immune responses and maintaining lymphocytes; they include the spleen, lymph nodes, tonsils, and mucous membranes, such as the bowel (Cruse *et al*, 2004; Kindt *et al*, 2007). Lymphocyte development of B and T cells is introduced in section 1.5.1.1.

DSBs are generated both in developing B and T lymphocytes and in mature B lymphocytes. At the early stages of B and T lymphocyte development, NHEJ is required to repair DSBs during V(D)J recombination, where immature B and T lymphocytes undergo antigen receptor gene rearrangements to increase the repertoire of B and T cell receptors. While, in mature B cells, NHEJ and A-EJ participate in a mechanism called class switch recombination (CSR), when constant regions of immunoglobulins switch from IgM to IgG, IgA, or IgE, playing a crucial role in the immune response through their effector functions. Thus, NHEJ is important for V(D)J recombination and CSR (Castaneda-Zegarra *et al.*, 2020a; Kumar *et al.*, 2014; Wang *et al.*, 2020b).

1.5.1 V(D)J recombination

V(D)J recombination is a physiological process required for developing B and T cell lymphocytes, where the *variable (V)*, *diversity (D)*, and *joining (J)* gene segments are assembled to form *V(D)J* exons that encode part of the B cell receptor (BCR) or T cell receptor (TCR) proteins that provide antigen-binding specificity (Castaneda-Zegarra *et al.*, 2020a;

Kumar *et al.*, 2014; Wang *et al.*, 2020b). The BCR is composed of two heavy immunoglobulin chains (IgH) and two immunoglobulin light chains (IgL), Igk or Igl, whereas a TCR is composed of TCR β and α or γ and δ proteins. The BCR development includes the rearrangement of the *V*, *D*, and *J* gene segments in the IgH chain locus and the *V* and *J* gene segments in the light chains loci. In contrast, a TCR is generated by rearrangement of the *V*, *D*, and *J* gene segments from β and δ receptor chains, while α and γ receptor chains are constituted of *V* and *J* gene variable segments (Jackson *et al.*, 2013; Wang *et al.*, 2020b).

V(D)J recombination is initiated by recruitment of a lymphoid-specific protein complex called recombination-activating gene (RAG) recombinase formed by RAG1 and RAG2. RAG recognizes and binds to short DNA elements termed recombination signal sequences (RSSs) flanking the *V*, *D*, and *J* gene segments. The RSSs are composed of three elements; a conserved heptamer (CACAGTG), a spacer region of 12 or 23 base pairs, and a conserved nonamer sequence (ACAAAACC) (Lescale & Deriano, 2017; Oettinger *et al.*, 1990; Zhang *et al.*, 2019b). A synapsis of a pair of RSSs takes place due to the recruitment of a second RSS by the RAG complex, where the RAG proteins cleave the 12RSS from the 23RSS during the cleavage phase introducing DSBs between the gene segments and the RSSs. Moreover, RSS cleavage by RAG generates two blunt 5' phosphorylated signal ends (SEs) and two covalently sealed coding ends (CEs), resulting in covalently sealed DNA hairpin structures (McBlane *et al.*, 1995). After cleavage, the SEs remained bound by RAG in a signal end complex (SEC), which after ligation forms a signal joint (SJ), and the two CEs are released to further processing by forming a coding joint (CJ). Prior to the formation of SJs and CJs, the NHEJ machinery recognizes the RAG-generated breaks, triggering the recruitment and access of NHEJ DNA repair factors in order to perform the end-processing and repair, followed by ligation, as illustrated in Figure 10 (Kumar *et al.*, 2014; Lescale & Deriano, 2017; Schatz & Swanson, 2011; Wang *et al.*, 2020b). RAG2 protein expression declines by at least 20-fold during the mitosis (M), G2, or S phases of the cell cycle compared to the G1 phase in precursors of both B and T lymphocytes (Lin & Desiderio, 1994). Furthermore, the RAG2 subunit is degraded outside the G1 phase by the Skp2-SCF ubiquitin ligase, which contributes to V(D)J restriction to the G1 phase (Desiderio, 2010; Jiang *et al.*, 2005).

In addition, other factors also participate in the V(D)J recombination. For instance, Artemis endonuclease cleaves the CE hairpins, promoting the CEs to be ligated to form a CJ. Moreover, palindromic insertions (P nucleotides) are added by polymerases of the PolX family (μ and λ) because Artemis cleavage often produces one long DNA strand and one short DNA strand (Bertocci *et al.*, 2003; Bertocci *et al.*, 2006; Malu *et al.*, 2012). Subsequently, the TdT

enzyme adds non-templated nucleotides to the V(D)J junctions in order to increase the diversity of the variable region exons (Desiderio *et al.*, 1984; Komori *et al.*, 1993; Ma *et al.*, 2002; Wang *et al.*, 2020b). Furthermore, WRN helicase also participates in V(D)J recombination through DSB processing during NHEJ prior gap filling and DNA ligation (Grundy *et al.*, 2016).

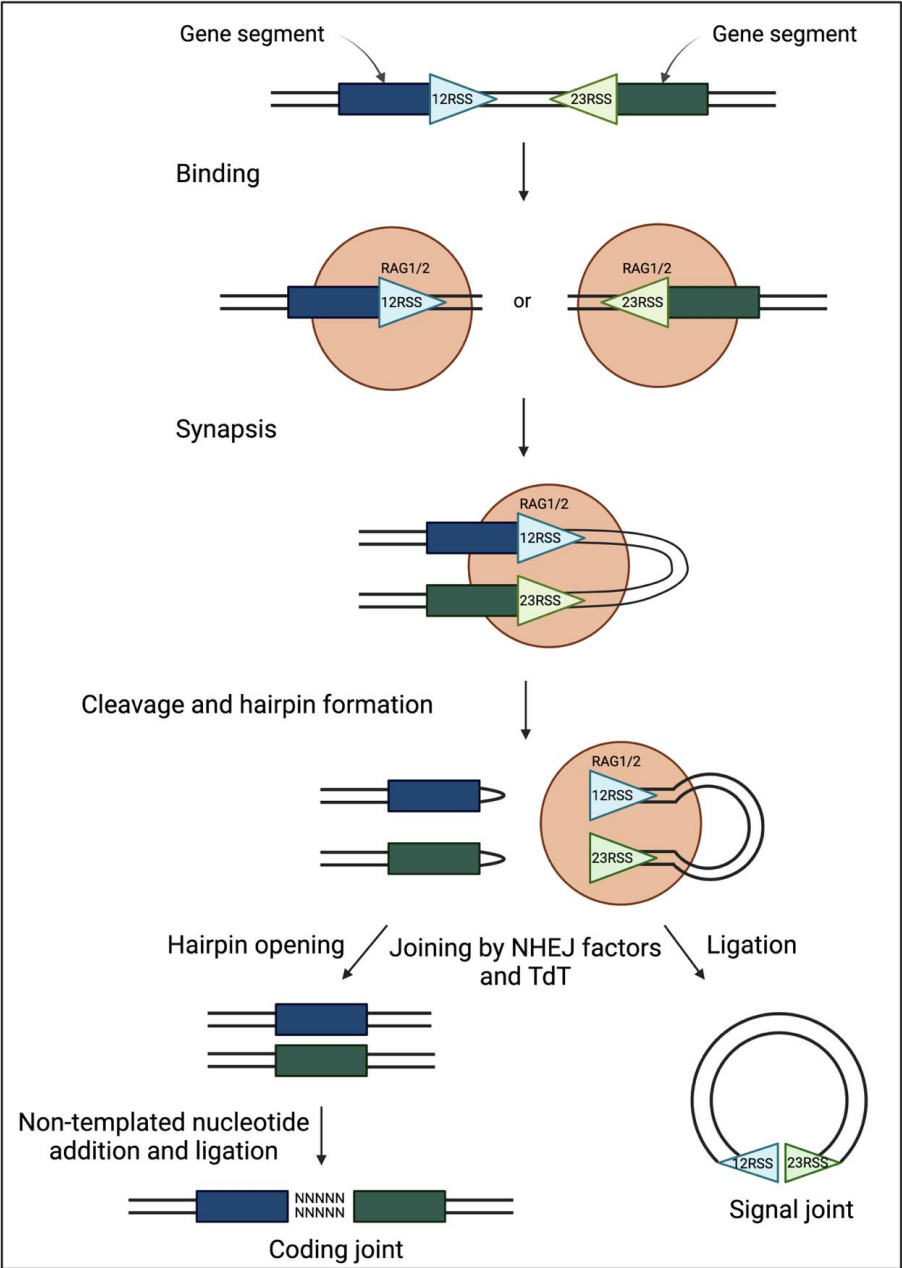


Figure 10. Schematic illustration of V(D)J recombination. Either 12RSS or a 23RSS flanks antigen receptor gene segments. Then, the RAG complex formed by RAG1 and RAG2 binds

either a 12RSS or a 23RSS. Subsequently, a synapsis process occurs due to the recruitment of a second RSS, where the RAG complex introduces DSBs between the gene segments and the RSSs, generating hairpin-sealed coding ends and blunt signal ends. The NHEJ pathway recognizes, processes, and repairs both the coding and signal ends. On the one hand, coding ends are imprecisely repaired through non-templated nucleotide addition by TdT to increase diversity to form the coding joint. On the other hand, RSS ends are commonly ligated without processing to form the signal joint. DSB, double-strand break; RAG, recombination-activating gene; RSS, recombination signal sequence; TdT, terminal deoxynucleotidyl transferase. This Figure was made in BioRender platform.

1.5.1.1 V(D)J recombination associated to B and T cell development

Susumu Tonegawa was awarded the Nobel Prize in Physiology or Medicine in 1987 "for his discovery of the genetic principle for generation of antibody diversity in B cells". B cell development begins in the fetal liver and continues after birth in the bone marrow in both humans and mice. This process involves the development of a diverse repertoire of functional VJ_H and VJ_L gene rearrangements encoding the BCR, which is essential for B cell survival, B cell development, and antibody production (Brack *et al*, 1978; Liu *et al*, 2020a; Wang *et al*, 2020c). The BCR formation occurs in three major stages during the B cell development: the progenitor B cell (pro-B), precursor B cell (pre-B), and immature B cell. In addition to the V(D)J recombination of the Ig loci, B cell development depending on their stage, pro-B cells, pre-B cells, and immature B cells, may express high, medium, or low levels of co-receptors, such as CD19, CD43, and CD45 (B220) (Mak *et al*, 2014a). For instance, CD19, a transmembrane glycoprotein, is a co-receptor expressed in almost all B cell stages except for the differentiated plasma B cells (Wang *et al*, 2012).

In the bone marrow, initial DNA rearrangement at the IgH locus (D_H to J_H) takes place at the pre-pro B cell stage, followed by rearrangement of V_H to D_HJ_H gene segments in late pro-B cells (Lescale & Deriano, 2016; Mak *et al.*, 2014a; Patton *et al*, 2014). Successful $V_H-D_H-J_H$ rearrangement leads to the expression of μ heavy chain (Ig μ). During the pre-B cell stage, cells downregulate CD43 and Ig μ assemblages with the surrogate light chain, formed by the $\lambda 5$ and VpreB proteins, and the signaling molecules Ig α and Ig β to form a pre-BCR. The pre-BCR stimulates the expansion of large pre-B cells. In addition, although a pre-BCR is not an Ig, and it cannot recognize antigens, it can bind to ligands on bone marrow stromal cells and sends them an intracellular signal indicating that a functional H chain has been synthesized in the cell (Lescale & Deriano, 2016; Mak *et al.*, 2014a; Patton *et al.*, 2014). The last rearrangement occurs in small pre-B cells, in the VL and JL segments on either $IgL\kappa$ or $IgL\lambda$ locus, which are no longer dividing, unlike large pre-B cells. It results in the expression of the κ or λ light chain,

which joins with Ig μ to generate a functional IgM protein and BCR signaling on immature B cells, as illustrated in Figure 11 (Lescale & Deriano, 2016; Wang *et al.*, 2020c).

Upon completing the BCR process, immature B cells are screened for central tolerance. Herein, immature B cells that recognize self-antigens with high avidity undergo apoptosis by negative selection. In the absence of self-antigen recognition, BCR-expressing cells are prone to positive selection and survival (Mak *et al.*, 2014a; Monroe *et al.*, 2003). In order to mature, immature B cells migrate to the spleen and express IgD (Noviski *et al.*, 2018). Subsequently, mature B cells, also known as naïve B cells, are activated by interaction with antigens (Ag) in secondary lymphoid tissue (Mak *et al.*, 2014a). In addition, CSR leads to changes in the H chains, for instance, from IgM to IgA, IgE, or IgG, giving rise to different effector functions depending on the recognized Ag (CSR is introduced in section 1.5.2).

Common lymphoid progenitors (CLPs) differentiate into B and T lymphocytes, but lymphoid-primed multipotent progenitors (LMPPs) develop into T lymphocytes more efficiently than CLPs (Ghaedi *et al.*, 2016). T cells undergo a developmental process to mature and express the TCR, and unlike B cells, T lymphocytes undergo most of their development in the thymus. Approximately 95% of the T cells in the thymus give rise to $\alpha\beta$ T cells; however, approximately 5% will express the TCR $\gamma\delta$ (Kragel, 2009; Lescale & Deriano, 2016).

T-cell precursors migrate from the bone marrow to the thymus. The earliest intrathymic T cell progenitors are termed early thymic progenitors (ETPs) or double-negative (DN) 1 cells. DN cells lack expression of the co-receptors CD4 and CD8 and can be sub-divided into four subsets (DN1-4) and are identified according to the expression of receptors, such as c-kit, CD44, and CD25 (Bhandoola *et al.*, 2007; Yui *et al.*, 2010). TCR β rearrangement takes place in DN2 and DN3 cells. Initially, the *D* and *J* gene segments from the β chain locus are rearranged in DN2 cells, followed by V_{β} - D_{β} J_{β} rearrangement in DN3 cells in order to express a functional TCR β chain. DN3 cells undergo a process called β -selection, where the β chain pairs with the surrogate chain, pre-T α , and CD3 components, producing a pre-TCR, analogous to the pre-BCR structure in pre-B cells. When β -chain rearrangement is successful, cells proliferate and continue their differentiation into DN4; in the opposite case, cells that do not endure β -selection die by apoptosis (Liu *et al.*, 2021; Mak *et al.*, 2014b). DN4 cells downregulate their expression of RAG and induce the expression of low levels of both CD4 and CD8 to become double-positive (DP) T cells. Upon entering the DP stage, V(D)J recombination and RAG expression are intensified, followed by rearrangements in the V_{α} and J_{α} gene segments in the α chain locus to form TCR $\alpha\beta$ (Mak *et al.*, 2014b; Wilson *et al.*, 1994; Yannoutsos *et al.*, 2001). DP T cells mature into single-positive (SP) cells, CD4⁺ (T helper) or CD8⁺ (T cytotoxic), as illustrated

in Figure 11, depending on the complex intracellular signaling pathways and the class of major histocompatibility complex (MHC) that is involved in the positive selection of the DP T cells. T helper cells activate B cells while T cytotoxic cells lyse infected target cells among the SP cell functions. Upon proliferation, SP cells migrate from the thymus to secondary lymphoid organs, ready to interact with specific antigens (Farhood *et al*, 2019; Zhu, 2018).

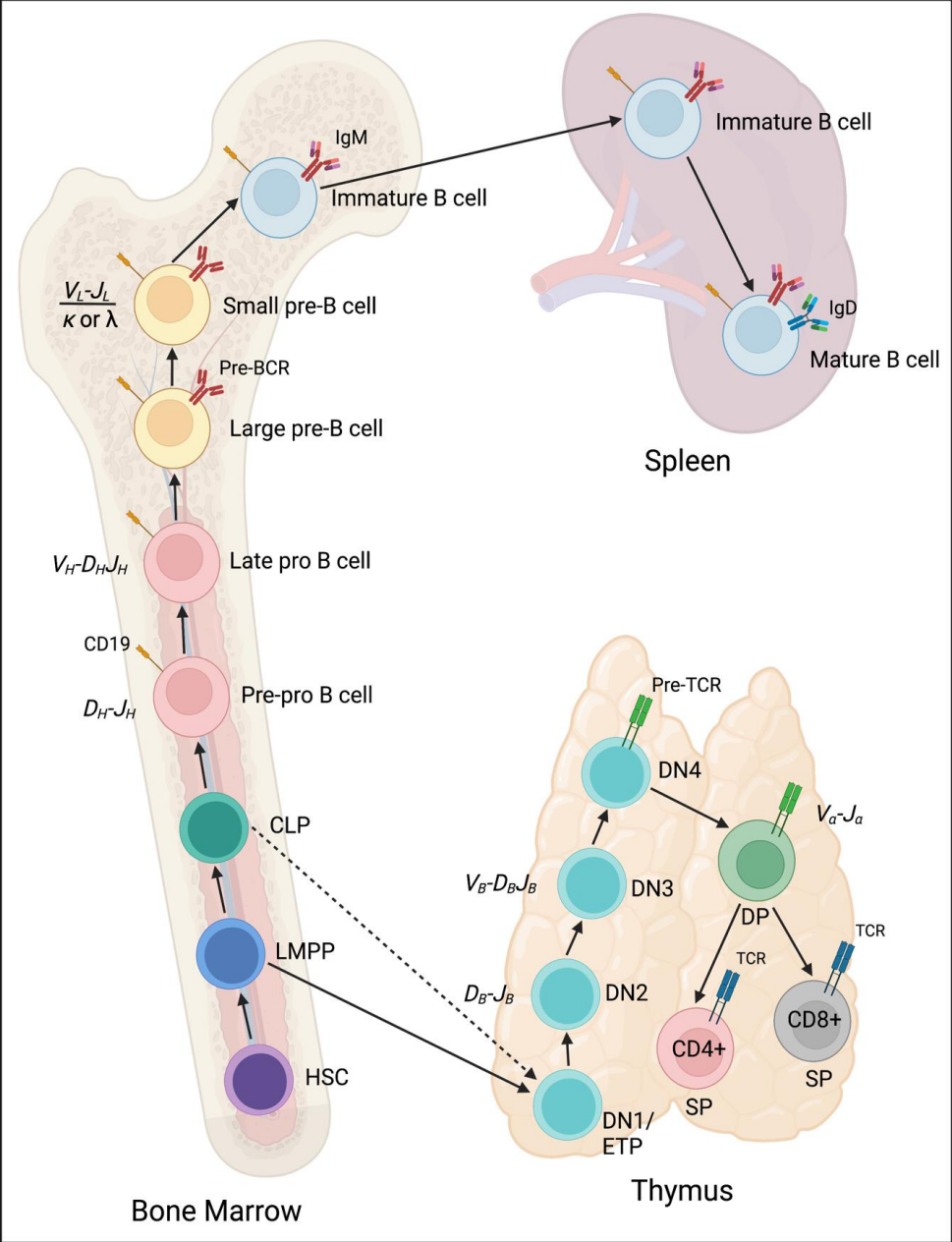


Figure 11. Schematic illustration of B and T cell development. On the one side, rearrangements of the *D* and *J* gene segments in the IgH locus occur in pre-pro B cells, followed by *V_H* segment rearrangement in late pro-B cells forming the pre-BCR on large pre-B cells. The *V_L* and *J_L* gene segments (κ or λ) are rearranged in small pre-B cells producing a functional IgM on immature B cells. Immature B cells migrate from bone marrow to the spleen to complete the maturation and express IgD. CD19 is a co-receptor expressed from late pro-B cells. On the other side, lymphoid progenitor cells travel from the bone marrow to the thymus to develop into mature T cells. Early committed T cells termed DN cells lack the expression of TCR $\alpha\beta$, CD4, and CD8. The TCR β is rearranged at the DN2 and DN3 stages. DN4 cells express the pre-TCR composed of the rearranged TCR β -chain and the surrogate chain pre-T α . Subsequently, *V α* and *J α* gene rearrangement takes place in DP cells and replacement of the pre-TCR α chain with a newly rearranged TCR α chain produces the TCR $\alpha\beta$. DP cells undergo differentiation and mature to SP cells, either CD4⁺ helper or CD8⁺ cytotoxic cells. CLP, common lymphoid progenitors; DN, double-negative T cell; DP, double-positive T cell; ETP, early thymic progenitor; HSC, hematopoietic stem cell; LMPP, lymphoid primed progenitor; Pre-B, precursor B cell; Pro-B, progenitor B cell; SP, single-positive T cell; TCR, T cell receptor. This Figure was made in BioRender platform.

1.5.2 Class switch recombination (CSR)

CSR occurs in mature B cells upon antigen stimulation, when constant regions of immunoglobulins switch from IgM to IgG, IgA or IgE, eliciting a new effector function (Castaneda-Zegarra *et al.*, 2020a; Shang & Meng, 2021; Wang *et al.*, 2020b; Xu *et al.*, 2012). Although CSR also produces IgD, it is a rare event restricted to a few B-cell subsets in specific lymphoid tissues in both mice and humans, with an unclear regulatory mechanism (Issaoui *et al.*, 2017). However, it has been evidenced that IgD CSR is independent of the presence of the 3'RR super-enhancer, which is required for conventional IgG, IgA, and IgE CSR (Rouaud *et al.*, 2014). Moreover, IgD CSR depicts junctions with micro-homology or insertions, unlike conventional CSR, showing that alternative pathways to repair DSB might have a role in this process, such as A-EJ and SSA (Xu *et al.*, 2021).

According to its decreasing abundance, IgG is divided into four subclasses (IgG1, IgG2, IgG3, and IgG4) in humans. For instance, IgG1 and IgG3 possess effector functions against viruses, while IgG2 responds against encapsulated bacteria and IgG4 against extracellular parasites (Vidarsson *et al.*, 2014; Xu *et al.*, 2012). Whereas IgA carries out responses against pathogenic bacteria and protection to mucosal surfaces (de Sousa-Pereira & Woof, 2019), while IgE possesses similar actions to IgG4 and is associated with allergies (Sutton *et al.*, 2019; Xu *et al.*, 2012).

The constant regions in the immunoglobulin heavy chain locus (*C_H*) encode a variety of immunoglobulin isotypes. In mice, *C_H* are ordered as C μ , C δ , C γ , C ϵ , and C α , respectively. Through CSR, the initial exons expressed IgH constant region (C μ) from IgM are replaced with

one of several sets of constant regions, such as $C\gamma$, $C\epsilon$ or $C\alpha$, allowing the switch to the isotypes IgG, IgA or IgE, respectively (Kumar *et al.*, 2014; Shang & Meng, 2021; Xu *et al.*, 2012). The C_H gene locus in humans is located on chromosome 14, and not on chromosome 12, as in mice. The human C_H contains nine functional genes ($C\mu$ - $C\delta$ - $C\gamma_3$ - $C\gamma_1$ - $C\alpha_1$ - $C\gamma_2$ - $C\gamma_4$ - $C\epsilon$ - $C\alpha_2$), and two pseudogenes ($C\psi\epsilon$ and $C\psi\gamma$), as illustrated in Figure 12.



Figure 12. Schematic illustration of the human constant region gene locus. Coding regions are shown with filled boxes and pseudogenes are indicated with striped boxes. This Figure was made in BioRender platform.

Cytokines secreted by T cells, and other cells, activate transcription promoters located upstream of each acceptor switch (S) region that induce CSR to a specific isotype. Transcription from these promoters produces germline transcripts (GLTs), which are spliced to the first exon of the corresponding C_H gene prior to CSR. Transcription through S regions forms R-loops (RNA:DNA hybrid structures), involving the template strand of DNA and a free non-template ssDNA (Pan-Hammarström *et al.*, 2007; Stavnezer & Schrader, 2014). Moreover, histone modifications are observed throughout transcribed S regions, which serve as markers of active chromatin conformation at promoter-proximal sites like hyperacetylated H3K9 (Ac-H3K9) and trimethyl histone H3 lysine 4 (H3K4me3) to modulate chromatin accessibility to AID (Matthews *et al.*, 2014; Wang *et al.*, 2009). AID initiates CSR by binding firmly to ssDNA previously formed. AID enzyme deaminates C's to U's at repetitive S regions upstream of each set of C_H coding exons (Muramatsu *et al.*, 2000; Zhang *et al.*, 2019a). UNG recognizes and excises the U's, leaving an AP site. The AP sites are cut by APEs, leading to SSBs. A DSB is produced if SSBs are sufficiently close on both DNA strands, whereas if SSBs are too far apart on opposing DNA strands to produce a DSB, as well as the MMR factors can convert the SSB to a DSB (Chi *et al.*, 2020; Stavnezer & Schrader, 2014). DSBs located in a donor S region upstream of $C\mu$ ($S\mu$) and a downstream acceptor S region (e.g., $S\gamma$, $S\epsilon$, $S\alpha$) are repaired to complete CSR, generating a different Ig, as illustrated in Figure 13 (Kumar *et al.*, 2014; Shang & Meng, 2021; Xu *et al.*, 2012).

It is generally observed that the microhomology between the $S\mu$ and the acceptor S region is 0 or 1 bp, which is a signature of NHEJ. However, if cells are deficient in an NHEJ protein, e.g. Ku, DNA-PKcs, or LIG4, further increased lengths of microhomology are present at S-S junctions, and the A-EJ pathway repairs them (Boboila *et al.*, 2012; Saha *et al.*, 2021). For example, both LIG1 and LIG3 may catalyze A-EJ for CSR (Boboila *et al.*, 2012; Lu *et al.*,

2016). Nevertheless, A-EJ possesses less CSR efficiency and is required when NHEJ is impaired (Boboila *et al.*, 2012; Saha *et al.*, 2021). In addition, processing DSBs during CSR activates the ATM and ATR signal-transducing pathways (Menolfi & Zha, 2020; Pan-Hammarström *et al.*, 2007) and different components of the DDR, such as H2AX (Petersen *et al.*, 2001; Reina-San-Martin *et al.*, 2003), 53BP1 (Manis *et al.*, 2004; Ward *et al.*, 2004), and MDC1 (Lou *et al.*, 2006).

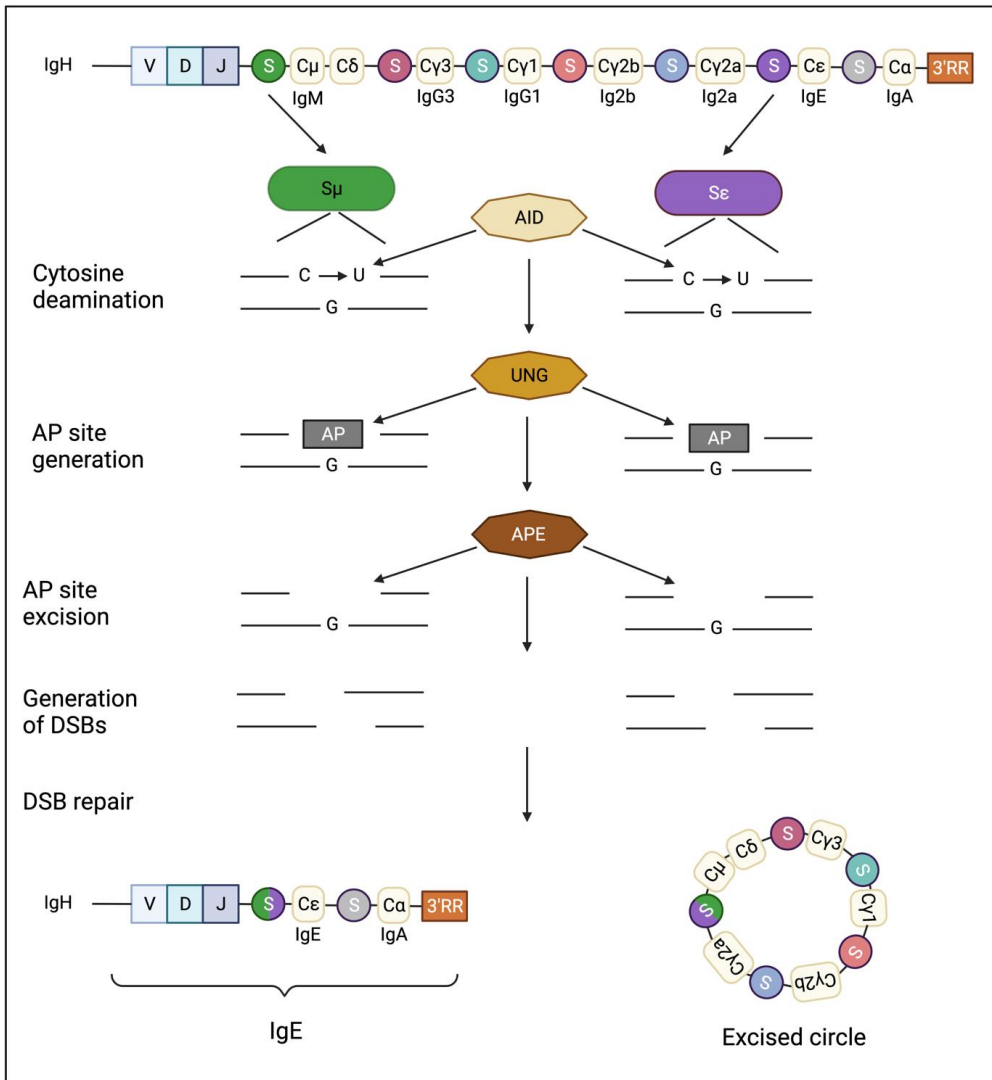


Figure 13. Schematic illustration of class switch recombination in mice. The figure depicts CSR between S μ and S ϵ in the immunoglobulin heavy chain (IgH) locus. The top line illustrates the mouse Ig heavy chain genes present in B cells expressing IgM. AID deaminates C within S μ and the downstream S region (S ϵ here) to initiate CSR. Then, UNG removes the U base from the DNA to generate an AP site, which is recognized and excised by APE, generating a

SSB. Relatively close nicks and gaps resolve into DSBs. Subsequently, NHEJ or A-EJ pathways repair DSBs to generate a recombined IgH locus and an excision circle. Consequently, in this example, the rearranged *VDJ* exon is transcribed together with a new constant region (C ϵ), which encodes for the switched isotype IgE. AID, activation-induced deaminase; AP, apurinic/aprimidinic; APE, AP endonuclease; A-EJ, alternative end-joining; C, cytosine; CSR, class switch recombination; DSB, double-strand break; NHEJ, non-homologous end-joining; SSB, single-strand break; U, uracil; UNG, uracil-DNA glycosylase. This Figure was made in BioRender platform.

1.5.3 Similarities between V(D)J and CSR processes

At the DNA level, V(D)J recombination is initiated by RAG (Libri *et al.*, 2022), while CSR is initiated by AID (Yu & Lieber, 2019). RAG-mediated cleavage is a “site specific” process rather than a “region specific” as CSR, as no consensus sequence has been identified at the junctions of recombined S regions. Nevertheless, both V(D)J recombination and CSR involve circular DNA excision, generation of DSBs during the switch reaction, participation of the NHEJ machinery, and some DDR factors, depending on each process (Chi *et al.*, 2020; Pan-Hammarström *et al.*, 2007).

On the one side, RAG proteins can be associated with a small region of highly active chromatin in each antigen receptor locus, forming a recombination center (RC) (Schatz & Ji, 2011). Furthermore, it has been shown that chromatin-based mechanisms may enhance the synapsis of functional cis-elements via loop extrusion (Zhang *et al.*, 2019b; Zhang *et al.*, 2022). On the other side, during CSR, the loop extrusion drives germline transcript promoter-enhancer contacts and juxtaposes a cohesin-loading site (e.g., 3' IgHRR) with upstream S μ to generate a CSR center (CSRC) (Shen *et al.*, 2021). When a synaptic S-region DSB reaches an associated cohesin ring, it stops extruding, aligning ends of the donor and acceptor DSBs (Zhang *et al.*, 2019a).

1.6 HUMAN DISEASES ASSOCIATED WITH DEFECTS IN DSB REPAIR

Patients with mutations in the genes associated with the NHEJ pathway and DDR display several clinical features, which might involve immunodeficiencies, SCID, radiosensitivity, and in many cases, neurological abnormalities (de Villartay, 2015; Morio, 2017; Wang *et al.*, 2020b). The updated information about NHEJ- and DDR-gene deficiency associated with syndromes is summarized in Table 1.

For instance, until 1999, only one patient with defective NHEJ was described (Riballo *et al.*, 1999). This patient had a missense mutation in the gene encoding *LIG4* that impairs the adenylation and ligation activities. The mentioned patient developed leukemia and radiosensitivity but surprisingly no immunodeficiency (Riballo *et al.*, 1999). However, a couple of years later, O'Driscoll *et al.* described four patients with *LIG4* mutations with biological consequences either in the ligase domain or impairment in the interaction between *LIG4* and *XRCC4*. The *LIG4*-deficient patients possessed immunodeficiency, developmental delay, and chromosomal instability; these clinical features were characterized as *LIG4* syndrome (O'Driscoll *et al.*, 2001). Later, several more *LIG4*-deficient patients were described by different scientific groups. For example, in 2006, Van Der Burg *et al.* described a *LIG4*-deficient patient with a severe block in the early B cell development and, consequently, shallow B lymphocytes level (van der Burg *et al.*, 2006). In the same year, Buck *et al.* described two siblings with *LIG4* deficiency, both patients possessed microcephaly and radiosensitive SCID (RS-SCID), represented by the remaining number of T cells and absence of B cells (Buck *et al.*, 2006b). Likewise, a patient with *LIG4* mutation showed characteristics similar to the Omenn syndrome (OS), which is characterized by SCID, erythrodermia, alopecia, lymphadenopathy, eosinophilia, and elevated serum IgE (Grunebaum *et al.*, 2008). Another *LIG4*-deficient patient showed dysembryoplastic neuroepithelial tumor (DNET), growth delay, and an inflammatory disorder similar to Behçet's disease (BD) (Taskiran *et al.*, 2019). Therefore, patients with different *LIG4* mutations might possess variable phenotypes among them a normal development with SCID or even developmental defects but with minor immunological deficiencies.

The first five patients with mutations in the *XLF/Cernunnos* gene were reported in 2006; they displayed radiosensitivity, growth retardation, microcephaly, and immunodeficiency characterized by a reduced number of B and T cells (Buck *et al.*, 2006a). Since that, several patients have been reported with *XLF* deficiency (Cipe *et al.*, 2014; Du *et al.*, 2012; Dutrannoy

et al, 2010; Recio *et al*, 2018; Sheikh *et al*, 2017). For instance, three siblings presenting null XLF deficiency showed combined immunodeficiency (CID), growth retardation, and microcephaly (Sheikh *et al.*, 2017). While in 2018, Recio *et al.* described two unrelated XLF-deficient patients with the same non-sense mutation showing a similar DNA repair defect but significant clinical and immunological differences (Recio *et al.*, 2018).

The first patient with mutations in the *DNA-PKCS/PRKDC* gene was reported in 2009. The mentioned patient possessed RS-SCID due to a missense mutation (L3062R), which did not affect the DNA-PKcs kinase but diminished the Artemis activation during the immunoglobulin gene coding joints (van der Burg *et al*, 2009). Furthermore, other DNA-PKcs-deficient patients have been reported, such as a DNA-PKcs-deficient patient who possessed SCID with severe reduction of B and T lymphocytes similar to *Dna-pkcs*^{-/-} mouse models (DNA-PKcs-deficient mouse models are introduced in section 1.7.1.1). However, this patient, in addition to the SCID phenotype and different from DNA-PKcs-deficient animal models, displayed severe growth failure, microcephaly, seizures, and impaired neurological function (Woodbine *et al*, 2013). Another two DNA-PKcs-deficient patients were described in 2015; one possessed diminished DNA-PKcs protein expression and kinase activity, while the second patient showed mutations in the *DNA-PKCS* gene without affecting the DNA-PKcs kinase activity but causing impairment during the Artemis activation. The first patient possessed more defects during CSR than the second patient, suggesting that DNA-PKcs by itself and/or its kinase activity have additional functions compared to Artemis functionality during CSR (Bjorkman *et al*, 2015). Mathieu *et al.* described two DNA-PKcs-deficient patients, where both of them showed deficiencies during V(D)J recombination and DNA DSB repair (Mathieu *et al*, 2015).

Unlike the other reported NHEJ-deficient patients, XRCC4-deficient patients did not display clinical immunodeficiency or V(D)J recombination deficiency. However, the mentioned patients showed a severe DSB repair impairment and marked neurological abnormalities, and progressive ataxia (Bee *et al*, 2015; Guo *et al*, 2015; Murray *et al*, 2015; Rosin *et al*, 2015).

Artemis, a protein involved in V(D)J recombination and often not essential in the NHEJ, plays a relevant role during the B and T cell development. Unlike NHEJ deficiencies, patients with *ARTEMIS/DCLRE1C* null mutations do not possess microcephaly and have no overt developmental abnormalities but they do possess a severe RS-SCID phenotype with a marked and total B and T cells deficiency (Ijspeert *et al*, 2011; O'Driscoll *et al*, 2004; Pannicke *et al*, 2010).

RAG1/2-deficient patients display a broad clinical spectrum that includes SCID, OS or even milder phenotypes (Villa *et al*, 2001). For example, a patient with a hypomorphic RAG1 mutation and around half of the wild-type (WT) protein functionality displayed immunodeficiency, B cell lymphoma and autoimmune neutropenia (Abolhassani *et al*, 2014).

One of the most known diseases caused by a DDR disorder is the Ataxia–telangiectasia syndrome (A–T). A–T is an autosomal recessive disease caused by mutations in the ATM gene (Savitsky *et al*, 1995). ATM-deficient cells do not stop their cell cycle during DNA DSB repair caused by ionizing radiation and V(D)J recombination. ATM-deficient patients are characterized by loss of coordination due to cerebellar ataxia, prominent blood vessels or also known as telangiectasia, radiosensitivity, neurodegeneration, and genomic instability. Immunologically, the mentioned patients possess severe lymphocytopenia both in B and T cells and reduced Ig levels (Nowak-Wegrzyn *et al*, 2004).

Nijmegen breakage syndrome (NBS) is another human disease associated with defects in the DDR. This genetic disorder is caused by mutations in the *NBS1/NBN* gene that encodes the NBS1 protein. NBS1 is a subunit of the MRN complex together with MRE11 and RAD50 (Tauchi *et al*, 2002). In 1981, Weemaes *et al*. described the first two patients with NBS deficiency. Both patients showed microcephaly, growth retardation, radiosensitivity, spontaneous chromosomal instability, B and T immunodeficiency and diminished IgG and IgA levels similar to A–T patients (Weemaes *et al*, 1981). However, NBS-deficient patients display neither telangiectasia nor cerebellar ataxia compared to A–T patients (Tauchi *et al.*, 2002).

Continuing with the diseases associated with the MRN complex, *MRE11*-deficient patients possess ataxia telangiectasia like disorder (ATLD), ocular apraxia, cerebellar atrophy, but without telangiectasia (Taylor *et al*, 2004; Uchisaka *et al*, 2009). For instance, in 2009, two siblings were characterized with mutations in the gene that encodes the MRE11 protein. Both patients displayed ATLD, lung adenocarcinoma, mental retardation, and ataxia (Uchisaka *et al.*, 2009). At the same time, a RAD50-deficient patient displayed microcephaly, mental retardation, and growth delay. The mentioned patient did not show immunological abnormalities, including average lymphocyte counts and immunoglobulin levels (Walters *et al*, 2009).

Another human disease associated with DDR deficiency is the RIDDLE syndrome (termed like that due to the clinical features of these patients; radiosensitivity, immunodeficiency, dysmorphic features, and learning difficulties) (Stewart *et al*, 2007). RIDDLE patients possess *RNF168* mutations, and their cells show impairment to recruit 53BP1

while other DDR factors, such as MDC1 and NBS1 remain unaffected during the DNA DSB repair (Stewart *et al*, 2009).

For several NHEJ and DDR factor genes, no syndrome is associated yet (e.g., Ku70, Ku80, PAXX, MRI, MDC1, and H2AX). One can suggest several reasons for this. For instance, on the one side, phenotypes from some mutated genes might be identified only by analyzing embryonic samples due to their essentiality in human cells. On the other side, due to their lack of clinical relevance, no harmful phenotype might not be reported in some mutated genes.

Table 1. Syndromes associated with NHEJ- and DDR-factors deficiency. Clinical features and associated-mutated genes data were obtained on the Orphanet (the portal for rare diseases and orphan drugs) and OMIM (Online Mendelian Inheritance in Man) websites. Prevalence data were obtained on Orphanet website.

Syndrome	Clinical features	Associated-mutated genes and prevalence
Severe combined immunodeficiency (SCID)	* Lack of functional T cells, associated with abnormal development of B and natural killer (NK) lymphocytes. In addition, early-onset severe respiratory infections, absent antibody response, and failure to thrive.	* Associated to several mutations. * Prevalence: <1/50 000
Radiosensitive severe combined immunodeficiency (RS-SCID)	* Complete absence of T and B lymphocytes, associated with increased cell sensitivity to ionizing radiation.	* A mutation in the <i>ARTESMIS/DCLRE1C</i> gene causes most common form of RS-SCID. * Prevalence: <1/500 000
Combined immunodeficiency (CID)	* Less severe form when compared to SCID. Defective development and/or functionality of T cells, high risk of infections. Infection-related mortality in the first year of life is uncommon compared to SCID patients.	* Associated to several mutations. * Prevalence: 1-20/100 000
LIG4 syndrome	* Pancytopenia (low amounts of red blood cells, white blood cells, and platelets), microcephaly, growth and developmental delay, skin anomalies, and unusual facial features.	* LIG4 deficiency * Prevalence: <1/1 000 000
Omenn syndrome (OS)	* Inflammatory condition associated with SCIDs, erythroderma, alopecia, failure to thrive, lymphadenopathy, desquamation, and chronic diarrhea.	* OS is not caused by a specific genetic defect. Most of the NHEJ- or DDR-associated patients possess hypomorphic mutations in <i>RAG1</i> , <i>RAG2</i> , <i>DCLRE1C</i> , and <i>LIG4</i> genes. * Prevalence: <1/1 000 000
Ataxia–telangiectasia	* SCID (mainly in B cells), progressive cerebellar ataxia, telangiectasia,	* ATM deficiency * Prevalence: 1-9/1 000 000

syndrome (A–T or AT)	increased susceptibility to infections, and cancer.	
Nijmegen breakage syndrome (NBS)	* Microcephaly, mild growth retardation, immune deficiency with recurrent respiratory tract infections, radiosensitivity, chromosomal instability, mild skeletal anomalies, and premature ovarian insufficiency in females.	* NBS1 deficiency * Prevalence: <1/1 000 000
Ataxia telangiectasia like disorder (ATLD)	* Oculomotor apraxia, slowly progressive cerebellar degeneration resulting in ataxia, increased frequency of spontaneous chromosomal aberrations, and hypersensitivity to ionizing radiation.	* MRE11 deficiency * Prevalence: Unknown
Radiosensitivity, immunodeficiency, dysmorphic features, and learning difficulties (RIDDLE)	* Increased radiosensitivity, CSR impairment, dysmorphic features, and learning difficulties.	* RNF168 deficiency * Prevalence: <1/1 000 000

1.7 GENETIC INTERACTION OF DNA DSB REPAIR FACTORS DURING LYMPHOCYTE DEVELOPMENT

Since mice and humans have numerous genetic and physiological similarities, mice are commonly used in medical research as models to study human biology (Perlman, 2016). For instance, Bosma et al. described an inbred strain of immunodeficient mice with SCID before transgenic mice became popular (Bosma *et al.*, 1983). Some years later, Araki et al. identified that the gene responsible to produce the lack of mature B and T lymphocytes as a result of impaired V(D)J recombination in the SCID mice reported by Bosma was a recessive mutation in the *Dna-pkcs* gene that resulted in the substitution of termination codon for the Tyr-4046 (Araki *et al.*, 1997). Since then, several mouse models have been developed to understand and explain the deficiency of DSB repair in mice with single and multiple mutated genes.

1.7.1 Single NHEJ factor-deficient mouse models

Several NHEJ-deficient mouse models have been developed and described, as summarized in Table 2. Furthermore, the different NHEJ-deficient mouse models are described below.

- The Ku heterodimer composed of 70 (Ku70) and 86 kDa (Ku80) subunits is essential for the V(D)J recombination attributable to its central role at the initial DNA end binding in NHEJ. In 1996, two independent groups reported that *Ku80*^{-/-} mice have growth retardation and lymphocyte development arrest at early progenitor stages. The latter is due to V(D)J recombination impairment and a reduced level of CJ at the chromosomal Ig and TCR loci in both B and T lymphocytes, respectively (Nussenzweig *et al.*, 1996; Zhu *et al.*, 1996a). Like Ku80-deficient mice, *Ku70*^{-/-} mice possess growth retardation and DSB repair deficiency. Moreover, Ku70-deficient mice have leaky SCID phenotype due to the lack of mature B cells but presence of mature CD4⁺CD8⁻ and CD4⁻CD8⁺ T cells with a severe joining impairment for V(D)J coding and recombination signal sequences (Gu *et al.*, 1997; Ouyang *et al.*, 1997). In addition, Li et al. found that *Ku70*^{-/-} mice develop thymic and disseminated T cell lymphomas, which shows that Ku70 plays a role in tumor suppression (Li *et al.*, 1998).
- Gao et al. developed the first *Xrcc4*^{-/-} mice via gene-targeted mutation (Gao *et al.*, 1998b). Herein, they found that XRCC4 deficiency in mice leads to late embryonic lethality at about E16.5, although two XRCC4 pups were delivered, albeit dead. Moreover, *Xrcc4*^{-/-} mice display defective neurogenesis manifested with massive neuronal apoptosis of newly generated postmitotic neuronal cells. In addition, XRCC4-deficient mice possess defective lymphocyte development at early progenitor stages

both in B and T cells due to V(D)J recombination impairment (Gao *et al.*, 1998b). Furthermore, *Xrcc4*^{-/-} mouse embryonic fibroblasts (MEFs) possess reduced ability to repair DSBs as well as reduced proliferative capacity compared to control cells (Gao *et al.*, 1998b). To overcome the embryonic lethality, Roch *et al.* generated a viable XRCC4-deficient mouse model throughout a single amino acid substitution (M61R), *Xrcc4*^{M61R} mice (Roch *et al.*, 2021). The mentioned mice possess a slightly reduced proportion of immature B cells in the bone marrow, but the total number of B cells was not affected compared to controls. Moreover, *Xrcc4*^{M61R} mice display reduced thymocyte counts and TCR repertoire due to suboptimal V(D)J recombination levels (Roch *et al.*, 2021). In order to elucidate the XRCC4 roles during CSR *in vivo*, Soulas-Sprauel *et al.* generated a conditional XRCC4 KO mouse model (Soulas-Sprauel *et al.*, 2007). These mice possess reduced CSR levels and use short microhomologies in S μ -S γ 1 junctions compared to controls, showing that a possible alternative pathway is active in repairing CSR DSB in the absence of XRCC4 (Soulas-Sprauel *et al.*, 2007).

- Similar to *Xrcc4*^{-/-} mice, deficiency for LIG4 leads to embryonic lethality (Frank *et al.*, 1998). *Lig4*^{-/-} embryos are smaller than littermates, possess blockage in the lymphopoiesis and severe impairment in V(D)J recombination. Furthermore, *Lig4*^{-/-} MEFs also display marked sensitivity to IR, premature senescence, and growth defects (Frank *et al.*, 1998). Rucci *et al.* generated an *in vivo* model that resembles the first LIG4 mutation reported in humans throughout a knock-in mouse model with a homozygous *Lig4* R278H mutation (*Lig4*^{R/R}) (Rucci *et al.*, 2010). *Lig4*^{R/R} mice possess growth retardation similar to Ku70- and Ku80-deficient mice. Moreover, the mentioned mice display a decreased life span, IR sensitivity, severe block in B and T cell development, and impaired CSR (Rucci *et al.*, 2010).
- Bosma *et al.* discovered the first SCID mice, which have an autosomal recessive mutation that severely impairs lymphopoiesis and possess low serum immunoglobulin levels (Bosma *et al.*, 1983). More than a decade later, Araki *et al.* identified that a T to A transversion at Tyr-4046 results in the substitution of termination codon in the *Dna-pkcs* (*Prkdc*) gene, being this mutation the responsible for the SCID phenotype in the mice previously described by Bosma (Araki *et al.*, 1997). The same year, Fujimori *et al.* identified that the murine *Dna-pkcs* gene consists of 86 exons and encodes a 465-kDa catalytic subunit DNA-dependent protein kinase (DNA-PK), which is associated with Ku (Fujimori *et al.*, 1997). Jhappan *et al.* generated DNA-PKcs null mice resulting in SCID phenotype and increasing predisposition to thymic lymphoblastic lymphomas,

suggesting that DNA-PKcs functions in mice as a T-cell tumor suppressor (Jhappan *et al.*, 1997). In addition, two independent DNA-PKcs-null mouse models display no growth retardation but IR hypersensitivity as well as severe B and T lymphocyte development arrest at early progenitor stages due to V(D)J recombination impairment (Gao *et al.*, 1998a; Kurimasa *et al.*, 1999; Taccioli *et al.*, 1998). Further studies in the *Dna-pkcs*^{-/-} mice generated by Gao and colleagues showed that DNA-PKcs deficiency does not result in increased death of developing embryonic neurons compared to *Ku70*^{-/-} and *Ku80*^{-/-} mice (Gu *et al.*, 2000). Jiang *et al.* generated a mouse model that expresses a catalytically inactive (Kinase dead “KD”) DNA-PKcs protein (*Dna-pkcs*^{KD/KD}) (Jiang *et al.*, 2015). In contrast to the normal development of *Dna-pkcs*^{-/-} mice, *Dna-pkcs*^{KD/KD} mice are embryonic lethal. Furthermore, *Dna-pkcs*^{KD/KD} embryos are visibly smaller, show abrogated end-ligation and possess severe neuronal apoptosis compared to WT controls (Jiang *et al.*, 2015). Activated DNA-PK phosphorylates DNA-PKcs at the S2056 and T2609 clusters, a mouse model carrying a loss of T2609 phosphorylation of DNA-PKcs by alanine substitutions (*Dna-pkcs*^{5A/5A}) displays no CSR deficiency (Crowe *et al.*, 2020). However, *Dna-pkcs*^{5A/5A} B cells show increased chromosomal translocations and preferential usage of microhomology, suggesting that the A-EJ pathway may compensate for NHEJ roles during CSR (Crowe *et al.*, 2020).

- Artemis-deficient mice is another *in vivo* model associated with NHEJ. *Artemis*^{-/-} mice display a severe impairment during B lymphocyte development, showing blocking at the pro-B cell stage (Rooney *et al.*, 2002). Moreover, *Artemis*^{-/-} mice possess detectable, although low numbers, DP and SP T cells, categorizing this type of SCID as “leaky SCID”. In addition, *Artemis*^{-/-} mice possess defects in opening and joining V(D)J coding hairpin ends and increased radiosensitivity (Rooney *et al.*, 2002). In order to elucidate the role of Artemis during CSR, Rivera-Munoz *et al.* developed an Artemis conditional knockout mouse model to bypass the absence of B cells. *Artemis*^{-/-} B cells show reduced CSR, although not as drastic as other SCID mouse models, and an increase in DNA microhomology usage at CSR junctions (Rivera-Munoz *et al.*, 2009).
- Mutations in the *Cernunnos* gene, later known as *Xlf*, were initially identified in five patients with growth retardation, microcephaly, and SCID. Furthermore, XLF-deficient patients displayed IR sensitivity, impaired DNA-end ligation process both *in vivo* and *in vitro*, and impaired V(D)J recombination (Buck *et al.*, 2006a). The same year, it was found that the XRCC4-like factor (XLF/Cernunnos) interacts with the XRCC4-LIG4 complex to promote NHEJ and its downregulation in human cell lines leads to impaired

NHEJ as well as increased IR sensitivity (Ahnesorg *et al.*, 2006a). Two years later, the first *Xlf^{-/-}* mouse model was generated and described as fertile, normal size, and born at expected Mendelian ratios (Li *et al.*, 2008). On the one hand, *Xlf^{-/-}* MEFs possess IR hypersensitivity, genomic instability, and severely impaired V(D)J recombination. On the other hand, *Xlf^{-/-}* mice are modestly impaired for lymphocyte development, characterized by a mild reduction in the total thymocyte numbers, nearly normal V(D)J recombination in pro-B cell lines but moderately defective for CSR (Li *et al.*, 2008). In addition, two independent *Xlf^{-/-}* mouse models were generated, displaying a similar phenotype to what has been shown by Li and colleagues in 2008 (Roch *et al.*, 2019; Vera *et al.*, 2013). Moreover, it was found that *Xlf^{-/-}* mice possess a reduced thymocyte life span and a characteristic TCR repertoire bias with loss of distal V_{α} and J_{α} rearrangements (Roch *et al.*, 2019; Vera *et al.*, 2013).

- In 2015, three independent laboratories identified a new NHEJ factor with structural similarity to XRCC4 and XLF called PAXX (Paralog of XRCC4 and XLF; also called C9orf142 or XLS) as a new XRCC4-superfamily member (Craxton *et al.*, 2015; Ochi *et al.*, 2015; Xing *et al.*, 2015). Moreover, it was shown that PAXX is dispensable for V(D)J recombination in murine vAbl pro-B cell lines (Hung *et al.*, 2017; Kumar *et al.*, 2016; Lescale *et al.*, 2016b). In addition, PAXX-deficient CH12F3 cells (derived from B-cell lymphoma cell line) possess nearly WT CSR levels (Dewan *et al.*, 2018; Kumar *et al.*, 2016). Different and independent PAXX-deficient mouse models were generated and published during 2016-2018 (Abramowski *et al.*, 2018; Balmus *et al.*, 2016; Gago-Fuentes *et al.*, 2018; Liu *et al.*, 2017b). *Paxx^{-/-}* mice are viable and possess similar weight, size, fertility status, spleen and thymus size, and genomic instability level, compared to WT controls (Abramowski *et al.*, 2018; Balmus *et al.*, 2016; Gago-Fuentes *et al.*, 2018; Liu *et al.*, 2017b). Furthermore, PAXX deficiency does not have any harmful impact on the V(D)J recombination process and CSR compared to WT controls (Balmus *et al.*, 2016; Gago-Fuentes *et al.*, 2018; Liu *et al.*, 2017b).
- In 2006, Agarwal *et al.* showed that overexpression of MRI (modulator of retrovirus infection) reverses the phenotype of a mutant hamster cell line (mutant 67-1) that is resistant to infection by retroviruses, such as human immunodeficiency virus-1 (HIV-1) and murine leukemia virus (MLV) (Agarwal *et al.*, 2006). A few years later, it was found that MRI physically interacts with the Ku heterodimer to enhance NHEJ in human cells (Slavoff *et al.*, 2014) and possesses a C-terminal XLF-like motif (XLM) similar to XLF and PAXX (Grundy *et al.*, 2016). Nevertheless, it was unclear if MRI

is really a bona fide NHEJ factor and whether it is necessary for embryonic development and lymphocyte development. As part of this thesis, we custom-generated MRI-deficient mice by introducing a frame-shift mutation to *exon 2* by CRISPR/Cas9 gene-editing approach. Herein, we found that *Mri*^{-/-} mice are born at expected Mendelian ratios, fertile, and possess normal body size. More details are discussed in Paper I (Castaneda-Zegarra *et al.*, 2019a).

Table 2. Summary of single-deficient NHEJ mouse models.

Mouse models	Fitness	Main phenotype	References
<i>Ku80</i> ^{-/-}	Viable	Growth retardation, SCID, and V(D)J recombination impairment	(Nussenzweig <i>et al.</i> , 1996; Zhu <i>et al.</i> , 1996a)
<i>Ku70</i> ^{-/-}	Viable	Growth retardation, V(D)J recombination impairment, and leaky SCID phenotype*	(Gu <i>et al.</i> , 1997; Li <i>et al.</i> , 1998; Ouyang <i>et al.</i> , 1997)
<i>Xrcc4</i> ^{-/-}	Embryonic lethal	Severe genomic instability, increased neuronal apoptosis, and V(D)J recombination impairment	(Gao <i>et al.</i> , 1998b)
<i>Lig4</i> ^{-/-}	Embryonic lethal	Similar to <i>Xrcc4</i> ^{-/-} mice	(Frank <i>et al.</i> , 1998)
<i>Dna-pkcs</i> ^{-/-}	Viable	SCID, V(D)J recombination impairment and increased IR sensitivity	(Gao <i>et al.</i> , 1998a; Jhappan <i>et al.</i> , 1997; Kurimasa <i>et al.</i> , 1999; Taccioli <i>et al.</i> , 1998)
<i>Artemis</i> ^{-/-}	Viable	V(D)J recombination impairment, IR hypersensitivity, and leaky SCID phenotype*	(Rivera-Munoz <i>et al.</i> , 2009; Rooney <i>et al.</i> , 2002)
<i>Xlf</i> ^{-/-}	Viable	Modest lymphocytopenia, nearly normal V(D)J recombination and CSR	(Li <i>et al.</i> , 2008; Roch <i>et al.</i> , 2019; Vera <i>et al.</i> , 2013)
<i>Paxx</i> ^{-/-}	Viable	Similar to WT mice	(Abramowski <i>et al.</i> , 2018; Balmus <i>et al.</i> , 2016; Gago-Fuentes <i>et al.</i> , 2018; Liu <i>et al.</i> , 2017b)
<i>Mri</i> ^{-/-}	Viable	Similar to WT mice**	(Castaneda-Zegarra <i>et al.</i> , 2019a; Hung <i>et al.</i> , 2018)

IR, ionizing radiation; SCID, severe combined immune deficiency.

“*” Leaky SCID phenotype involves lack of mature B cells but presence of mature SP T cells.

“**” Results are presented in the Paper I as part of the PhD thesis.

1.7.2 Synthetic lethal NHEJ mouse models

Although deficiency of several NHEJ and DDR factors does not result in embryonic lethality in mice, it can lead to synthetic lethality when combined with a deficiency of other factors. A major reason is that their functions are compensated by each other due to the extensive genetic interaction inside the NHEJ and DDR pathways. Some examples are listed below:

- Almost ten years ago the first mouse model showing genetic interaction between *Xlf* and another NHEJ factor *in vivo* was reported, *Xlf^{-/-}Dna-pkcs^{-/-}* (Oksenyich *et al.*, 2013a). Although *Xlf^{-/-}Dna-pkcs^{-/-}* embryos have nearly Mendelian-expected ratios at E15.5, they possess perinatal lethality. Moreover, only a few *Xlf^{-/-}Dna-pkcs^{-/-}* double-deficient mice appeared to be born, however, none survived past P10, and these pups were significantly smaller than their littermates. In addition, *Xlf^{-/-}Dna-pkcs^{-/-}* double-deficient mice display increased genomic instability and dramatic V(D)J recombination abrogation due to nearly no NHEJ (Oksenyich *et al.*, 2013a). Furthermore, functional redundancy between XLF and DNA-PKcs was shown in human HAP1 (HAP is short for haploid) cell lines when exposed to DSB-inducing agents. HAP1 is a near-haploid human cell line derived from KBM-7, which is a male chronic myelogenous leukemia cell line (Xing & Oksenyich, 2019).
- Although PAXX is dispensable for V(D)J recombination in murine vAbl pro-B cell lines, combined deficiency of PAXX and XLF abrogates V(D)J recombination and increase IR sensitivity comparable to LIG4-deficient cells (Hung *et al.*, 2017; Kumar *et al.*, 2016; Lescale *et al.*, 2016b). The latter evidenced that PAXX and XLF might have functional redundancy in NHEJ. Later, four independent research groups, including our laboratory, characterized the genetic interaction between *Xlf* and *Paxx* *in vivo* (Abramowski *et al.*, 2018; Balmus *et al.*, 2016; Castaneda-Zegarra *et al.*, 2019b; Liu *et al.*, 2017b). *Xlf^{-/-}Paxx^{-/-}* double-deficient mice possess late embryonic lethality, increased genomic instability, and widespread neuronal apoptosis. Moreover, embryos lacking both XLF and PAXX display severe blockage of B- and T-cell development (Abramowski *et al.*, 2018; Balmus *et al.*, 2016; Castaneda-Zegarra *et al.*, 2019b; Liu *et al.*, 2017b). Balmus *et al.* found an *Xlf^{-/-}Paxx^{-/-}* double-deficient mouse was born out of 25 expected, indicating that, apparently due to alternative end-joining activity, embryonic lethality can be overcome in NHEJ ligation-deficient mice (Balmus *et al.*, 2016).

- Hung et al. found that mice lacking both XLF and MRI possess late embryonic lethality (Hung *et al.*, 2018). *Xlf^{-/-}Mri^{-/-}* embryos have roughly Mendelian-expected ratios at E14.5, but the mentioned embryos are significantly smaller in size compared to WT and single knockout *Xlf^{-/-}* and *Mri^{-/-}* embryos. Furthermore, *Xlf^{-/-}Mri^{-/-}* double-deficient embryos display impaired CNS development with massive neuronal apoptosis. Moreover, *Xlf^{-/-}Mri^{-/-}* vAbl pre-B cells show a severe block in V(D)J recombination (Hung *et al.*, 2018).
- Concerning mouse development, both MRI (Hung *et al.*, 2018) and DNA-PKcs (Oksenyich *et al.*, 2013a) have redundant functions with XLF. Research conducted by our laboratory shows that combined inactivation of *Mri* and *Dna-pkcs* leads to late embryonic lethality, with more details discussed in Paper III (Castaneda-Zegarra *et al.*, 2020b).

1.7.3 Complex viable NHEJ mouse models

Inactivation of transformation-related protein 53 (*Trp53*, encoding for p53), *Ku*, or *Atm* rescues embryonic lethality of different mouse models, which are going to be discussed in this section, as illustrated in Figure 14. p53 is stabilized in response to various cellular stresses, including replication stress and DNA damage. Moreover, p53 promotes a set of physiological responses, such as apoptosis, cell cycle arrest, cellular senescence, and DNA repair (Kastenhuber & Lowe, 2017). Furthermore, it is worth mentioning that mice deficient for p53 are developmentally normal but susceptible to spontaneous tumors when they reach 6 or 9 months of age in p53 deficiency (*Trp53^{-/-}*) or p53 haploinsufficiency (*Trp53^{+/-}*), respectively (Donehower *et al.*, 1992). Although, p53 deficiency rescues several embryonic mouse models, the altered expression of *Trp53* does not always rescue this lethality. For instance, the p53 loss promotes the aging and increasing cells that undergo apoptosis in embryos of an ATR-Seckel syndrome mouse model (Murga *et al.*, 2009). Moreover, PLK1-interacting checkpoint helicase (PICH)-deficient mice display embryonic lethality, and the absence of p53 does not rescue its viability (Albers *et al.*, 2018). As a result of defects in downstream factors, the Ku proteins may have toxic effects as they can cause chromosomal aggregates when the NHEJ pathway is blocked (Kovalchuk, 2021). In addition, it is possible that the Ku proteins may lead to unrepaired DSBs, activation of p53, and apoptosis by preventing DNA ligation and blocking the DSB sites from other DNA repair pathway proteins. Rescuing the lethality by ATM deficiency may be associated with its functions, such as activation of CHK1, CHK2, and p53 triggering apoptosis (Blackford & Jackson, 2017; Shiloh & Ziv, 2013).

- The first NHEJ embryonic mice rescued by inactivation of *Trp53* was the XRCC4-deficient mouse model (Gao *et al*, 2000). p53-deficiency rescues the embryonic lethality and neuronal apoptosis from XRCC4-deficient mice. Both *Xrcc4^{-/-}Trp53^{-/-}* and *Xrcc4^{-/-}Trp53^{+/-}* mice displayed growth retardation, impaired V(D)J recombination, and arrest of B and T lymphocyte development at early stages. Furthermore, *Xrcc4^{-/-}Trp53^{+/-}* mice generally died within 3-4 postnatal weeks, while *Xrcc4^{-/-}Trp53^{-/-}* mice became ill and displayed pro-B-cell lymphomas after the sixth postnatal week (Gao *et al.*, 2000).
- Similar to double deficient mice for XRCC4 and p53, p53-deficiency rescues the embryonic lethality and neuronal apoptosis in LIG4-deficient mice (Frank *et al*, 2000). *Lig4^{-/-}Trp53^{+/-}* and *Lig4^{-/-}Trp53^{-/-}* mice possessed approximately 25% and 50% of weight, respectively, compared to WT mice. Furthermore, lifespan is affected in *Lig4^{-/-}Trp53^{+/-}* and *Lig4^{-/-}Trp53^{-/-}* mice, which generally die in the first eight weeks. In addition, the mentioned mice showed minimal rescue of B and T lymphocyte development, where pro-B cells and DP T cells were identified (Frank *et al.*, 2000). In 2001, Sekiguchi *et al.* reported that ATM deficiency partially rescues the embryonic lethality of LIG4-deficient mice (Sekiguchi *et al*, 2001). Although *Lig4^{-/-}Atm^{+/-}* and *Lig4^{-/-}Atm^{-/-}* mice were born alive, they possessed growth retardation, and most of them did not survive beyond P2 (Sekiguchi *et al.*, 2001). Furthermore, complete inactivation of Ku70 (Boboila *et al*, 2010) or Ku80 (Karanjawala *et al*, 2002) has also rescued the lethality of LIG4-deficient mice. Moreover, *Lig4^{-/-}Ku70^{-/-}* and *Lig4^{-/-}Ku80^{-/-}* mice displayed a similar phenotype to *Ku70^{-/-}* and *Ku80^{-/-}* mice (Boboila *et al.*, 2010; Karanjawala *et al.*, 2002).
- Xing *et al.* demonstrated that synthetic lethality of *Xlf^{-/-}Dna-pkcs^{-/-}* double-deficient mice is rescued by complete inactivation of *Ku70*. *Xlf^{-/-}Dna-pkcs^{-/-}Ku70^{-/-}* mice were born at Mendelian-expected ratios and indistinguishable from *Ku70^{-/-}* littermates by size or levels of genomic instability. In addition, p53-haploinsufficiency also rescues the synthetic lethality of *Xlf^{-/-}Dna-pkcs^{-/-}* double-deficient mice (Xing *et al*, 2017). Although later, only one *Xlf^{-/-}Dna-pkcs^{-/-}Trp53^{-/-}* triple knockout mouse was identified from 20 expected mice according to Mendelian distribution (Castaneda-Zegarra *et al.*, 2019b). The *Xlf^{-/-}Dna-pkcs^{-/-}Trp53^{-/-}* mouse died at postnatal day 55, displaying signs of lymphoma, including three large lymph nodes (Castaneda-Zegarra *et al.*, 2019b).
- Inactivation of *Trp53* also rescues the synthetic lethality of *Xlf^{-/-}Paxx^{-/-}* mice. Both *Xlf^{-/-}Paxx^{-/-}Trp53^{+/-}* and *Xlf^{-/-}Paxx^{-/-}Trp53^{-/-}* mice were born at nearly Mendelian-expected

ratios (Castaneda-Zegarra *et al.*, 2019b). *Xlf^{-/-}Paxx^{-/-}Trp53^{-/-}* mice possessed reduced body size and severe lymphocytopenia. More details are discussed in this thesis in Paper III (Castaneda-Zegarra *et al.*, 2020b).

- In addition, as part of the present thesis, we rescued the embryonic lethality of *Xlf^{-/-}Mri^{-/-}* double-deficient mice by inactivation of *Trp53*, with more details discussed in Paper III (Castaneda-Zegarra *et al.*, 2020b).

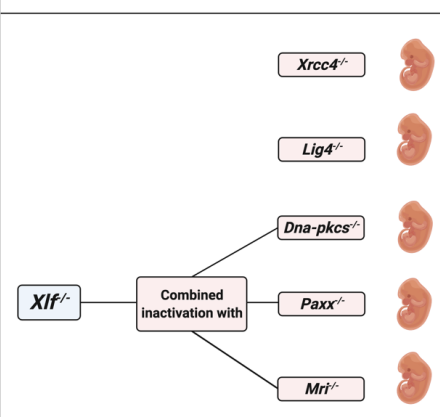










Embryonic lethality	Lethality rescue by <i>Trp53^{-/-}</i>	References
 <p><i>Xrcc4^{-/-}</i> </p> <p><i>Lig4^{-/-}</i> </p> <p><i>Dna-pkcs^{-/-}</i> </p> <p><i>Paxx^{-/-}</i> </p> <p><i>Mri^{-/-}</i> </p>	<p><i>Xrcc4^{-/-}Trp53^{-/-}</i> </p> <p><i>Lig4^{-/-}Trp53^{-/-}</i> </p> <p><i>Xlf^{-/-}Dna-pkcs^{-/-}Trp53^{-/-}</i> </p> <p><i>Xlf^{-/-}Paxx^{-/-}Trp53^{-/-}</i> </p> <p><i>Xlf^{-/-}Mri^{-/-}Trp53^{-/-}</i> </p>	<p>(Gao <i>et al.</i>, 2000)</p> <p>(Frank <i>et al.</i>, 2000)*</p> <p>(Xing <i>et al.</i>, 2017; Castaneda-Zegarra <i>et al.</i>, 2019b)**</p> <p>(Castaneda-Zegarra <i>et al.</i>, 2019b) and Paper III***</p> <p>Paper III***</p>

Figure 14. Rescue of NHEJ embryonic mouse models by inactivation of the *Trp53* gene. Single inactivation of *Xrcc4* or *Lig4* as well as combined inactivation of *Xlf/Dna-pkcs*, *Xlf/Paxx*, *Xlf/Mri* leads to embryonic lethality in mice that correlate with high levels of genomic instability and nearly no NHEJ activity. Accumulated DSBs activate the ATM-dependent DNA damage response (DDR) pathway; ATM phosphorylates CHK checkpoint proteins that further trigger cell cycle arrest and apoptosis by p53. The presence of Ku70/Ku80 blocks alternative end-joining. Inactivation of one or two alleles of *Trp53* rescues embryonic lethality of *Xrcc4^{-/-}*, *Lig4^{-/-}*, *Xlf^{-/-}Dna-pkcs^{-/-}*, *Xlf^{-/-}Paxx^{-/-}*, and *Xlf^{-/-}Mri^{-/-}* mice. Lack of p53 prevents massive apoptosis and thus results in alive mice. Sizes of the triple-deficient mice are reduced, as one option, due to DNA damage-dependent cell cycle arrest in multiple cells of the body. *Trp53* is the gene that encodes p53 protein in mice. (*) Embryonic lethality in *Lig4^{-/-}* mice is also rescued by inactivation of *Atm* (Sekiguchi *et al.*, 2001) or *Ku70* (Boboila *et al.*, 2010) or *Ku80* (Karanjawala *et al.*, 2002). (**) Embryonic lethality in *Xlf^{-/-}Dna-pkcs^{-/-}* mice is also rescued by the inactivation of *Ku70* (Xing *et al.*, 2017). (***) Results are presented in extended in Paper III as part of the PhD thesis (Castaneda-Zegarra *et al.*, 2020b). The embryonic lethality in mice lacking *Xlf/Paxx* and *Xlf/Mri* is likely to be rescued by the inactivation of Ku70 or Ku80. Light blue and pink colors represent viable and embryonic mouse models, respectively. This Figure was made in BioRender platform.

1.7.4 DDR mouse models

The generated DSBs induced by RAG and AID activate the ATM signal-transducing pathway, which phosphorylates multiple substrates, including NHEJ and DDR factors

(Helmink & Sleckman, 2012; Menolfi & Zha, 2020; Oksenykh & Kainov, 2021; Pan-Hammarström *et al.*, 2007). Although V(D)J recombination and CSR relies on NHEJ, it has been shown that several DDR factors also accomplish roles in the mentioned processes but seem to be either more “V(D)J-specific” or “CSR-specific”. A set of examples of DDR mouse models is listed below. How does the deficiency of one or more DDR factors affects the V(D)J and CSR *in vivo* is summarized in Table 3.

Both *Rag1*^{-/-} (Mombaerts *et al.*, 1992) and *Rag2*^{-/-} mice (Shinkai *et al.*, 1992) display small lymphoid organs that lack B and T lymphocytes. In both mouse models, B- and T-cell development is blocked at the pro-B cell stage in the bone marrow and the DN stage in the thymus, respectively, due to the inability to perform V(D)J recombination (Mombaerts *et al.*, 1992; Shinkai *et al.*, 1992).

DDR factors were thought to be dispensable for the V(D)J recombination. For instance, mice with germline inactivation of ATM possess functional B and T cells but a reduced number of mature T cells in the peripheral lymphoid organs, which shows that ATM is involved in the thymocyte expansion (Chao *et al.*, 2000; Lumsden *et al.*, 2004; Perkins *et al.*, 2002; Reina-San-Martin *et al.*, 2004; Xu *et al.*, 1996). In addition, it was shown that *Atm*^{-/-} mice display no V(D)J recombination impairment, but they do possess CSR deficiency (Lumsden *et al.*, 2004; Reina-San-Martin *et al.*, 2004). Mice lacking H2AX possess IR hypersensitivity, genomic instability, and growth retardation (Bassing *et al.*, 2002; Celeste *et al.*, 2002). Moreover, *H2ax*^{-/-} mice exhibit almost normal V(D)J recombination (Bassing *et al.*, 2002) but they do display impaired CSR (Reina-San-Martin *et al.*, 2003). 53BP1-deficient mice show growth retardation, increased IR sensitivity, reduced CSR efficiency, and modest effects on V(D)J recombination or lymphocyte development, being implicated in promoting DNA end mobility and long-range joining (Difilippantonio *et al.*, 2008; Manis *et al.*, 2004; Ward *et al.*, 2004). MDC1-deficient mice display a phenotype that includes severe growth retardation, IR hypersensitivity, modest CSR defect but efficient V(D)J recombination (Lou *et al.*, 2006). RNF8-deficient mice are viable and possess a mild reduction in the number of B and T cells; however, V(D)J recombination is not compromised (Santos *et al.*, 2010). Moreover, *Rnf8*^{-/-} mice display a CSR impairment but less severe than observed in *53bp1*^{-/-} mice (Santos *et al.*, 2010). Contrary to *Rnf8*^{-/-} mice, *Rnf168*^{-/-} mice display normal lymphocyte counts, in line with lack of lymphopenia in patients with RIDDLE syndrome (Bohgaki *et al.*, 2011). In addition, RNF168-deficient mice display CSR impairment, which is nevertheless milder compared to *Rnf8*^{-/-} mice and modest effects on V(D)J recombination similar to *53bp1*^{-/-} mice (Bohgaki *et al.*, 2011).

The phosphorylation of H2AX is related to the acetylation of histones, including histone H3K9. The acetylation of histone H3K9 is mediated by general control non-depressible 5 (GCN5) GCN5 and p300/CBP-associated factor (PCAF) (Jin *et al.*, 2011; Lee *et al.*, 2010). The germline inactivation of GCN5 in mice leads to embryonic lethality due to the role of the protein in neurogenesis, whereas *Pcaf*^{-/-} mice have no detectable phenotype (Xu *et al.*, 2000). However, double-deficient mice for GCN5 and PCAF display embryonic lethality, dying several days earlier than the *Gcn5*^{-/-} mice. A recent study developed a complex mouse model with germline-inactivated *Pcaf* and conditional-inactivated *Gcn5* in B-cell lineages in order to elucidate whether GCN5, PCAF or both are required for lymphocyte development *in vivo* (Oksenyich *et al.*, 2022). The mentioned mice showed a reduced number of mature B cells in the bone marrow and peripheral organs, accumulation of pro-B cells in the bone marrow, and impaired CSR levels proving that GCN5 is required for robust CSR (Oksenyich *et al.*, 2022).

Furthermore, several factors with no known function in V(D)J recombination or CSR are being identified during the last years. It is the case of FAM72A, a protein overexpressed in multiple cancers that interacts with the nuclear isoform of UNG (UNG2) (Guo *et al.*, 2008). The participation of FAM72A in CSR was identified throughout a genome-wide CRISPR–Cas9 knockout screen for genes involved in CSR. Mice lacking FAM72A exhibit reduced CSR due to increased UNG2 but normal B cell development; this suggests that FAM72A is not necessary for V(D)J recombination (Feng *et al.*, 2021; Rogier *et al.*, 2021).

Table 3. Impact of single DDR-deficiency on V(D)J recombination and CSR in mice.

Mouse model	V(D)J recombination	CSR	References
<i>Atm</i> ^{-/-}	Normal	Reduced	(Chao <i>et al.</i> , 2000; Lumsden <i>et al.</i> , 2004; Perkins <i>et al.</i> , 2002; Reina-San-Martin <i>et al.</i> , 2004; Xu <i>et al.</i> , 1996)
<i>H2ax</i> ^{-/-}	Normal	Reduced	(Bassing <i>et al.</i> , 2002; Celeste <i>et al.</i> , 2002; Reina-San-Martin <i>et al.</i> , 2003)
<i>53bp1</i> ^{-/-}	Normal	Reduced	(Difilippantonio <i>et al.</i> , 2008; Manis <i>et al.</i> , 2004; Ward <i>et al.</i> , 2004)
<i>Mdc1</i> ^{-/-}	Normal	Reduced	(Lou <i>et al.</i> , 2006)
<i>Rnf8</i> ^{-/-}	Normal	Reduced	(Santos <i>et al.</i> , 2010)
<i>Rnf168</i> ^{-/-}	Normal	Reduced	(Bohgaki <i>et al.</i> , 2011)
<i>Gcn5</i> ^{-/-}	?	Reduced	(Oksenyich <i>et al.</i> , 2022; Xu <i>et al.</i> , 2000)
<i>Pcaf</i> ^{-/-}	?	Normal	(Oksenyich <i>et al.</i> , 2022; Xu <i>et al.</i> , 2000)
<i>Fam72a</i> ^{-/-}	Normal	Reduced	(Feng <i>et al.</i> , 2021; Rogier <i>et al.</i> , 2021)

“?” no direct evidence that supports that the factor is involved in the respective process.

1.7.5 Genetic interaction between ATM-DDR and NHEJ factors

DNA damage response factors genetically interact with NHEJ components *in vivo*. *Atm* genetically interacts with *Ku70*, *Ku80*, and *Dna-pkcs*. *Atm*^{-/-}*Ku70*^{-/-}, *Atm*^{-/-}*Ku80*^{-/-}, and *Atm*^{-/-}*Dna-pkcs*^{-/-} mice possess early embryonic lethality. This is possible since DNA-PK holoenzymes and ATM functions overlap in detecting DNA lesions, phosphorylating a spectrum of substrates, and triggering subsequent cellular responses that cause embryos to die early (Menolfi & Zha, 2020). Moreover, combined deficiency of ATM and XLF nearly blocks mouse lymphocyte development due to V(D)J recombination impairment (Zha *et al*, 2011). Unlike *Xlf*, *Atm* does not interact genetically with *Paxx* and *Mri*. Both *Atm*^{-/-}*Paxx*^{-/-} and *Atm*^{-/-}*Mri*^{-/-} mice are indistinguishable from *Atm*^{-/-} mice (Balmus *et al.*, 2016; Hung *et al.*, 2018). Interestingly, several studies have shown that *Xlf* also genetically interacts with *Rag2* (Lescale *et al*, 2016a) and other DDR factors, such as *53bp1*, *H2ax*, *Mdc1*, *Rnf8* and *Rnf168* (Beck *et al*, 2019; Chen *et al*, 2021; Liu *et al*, 2012; Oksenysh *et al*, 2012) for V(D)J recombination during lymphocyte development, as illustrated in Figure 15. Mice lacking the RAG2 C-terminus domain that results in the truncated protein ‘core Rag2’ (*Rag2*^{c/c} mice) support DSB formation and DNA repair in developing B and T lymphocytes. Nevertheless, *Rag2*^{c/c}*Xlf*^{-/-} mice display deficient numbers of splenocytes and thymocytes associated with severe blockage at the pro-B cell stage and DN T cells, respectively. Although T-cell development was not wholly abolished in *Rag2*^{c/c}*Xlf*^{-/-} mice compared to B-cell development. Therefore, *Rag2*^{c/c}*Xlf*^{-/-} mice possess a “leaky” SCID phenotype (Lescale *et al.*, 2016a). On the one side, *Xlf*^{-/-}*H2ax*^{-/-} and *Xlf*^{-/-}*Mdc1*^{-/-} are embryonic lethal (Beck *et al.*, 2019; Zha *et al.*, 2011). On the other side, compared to individual deficiencies, mice with a combined loss of XLF and 53BP1 possess reduced body weight, increased genomic instability, and severe lymphocytopenia due to the inability to process and join chromosomal V(D)J recombination DSB intermediates in developing B and T cells (Liu *et al.*, 2012; Oksenysh *et al.*, 2012). Similarly, a recent study has shown that *Xlf* also possesses genetic interaction with other DDR factors, such as *Ercc6l2*, *Rnf8* and *Rnf168*. Following a CRISPR knockout screening, ERCC6L2, a suggested DSB response factor, was identified as an inductor of DSBs in Knockout conditions when treated with Zeocin. ERCC6L2-deficient B cells showed decreased CSR, and it was shown that ERCC6L2 plays a functionally redundant role with the XLF end-joining factor in V(D)J recombination (Liu *et al*, 2020b). Either deficiency of RNF8 or RNF168 does not lead to a demonstrable defect in RAG DSB repair during V(D)J recombination. However, *Xlf*^{-/-}*Rnf8*^{-/-}

and $Xlf^{f/-}Rnf168^{-/-}$ B cells show NHEJ impairment during V(D)J recombination (Chen *et al.*, 2021).

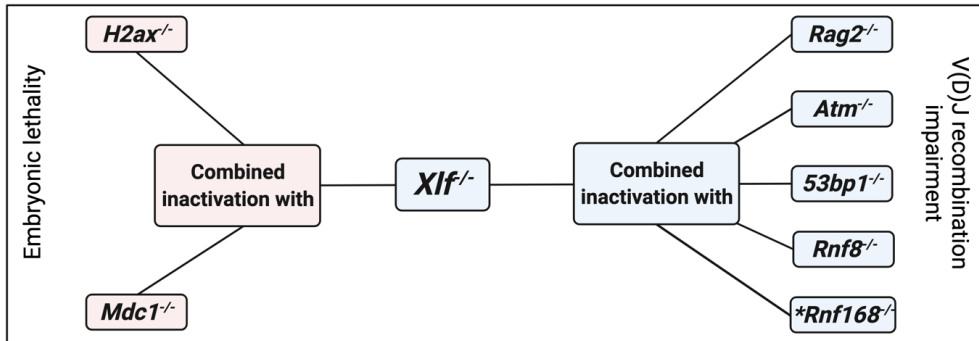


Figure 15. Genetic interactions between Xlf and DDR factors/ $Rag2$ in mice. Mice with single deficiency of shown genes are born alive and display either normal or moderately-reduced V(D)J recombination efficiency. On the one side, combined deficiency between Xlf and either $H2ax$ or $Mdc1$ leads to embryonic lethality *in vivo*. On the other side, $Xlf^{-/-}Rag2^{-/-}$, $Xlf^{-/-}Atm^{-/-}$, $Xlf^{-/-}53bp1^{-/-}$, and $Xlf^{-/-}Rnf8^{-/-}$ mice are born alive but possess V(D)J recombination impairment among the phenotype shown. * V(D)J recombination impairment in $Xlf^{-/-}Rnf168^{-/-}$ B cells was shown in B cells generated from $Xlf^{f/-}$ B cells through the CRISPR/Cas9-mediated inactivation of both $Rnf168$ alleles. Light blue and pink colors represent viable and embryonic lethal mouse models, respectively. This Figure was made in BioRender platform.

1.7.6 Shieldin-deficient mouse models and CSR

Mechanistically, RIF1 is recruited to DSBs via 53BP1, and both proteins cooperate to block DSB resection to promote NHEJ in G1. Similar to 53BP1-deficient mice, $Rif1^{-/-}$ mice display CSR defects (Chapman *et al.*, 2013). Immediately downstream of the 53BP1-RIF1 axis and promoting DSB repair by NHEJ lies the Shieldin complex formed by REV7, SHLD1, SHLD2, and SHLD3 (Dev *et al.*, 2018; Findlay *et al.*, 2018; Ghezraoui *et al.*, 2018; Gupta *et al.*, 2018; Ling *et al.*, 2020; Noordermeer *et al.*, 2018; Tomida *et al.*, 2018). *In vitro* assays showed that mutations of each shieldin subunit compromised CSR, but $Shld1^{-/-}$ B cells displayed a milder phenotype (Gupta *et al.*, 2018; Noordermeer *et al.*, 2018). It was confirmed *in vivo* that SHLD2-deficient mice possess CSR impairment but normal V(D)J recombination and unaffected B- and T-cell development (Ling *et al.*, 2020). Furthermore, a mouse model with conditional-inactivated $Rev7$ in B cells showed defective CSR although similar B cell numbers compared to WT mice (Yang *et al.*, 2020).

2. AIMS OF THE STUDY

Paper I:

To test the hypothesis that MRI is required for mouse development in general and lymphocyte development in particular.

Paper II:

To test the hypotheses that 1) MDC1 is involved in V(D)J recombination, and 2) MDC1 and XLF are functionally redundant in V(D)J recombination and mouse development.

Paper III:

To test the hypotheses that 1) p53 deficiency can rescue the synthetic lethality of *Xlf^{-/-}Mri^{-/-}* mice; and 2) combined deficiency of XLF and MRI abrogates the B and T cell development *in vivo*; 3) combined deficiency of XLF and PAXX abrogates B and T cell development *in vivo*; 4) *Mri* and *Paxx* interact genetically *in vivo*; 5) *Mri* and *Dna-pkcs* interact genetically *in vivo*.

3. SUMMARY OF PAPERS

3.1 PAPER I

Generation of a Mouse Model Lacking the Non-Homologous End-Joining Factor Mri/Cyren.

Biomolecules, 9(12), 798. (2019)

Castañeda-Zegarra S, Huse C, Røsand Ø, Sarno A, Xing M, Gago-Fuentes R, Zhang Q, Alirezaylavasani A, Werner J, Ji P, Liabakk N, Wang W, Bjørås M, Oksenysh V.

Mice lacking LIG4 (Barnes *et al.*, 1998; Frank *et al.*, 1998) or XRCC4 (Gao *et al.*, 1998b) are embryonic lethal. It has been demonstrated that p53 deficiency or haploinsufficiency rescued their embryonic lethality (Frank *et al.*, 2000; Gao *et al.*, 2000). Furthermore, the deficiency of other NHEJ factors, such as Ku70 (Gu *et al.*, 1997; Ouyang *et al.*, 1997), Ku80 (Bogue *et al.*, 1997; Nussenzweig *et al.*, 1996; Zhu *et al.*, 1996b), DNA-PKcs (Gao *et al.*, 1998a; Jhappan *et al.*, 1997; Kurimasa *et al.*, 1999; Taccioli *et al.*, 1998), or Artemis (Li *et al.*, 2005; Rooney *et al.*, 2002) results in SCID phenotype. Moreover, XLF-deficient mice possess a 2-3-fold reduction of B and T cell counts (Li *et al.*, 2008; Vera *et al.*, 2013). However, PAXX-deficient mice (Abramowski *et al.*, 2018; Balmus *et al.*, 2016; Gago-Fuentes *et al.*, 2018; Liu *et al.*, 2017b) show a very modest phenotype due to functional redundancy with XLF (Abramowski *et al.*, 2018; Balmus *et al.*, 2016; Castaneda-Zegarra *et al.*, 2019b; Liu *et al.*, 2017b).

In 2006, the modulator of retrovirus infection (MRI, or CYREN), was described as an open reading frame at human chromosome 7 (C7orf49) that reverses the resistance to retroviral infection in cell lines (Agarwal *et al.*, 2006). A few years later, it was found that MRI enhances NHEJ in human cells (Slavoff *et al.*, 2014) and possesses a C-terminal XLF-like motif (XLM) similar to PAXX and XLF (Grundy *et al.*, 2016). However, it was unclear if MRI was indeed a bona fide NHEJ factor and whether it was required for embryonic development in general and lymphocyte development in particular.

To study the specific functions of MRI *in vivo*, we custom-generated *Mri*^{-/-} mice by introducing a frame-shift mutation to *exon 2* by CRISPR/Cas9 gene-editing approach giving rise to a 14 bp deletion, which resulted in a premature stop codon. The *Mri*^{-/-} mice were generated using C57BL/6 strain as a starting point. Genetic alterations were confirmed by DNA sequencing and PCR. No commercially available and functional antibody was available to validate the lack of MRI protein in MRI-deficient mice at that time. For routine genotype

analyses, two consecutive PCRs were performed, the first PCR detected the *Mri* WT allele (428 bp) and *Mri* null allele (414 bp), which allowed to recognize heterozygous samples at a glance but not differentiate with certainty the *Mri* null allele from *Mri* WT allele due to the small difference. However, the second PCR was designed to detect only the *Mri* WT allele. In order to validate the results, both PCRs were run simultaneously for every sample to distinguish *Mri*^{-/-} mice from heterozygous and WT littermates.

Mri^{-/-} mice were born from heterozygous parents at nearly Mendelian-expected ratios (1:2:1, which corresponds to 25%) and were fertile. In addition, we found that MRI-deficient mice had a normal body size and development of lymphoid organs, including spleens and thymi. *Mri*^{-/-} mice possessed similar proportions of B and T cells in the spleen and T cells in the thymus compared to *Mri*^{+/+} and *Mri*^{+/-} mice. Moreover, CSR to IgG1 was performed in order to determine if DNA repair-dependent immunoglobulin production was affected in mature B cells lacking MRI. We showed that *Mri*^{-/-} mature B cells had reduced CSR to IgG1 compared to *Mri*^{+/+} B cells but higher than the *Ung*^{-/-} negative controls. Additionally, we used neuronal stem progenitor cells (NSPC) to determine the impact of MRI on the developing nervous system. Here, we found that the proliferation of NSPCs from *Mri*^{-/-} brains was slower when compared to WT controls. However, self-renewal capacity of NSPCs was similar between MRI-deficient mice and WT controls.

Furthermore, we used HAP1 human cell line model in order to characterize the impact of MRI on cellular sensitivity to DSBs. Here, we exposed two independent MRI-deficient clones (*MRI*^{Δ1} and *MRI*^{Δ2}) to bleomycin, doxorubicin, and etoposide. Neither *MRI*^{Δ1} nor *MRI*^{Δ2} possessed proliferation defects or hypersensitivity to the DNA damaging agents when compared to WT control unlike *XRCC4*^Δ-deficient controls.

Independently, the Sleckman group published a different *Mri* knockout model (Hung *et al.*, 2018) with a similar phenotype to ours. Therefore, we concluded that *Mri*^{-/-} mice possess a nearly normal phenotype, and it is likely that the MRI functions are compensated by other NHEJ factors, such as XLF. This new *Mri* knockout model is available to be used for further *in vivo* studies.

3.2 PAPER II

Mediator of DNA Damage Checkpoint Protein 1 Facilitates V(D)J Recombination in Cells Lacking DNA Repair Factor XLF.

Biomolecules, 10(1), 60. (2020)

Beck C, Castañeda-Zegarra S, Huse C, Xing M, Oksenyich V.

Both NHEJ and DDR pathways function in response to the V(D)J recombination during the B and T lymphocyte development. On the one side, NHEJ factors, XRCC4 (Gao *et al.*, 1998b) and LIG4 (Barnes *et al.*, 1998; Frank *et al.*, 1998) deficiency in mice cause embryonic lethality. Inactivation of *Ku70* (Gu *et al.*, 1997; Ouyang *et al.*, 1997) and *Ku80* (Bogue *et al.*, 1997; Nussenzweig *et al.*, 1996; Zhu *et al.*, 1996b) ablates V(D)J recombination in mice. Whereas modest or no impact on V(D)J recombination is registered in *Xlf^{-/-}* (Li *et al.*, 2008; Vera *et al.*, 2013), *Paxx^{-/-}* (Abramowski *et al.*, 2018; Balmus *et al.*, 2016; Gago-Fuentes *et al.*, 2018; Liu *et al.*, 2017b) and *Mri^{-/-}* (Castaneda-Zegarra *et al.*, 2019a; Hung *et al.*, 2018) mice. Moreover, XLF is functionally redundant with DNA-PKcs (Castaneda-Zegarra *et al.*, 2019b; Oksenyich *et al.*, 2013a; Xing *et al.*, 2017), PAXX (Abramowski *et al.*, 2018; Balmus *et al.*, 2016; Castaneda-Zegarra *et al.*, 2019b; Liu *et al.*, 2017b), and MRI (Castaneda-Zegarra *et al.*, 2019a; Hung *et al.*, 2018). On the other side, the germline inactivation of DDR factors, such as *H2ax* (Bassing *et al.*, 2002; Bassing *et al.*, 2003; Celeste *et al.*, 2002), *Atm* (Zha *et al.*, 2008), *Mdc1* (Lou *et al.*, 2006), or *53bp1* (Manis *et al.*, 2004) shows modest or no effect on early stages of B and T lymphocyte development, which could suggest that DDR factors are dispensable for the V(D)J recombination. Nevertheless, combined inactivation of *Xlf* and *Atm* (Zha *et al.*, 2011), or *Xlf* and *53bp1* (Liu *et al.*, 2012; Oksenyich *et al.*, 2012), resulted in V(D)J recombination impairment with very low counts of mature B and T lymphocytes in double-deficient mice.

Both MDC1 and XLF were suggested to tether the DNA at the DSB sites before the DNA ligation (Kumar *et al.*, 2014; Leimbacher *et al.*, 2019). Therefore, in this project, we addressed the role of combined inactivation of *Mdc1* and *Xlf* on V(D)J recombination both *in vivo* and *in vitro*.

In order to elucidate the *in vivo* impact of *Mdc1^{-/-}Xlf^{-/-}* double deficiency, we intercrossed *Mdc1^{+/-}Xlf^{-/-}* mice. Here, we identified 34 *Mdc1^{+/+}Xlf^{-/-}*, 70 *Mdc1^{+/-}Xlf^{-/-}* and 0 *Mdc1^{-/-}Xlf^{-/-}* mice from 104 pups. According to Mendelian distribution (1:2:1), 26 *Mdc1^{-/-}Xlf^{-/-}* mice were expected. Thus, combined inactivation of *Mdc1* and *Xlf* resulted in embryonic lethality.

To further investigate the functions of MDC1, we generated *Mdc1*^{-/-} vAbl cell lines from the bone marrow of three-week-old *Mdc1*^{-/-} *Eμ-Bcl2*⁺ mice. Furthermore, we inactivated the *Xlf* gene by targeting its *exon 3* in WT and *Mdc1*^{-/-} vAbl cells using the CRISPR/Cas9 gene-editing approach to generate *Xlf*^{-/-} knockout and *Mdc1*^{-/-} *Xlf*^{-/-} double knockout vAbl cell lines. The lack of XLF in newly-generated vAbl cell lines was validated by western blot and DNA sequencing.

To investigate if V(D)J recombination was compromised, we chromosomally-integrated the cassette-carrying GFP gene in reverse orientation and flanked by DNA sequences recognized by RAG (pMX-INV) in WT, two *Xlf*^{-/-} (#1 and #2), two *Mdc1*^{-/-} (#1 and #2), four *Mdc1*^{-/-} *Xlf*^{-/-} (#1 to #4) and *Dna-pkcs*^{-/-} *Xlf*^{-/-} vAbl cell lines. V(D)J recombination was measured by GFP fluorescence through flow cytometry after RAG induction. Robust V(D)J recombination was evidenced in the two independently-generated *Mdc1*^{-/-} vAbl cell lines compared to WT controls. However, the four *Mdc1*^{-/-} *Xlf*^{-/-} vAbl cell lines showed a significantly reduced proportion of GFP-expressing vAbl cells in approximately from 30 to 40% when compared to WT and single knockout controls and higher than the recombination levels observed in the *Dna-pkcs*^{-/-} *Xlf*^{-/-} negative controls, the latter possessed almost background levels of V(D)J recombination. Therefore, MDC1 stimulates the V(D)J recombination in *Xlf*^{-/-} cells due to functional complementarity between MDC1 and XLF.

Additionally, we evaluated the proliferation of WT, *Mdc1*^{-/-}, *Xlf*^{-/-} and *Mdc1*^{-/-} *Xlf*^{-/-} vAbl cells every 24 hours for 72 hours. No significant difference was detected between WT and single knockouts *Mdc1*^{-/-} and *Xlf*^{-/-} vAbl cells during the whole experiment. Nevertheless, double knockout *Mdc1*^{-/-} *Xlf*^{-/-} vAbl cells showed reduced proliferation at 48 and 72 hours of the experiment compared to WT, *Mdc1*^{-/-} and *Xlf*^{-/-} vAbl cells, suggesting that the lack of MDC1 was compensated by the presence of XLF in murine cells. Moreover, in a similar experiment using HAP1 human cell lines, we found that the proliferation rate was reduced when the *Mdc1* gene was inactivated in HAP1 cells at 96 and 120 hours compared to WT HAP1 cells, but no difference was detected during the first 72 hours. These results suggested that MDC1 is required for the cell cycle progression and general proliferation in human cells, and XLF compensates for the lack of MDC1 in murine cells.

In conclusion, XLF and MDC1 are functionally redundant in V(D)J recombination. Complex genetic *in vivo* and *in vitro* models would be appropriate to uncover specific functions of DDR factors in B and T lymphocyte development.

3.3 PAPER III

Leaky severe combined immunodeficiency in mice lacking non-homologous end joining factors XLF and MRI.

Aging, 12(23), 23578-23597. (2020)

Castañeda-Zegarra S, Zhang Q, Alirezaylavasani A, Fernandez-Berrocal M, Yao R, Oksenyich V.

Different proteins, such as Ku70, Ku80, DNA-PKcs, Artemis, XRCC4, LIG4, XLF, PAXX and MRI are involved in NHEJ, which is required for B and T lymphocyte development (Castaneda-Zegarra *et al.*, 2020a). Inactivation of *Xrcc4* (Gao *et al.*, 1998b) or *Lig4* (Barnes *et al.*, 1998; Frank *et al.*, 1998) results in late embryonic lethality in mice, which correlates with increased apoptosis in the central nervous system. Deletion of *Ku70* (Gu *et al.*, 1997; Ouyang *et al.*, 1997), *Ku80* (Bogue *et al.*, 1997; Nussenzweig *et al.*, 1996; Zhu *et al.*, 1996b), *Dna-pkcs* (Gao *et al.*, 1998a), or *Artemis* (Li *et al.*, 2005; Ma *et al.*, 2002; Rooney *et al.*, 2002) results in SCID phenotype, characterized by severe reduction of mature B and T lymphocytes. Mice lacking *Xlf* results in modest immunodeficiency (Li *et al.*, 2008; Roch *et al.*, 2019; Vera *et al.*, 2013). Inactivation of *Paxx* shows no overt phenotype compared to WT (Abramowski *et al.*, 2018; Balmus *et al.*, 2016; Gago-Fuentes *et al.*, 2018; Liu *et al.*, 2017b), while *Mri* deficient mice possess normal body size and number of B and T cells, but reduced CSR process in mature B cells compared to WT mice (Castaneda-Zegarra *et al.*, 2019a; Hung *et al.*, 2018)

Several studies demonstrated that XLF is functionally redundant with NHEJ factors, such as DNA-PKcs (Oksenyich *et al.*, 2013a; Xing *et al.*, 2017), PAXX (Abramowski *et al.*, 2018; Balmus *et al.*, 2016; Castaneda-Zegarra *et al.*, 2019b; Liu *et al.*, 2017b), and MRI (Hung *et al.*, 2018), which challenged study of DNA-PKcs, XLF, PAXX and MRI functions *in vivo*. Furthermore, it has been reported that lethality in mice with deficiency in *Xrcc4* (Gao *et al.*, 2000), *Lig4* (Frank *et al.*, 2000), *Xlf* and *Dna-pkcs* (Xing *et al.*, 2017), or *Xlf* and *Paxx* (Castaneda-Zegarra *et al.*, 2019b) can be rescued by inactivation of the *Trp53* gene. Moreover, it has not been clear whether the B and T cell development is affected in the *Xlf^{-/-}Paxx^{-/-}Trp53^{+/-}* mice as well as whether synthetic lethality between *Xlf* and *Mri* is *Trp53*-dependent. Therefore, in this project, we elucidated if the inactivation of one or two alleles of *Trp53* could rescue the lethality of *Xlf^{-/-}Mri^{-/-}* mice, and whether combined deficiency of XLF and MRI, or XLF and PAXX *in vivo* abrogates the B and T cell development. In addition, whether *Mri* and *Paxx* or *Mri* and *Dna-pkcs* interact genetically *in vivo*.

We intercrossed $Xlf^{f/-}Mri^{+/-}Trp53^{+/-}$ mice in order to generate $Xlf^{f/-}Mri^{f/-}$ deficient mice with altered expression of *Trp53*. Here, we identified 11 $Xlf^{f/-}Mri^{f/-}Trp53^{+/-}$, 2 $Xlf^{f/-}Mri^{f/-}Trp53^{-/-}$ and strikingly, 1 $Xlf^{f/-}Mri^{f/-}Trp53^{+/+}$ mouse. The only $Xlf^{f/-}Mri^{f/-}Trp53^{+/+}$ mouse was very sick, born smaller and clearly distinguishable from its littermates. $Xlf^{f/-}Mri^{f/-}Trp53^{+/-}$ and $Xlf^{f/-}Mri^{f/-}Trp53^{-/-}$ mice were viable up to 63 days and died for unknown reasons. $Xlf^{f/-}Mri^{f/-}Trp53^{+/-}$ mice were used to characterize the development of B and T lymphocytes *in vivo*. We found that $Xlf^{f/-}Mri^{f/-}Trp53^{+/-}$ mice had reduced body size, spleen, and thymus weight, as well as splenocytes and thymocytes count when compared to WT and single-deficient controls. In addition, $Xlf^{f/-}Mri^{f/-}Trp53^{+/-}$ mice showed a reduced number of CD19⁺ B and CD3⁺ T cells in the spleen compared with WT and single-deficient controls. Likewise, counts of T helper (CD4⁺) and T cytotoxic (CD8⁺) cells were significantly reduced both in the spleen and thymus of $Xlf^{f/-}Mri^{f/-}Trp53^{+/-}$ mice compared to WT, $Xlf^{f/-}$ and $Mri^{f/-}$ controls. Thus, XLF and MRI are functionally redundant during B and T lymphocytes development in mice.

Previously, we rescued the synthetic lethality of $Xlf^{f/-}Paxx^{f/-}$ double-deficient mice by inactivation of *Trp53* (Castaneda-Zegarra *et al.*, 2019b). In addition, in that study, we identified that $Xlf^{f/-}Paxx^{f/-}Trp53^{+/-}$ mice possessed reduced body size, spleen, and thymus weight, as well as splenocytes and thymocytes count. However, it was not clear if this combined deficiency certainly abrogated the B and T cell development. During this study, we further investigated the XLF and PAXX roles during the B and T lymphocyte development. Here, we reported that altered *Trp53* genotype did not directly influence lymphocyte development of XLF and PAXX double-deficient mice. Moreover, we evidenced that $Xlf^{f/-}Paxx^{f/-}Trp53^{+/-}$ mice had a severe reduction of CD19⁺ B and CD3⁺ T cell count in the spleen compared to WT and single knockout controls. Likewise, we found a significant reduction of T helper, T cytotoxic, and double-positive CD4⁺CD8⁺ T cells in the thymus of $Xlf^{f/-}Paxx^{f/-}Trp53^{+/-}$ mice when compared to WT, $Xlf^{f/-}$, and $Paxx^{f/-}$ mice. Therefore, it was possible to conclude that XLF and PAXX are functionally redundant during the B and T lymphocyte development *in vivo*.

Furthermore, we evaluated the B cell development from isolated bone marrow cells of mice lacking XLF, MRI, PAXX or both XLF and MRI, as well as XLF and PAXX, and analyzed the proportions of B220⁺CD43⁺IgM⁻ pro-B cells and B220⁺CD43⁻IgM⁺ immature and mature B cells. Both $Xlf^{f/-}Mri^{f/-}Trp53^{+/-}$ and $Xlf^{f/-}Paxx^{f/-}Trp53^{+/-}$ mice possessed a higher proportion of pro-B cells but background levels of B220⁺CD43⁻IgM⁺ B cells compared to WT and their respective single-deficient controls. Therefore, early B cell development is abrogated in mice lacking XLF and MRI, or XLF and PAXX.

To further investigate the MRI functions *in vivo*, we focused on whether *Mri* genetically interacts with *Paxx* and *Dna-pkcs* through the generation of *Paxx*^{-/-}*Mri*^{-/-} and *Mri*^{-/-}*Dna-pkcs*^{-/-} mice. On the one hand, we intercrossed *Paxx*^{-/-}*Mri*^{+/-} mice, and we identified 2 *Paxx*^{-/-}*Mri*^{+/+}, 4 *Paxx*^{-/-}*Mri*^{+/-}, and 7 *Paxx*^{-/-}*Mri*^{-/-} mice among the resulting offspring. *Paxx*^{-/-}*Mri*^{-/-} mice were live-born, fertile, had a similar body size, spleen, and thymus weight, as well as splenocytes and thymocytes count when compared to WT controls. However, we identified that *Paxx*^{-/-}*Mri*^{-/-} double-deficient mice possessed a reduction of splenic B cells compared to WT, *Paxx*^{-/-} and *Mri*^{-/-}, but similar to *Xlf*^{-/-} mice. Moreover, CSR was evaluated in order to determine if DNA repair-dependent immunoglobulin production was affected in mature B cells lacking PAXX and MRI. Here, we found that *Paxx*^{-/-}*Mri*^{-/-} mature B cells had similar IgG1⁺ cells after CSR compared to *Mri*^{-/-} B cells. Nevertheless, T cell development was not affected both in thymus and spleen of *Paxx*^{-/-}*Mri*^{-/-} mice compared to WT, *Paxx*^{-/-} and *Mri*^{-/-} controls. Therefore, there is a genetic interaction between *Paxx* and *Mri* *in vivo*, and it is evidenced only in the modest B cell phenotype.

On the other hand, *Mri*^{-/-}*Dna-pkcs*^{+/-} mice were intercrossed in order to generate *Mri*^{-/-}*Dna-pkcs*^{-/-} double-deficient mice. However, 12 *Mri*^{-/-}*Dna-pkcs*^{+/+} and 12 *Mri*^{-/-}*Dna-pkcs*^{+/-}, but no *Mri*^{-/-}*Dna-pkcs*^{-/-} mice (out of 6 expected) were identified, giving a Mendelian distribution close to 1:2:0. In order to elucidate if *Mri*^{-/-}*Dna-pkcs*^{-/-} were embryonic lethal, embryos at day E14.5 from *Mri*^{-/-}*Dna-pkcs*^{+/-} crossbreeding were analyzed. Here, we identified two *Mri*^{-/-}*Dna-pkcs*^{-/-} embryos (out of 2.5 expected), which were about 40% lighter than *Mri*^{-/-} littermates. Therefore, it was suggested that *Mri*^{-/-}*Dna-pkcs*^{-/-} is synthetic lethal, and there is genetic interaction between *Mri* and *Dna-pkcs* *in vivo*.

In conclusion, synthetic lethality between *Xlf* and *Mri* is rescued by inactivating one or two alleles of *Trp53*. Moreover, both *Xlf*^{-/-}*Mri*^{-/-}*Trp53*^{+/-} and *Xlf*^{-/-}*Paxx*^{-/-}*Trp53*^{+/-} mice possess a leaky SCID phenotype with severely impaired B and T development. Finally, we demonstrate that *Paxx*^{-/-}*Mri*^{-/-} mice develop phenotypes similar to single-deficient controls, and *Mri* genetically interacts with *Dna-pkcs*, the latter is reflected in embryonic lethality.

4. GENERAL DISCUSSION AND FUTURE PERSPECTIVES

V(D)J recombination in developing B and T lymphocytes and CSR in activated mature B cells produce physiological DSBs. During the V(D)J recombination in mammalian cells, both NHEJ and DDR pathways function in response to the recombination activating gene (RAG)-induced DSBs; and to the activation induced-deaminase (AID)-induced DSBs during the CSR (Kumar *et al.*, 2014).

Mutations in genes encoding NHEJ factors have been associated with human disorders, including immunodeficiency and neurological abnormalities. For instance, patients with mutations in *DNA-PKCS/PRKDC* mainly display SCID, delayed growth, neurological abnormalities, and impairments during CSR (Bjorkman *et al.*, 2015; van der Burg *et al.*, 2009; Woodbine *et al.*, 2013). Similar features are evidenced in *LIG4*-deficient (Enders *et al.*, 2006; O'Driscoll *et al.*, 2001; Riballo *et al.*, 1999) and *XLF/CERNUNNOS*-deficient patients (Buck *et al.*, 2006a; Du *et al.*, 2012; Recio *et al.*, 2018). While *ARTEMIS/DCLRE1C* mutant patients, in addition to the severe depletion of B and T cells, possess radiosensitivity (RS-SCID) but no neurological defects (Moshous *et al.*, 2001; O'Driscoll *et al.*, 2004). All these syndromes and phenotypes demonstrate the relevance of the NHEJ pathway in the normal development of humans' immune system. Nevertheless, although XRCC4 interacts with LIG4 by forming a highly stable complex (Grawunder *et al.*, 1997), XRCC4-deficient patients showed an unexpected phenotype for an NHEJ deficiency (Bee *et al.*, 2015; Guo *et al.*, 2015; Murray *et al.*, 2015; Rosin *et al.*, 2015). For instance, an XRCC4 mutant patient with reduced levels of XRCC4 possessed marked neurological abnormalities, progressive ataxia, and severely defective DSB repair, but neither clinical immunodeficiency nor V(D)J recombination deficiency (Guo *et al.*, 2015). Previously, it has been identified that XRCC4 forms polymeric arrangements, or filaments, with XLF, which stabilizes the DNA ends prior ligation (Hammel *et al.*, 2010; Ropars *et al.*, 2011). Therefore, it is suggested that although XRCC4 stabilizes LIG4 during V(D)J recombination, it would not be mandatory for coding-ends tethering during V(D)J recombination. This suggestion is reinforced with the data provided by an article published last year (Roch *et al.*, 2021). In the mentioned article, authors developed a viable XRCC4-deficient mouse model with a single amino acid substitution, M61R (*Xrcc4*^{M61R} mice). XRCC4^{M61R} protein does not interact with XLF but preserves the ability to stabilize LIG4. In comparison to XLF-deficient mice, *Xrcc4*^{M61R} mice exhibited similar phenotypes. In addition, the adaptive immune system was not adversely affected in XRCC4^{M61R}-deficient mice (Roch *et al.*, 2021). However, Roch *et al.* showed that M61R mutation induces alternative splicing in

exon 3 (Roch *et al.*, 2021), becoming difficult to affirm the relevance of XRCC4 in the V(D)J recombination conclusively. Therefore, more research would be needed to clarify whether XRCC4 is not essential for V(D)J recombination coding ends tethering at all and whether compensatory functions by other DNA repair factors exist.

Transgenic mouse models are one of the major tools to study the diverse functions of NHEJ factors and how they genetically interact with each other. Each NHEJ-deficient mouse models' phenotype depends on which gene is mutated and if two or more genes are simultaneously mutated, and whether their respective protein functions accomplish a compensatory functionality or not. Inactivation of *Ku70* (Gu *et al.*, 1997; Ouyang *et al.*, 1997), *Ku80* (Bogue *et al.*, 1997; Nussenzweig *et al.*, 1996; Zhu *et al.*, 1996b), *Dna-pkcs* (Gao *et al.*, 1998a; Jhappan *et al.*, 1997; Kurimasa *et al.*, 1999; Taccioli *et al.*, 1998), or *Artemis* (Li *et al.*, 2005; Rooney *et al.*, 2002) resulted in live-born mice with SCID phenotype. While *Xlf* deficient mice possess only modest immunodeficiency (Li *et al.*, 2008; Roch *et al.*, 2019; Vera *et al.*, 2013), and *Paxx*^{-/-} mice (Abramowski *et al.*, 2018; Balmus *et al.*, 2016; Gago-Fuentes *et al.*, 2018; Liu *et al.*, 2017b) or *Mri*^{-/-} mice (Hung *et al.*, 2018) display modest phenotype (another *Mri*^{-/-} mouse model is discussed in the Paper I). Nevertheless, both *Xrcc4*^{-/-} (Gao *et al.*, 1998b) and *Lig4*^{-/-} (Barnes *et al.*, 1998; Frank *et al.*, 1998) mice possess a strong phenotype reflected upon late embryonic lethality.

Furthermore, double-deficient *Xlf*^{-/-}*Dna-pkcs*^{-/-} mice showed to be synthetic lethal with increased genomic instability due to nearly no NHEJ (Oksenyich *et al.*, 2013a), which evidenced the first mouse model that featured genetic interaction between *Xlf* and other NHEJ factors. Likewise, genetic interaction between *Xlf* and *Paxx* (Abramowski *et al.*, 2018; Balmus *et al.*, 2016; Castaneda-Zegarra *et al.*, 2019b; Liu *et al.*, 2017b) or *Xlf* and *Mri* (Hung *et al.*, 2018) resulted in late embryonic lethality in mice. In addition, mice with combined deficiency of XLF and core RAG2 showed a severe reduction of B and T cells associated due to intensive defects in V(D)J recombination (Lescale *et al.*, 2016a).

Remarkably, it was evidenced that p53 deficiency or haploinsufficiency rescued the embryonic lethality of several single- and combined deficient NHEJ mouse models, such as *Lig4*^{-/-} (Frank *et al.*, 2000), *Xrcc4*^{-/-} (Gao *et al.*, 2000), *Xlf*^{-/-}*Dna-pkcs*^{-/-} (Xing *et al.*, 2017) and *Xlf*^{-/-}*Paxx*^{-/-} (Castaneda-Zegarra *et al.*, 2019b) mice. It was not clear whether the inactivation of *Trp53* could also rescue the synthetic lethality of *Xlf*^{-/-}*Mri*^{-/-} mice, and this question was addressed in the Paper III. Furthermore, inactivation of *Ku70* or *Ku80* has rescued the embryonic lethality of some NHEJ-deficient mouse models, such as *Lig4*^{-/-} and *Xlf*^{-/-}*Dna-pkcs*^{-/-} mice (Boboila *et al.*, 2010; Karanjawala *et al.*, 2002; Xing *et al.*, 2017). In addition, all three

mouse models, *Lig4^{-/-}Ku70^{-/-}* (Boboila *et al.*, 2010), *Lig4^{-/-}Ku80^{-/-}* (Karanjawala *et al.*, 2002) and *Xlf^{-/-}Dna-pkcs^{-/-}Ku70^{-/-}* (Xing *et al.*, 2017) possess SCID phenotype and they are indistinguishable from Ku-deficient mice. Moreover, ATM deficiency also rescued the lethality in LIG4-deficient mice (Sekiguchi *et al.*, 2001). However, in contrast to LIG4-deficient mice rescued by *Trp53*, *Ku70* and *Ku80*, both *Lig4^{-/-}Atm^{+/-}* and *Lig4^{-/-}Atm^{-/-}* mice were born at numbers below the predicted Mendelian frequency and the rescued pups did not survive beyond postnatal day P2 (Sekiguchi *et al.*, 2001).

Several ATM-dependent DDR mouse models, such as *Atm^{-/-}* (Zha *et al.*, 2008), *H2ax^{-/-}* (Bassing *et al.*, 2002; Bassing *et al.*, 2003), *53bp1^{-/-}* (Manis *et al.*, 2004), *Mdc1^{-/-}* (Lou *et al.*, 2006), *Rnf8^{-/-}* (Santos *et al.*, 2010), and *Rnf168^{-/-}* (Bohgaki *et al.*, 2011) resulted in no or small defect during early stages of B and T lymphocyte development. Although RNF8 and RNF168 deficiency on their own do not result in a V(D)J recombination defect, it has been reported that *Xlf^{-/-}Rnf8^{-/-}* and *Xlf^{-/-}Rnf168^{-/-}* vAbl pre-B cells possess defects during the V(D)J recombination (Chen *et al.*, 2021). In addition, combined inactivation of *Xlf* and *Atm* (Zha *et al.*, 2011), or *Xlf* and *53bp1* *in vivo* (Liu *et al.*, 2012; Oksenysh *et al.*, 2012), resulted in live-born mice but with impaired V(D)J recombination, and as a consequence, no mature B and T lymphocytes. Moreover, *Xlf^{-/-}H2ax^{-/-}* mice resulted in embryonic lethality (Zha *et al.*, 2011). Nevertheless, it was not known whether MDC1 participates in the V(D)J recombination as well as whether *Mdc1* genetically interacts with *Xlf*, and this question was addressed in the Paper II.

In **Paper I**, we generated *Mri^{-/-}* mice. Here, we showed that MRI-deficient mice possessed normal body size and number of B and T lymphocytes compared to WT mice. Nevertheless, MRI was found to be required for an efficient CSR process in mature B cells, and *Mri^{-/-}* neurospheres had a reduced proliferation rate, but similar self-renewal capacity, when compared to WT neurospheres.

Hung *et al.* generated and published an independent *Mri* knockout mouse model by replacing the entire protein-coding region with a LacZ cDNA cassette (Hung *et al.*, 2018). In contrast, our *Mri^{-/-}* mice were generated by introducing a frame-shift mutation to *exon 2*, which led to a 14 bp deletion and a premature stop codon.

It might be interesting to study further why *Mri^{-/-}* mature B cells exhibit defects in CSR. One idea could be to determine if the S-S junctions of MRI-deficient B cells are affected and if they possess increased lengths of junctional microhomology. For example, by using high-throughput genome-wide translocation sequencing (HTGTS) technology. HTGTS allows the detection of thousands of independent translocation junctions involving DSBs within the IgH locus of B lymphocytes. In addition, HTGTS analyzes not only the junctions at the peripheral

edges of S regions, which are generally identified by classical methods based on PCRs but also the junctions across the repetitive core of downstream acceptor S regions, where most of the CSR take place (Chiarle *et al.*, 2011; Frock *et al.*, 2015; Panchakshari *et al.*, 2018). Compared to CSR-deficient cells, WT mice show little microhomology between the donor S μ and acceptor S regions at the junction (Boboila *et al.*, 2012; Du *et al.*, 2012; Yan *et al.*, 2007). CSR-deficient cells normally possess up to 10 bp or more microhomology, as reported in *Xrcc4^{-/-}Trp53^{+/-}* mouse B cells (Yan *et al.*, 2007) and XLF-deficient human B cells (Du *et al.*, 2012).

In addition, we demonstrated that human nearly-haploid HAP1 cell lines lacking MRI do not possess DSB sensitivity to etoposide, doxorubicin, and bleomycin, while another research group showed that *Mri^{-/-}* MEFs display a hypersensitivity to IR compared to WT controls (Hung *et al.*, 2018). Thus, it would be worthwhile to elucidate the specific DNA repair functions of MRI in murine and human models, facing both kinds of cells to different DNA damaging agents.

Particularly, NSPCs possess the ability to differentiate into multiple cells, such as neurons, astrocytes, and oligodendrocytes. Furthermore, the formation and repair of endogenous DSBs in NSPCs possess a relevant role in neurogenesis and neurodevelopmental disorders. For instance, aberrant NSPC functions could lead to psychiatric diseases and neurodegenerative diseases, such as Alzheimer's disease and Parkinson's disease, as well as defects in the NSPCs might be associated with macrocephaly and autism spectrum disorder (Ladran *et al.*, 2013; Wang *et al.*, 2020a). Besides, it was shown that Filia, a regional regulator expressed in mouse hippocampal NSPC, is required for neurodevelopment and learning, memory, and mood regulation processes *in vivo* (Li *et al.*, 2020). In addition, a study published by our group in 2020 showed how the proliferation, self-renewal capacity, and differentiation in NSPCs are affected in *Xlf^{-/-}*, *Paxx^{-/-}*, *Dna-pkcs^{-/-}* and double-deficient *Xlf^{-/-}Paxx^{-/-}*, and *Xlf^{-/-}Dna-pkcs^{-/-}* compared to WT mice. For instance, XLF was found to be required for NSPC proliferation, evidenced in the significantly lower proliferation of *Xlf^{-/-}* and double-deficient *Xlf^{-/-}Paxx^{-/-}*, and *Xlf^{-/-}Dna-pkcs^{-/-}* compared to WT mice. Moreover, self-renewal capacity was reduced in *Xlf^{-/-}*, *Paxx^{-/-}* and double-deficient *Xlf^{-/-}Paxx^{-/-}* NSPCs compared to WT and single-deficient controls. Additionally, NSPCs with combined deficiency of XLF and DNA-PKcs possessed a reduced NSPC differentiation towards neurons compared to WT and single-deficient controls (Gago-Fuentes & Oksenysh, 2020). Other NSPC models displayed that XRCC4 and ATM are likely required to repair DSBs during neuronal development (Alt & Schwer, 2018; Glover & Wilson, 2016; Schwer *et al.*, 2016; Wei *et al.*, 2016). Therefore, it is suggested that additional NHEJ factors and ATM-dependent DDR factors might have similar

functions in neurodevelopment. Particularly, given that we found that NSPCs from *Mri*^{-/-} brains possess slower proliferation than WT mice, it would be interesting to test whether learning, memory, and mood regulation processes might be affected in the MRI-deficient mice.

In **Paper II**, we found that the DDR factor *Mdc1* genetically interacts with the NHEJ factor *Xlf*, resulting in synthetic lethality in mice. Furthermore, we generated MDC1/XLF double-deficient murine vAbl pro-B cell lines in order to study the V(D)J recombination effects *in vitro*. *Mdc1*^{-/-}*Xlf*^{+/+} vAbl cell lines showed reduced V(D)J recombination compared to WT but higher than *Dna-pkcs*^{-/-}*Xlf*^{+/+} negative controls. Therefore, it can be concluded that MDC1 stimulates the V(D)J recombination in cells lacking XLF. In addition, it is proposed that MDC1 and XLF are functionally redundant during the mouse development and the V(D)J recombination.

It would be interesting to study how MDC1 contributes to the V(D)J recombination in developing B and T lymphocytes *in vivo*. For this, one option could be to test whether the inactivation of the *Trp53* gene rescues the synthetic lethality of *Mdc1*^{-/-}*Xlf*^{+/+} double-deficient mice, similar to what was performed before for other lethal mouse models (Castaneda-Zegarra *et al.*, 2019b; Frank *et al.*, 2000; Gao *et al.*, 2000; Xing *et al.*, 2017). Another option could be to generate conditional knockout models for combined inactivation of *Mdc1* and *Xlf* in developing B and T lymphocytes, as de Villartay lab made to study XLF and PAXX double deficiency in mice (Musilli *et al.*, 2020).

Finally, several DDR factors possibly share functions with XLF and/or contribute to distinct but complementary to XLF aspects in DNA repair. However, further studies are required to determine their specific roles in DNA repair.

In **Paper III**, we found that inactivation of *Trp53* rescues the embryonic lethality of *Xlf*^{+/+}*Mri*^{-/-} in mice, similar to what we found for *Xlf*^{+/+}*Paxx*^{-/-} double-deficient mice in 2019 (Castaneda-Zegarra *et al.*, 2019b). In addition, we showed that the triple knockouts *Xlf*^{+/+}*Mri*^{-/-}*Trp53*^{+/-} and *Xlf*^{+/+}*Paxx*^{-/-}*Trp53*^{+/-} mice possess severely impaired B and T lymphocyte development. Therefore, we concluded that this leaky SCID phenotype is due to impaired V(D)J recombination, and our findings are supported by different cell line-based research published previously (Hung *et al.*, 2017; Hung *et al.*, 2018; Kumar *et al.*, 2016; Lescale *et al.*, 2016b). Furthermore, we found that combined deficiency of MRI and PAXX results in live-born and fertile mice with an almost normal B and T lymphocyte development, where only the number of splenic B cells is affected, giving rise to a modest phenotype. In contrast, we found that combined inactivation of *Mri* and *Dna-pkcs* results in embryonic lethality.

Moreover, we showed that *Xlf^{-/-}Mri^{-/-}Trp53^{+/-}* and *Xlf^{-/-}Paxx^{-/-}Trp53^{+/-}* mice possess more mature T cells than B cells. Therefore, there are two intriguing hypotheses to test. First, whether *Xlf^{-/-}Mri^{-/-}* and *Xlf^{-/-}Paxx^{-/-}* mice possess reduced T cells' repertoire similar to those reported for *Xlf^{-/-}* deficient mice (Vera *et al.*, 2013). In that case, a possible explanation would be that detected T lymphocytes are descendants of a few clones, which were competent to bypass or complete the V(D)J recombination. Second, because B cells are predominantly short-lived in the bone marrow (Fulcher & Basten, 1997; Ropke *et al.*, 1975) and naïve T cells possess a long-life span (Tough & Sprent, 1994, 1995), it would be possible that the T cells in our model context possess a longer lifespan than B cells. Consequently, T cells would accumulate over time following the low V(D)J recombination efficiency, while B cells would be eliminated faster from the pool due to the different physiology.

Furthermore, another intriguing hypothesis to test is whether the inactivation of *Trp53* could also rescue the synthetic lethality of *Mri^{-/-}Dna-pkcs^{-/-}* mice. In addition, due to the inactivation of *Ku70*, or *Ku80* rescued some NHEJ embryonic mouse models (Karanjawala *et al.*, 2002; Xing *et al.*, 2017), it is possible to speculate that the inactivation of one of these genes will also rescue the synthetic lethality of *Xlf* and *Paxx*, *Xlf* and *Mri*, or *Mri* and *Dna-pkcs*. Finally, it is tantalizing to hypothesize that mice lacking all known NHEJ factors (e.g., *Ku70^{-/-}Ku80^{-/-}Artemis^{-/-}Dna-pkcs^{-/-}Xlf^{-/-}Xrcc4^{-/-}Lig4^{-/-}Paxx^{-/-}Mri^{-/-}*) are still viable, and they would be indistinguishable from Ku-deficient mice; hence this new mouse model would provide new insights into the DNA repair field and would be a clean model to study alternative end-joining pathway.

5. CONCLUDING REMARKS

There are complex genetic interactions between the NHEJ pathway genes and between NHEJ and DDR factors. Genetically modified mouse models and murine cell lines have contributed to elucidate specific functions of DNA repair factors previously hidden due to the functional redundancy. For example, PAXX and MRI possess functional redundancy with XLF, and it is reflected in the synthetic lethality of $Xlf^{e/-}Paxx^{-/-}$ and $Xlf^{e/-}Mri^{-/-}$ mice. Nevertheless, p53 inactivation can rescue the lethality of both models, becoming possible to determine that PAXX and MRI are required for B and T lymphocyte development *in vivo*. Likewise, MDC1 and XLF are clear examples of functional redundancy between the DDR and NHEJ pathways. The latter is evidenced during mouse development, and particularly in the V(D)J recombination. Finally, further studies will uncover additional genetic interactions between the DNA repair factors, which will contribute to detections and treatments of future human patients.

6. REFERENCES

- Abolhassani H, Wang N, Aghamohammadi A, Rezaei N, Lee YN, Frugoni F, Notarangelo LD, Pan-Hammarstrom Q, Hammarstrom L (2014) A hypomorphic recombination-activating gene 1 (RAG1) mutation resulting in a phenotype resembling common variable immunodeficiency. *J Allergy Clin Immunol* 134: 1375-1380
- Abramowski V, Etienne O, Elsaid R, Yang J, Berland A, Kermasson L, Roch B, Musilli S, Moussu JP, Lipson-Ruffert K *et al* (2018) PAXX and Xlf interplay revealed by impaired CNS development and immunodeficiency of double KO mice. *Cell Death Differ* 25: 444-452
- Agarwal S, Harada J, Schreifels J, Lech P, Nikolai B, Yamaguchi T, Chanda SK, Somia NV (2006) Isolation, characterization, and genetic complementation of a cellular mutant resistant to retroviral infection. *Proc Natl Acad Sci U S A* 103: 15933-15938
- Aggarwal V, Tuli HS, Varol A, Thakral F, Yerer MB, Sak K, Varol M, Jain A, Khan MA, Sethi G (2019) Role of Reactive Oxygen Species in Cancer Progression: Molecular Mechanisms and Recent Advancements. *Biomolecules* 9
- Ahnesorg P, Smith P, Jackson SP (2006a) XLF interacts with the XRCC4-DNA ligase IV complex to promote DNA nonhomologous end-joining. *Cell* 124: 301-313
- Ahnesorg P, Smith P, Jackson SP (2006b) XLF Interacts with the XRCC4-DNA Ligase IV Complex to Promote DNA Nonhomologous End-Joining. *Cell* 124: 301-313
- Albers E, Sbroggiò M, Pladevall-Morera D, Bizard AH, Avram A, Gonzalez P, Martin-Gonzalez J, Hickson ID, Lopez-Contreras AJ (2018) Loss of PICH Results in Chromosomal Instability, p53 Activation, and Embryonic Lethality. *Cell Reports* 24: 3274-3284
- Alt FW, Schwer B (2018) DNA double-strand breaks as drivers of neural genomic change, function, and disease. *DNA Repair (Amst)* 71: 158-163
- Araki R, Fujimori A, Hamatani K, Mita K, Saito T, Mori M, Fukumura R, Morimyo M, Muto M, Itoh M *et al* (1997) Nonsense mutation at Tyr-4046 in the DNA-dependent protein kinase catalytic subunit of severe combined immune deficiency mice. *Proc Natl Acad Sci U S A* 94: 2438-2443
- Aravind L, Koonin EV (2001) Prokaryotic homologs of the eukaryotic DNA-end-binding protein Ku, novel domains in the Ku protein and prediction of a prokaryotic double-strand break repair system. *Genome Res* 11: 1365-1374
- Bai W, Zhu G, Xu J, Chen P, Meng F, Xue H, Chen C, Dong J (2021) The 3'-flap endonuclease XPF-ERCC1 promotes alternative end joining and chromosomal translocation during B cell class switching. *Cell Reports* 36: 109756
- Balcome S, Park S, Quirk Dorr DR, Hafner L, Phillips L, Tretyakova N (2004) Adenine-containing DNA-DNA cross-links of antitumor nitrogen mustards. *Chem Res Toxicol* 17: 950-962

- Balmus G, Barros AC, Wijnhoven PW, Lescale C, Hasse HL, Boroviak K, le Sage C, Doe B, Speak AO, Galli A *et al* (2016) Synthetic lethality between PAXX and XLF in mammalian development. *Genes Dev* 30: 2152-2157
- Barlogie B, Shaughnessy J, Tricot G, Jacobson J, Zangari M, Anaissie E, Walker R, Crowley J (2004) Treatment of multiple myeloma. *Blood* 103: 20-32
- Barnes DE, Stamp G, Rosewell I, Denzel A, Lindahl T (1998) Targeted disruption of the gene encoding DNA ligase IV leads to lethality in embryonic mice. *Curr Biol* 8: 1395-1398
- Bassing CH, Chua KF, Sekiguchi J, Suh H, Whitlow SR, Fleming JC, Monroe BC, Ciccone DN, Yan C, Vlasakova K *et al* (2002) Increased ionizing radiation sensitivity and genomic instability in the absence of histone H2AX. *Proc Natl Acad Sci U S A* 99: 8173-8178
- Bassing CH, Suh H, Ferguson DO, Chua KF, Manis J, Eckersdorff M, Gleason M, Bronson R, Lee C, Alt FW (2003) Histone H2AX: a dosage-dependent suppressor of oncogenic translocations and tumors. *Cell* 114: 359-370
- Bebenek K, Pedersen LC, Kunkel TA (2014) Structure-function studies of DNA polymerase λ . *Biochemistry* 53: 2781-2792
- Beck C, Castaneda-Zegarra S, Huse C, Xing M, Oksenyich V (2019) Mediator of DNA Damage Checkpoint Protein 1 Facilitates V(D)J Recombination in Cells Lacking DNA Repair Factor XLF. *Biomolecules* 10
- Bee L, Nasca A, Zanolini A, Cendron F, d'Adamo P, Costa R, Lamperti C, Celotti L, Ghezzi D, Zeviani M (2015) A nonsense mutation of human XRCC4 is associated with adult-onset progressive encephalomyopathy. *EMBO Mol Med* 7: 918-929
- Bertocci B, De Smet A, Berek C, Weill J-C, Reynaud C-A (2003) Immunoglobulin κ Light Chain Gene Rearrangement Is Impaired in Mice Deficient for DNA Polymerase Mu. *Immunity* 19: 203-211
- Bertocci B, De Smet A, Weill J-C, Reynaud C-A (2006) Nonoverlapping Functions of DNA Polymerases Mu, Lambda, and Terminal Deoxynucleotidyltransferase during Immunoglobulin V(D)J Recombination In Vivo. *Immunity* 25: 31-41
- Betermier M, Bertrand P, Lopez BS (2014) Is non-homologous end-joining really an inherently error-prone process? *PLoS Genet* 10: e1004086
- Bhandoola A, von Boehmer H, Petrie HT, Zúñiga-Pflücker JC (2007) Commitment and Developmental Potential of Extrathymic and Intrathymic T Cell Precursors: Plenty to Choose from. *Immunity* 26: 678-689
- Bhargava R, Onyango DO, Stark JM (2016) Regulation of Single-Strand Annealing and its Role in Genome Maintenance. *Trends Genet* 32: 566-575
- Bjorkman A, Du L, Felgentreff K, Rosner C, Pankaj Kamdar R, Kokaraki G, Matsumoto Y, Davies EG, van der Burg M, Notarangelo LD *et al* (2015) DNA-PKcs Is Involved in Ig Class Switch Recombination in Human B Cells. *J Immunol* 195: 5608-5615

Blackford AN, Jackson SP (2017) ATM, ATR, and DNA-PK: The Trinity at the Heart of the DNA Damage Response. *Mol Cell* 66: 801-817

Blasiak J (2021) Single-Strand Annealing in Cancer. *Int J Mol Sci* 22

Blier PR, Griffith AJ, Craft J, Hardin JA (1993) Binding of Ku protein to DNA. Measurement of affinity for ends and demonstration of binding to nicks. *Journal of Biological Chemistry* 268: 7594-7601

Boboila C, Oksenysh V, Gostissa M, Wang JH, Zha S, Zhang Y, Chai H, Lee CS, Jankovic M, Saez LM *et al* (2012) Robust chromosomal DNA repair via alternative end-joining in the absence of X-ray repair cross-complementing protein 1 (XRCC1). *Proc Natl Acad Sci U S A* 109: 2473-2478

Boboila C, Yan C, Wesemann DR, Jankovic M, Wang JH, Manis J, Nussenzweig A, Nussenzweig M, Alt FW (2010) Alternative end-joining catalyzes class switch recombination in the absence of both Ku70 and DNA ligase 4. *J Exp Med* 207: 417-427

Boehm T, Swann JB (2014) Origin and Evolution of Adaptive Immunity. *Annual Review of Animal Biosciences* 2: 259-283

Boersma V, Moatti N, Segura-Bayona S, Peuscher MH, van der Torre J, Wevers BA, Orthwein A, Durocher D, Jacobs JLL (2015) MAD2L2 controls DNA repair at telomeres and DNA breaks by inhibiting 5' end resection. *Nature* 521: 537-540

Bogue MA, Wang C, Zhu C, Roth DB (1997) V(D)J recombination in Ku86-deficient mice: distinct effects on coding, signal, and hybrid joint formation. *Immunity* 7: 37-47

Bohgaki M, Bohgaki T, El Ghamrasni S, Srikumar T, Maire G, Panier S, Fradet-Turcotte A, Stewart GS, Raught B, Hakem A *et al* (2013) RNF168 ubiquitylates 53BP1 and controls its response to DNA double-strand breaks. *Proc Natl Acad Sci U S A* 110: 20982-20987

Bohgaki T, Bohgaki M, Cardoso R, Panier S, Zeegers D, Li L, Stewart GS, Sanchez O, Hande MP, Durocher D *et al* (2011) Genomic instability, defective spermatogenesis, immunodeficiency, and cancer in a mouse model of the RIDDLE syndrome. *PLoS Genet* 7: e1001381

Borrego-Soto G, Ortiz-Lopez R, Rojas-Martinez A (2015) Ionizing radiation-induced DNA injury and damage detection in patients with breast cancer. *Genet Mol Biol* 38: 420-432

Bosma GC, Custer RP, Bosma MJ (1983) A severe combined immunodeficiency mutation in the mouse. *Nature* 301: 527-530

Brack C, Hiram M, Lenhard-Schuller R, Tonegawa S (1978) A complete immunoglobulin gene is created by somatic recombination. *Cell* 15: 1-14

Brandt JP, Gerriets V (2021) Bleomycin. In: *StatPearls*, Treasure Island (FL)

Brettel K, Byrdin M (2010) Reaction mechanisms of DNA photolyase. *Curr Opin Struct Biol* 20: 693-701

- Bryant HE, Schultz N, Thomas HD, Parker KM, Flower D, Lopez E, Kyle S, Meuth M, Curtin NJ, Helleday T (2005) Specific killing of BRCA2-deficient tumours with inhibitors of poly(ADP-ribose) polymerase. *Nature* 434: 913-917
- Buck D, Malivert L, de Chasseval R, Barraud A, Fondaneche MC, Sanal O, Plebani A, Stephan JL, Hufnagel M, le Deist F *et al* (2006a) Cernunnos, a novel nonhomologous end-joining factor, is mutated in human immunodeficiency with microcephaly. *Cell* 124: 287-299
- Buck D, Moshous D, de Chasseval R, Ma Y, le Deist F, Cavazzana-Calvo M, Fischer A, Casanova JL, Lieber MR, de Villartay JP (2006b) Severe combined immunodeficiency and microcephaly in siblings with hypomorphic mutations in DNA ligase IV. *Eur J Immunol* 36: 224-235
- Burma S, Chen BP, Murphy M, Kurimasa A, Chen DJ (2001) ATM phosphorylates histone H2AX in response to DNA double-strand breaks. *J Biol Chem* 276: 42462-42467
- Cadet J, Davies KJA (2017) Oxidative DNA damage & repair: An introduction. *Free Radic Biol Med* 107: 2-12
- Cadet J, Douki T, Ravanat JL (2008) Oxidatively generated damage to the guanine moiety of DNA: mechanistic aspects and formation in cells. *Acc Chem Res* 41: 1075-1083
- Callen E, Di Virgilio M, Kruhlak MJ, Nieto-Soler M, Wong N, Chen HT, Faryabi RB, Polato F, Santos M, Starnes LM *et al* (2013) 53BP1 mediates productive and mutagenic DNA repair through distinct phosphoprotein interactions. *Cell* 153: 1266-1280
- Caracciolo D, Montesano M, Tagliaferri P, Tassone P (2019) Alternative non-homologous end joining repair: a master regulator of genomic instability in cancer. *Precision Cancer Medicine* 2
- Carter RJ, Parsons JL (2016) Base Excision Repair, a Pathway Regulated by Posttranslational Modifications. *Mol Cell Biol* 36: 1426-1437
- Castaneda-Zegarra S, Fernandez-Berrocal M, Tkachov M, Yao R, Upfold NLE, Oksenyich V (2020a) Genetic interaction between the non-homologous end-joining factors during B and T lymphocyte development: In vivo mouse models. *Scand J Immunol* 92: e12936
- Castaneda-Zegarra S, Huse C, Rosand O, Sarno A, Xing M, Gago-Fuentes R, Zhang Q, Alirezaylavasani A, Werner J, Ji P *et al* (2019a) Generation of a Mouse Model Lacking the Non-Homologous End-Joining Factor Mri/Cyren. *Biomolecules* 9
- Castaneda-Zegarra S, Xing M, Gago-Fuentes R, Saeterstad S, Oksenyich V (2019b) Synthetic lethality between DNA repair factors Xlf and Paxx is rescued by inactivation of Trp53. *DNA Repair (Amst)* 73: 164-169
- Castaneda-Zegarra S, Zhang Q, Alirezaylavasani A, Fernandez-Berrocal M, Yao R, Oksenyich V (2020b) Leaky severe combined immunodeficiency in mice lacking non-homologous end joining factors XLF and MRI. *Aging (Albany NY)* 12: 23578-23597
- Ceccaldi R, Rondinelli B, D'Andrea AD (2016) Repair Pathway Choices and Consequences at the Double-Strand Break. *Trends Cell Biol* 26: 52-64

- Celeste A, Petersen S, Romanienko PJ, Fernandez-Capetillo O, Chen HT, Sedelnikova OA, Reina-San-Martin B, Coppola V, Meffre E, Difilippantonio MJ *et al* (2002) Genomic instability in mice lacking histone H2AX. *Science* 296: 922-927
- Chang HHY, Pannunzio NR, Adachi N, Lieber MR (2017) Non-homologous DNA end joining and alternative pathways to double-strand break repair. *Nat Rev Mol Cell Biol* 18: 495-506
- Chanut P, Britton S, Coates J, Jackson SP, Calsou P (2016) Coordinated nuclease activities counteract Ku at single-ended DNA double-strand breaks. *Nature Communications* 7: 12889
- Chao C, Yang EM, Xu Y (2000) Rescue of Defective T Cell Development and Function in $\text{Atm}^{-/-}$ Mice by a Functional TCR $\alpha\beta$ Transgene. *The Journal of Immunology* 164: 345
- Chapman JR, Barral P, Vannier J-B, Borel V, Steger M, Tomas-Loba A, Sartori Alessandro A, Adams Ian R, Batista Facundo D, Boulton Simon J (2013) RIF1 Is Essential for 53BP1-Dependent Nonhomologous End Joining and Suppression of DNA Double-Strand Break Resection. *Molecular Cell* 49: 858-871
- Chatterjee N, Walker GC (2017) Mechanisms of DNA damage, repair, and mutagenesis. *Environ Mol Mutagen* 58: 235-263
- Chen BR, Wang Y, Shen ZJ, Bennett A, Hindi I, Tyler JK, Sleckman BP (2021) The RNF8 and RNF168 Ubiquitin Ligases Regulate Pro- and Anti-Resection Activities at Broken DNA Ends During Non-Homologous End Joining. *DNA Repair (Amst)* 108: 103217
- Chen J, Feng W, Jiang J, Deng Y, Huen MS (2012) Ring finger protein RNF169 antagonizes the ubiquitin-dependent signaling cascade at sites of DNA damage. *J Biol Chem* 287: 27715-27722
- Chi X, Li Y, Qiu X (2020) V(D)J recombination, somatic hypermutation and class switch recombination of immunoglobulins: mechanism and regulation. *Immunology* 160: 233-247
- Chiarle R, Zhang Y, Frock RL, Lewis SM, Molinie B, Ho YJ, Myers DR, Choi VW, Compagno M, Malkin DJ *et al* (2011) Genome-wide translocation sequencing reveals mechanisms of chromosome breaks and rearrangements in B cells. *Cell* 147: 107-119
- Cipe FE, Aydogmus C, Babayigit Hocaoglu A, Kilic M, Kaya GD, Yilmaz Gulec E (2014) Cernunnos/XLF Deficiency: A Syndromic Primary Immunodeficiency. *Case Rep Pediatr* 2014: 614238
- Coin F, Oksenysh V, Egly JM (2007) Distinct roles for the XPB/p52 and XPD/p44 subcomplexes of TFIIH in damaged DNA opening during nucleotide excision repair. *Mol Cell* 26: 245-256
- Coin F, Oksenysh V, Mocquet V, Groh S, Blattner C, Egly JM (2008) Nucleotide excision repair driven by the dissociation of CAK from TFIIH. *Mol Cell* 31: 9-20
- Cong K, Peng M, Kousholt AN, Lee WTC, Lee S, Nayak S, Kraus J, VanderVere-Carozza PS, Pawelczak KS, Calvo J *et al* (2021) Replication gaps are a key determinant of PARP inhibitor synthetic lethality with BRCA deficiency. *Molecular Cell* 81: 3128-3144.e3127

- Cooper MD, Alder MN (2006) The Evolution of Adaptive Immune Systems. *Cell* 124: 815-822
- Cortez D (2019) Replication-Coupled DNA Repair. *Mol Cell* 74: 866-876
- Covo S, Ma W, Westmoreland JW, Gordenin DA, Resnick MA (2012) Understanding the origins of UV-induced recombination through manipulation of sister chromatid cohesion. *Cell Cycle* 11: 3937-3944
- Craxton A, Somers J, Munnur D, Jukes-Jones R, Cain K, Malewicz M (2015) XLS (c9orf142) is a new component of mammalian DNA double-stranded break repair. *Cell Death Differ* 22: 890-897
- Crowe JL, Wang XS, Shao Z, Lee BJ, Estes VM, Zha S (2020) DNA-PKcs phosphorylation at the T2609 cluster alters the repair pathway choice during immunoglobulin class switch recombination. *Proc Natl Acad Sci U S A* 117: 22953-22961
- Cruse JM, Lewis RE, Wang H (2004) Immunology Guidebook. MOLECULES, CELLS, AND TISSUES OF IMMUNITY. In: pp. 1-15. Academic Press: San Diego
- Daniel JA, Nussenzweig A (2013) The AID-induced DNA damage response in chromatin. *Mol Cell* 50: 309-321
- de Sousa-Pereira P, Woof JM (2019) IgA: Structure, Function, and Developability. *Antibodies (Basel)* 8
- de Villartay JP (2015) Congenital defects in V(D)J recombination. *Br Med Bull* 114: 157-167
- Desiderio S (2010) Temporal and spatial regulatory functions of the V(D)J recombinase. *Seminars in Immunology* 22: 362-369
- Desiderio SV, Yancopoulos GD, Paskind M, Thomas E, Boss MA, Landau N, Alt FW, Baltimore D (1984) Insertion of N regions into heavy-chain genes is correlated with expression of terminal deoxynucleotidyl transferase in B cells. *Nature* 311: 752-755
- Dev H, Chiang TW, Lescale C, de Krijger I, Martin AG, Pilger D, Coates J, Sczaniecka-Clift M, Wei W, Ostermaier M *et al* (2018) Shieldin complex promotes DNA end-joining and counters homologous recombination in BRCA1-null cells. *Nat Cell Biol* 20: 954-965
- DeVita VT, Jr., Chu E (2008) A history of cancer chemotherapy. *Cancer Res* 68: 8643-8653
- Dewan A, Xing M, Lundbaek MB, Gago-Fuentes R, Beck C, Aas PA, Liabakk NB, Saeterstad S, Chau KTP, Kavli BM *et al* (2018) Robust DNA repair in PAXX-deficient mammalian cells. *FEBS Open Bio* 8: 442-448
- Difilippantonio S, Gapud E, Wong N, Huang C-Y, Mahowald G, Chen HT, Kruhlak MJ, Callen E, Livak F, Nussenzweig MC *et al* (2008) 53BP1 facilitates long-range DNA end-joining during V(D)J recombination. *Nature* 456: 529-533
- Dizdaroglu M (2017) Oxidatively Induced DNA Damage and Its Repair. In: *Reference Module in Life Sciences*, Elsevier:

- Dobzhansky T (1946) Genetics of natural populations; recombination and variability in populations of *Drosophila pseudoobscura*. *Genetics* 31: 269-290
- Donehower LA, Harvey M, Slagle BL, McArthur MJ, Montgomery CA, Butel JS, Bradley A (1992) Mice deficient for p53 are developmentally normal but susceptible to spontaneous tumours. *Nature* 356: 215-221
- Du L, Peng R, Bjorkman A, Filipe de Miranda N, Rosner C, Kotnis A, Berglund M, Liu C, Rosenquist R, Enblad G *et al* (2012) Cernunnos influences human immunoglobulin class switch recombination and may be associated with B cell lymphomagenesis. *J Exp Med* 209: 291-305
- Duan M, Ulibarri J, Liu KJ, Mao P (2020) Role of Nucleotide Excision Repair in Cisplatin Resistance. *Int J Mol Sci* 21
- Duraturro F, Liccardo R, De Rosa M, Izzo P (2019) Genetics, diagnosis and treatment of Lynch syndrome: Old lessons and current challenges. *Oncol Lett* 17: 3048-3054
- Dutrannoy V, Demuth I, Baumann U, Schindler D, Konrat K, Neitzel H, Gillissen-Kaesbach G, Radszewski J, Rothe S, Schellenberger MT *et al* (2010) Clinical variability and novel mutations in the NHEJ1 gene in patients with a Nijmegen breakage syndrome-like phenotype. *Hum Mutat* 31: 1059-1068
- Enders A, Fisch P, Schwarz K, Duffner U, Pannicke U, Nikolopoulos E, Peters A, Orłowska-Volk M, Schindler D, Friedrich W *et al* (2006) A severe form of human combined immunodeficiency due to mutations in DNA ligase IV. *J Immunol* 176: 5060-5068
- Episkopou H, Kyrtopoulos SA, Sfrikakis PP, Fousteri M, Dimopoulos MA, Mullenders LH, Souliotis VL (2009) Association between transcriptional activity, local chromatin structure, and the efficiencies of both subpathways of nucleotide excision repair of melphalan adducts. *Cancer Res* 69: 4424-4433
- Escribano-Díaz C, Orthwein A, Fradet-Turcotte A, Xing M, Young Jordan TF, Tkáč J, Cook Michael A, Rosebrock Adam P, Munro M, Canny Marella D *et al* (2013) A Cell Cycle-Dependent Regulatory Circuit Composed of 53BP1-RIF1 and BRCA1-CtIP Controls DNA Repair Pathway Choice. *Molecular Cell* 49: 872-883
- Esma F, Salvini M, Troia R, Boccadoro M, Larocca A, Pautasso C (2017) Melphalan hydrochloride for the treatment of multiple myeloma. *Expert Opin Pharmacother* 18: 1127-1136
- Farhood B, Najafi M, Mortezaee K (2019) CD8(+) cytotoxic T lymphocytes in cancer immunotherapy: A review. *J Cell Physiol* 234: 8509-8521
- Farmer H, McCabe N, Lord CJ, Tutt AN, Johnson DA, Richardson TB, Santarosa M, Dillon KJ, Hickson I, Knights C *et al* (2005) Targeting the DNA repair defect in BRCA mutant cells as a therapeutic strategy. *Nature* 434: 917-921
- Feng Y, Li C, Stewart JA, Barbulescu P, Desivo NS, Álvarez-Quilón A, Pezo RC, Perera MLW, Chan K, Tong AHY *et al* (2021) FAM72A antagonizes UNG2 to promote mutagenic repair during antibody maturation. *Nature* 600: 324-328

- Findlay S, Heath J, Luo VM, Malina A, Morin T, Coulombe Y, Djerir B, Li Z, Samiei A, Simo-Cheyou E *et al* (2018) SHLD2/FAM35A co-operates with REV7 to coordinate DNA double-strand break repair pathway choice. *EMBO J* 37
- Flajnik MF, Kasahara M (2010) Origin and evolution of the adaptive immune system: genetic events and selective pressures. *Nature Reviews Genetics* 11: 47-59
- Frank KM, Sekiguchi JM, Seidl KJ, Swat W, Rathbun GA, Cheng HL, Davidson L, Kangaloo L, Alt FW (1998) Late embryonic lethality and impaired V(D)J recombination in mice lacking DNA ligase IV. *Nature* 396: 173-177
- Frank KM, Sharpless NE, Gao Y, Sekiguchi JM, Ferguson DO, Zhu C, Manis JP, Horner J, DePinho RA, Alt FW (2000) DNA ligase IV deficiency in mice leads to defective neurogenesis and embryonic lethality via the p53 pathway. *Mol Cell* 5: 993-1002
- Friedberg EC (2008) A brief history of the DNA repair field. *Cell Res* 18: 3-7
- Frit P, Ropars V, Modesti M, Charbonnier JB, Calsou P (2019) Plugged into the Ku-DNA hub: The NHEJ network. *Progress in Biophysics and Molecular Biology* 147: 62-76
- Frock RL, Hu J, Meyers RM, Ho YJ, Kii E, Alt FW (2015) Genome-wide detection of DNA double-stranded breaks induced by engineered nucleases. *Nat Biotechnol* 33: 179-186
- Frock RL, Sadeghi C, Meng J, Wang JL (2021) DNA End Joining: G0-ing to the Core. *Biomolecules* 11
- Fujimori A, Araki R, Fukumura R, Saito T, Mori M, Mita K, Tatsumi K, Abe M (1997) The murine DNA-PKcs gene consists of 86 exons dispersed in more than 250 kb. *Genomics* 45: 194-199
- Fulcher DA, Basten A (1997) B cell life span: a review. *Immunol Cell Biol* 75: 446-455
- Gago-Fuentes R, Oksenysh V (2020) Non-Homologous End Joining Factors XLF, PAXX and DNA-PKcs Maintain the Neural Stem and Progenitor Cell Population. *Biomolecules* 11
- Gago-Fuentes R, Xing M, Saeterstad S, Sarno A, Dewan A, Beck C, Bradamante S, Bjoras M, Oksenysh V (2018) Normal development of mice lacking PAXX, the paralogue of XRCC4 and XLF. *FEBS Open Bio* 8: 426-434
- Gao Y, Chaudhuri J, Zhu C, Davidson L, Weaver DT, Alt FW (1998a) A targeted DNA-PKcs-null mutation reveals DNA-PK-independent functions for KU in V(D)J recombination. *Immunity* 9: 367-376
- Gao Y, Ferguson DO, Xie W, Manis JP, Sekiguchi J, Frank KM, Chaudhuri J, Horner J, DePinho RA, Alt FW (2000) Interplay of p53 and DNA-repair protein XRCC4 in tumorigenesis, genomic stability and development. *Nature* 404: 897-900
- Gao Y, Sun Y, Frank KM, Dikkes P, Fujiwara Y, Seidl KJ, Sekiguchi JM, Rathbun GA, Swat W, Wang J *et al* (1998b) A critical role for DNA end-joining proteins in both lymphogenesis and neurogenesis. *Cell* 95: 891-902

- Gell D, Jackson SP (1999) Mapping of protein-protein interactions within the DNA-dependent protein kinase complex. *Nucleic Acids Research* 27: 3494-3502
- Ghaedi M, Steer Catherine A, Martinez-Gonzalez I, Halim Timotheus YF, Abraham N, Takei F (2016) Common-Lymphoid-Progenitor-Independent Pathways of Innate and T Lymphocyte Development. *Cell Reports* 15: 471-480
- Ghezraoui H, Oliveira C, Becker JR, Bilham K, Moralli D, Anzilotti C, Fischer R, Deobagkar-Lele M, Sanchiz-Calvo M, Fueyo-Marcos E *et al* (2018) 53BP1 cooperation with the REV7–shieldin complex underpins DNA structure-specific NHEJ. *Nature* 560: 122-127
- Ghosh S (2019) Cisplatin: The first metal based anticancer drug. *Bioorg Chem* 88: 102925
- Glover TW, Wilson TE (2016) Molecular biology: Breaks in the brain. *Nature* 532: 46-47
- Gonzalez-Gutierrez AM, Ortiz-Muniz R, Garcia-Rodriguez MDC, Cortes-Barberena E (2019) Phosphorylated ATM and H2AX in T and B lymphocytes from rats with moderate and severe malnutrition. *DNA Repair (Amst)* 83: 102640
- Graham TGW, Walter JC, Loparo JJ (2016) Two-Stage Synapsis of DNA Ends during Non-homologous End Joining. *Molecular cell* 61: 850-858
- Grawunder U, Wilm M, Wu X, Kulesza P, Wilson TE, Mann M, Lieber MR (1997) Activity of DNA ligase IV stimulated by complex formation with XRCC4 protein in mammalian cells. *Nature* 388: 492-495
- Greber BJ, Toso DB, Fang J, Nogales E (2019) The complete structure of the human TFIIH core complex. *Elife* 8
- Grundy GJ, Parsons JL (2020) Base excision repair and its implications to cancer therapy. *Essays Biochem* 64: 831-843
- Grundy GJ, Rulten SL, Arribas-Bosacoma R, Davidson K, Kozik Z, Oliver AW, Pearl LH, Caldecott KW (2016) The Ku-binding motif is a conserved module for recruitment and stimulation of non-homologous end-joining proteins. *Nat Commun* 7: 11242
- Grundy GJ, Rulten SL, Zeng Z, Arribas-Bosacoma R, Iles N, Manley K, Oliver A, Caldecott KW (2013) APLF promotes the assembly and activity of non-homologous end joining protein complexes. *Embo j* 32: 112-125
- Grunebaum E, Bates A, Roifman CM (2008) Omenn syndrome is associated with mutations in DNA ligase IV. *J Allergy Clin Immunol* 122: 1219-1220
- Gu J, Lu H, Tsai AG, Schwarz K, Lieber MR (2007) Single-stranded DNA ligation and XLF-stimulated incompatible DNA end ligation by the XRCC4-DNA ligase IV complex: influence of terminal DNA sequence. *Nucleic Acids Res* 35: 5755-5762
- Gu Y, Seidl KJ, Rathbun GA, Zhu C, Manis JP, van der Stoep N, Davidson L, Cheng H-L, Sekiguchi JM, Frank K *et al* (1997) Growth Retardation and Leaky SCID Phenotype of Ku70-Deficient Mice. *Immunity* 7: 653-665

- Gu Y, Sekiguchi J, Gao Y, Dikkes P, Frank K, Ferguson D, Hasty P, Chun J, Alt FW (2000) Defective embryonic neurogenesis in Ku-deficient but not DNA-dependent protein kinase catalytic subunit-deficient mice. *Proc Natl Acad Sci U S A* 97: 2668-2673
- Guillotin D, Martin SA (2014) Exploiting DNA mismatch repair deficiency as a therapeutic strategy. *Experimental Cell Research* 329: 110-115
- Guo C, Nakazawa Y, Woodbine L, Bjorkman A, Shimada M, Fawcett H, Jia N, Ohyama K, Li TS, Nagayama Y *et al* (2015) XRCC4 deficiency in human subjects causes a marked neurological phenotype but no overt immunodeficiency. *J Allergy Clin Immunol* 136: 1007-1017
- Guo C, Zhang X, Fink SP, Platzer P, Wilson K, Willson JK, Wang Z, Markowitz SD (2008) Ugene, a newly identified protein that is commonly overexpressed in cancer and binds uracil DNA glycosylase. *Cancer Res* 68: 6118-6126
- Gupta R, Somyajit K, Narita T, Maskey E, Stanlie A, Kremer M, Typas D, Lammers M, Mailand N, Nussenzweig A *et al* (2018) DNA Repair Network Analysis Reveals Shieldin as a Key Regulator of NHEJ and PARP Inhibitor Sensitivity. *Cell* 173: 972-988 e923
- Gutierrez R, O'Connor T (2021) DNA direct reversal repair and alkylating agent drug resistance. *Cancer Drug Resist* 4: 414-423
- Hammel M, Yu Y, Fang S, Lees-Miller SP, Tainer JA (2010) XLF regulates filament architecture of the XRCC4.ligase IV complex. *Structure* 18: 1431-1442
- Hegde ML, Hazra TK, Mitra S (2008) Early steps in the DNA base excision/single-strand interruption repair pathway in mammalian cells. *Cell Res* 18: 27-47
- Hegde ML, Izumi T, Mitra S (2012) Oxidized base damage and single-strand break repair in mammalian genomes: role of disordered regions and posttranslational modifications in early enzymes. *Prog Mol Biol Transl Sci* 110: 123-153
- Helleday T (2011) The underlying mechanism for the PARP and BRCA synthetic lethality: clearing up the misunderstandings. *Mol Oncol* 5: 387-393
- Helmink BA, Sleckman BP (2012) The response to and repair of RAG-mediated DNA double-strand breaks. *Annu Rev Immunol* 30: 175-202
- Hosoya N, Miyagawa K (2014) Targeting DNA damage response in cancer therapy. *Cancer Sci* 105: 370-388
- Huang J, Huen MS, Kim H, Leung CC, Glover JN, Yu X, Chen J (2009) RAD18 transmits DNA damage signalling to elicit homologous recombination repair. *Nat Cell Biol* 11: 592-603
- Huang X, Pan Y, Cao D, Fang S, Huang K, Chen J, Chen A (2017) UVA-induced upregulation of progerin suppresses 53BP1 mediated NHEJ DSB repair in human keratinocytes via progerin-lamin A complex formation. *Oncol Rep* 37: 3617-3624
- Huang Y, Li GM (2018) DNA mismatch repair preferentially safeguards actively transcribed genes. *DNA Repair (Amst)* 71: 82-86

- Hung PJ, Chen BR, George R, Liberman C, Morales AJ, Colon-Ortiz P, Tyler JK, Sleckman BP, Bredemeyer AL (2017) Deficiency of XLF and PAXX prevents DNA double-strand break repair by non-homologous end joining in lymphocytes. *Cell Cycle* 16: 286-295
- Hung PJ, Johnson B, Chen BR, Byrum AK, Bredemeyer AL, Yewdell WT, Johnson TE, Lee BJ, Deivasigamani S, Hindi I *et al* (2018) MRI Is a DNA Damage Response Adaptor during Classical Non-homologous End Joining. *Mol Cell* 71: 332-342 e338
- Hutchinson MND, Mierzwa M, D'Silva NJ (2020) Radiation resistance in head and neck squamous cell carcinoma: dire need for an appropriate sensitizer. *Oncogene* 39: 3638-3649
- Ijspeert H, Lankester AC, van den Berg JM, Wiegant W, van Zelm MC, Weemaes CM, Warris A, Pan-Hammarstrom Q, Pastink A, van Tol MJ *et al* (2011) Artemis splice defects cause atypical SCID and can be restored in vitro by an antisense oligonucleotide. *Genes Immun* 12: 434-444
- Ikehata H, Ono T (2011) The mechanisms of UV mutagenesis. *J Radiat Res* 52: 115-125
- Issaoui H, Ghazzoui N, Saintamand A, Denizot Y, Boyer F (2017) IgD class switch recombination is not controlled through the immunoglobulin heavy chain 3' regulatory region super-enhancer. *Cellular & Molecular Immunology* 14: 871-874
- Jackson K, Kidd M, Wang Y, Collins A (2013) The Shape of the Lymphocyte Receptor Repertoire: Lessons from the B Cell Receptor. *Frontiers in Immunology* 4
- Jackson SP, Bartek J (2009) The DNA-damage response in human biology and disease. *Nature* 461: 1071-1078
- Jackson SP, Helleday T (2016) DNA REPAIR. Drugging DNA repair. *Science* 352: 1178-1179
- Jang S, Kumar N, Beckwitt EC, Kong M, Fouquerel E, Rapic-Otrin V, Prasad R, Watkins SC, Khuu C, Majumdar C *et al* (2019) Damage sensor role of UV-DDB during base excision repair. *Nat Struct Mol Biol* 26: 695-703
- Jhappan C, Morse HC, 3rd, Fleischmann RD, Gottesman MM, Merlino G (1997) DNA-PKcs: a T-cell tumour suppressor encoded at the mouse scid locus. *Nat Genet* 17: 483-486
- Jiang A, Maibach H (2018) Dermatotoxicology of sulfur mustard: Historical perspectives from World War I. *J Appl Toxicol* 38: 108-112
- Jiang H, Chang FC, Ross AE, Lee J, Nakayama K, Nakayama K, Desiderio S (2005) Ubiquitylation of RAG-2 by Skp2-SCF links destruction of the V(D)J recombinase to the cell cycle. *Mol Cell* 18: 699-709
- Jiang W, Crowe Jennifer L, Liu X, Nakajima S, Wang Y, Li C, Lee Brian J, Dubois Richard L, Liu C, Yu X *et al* (2015) Differential Phosphorylation of DNA-PKcs Regulates the Interplay between End-Processing and End-Ligation during Nonhomologous End-Joining. *Molecular Cell* 58: 172-185
- Jin Q, Yu LR, Wang L, Zhang Z, Kasper LH, Lee JE, Wang C, Brindle PK, Dent SY, Ge K (2011) Distinct roles of GCN5/PCAF-mediated H3K9ac and CBP/p300-mediated H3K18/27ac in nuclear receptor transactivation. *EMBO J* 30: 249-262

- Kaneto H, Katakami N, Matsuhisa M, Matsuoka TA (2010) Role of reactive oxygen species in the progression of type 2 diabetes and atherosclerosis. *Mediators Inflamm* 2010: 453892
- Karanjwala ZE, Adachi N, Irvine RA, Oh EK, Shibata D, Schwarz K, Hsieh CL, Lieber MR (2002) The embryonic lethality in DNA ligase IV-deficient mice is rescued by deletion of Ku: implications for unifying the heterogeneous phenotypes of NHEJ mutants. *DNA Repair (Amst)* 1: 1017-1026
- Karmakar P, Piotrowski J, Brosh RM, Jr., Sommers JA, Miller SP, Cheng WH, Snowden CM, Ramsden DA, Bohr VA (2002) Werner protein is a target of DNA-dependent protein kinase in vivo and in vitro, and its catalytic activities are regulated by phosphorylation. *J Biol Chem* 277: 18291-18302
- Kastenhuber ER, Lowe SW (2017) Putting p53 in Context. *Cell* 170: 1062-1078
- Kavakli IH, Ozturk N, Gul S (2019) Chapter One - DNA repair by photolyases. In: *Advances in Protein Chemistry and Structural Biology*, Donev R. (ed.) pp. 1-19. Academic Press:
- Kim H, Chen J, Yu X (2007) Ubiquitin-binding protein RAP80 mediates BRCA1-dependent DNA damage response. *Science* 316: 1202-1205
- Kindt TJ, Goldsby RA, Osborne BA, Kuby J (2007) *Kuby immunology*. W.H. Freeman, New York
- Kolas NK, Chapman JR, Nakada S, Ylanko J, Chahwan R, Sweeney FD, Panier S, Mendez M, Wildenhain J, Thomson TM *et al* (2007) Orchestration of the DNA-damage response by the RNF8 ubiquitin ligase. *Science* 318: 1637-1640
- Komori T, Okada A, Stewart V, Alt FW (1993) Lack of N regions in antigen receptor variable region genes of TdT-deficient lymphocytes. *Science* 261: 1171-1175
- Kovalchuk I (2021) Chapter 11 - Genome stability in *Caenorhabditis elegans*☆. In: *Genome Stability (Second Edition)*, Kovalchuk I., Kovalchuk O. (eds.) pp. 177-200. Academic Press: Boston
- Krangel MS (2009) Mechanics of T cell receptor gene rearrangement. *Current Opinion in Immunology* 21: 133-139
- Krokan HE, Drablos F, Slupphaug G (2002) Uracil in DNA--occurrence, consequences and repair. *Oncogene* 21: 8935-8948
- Kumar V, Alt FW, Frock RL (2016) PAXX and XLF DNA repair factors are functionally redundant in joining DNA breaks in a G1-arrested progenitor B-cell line. *Proc Natl Acad Sci U S A* 113: 10619-10624
- Kumar V, Alt FW, Oksenyuk V (2014) Functional overlaps between XLF and the ATM-dependent DNA double strand break response. *DNA Repair (Amst)* 16: 11-22
- Kunkel TA, Erie DA (2015) Eukaryotic Mismatch Repair in Relation to DNA Replication. *Annual review of genetics* 49: 291-313

Kurimasa A, Ouyang H, Dong LJ, Wang S, Li X, Cordon-Cardo C, Chen DJ, Li GC (1999) Catalytic subunit of DNA-dependent protein kinase: impact on lymphocyte development and tumorigenesis. *Proc Natl Acad Sci U S A* 96: 1403-1408

Ladran I, Tran N, Topol A, Brennan KJ (2013) Neural stem and progenitor cells in health and disease. *Wiley Interdiscip Rev Syst Biol Med* 5: 701-715

LaFargue CJ, Dal Molin GZ, Sood AK, Coleman RL (2019) Exploring and comparing adverse events between PARP inhibitors. *Lancet Oncol* 20: e15-e28

Lavoie JM, Kollmannsberger CK (2019) Current Management of Disseminated Germ Cell Tumors. *Urol Clin North Am* 46: 377-388

Lee H-S, Park J-H, Kim S-J, Kwon S-J, Kwon J (2010) A cooperative activation loop among SWI/SNF, γ -H2AX and H3 acetylation for DNA double-strand break repair. *The EMBO Journal* 29: 1434-1445

Lee TH, Kang TH (2019) DNA Oxidation and Excision Repair Pathways. *Int J Mol Sci* 20

Leegte B, van der Hout AH, Deffenbaugh AM, Bakker MK, Mulder IM, ten Berge A, Leenders EP, Wesseling J, de Hullu J, Hoogerbrugge N *et al* (2005) Phenotypic expression of double heterozygosity for BRCA1 and BRCA2 germline mutations. *J Med Genet* 42: e20

Leimbacher PA, Jones SE, Shorrocks AK, de Marco Zompit M, Day M, Blaauwendraad J, Bundschuh D, Bonham S, Fischer R, Fink D *et al* (2019) MDC1 Interacts with TOPBP1 to Maintain Chromosomal Stability during Mitosis. *Mol Cell* 74: 571-583 e578

Leoni LM, Bailey B, Reifert J, Bendall HH, Zeller RW, Corbeil J, Elliott G, Niemeyer CC (2008) Bendamustine (Treanda) displays a distinct pattern of cytotoxicity and unique mechanistic features compared with other alkylating agents. *Clin Cancer Res* 14: 309-317

Lescale C, Abramowski V, Bedora-Faure M, Murigneux V, Vera G, Roth DB, Revy P, de Villartay JP, Deriano L (2016a) RAG2 and XLF/Cernunnos interplay reveals a novel role for the RAG complex in DNA repair. *Nat Commun* 7: 10529

Lescale C, Deriano L (2016) V(D)J Recombination: Orchestrating Diversity without Damage. In: *Encyclopedia of Cell Biology*, Bradshaw R.A., Stahl P.D. (eds.) pp. 550-566. Academic Press: Waltham

Lescale C, Deriano L (2017) The RAG recombinase: Beyond breaking. *Mech Ageing Dev* 165: 3-9

Lescale C, Lenden Hasse H, Blackford AN, Balmus G, Bianchi JJ, Yu W, Bacoccina L, Jarade A, Clouin C, Sivapalan R *et al* (2016b) Specific Roles of XRCC4 Paralogs PAXX and XLF during V(D)J Recombination. *Cell Rep* 16: 2967-2979

Letavayova L, Markova E, Hermanska K, Vlckova V, Vlasakova D, Chovanec M, Brozmanova J (2006) Relative contribution of homologous recombination and non-homologous end-joining to DNA double-strand break repair after oxidative stress in *Saccharomyces cerevisiae*. *DNA Repair (Amst)* 5: 602-610

- Li B, Comai L (2000) Functional interaction between Ku and the werner syndrome protein in DNA end processing. *J Biol Chem* 275: 28349-28352
- Li G, Alt FW, Cheng HL, Brush JW, Goff PH, Murphy MM, Franco S, Zhang Y, Zha S (2008) Lymphocyte-specific compensation for XLF/cernunnos end-joining functions in V(D)J recombination. *Mol Cell* 31: 631-640
- Li GC, Ouyang H, Li X, Nagasawa H, Little JB, Chen DJ, Ling CC, Fuks Z, Cordon-Cardo C (1998) Ku70: a candidate tumor suppressor gene for murine T cell lymphoma. *Mol Cell* 2: 1-8
- Li J, Shang Y, Wang L, Zhao B, Sun C, Li J, Liu S, Li C, Tang M, Meng FL *et al* (2020) Genome integrity and neurogenesis of postnatal hippocampal neural stem/progenitor cells require a unique regulator Folia. *Sci Adv* 6
- Li L, Salido E, Zhou Y, Bhattacharyya S, Yannone SM, Dunn E, Meneses J, Feeney AJ, Cowan MJ (2005) Targeted disruption of the Artemis murine counterpart results in SCID and defective V(D)J recombination that is partially corrected with bone marrow transplantation. *J Immunol* 174: 2420-2428
- Liang Z, Kumar V, Le Bouteiller M, Zurita J, Kenrick J, Lin SG, Lou J, Hu J, Ye AY, Boboila C *et al* (2021) Ku70 suppresses alternative end joining in G1-arrested progenitor B cells. *Proc Natl Acad Sci U S A* 118
- Libri A, Marton T, Deriano L (2022) The (Lack of) DNA Double-Strand Break Repair Pathway Choice During V(D)J Recombination. *Frontiers in Genetics* 12: 2726
- Lieber MR (2006) The Polymerases for V(D)J Recombination. *Immunity* 25: 7-9
- Lin WC, Desiderio S (1994) Cell cycle regulation of V(D)J recombination-activating protein RAG-2. *Proc Natl Acad Sci U S A* 91: 2733-2737
- Lindahl T (1993) Instability and decay of the primary structure of DNA. *Nature* 362: 709-715
- Lindahl T, Barnes DE (2000) Repair of endogenous DNA damage. *Cold Spring Harb Symp Quant Biol* 65: 127-133
- Ling AK, Munro M, Chaudhary N, Li C, Berru M, Wu B, Durocher D, Martin A (2020) SHLD2 promotes class switch recombination by preventing inactivating deletions within the Igh locus. *EMBO Rep* 21: e49823
- Liu D, Keijzers G, Rasmussen LJ (2017a) DNA mismatch repair and its many roles in eukaryotic cells. *Mutat Res Rev Mutat Res* 773: 174-187
- Liu W, Tolar P, Song W, Kim TJ (2020a) Editorial: BCR Signaling and B Cell Activation. *Frontiers in Immunology* 11
- Liu X, Jiang W, Dubois RL, Yamamoto K, Wolner Z, Zha S (2012) Overlapping functions between XLF repair protein and 53BP1 DNA damage response factor in end joining and lymphocyte development. *Proc Natl Acad Sci U S A* 109: 3903-3908

Liu X, Liu T, Shang Y, Dai P, Zhang W, Lee BJ, Huang M, Yang D, Wu Q, Liu LD *et al* (2020b) ERCC6L2 promotes DNA orientation-specific recombination in mammalian cells. *Cell Res* 30: 732-744

Liu X, Shao Z, Jiang W, Lee BJ, Zha S (2017b) PAXX promotes KU accumulation at DNA breaks and is essential for end-joining in XLF-deficient mice. *Nat Commun* 8: 13816

Liu X, Yu J, Xu L, Umphred-Wilson K, Peng F, Ding Y, Barton BM, Lv X, Zhao MY, Sun S *et al* (2021) Notch-induced endoplasmic reticulum-associated degradation governs mouse thymocyte beta-selection. *Elife* 10

Lomax ME, Folkes LK, O'Neill P (2013) Biological consequences of radiation-induced DNA damage: relevance to radiotherapy. *Clin Oncol (R Coll Radiol)* 25: 578-585

Lou Z, Minter-Dykhouse K, Franco S, Gostissa M, Rivera MA, Celeste A, Manis JP, van Deursen J, Nussenzweig A, Paull TT *et al* (2006) MDC1 maintains genomic stability by participating in the amplification of ATM-dependent DNA damage signals. *Mol Cell* 21: 187-200

Liu G, Duan J, Shu S, Wang X, Gao L, Guo J, Zhang Y (2016) Ligase I and ligase III mediate the DNA double-strand break ligation in alternative end-joining. *Proc Natl Acad Sci U S A* 113: 1256-1260

Lumsden JM, McCarty T, Petiniot LK, Shen R, Barlow C, Wynn TA, Morse HC, 3rd, Gearhart PJ, Wynshaw-Boris A, Max EE *et al* (2004) Immunoglobulin class switch recombination is impaired in Atm-deficient mice. *J Exp Med* 200: 1111-1121

Ma Y, Lu H, Tippin B, Goodman MF, Shimazaki N, Koiwai O, Hsieh CL, Schwarz K, Lieber MR (2004) A biochemically defined system for mammalian nonhomologous DNA end joining. *Mol Cell* 16: 701-713

Ma Y, Pannicke U, Schwarz K, Lieber MR (2002) Hairpin opening and overhang processing by an Artemis/DNA-dependent protein kinase complex in nonhomologous end joining and V(D)J recombination. *Cell* 108: 781-794

Mailand N, Bekker-Jensen S, Fastrup H, Melander F, Bartek J, Lukas C, Lukas J (2007) RNF8 Ubiquitylates Histones at DNA Double-Strand Breaks and Promotes Assembly of Repair Proteins. *Cell* 131: 887-900

Mak TW, Saunders ME, Jett BD (2014a) Chapter 5 - B Cell Development, Activation and Effector Functions. In: *Primer to the Immune Response (Second Edition)*, pp. 111-142. Academic Cell: Boston

Mak TW, Saunders ME, Jett BD (2014b) Chapter 9 - T Cell Development, Activation and Effector Functions. In: *Primer to the Immune Response (Second Edition)*, pp. 197-226. Academic Cell: Boston

Makharashvili N, Paull TT (2015) CtIP: A DNA damage response protein at the intersection of DNA metabolism. *DNA Repair* 32: 75-81

Malu S, Malshetty V, Francis D, Cortes P (2012) Role of non-homologous end joining in V(D)J recombination. *Immunologic Research* 54: 233-246

- Manis JP, Morales JC, Xia Z, Kutok JL, Alt FW, Carpenter PB (2004) 53BP1 links DNA damage-response pathways to immunoglobulin heavy chain class-switch recombination. *Nat Immunol* 5: 481-487
- Mao Z, Bozzella M, Seluanov A, Gorbunova V (2008) DNA repair by nonhomologous end joining and homologous recombination during cell cycle in human cells. *Cell Cycle* 7: 2902-2906
- Mari P-O, Florea BI, Persengiev SP, Verkaik NS, Brüggewirth HT, Modesti M, Giglia-Mari G, Bezstarosti K, Demmers JAA, Luider TM *et al* (2006) Dynamic assembly of end-joining complexes requires interaction between Ku70/80 and XRCC4. *Proceedings of the National Academy of Sciences* 103: 18597-18602
- Marshall JS, Warrington R, Watson W, Kim HL (2018) An introduction to immunology and immunopathology. *Allergy, Asthma & Clinical Immunology* 14: 49
- Mathieu AL, Verronese E, Rice GI, Fouyssac F, Bertrand Y, Picard C, Chansel M, Walter JE, Notarangelo LD, Butte MJ *et al* (2015) PRKDC mutations associated with immunodeficiency, granuloma, and autoimmune regulator-dependent autoimmunity. *J Allergy Clin Immunol* 135: 1578-1588 e1575
- Matthews AJ, Zheng S, DiMenna LJ, Chaudhuri J (2014) Regulation of immunoglobulin class-switch recombination: choreography of noncoding transcription, targeted DNA deamination, and long-range DNA repair. *Adv Immunol* 122: 1-57
- Mattiroli F, Vissers JH, van Dijk WJ, Ikpa P, Citterio E, Vermeulen W, Martejn JA, Sixma TK (2012) RNF168 ubiquitinates K13-15 on H2A/H2AX to drive DNA damage signaling. *Cell* 150: 1182-1195
- McBlane JF, van Gent DC, Ramsden DA, Romeo C, Cuomo CA, Gellert M, Oettinger MA (1995) Cleavage at a V(D)J recombination signal requires only RAG1 and RAG2 proteins and occurs in two steps. *Cell* 83: 387-395
- McBride WH, Schae D (2020) Radiation-induced tissue damage and response. *J Pathol* 250: 647-655
- Menolfi D, Zha S (2020) ATM, ATR and DNA-PKcs kinases—the lessons from the mouse models: inhibition ≠ deletion. *Cell & Bioscience* 10: 8
- Meynard G, Mansi L, Lebahar P, Villanueva C, Klajer E, Calcagno F, Vivalta A, Chaix M, Collonge-Rame MA, Populaire C *et al* (2017) First description of a double heterozygosity for BRCA1 and BRCA2 pathogenic variants in a French metastatic breast cancer patient: A case report. *Oncol Rep* 37: 1573-1578
- Mirman Z, Lottersberger F, Takai H, Kibe T, Gong Y, Takai K, Bianchi A, Zimmermann M, Durocher D, de Lange T (2018) 53BP1–RIF1–shieldin counteracts DSB resection through CST- and Pol α -dependent fill-in. *Nature* 560: 112-116
- Modrich P (2016) Mechanisms in E. coli and Human Mismatch Repair (Nobel Lecture). *Angew Chem Int Ed Engl* 55: 8490-8501

- Mombaerts P, Iacomini J, Johnson RS, Herrup K, Tonegawa S, Papaioannou VE (1992) RAG-1-deficient mice have no mature B and T lymphocytes. *Cell* 68: 869-877
- Monroe JG, Bannish G, Fuentes-Panana EM, King LB, Sandel PC, Chung J, Sater R (2003) Positive and negative selection during B lymphocyte development. *Immunologic Research* 27: 427-442
- Montecucco A, Zanetta F, Biamonti G (2015) Molecular mechanisms of etoposide. *EXCLI J* 14: 95-108
- Moon AF, Pryor JM, Ramsden DA, Kunkel TA, Bebenek K, Pedersen LC (2014) Sustained active site rigidity during synthesis by human DNA polymerase μ . *Nat Struct Mol Biol* 21: 253-260
- Morio T (2017) Recent advances in the study of immunodeficiency and DNA damage response. *Int J Hematol* 106: 357-365
- Moshous D, Callebaut I, de Chasseval R, Corneo B, Cavazzana-Calvo M, Le Deist F, Tezcan I, Sanal O, Bertrand Y, Philippe N *et al* (2001) Artemis, a novel DNA double-strand break repair/V(D)J recombination protein, is mutated in human severe combined immune deficiency. *Cell* 105: 177-186
- Muramatsu M, Kinoshita K, Fagarasan S, Yamada S, Shinkai Y, Honjo T (2000) Class switch recombination and hypermutation require activation-induced cytidine deaminase (AID), a potential RNA editing enzyme. *Cell* 102: 553-563
- Murga M, Bunting S, Montaña MF, Soria R, Mulero F, Cañamero M, Lee Y, McKinnon PJ, Nussenzweig A, Fernandez-Capetillo O (2009) A mouse model of ATR-Seckel shows embryonic replicative stress and accelerated aging. *Nature Genetics* 41: 891-898
- Murray JE, van der Burg M, H IJ, Carroll P, Wu Q, Ochi T, Leitch A, Miller ES, Kysela B, Jawad A *et al* (2015) Mutations in the NHEJ component XRCC4 cause primordial dwarfism. *Am J Hum Genet* 96: 412-424
- Murray V, Chen JK, Chung LH (2018) The Interaction of the Metallo-Glycopeptide Anti-Tumour Drug Bleomycin with DNA. *Int J Mol Sci* 19
- Musilli S, Abramowski V, Roch B, de Villartay JP (2020) An in vivo study of the impact of deficiency in the DNA repair proteins PAXX and XLF on development and maturation of the hemolymphoid system. *J Biol Chem* 295: 2398-2406
- Nakamura J, Walker VE, Upton PB, Chiang SY, Kow YW, Swenberg JA (1998) Highly sensitive apurinic/apyrimidinic site assay can detect spontaneous and chemically induced depurination under physiological conditions. *Cancer Res* 58: 222-225
- Noordermeer SM, Adam S, Setiapatra D, Barazas M, Pettitt SJ, Ling AK, Olivieri M, Alvarez-Quilon A, Moatti N, Zimmermann M *et al* (2018) The shieldin complex mediates 53BP1-dependent DNA repair. *Nature* 560: 117-121
- Noviski M, Mueller JL, Satterthwaite A, Garrett-Sinha LA, Brombacher F, Zikherman J (2018) IgM and IgD B cell receptors differentially respond to endogenous antigens and control B cell fate. *Elife* 7

Nowak-Wegrzyn A, Crawford TO, Winkelstein JA, Carson KA, Lederman HM (2004) Immunodeficiency and infections in ataxia-telangiectasia. *J Pediatr* 144: 505-511

Nowsheen S, Aziz K, Aziz A, Deng M, Qin B, Luo K, Jeganathan KB, Zhang H, Liu T, Yu J *et al* (2018) L3MBTL2 orchestrates ubiquitin signalling by dictating the sequential recruitment of RNF8 and RNF168 after DNA damage. *Nat Cell Biol* 20: 455-464

Nussenzweig A, Chen C, da Costa Soares V, Sanchez M, Sokol K, Nussenzweig MC, Li GC (1996) Requirement for Ku80 in growth and immunoglobulin V(D)J recombination. *Nature* 382: 551-555

O'Driscoll M, Cerosaletti KM, Girard PM, Dai Y, Stumm M, Kysela B, Hirsch B, Gennery A, Palmer SE, Seidel J *et al* (2001) DNA ligase IV mutations identified in patients exhibiting developmental delay and immunodeficiency. *Mol Cell* 8: 1175-1185

O'Driscoll M, Gennery AR, Seidel J, Concannon P, Jeggo PA (2004) An overview of three new disorders associated with genetic instability: LIG4 syndrome, RS-SCID and ATR-Seckel syndrome. *DNA Repair (Amst)* 3: 1227-1235

Ochi T, Blackford AN, Coates J, Jhujh S, Mehmood S, Tamura N, Travers J, Wu Q, Draviam VM, Robinson CV *et al* (2015) DNA repair. PAXX, a paralog of XRCC4 and XLF, interacts with Ku to promote DNA double-strand break repair. *Science* 347: 185-188

Oettinger MA, Schatz DG, Gorka C, Baltimore D (1990) RAG-1 and RAG-2, adjacent genes that synergistically activate V(D)J recombination. *Science* 248: 1517-1523

Oksenyich V, Alt FW, Kumar V, Schwer B, Wesemann DR, Hansen E, Patel H, Su A, Guo C (2012) Functional redundancy between repair factor XLF and damage response mediator 53BP1 in V(D)J recombination and DNA repair. *Proc Natl Acad Sci U S A* 109: 2455-2460

Oksenyich V, Bernardes de Jesus B, Zhovmer A, Egly JM, Coin F (2009) Molecular insights into the recruitment of TFIIF to sites of DNA damage. *EMBO J* 28: 2971-2980

Oksenyich V, Coin F (2010) The long unwinding road: XPB and XPD helicases in damaged DNA opening. *Cell Cycle* 9: 90-96

Oksenyich V, Kainov DE (2021) DNA Damage Response. *Biomolecules* 11: 123

Oksenyich V, Kumar V, Liu X, Guo C, Schwer B, Zha S, Alt FW (2013a) Functional redundancy between the XLF and DNA-PKcs DNA repair factors in V(D)J recombination and nonhomologous DNA end joining. *Proc Natl Acad Sci U S A* 110: 2234-2239

Oksenyich V, Su D, Daniel JA (2022) Acetyltransferases GCN5 and PCAF Are Required for B Lymphocyte Maturation in Mice. *Biomolecules* 12

Oksenyich V, Zhovmer A, Ziani S, Mari PO, Eberova J, Nardo T, Stefanini M, Giglia-Mari G, Egly JM, Coin F (2013b) Histone methyltransferase DOT1L drives recovery of gene expression after a genotoxic attack. *PLoS Genet* 9: e1003611

OPCW (2021) Conference of the States Parties Setting the OPCW's strategic direction. <https://www.opcw.org/about/conference-states-parties>

- Oster S, Aqeilan RI (2020) Programmed DNA Damage and Physiological DSBs: Mapping, Biological Significance and Perturbations in Disease States. *Cells* 9
- Ouyang H, Nussenzweig A, Kurimasa A, Soares VC, Li X, Cordon-Cardo C, Li W, Cheong N, Nussenzweig M, Iliakis G *et al* (1997) Ku70 is required for DNA repair but not for T cell antigen receptor gene recombination In vivo. *J Exp Med* 186: 921-929
- Pan-Hammarström Q, Zhao Y, Hammarström L (2007) Class switch recombination: a comparison between mouse and human. *Adv Immunol* 93: 1-61
- Panahi Y, Fattahi A, Nejabat HR, Abroon S, Latifi Z, Akbarzadeh A, Ghasemnejad T (2018) DNA repair mechanisms in response to genotoxicity of warfare agent sulfur mustard. *Environ Toxicol Pharmacol* 58: 230-236
- Panchakshari RA, Zhang X, Kumar V, Du Z, Wei PC, Kao J, Dong J, Alt FW (2018) DNA double-strand break response factors influence end-joining features of IgH class switch and general translocation junctions. *Proc Natl Acad Sci U S A* 115: 762-767
- Pannicke U, Honig M, Schulze I, Rohr J, Heinz GA, Braun S, Janz I, Rump EM, Seidel MG, Matthes-Martin S *et al* (2010) The most frequent DCLRE1C (ARTEMIS) mutations are based on homologous recombination events. *Hum Mutat* 31: 197-207
- Pannunzio NR, Watanabe G, Lieber MR (2018) Nonhomologous DNA end-joining for repair of DNA double-strand breaks. *J Biol Chem* 293: 10512-10523
- Paris Ü, Mikkel K, Tavita K, Saumaa S, Teras R, Kivisaar M (2015) NHEJ enzymes LigD and Ku participate in stationary-phase mutagenesis in *Pseudomonas putida*. *DNA Repair* 31: 11-18
- Patton DT, Plumb AW, Abraham N (2014) The Survival and Differentiation of Pro-B and Pre-B Cells in the Bone Marrow Is Dependent on IL-7R α Tyr⁴⁴⁹. *The Journal of Immunology* 193: 3446-3455
- Pecina-Slaus N, Kafka A, Salamon I, Bukovac A (2020) Mismatch Repair Pathway, Genome Stability and Cancer. *Front Mol Biosci* 7: 122
- Perkins EJ, Nair A, Cowley DO, Van Dyke T, Chang Y, Ramsden DA (2002) Sensing of intermediates in V(D)J recombination by ATM. *Genes & development* 16: 159-164
- Perlman RL (2016) Mouse models of human disease: An evolutionary perspective. *Evol Med Public Health* 2016: 170-176
- Petersen S, Casellas R, Reina-San-Martin B, Chen HT, Difilippantonio MJ, Wilson PC, Hanitsch L, Celeste A, Muramatsu M, Pilch DR *et al* (2001) AID is required to initiate Nbs1/ γ -H2AX focus formation and mutations at sites of class switching. *Nature* 414: 660-665
- Pilger D, Seymour LW, Jackson SP (2021) Interfaces between cellular responses to DNA damage and cancer immunotherapy. *Genes Dev* 35: 602-618
- Polyak K, Garber J (2011) Targeting the missing links for cancer therapy. *Nat Med* 17: 283-284

- Prindle MJ, Loeb LA (2012) DNA polymerase delta in DNA replication and genome maintenance. *Environ Mol Mutagen* 53: 666-682
- Ragunathan K, Upfold NLE, Oksenysh V (2020) Interaction between Fibroblasts and Immune Cells Following DNA Damage Induced by Ionizing Radiation. *International Journal of Molecular Sciences* 21: 8635
- Ranjha L, Howard SM, Cejka P (2018) Main steps in DNA double-strand break repair: an introduction to homologous recombination and related processes. *Chromosoma* 127: 187-214
- Rastogi RP, Richa, Kumar A, Tyagi MB, Sinha RP (2010) Molecular mechanisms of ultraviolet radiation-induced DNA damage and repair. *J Nucleic Acids* 2010: 592980
- Recio MJ, Dominguez-Pinilla N, Perrig MS, Rodriguez Vigil-Iturrate C, Salmon-Rodriguez N, Martinez Faci C, Castro-Panete MJ, Blas-Espada J, Lopez-Nevado M, Ruiz-Garcia R *et al* (2018) Extreme Phenotypes With Identical Mutations: Two Patients With Same Non-sense NHEJ1 Homozygous Mutation. *Front Immunol* 9: 2959
- Reid DA, Keegan S, Leo-Macias A, Watanabe G, Strande NT, Chang HH, Oksuz BA, Fenyo D, Lieber MR, Ramsden DA *et al* (2015) Organization and dynamics of the nonhomologous end-joining machinery during DNA double-strand break repair. *Proc Natl Acad Sci U S A* 112: E2575-2584
- Reina-San-Martin B, Chen HT, Nussenzweig A, Nussenzweig MC (2004) ATM is required for efficient recombination between immunoglobulin switch regions. *J Exp Med* 200: 1103-1110
- Reina-San-Martin B, Difilippantonio S, Hanitsch L, Masilamani RF, Nussenzweig A, Nussenzweig MC (2003) H2AX is required for recombination between immunoglobulin switch regions but not for intra-switch region recombination or somatic hypermutation. *J Exp Med* 197: 1767-1778
- Reyhanoglu G, Tadi P (2021) Etoposide. In: *StatPearls*, Treasure Island (FL)
- Reynolds P, Anderson JA, Harper JV, Hill MA, Botchway SW, Parker AW, O'Neill P (2012) The dynamics of Ku70/80 and DNA-PKcs at DSBs induced by ionizing radiation is dependent on the complexity of damage. *Nucleic Acids Res* 40: 10821-10831
- Rhoads CP (1946) Nitrogen mustards in the treatment of neoplastic disease; official statement. *J Am Med Assoc* 131: 656-658
- Riballo E, Critchlow SE, Teo SH, Doherty AJ, Priestley A, Broughton B, Kysela B, Beamish H, Plowman N, Arlett CF *et al* (1999) Identification of a defect in DNA ligase IV in a radiosensitive leukaemia patient. *Curr Biol* 9: 699-702
- Rivera-Munoz P, Soulas-Sprauel P, Le Guyader G, Abramowski V, Bruneau S, Fischer A, Pâques F, de Villartay JP (2009) Reduced immunoglobulin class switch recombination in the absence of Artemis. *Blood* 114: 3601-3609
- Roch B, Abramowski V, Chaumeil J, de Villartay JP (2019) Cernunnos/Xlf Deficiency Results in Suboptimal V(D)J Recombination and Impaired Lymphoid Development in Mice. *Front Immunol* 10: 443

- Roch B, Abramowski V, Etienne O, Musilli S, David P, Charbonnier J-B, Callebaut I, Boussin FD, de Villartay J-P (2021) A XRCC4 mutant mouse, a model for human X4 syndrome, reveals interplays with Xlf, PAXX, and ATM in lymphoid development. *eLife* 10: e69353
- Rogakou EP, Pilch DR, Orr AH, Ivanova VS, Bonner WM (1998) DNA double-stranded breaks induce histone H2AX phosphorylation on serine 139. *J Biol Chem* 273: 5858-5868
- Rogier M, Moritz J, Robert I, Lescale C, Heyer V, Abello A, Martin O, Capitani K, Thomas M, Thomas-Claudepierre A-S *et al* (2021) Fam72a enforces error-prone DNA repair during antibody diversification. *Nature* 600: 329-333
- Rooney S, Sekiguchi J, Zhu C, Cheng HL, Manis J, Whitlow S, DeVido J, Foy D, Chaudhuri J, Lombard D *et al* (2002) Leaky Scid phenotype associated with defective V(D)J coding end processing in Artemis-deficient mice. *Mol Cell* 10: 1379-1390
- Ropars V, Drevet P, Legrand P, Baconnais S, Amram J, Faure G, Marquez JA, Pietrement O, Guerois R, Callebaut I *et al* (2011) Structural characterization of filaments formed by human Xrcc4-Cernunnos/XLF complex involved in nonhomologous DNA end-joining. *Proc Natl Acad Sci U S A* 108: 12663-12668
- Ropke C, Hougén HP, Everett NB (1975) Long-lived T and B lymphocytes in the bone marrow and thoracic duct lymph of the mouse. *Cell Immunol* 15: 82-93
- Rose M, Burgess JT, O'Byrne K, Richard DJ, Bolderson E (2020) PARP Inhibitors: Clinical Relevance, Mechanisms of Action and Tumor Resistance. *Front Cell Dev Biol* 8: 564601
- Rosin N, Elcioglu NH, Beleggia F, Isguven P, Altmüller J, Thiele H, Steindl K, Joset P, Rauch A, Nurnberg P *et al* (2015) Mutations in XRCC4 cause primary microcephaly, short stature and increased genomic instability. *Hum Mol Genet* 24: 3708-3717
- Rouaud P, Saintamand A, Saad F, Carrion C, Lecardeur S, Cogné M, Denizot Y (2014) Elucidation of the enigmatic IgD class-switch recombination via germline deletion of the IgH 3' regulatory region. *Journal of Experimental Medicine* 211: 975-985
- Roy S (2017) Impact of UV Radiation on Genome Stability and Human Health. *Adv Exp Med Biol* 996: 207-219
- Rucci F, Notarangelo LD, Fazeli A, Patrizi L, Hickernell T, Paganini T, Coakley KM, Detre C, Keszei M, Walter JE *et al* (2010) Homozygous DNA ligase IV R278H mutation in mice leads to leaky SCID and represents a model for human LIG4 syndrome. *Proceedings of the National Academy of Sciences* 107: 3024-3029
- Saha T, Sundaravinayagam D, Di Virgilio M (2021) Charting a DNA Repair Roadmap for Immunoglobulin Class Switch Recombination. *Trends Biochem Sci* 46: 184-199
- Saleh-Gohari N, Helleday T (2004) Conservative homologous recombination preferentially repairs DNA double-strand breaks in the S phase of the cell cycle in human cells. *Nucleic Acids Res* 32: 3683-3688
- Sallmyr A, Tomkinson AE (2018) Repair of DNA double-strand breaks by mammalian alternative end-joining pathways. *J Biol Chem* 293: 10536-10546

- San Filippo J, Sung P, Klein H (2008) Mechanism of eukaryotic homologous recombination. *Annu Rev Biochem* 77: 229-257
- Santos MA, Huen MS, Jankovic M, Chen HT, Lopez-Contreras AJ, Klein IA, Wong N, Barbancho JL, Fernandez-Capetillo O, Nussenzweig MC *et al* (2010) Class switching and meiotic defects in mice lacking the E3 ubiquitin ligase RNF8. *J Exp Med* 207: 973-981
- Savitsky K, Bar-Shira A, Gilad S, Rotman G, Ziv Y, Vanagaite L, Tagle DA, Smith S, Uziel T, Sfez S *et al* (1995) A single ataxia telangiectasia gene with a product similar to PI-3 kinase. *Science* 268: 1749-1753
- Schatz DG, Ji Y (2011) Recombination centres and the orchestration of V(D)J recombination. *Nat Rev Immunol* 11: 251-263
- Schatz DG, Swanson PC (2011) V(D)J recombination: mechanisms of initiation. *Annu Rev Genet* 45: 167-202
- Schimmel J, Munoz-Subirana N, Kool H, van Schendel R, Tijsterman M (2021) Small tandem DNA duplications result from CST-guided Pol alpha-primase action at DNA break termini. *Nat Commun* 12: 4843
- Schwer B, Wei PC, Chang AN, Kao J, Du Z, Meyers RM, Alt FW (2016) Transcription-associated processes cause DNA double-strand breaks and translocations in neural stem/progenitor cells. *Proc Natl Acad Sci U S A* 113: 2258-2263
- Scully R, Panday A, Elango R, Willis NA (2019) DNA double-strand break repair-pathway choice in somatic mammalian cells. *Nat Rev Mol Cell Biol* 20: 698-714
- Sekiguchi J, Ferguson DO, Chen HT, Yang EM, Earle J, Frank K, Whitlow S, Gu Y, Xu Y, Nussenzweig A *et al* (2001) Genetic interactions between ATM and the nonhomologous end-joining factors in genomic stability and development. *Proc Natl Acad Sci U S A* 98: 3243-3248
- Sekine S, Mori T, Ogawa R, Tanaka M, Yoshida H, Taniguchi H, Nakajima T, Sugano K, Yoshida T, Kato M *et al* (2017) Mismatch repair deficiency commonly precedes adenoma formation in Lynch Syndrome-Associated colorectal tumorigenesis. *Mod Pathol* 30: 1144-1151
- Setiaputra D, Durocher D (2019) Shieldin - the protector of DNA ends. *EMBO Rep* 20
- Shang Y, Meng FL (2021) Repair of programmed DNA lesions in antibody class switch recombination: common and unique features. *Genome Instab Dis*: 1-11
- Sharda M, Badrinarayanan A, Seshasayee ASN (2020) Evolutionary and Comparative Analysis of Bacterial Nonhomologous End Joining Repair. *Genome Biology and Evolution* 12: 2450-2466
- Sharif H, Li Y, Dong Y, Dong L, Wang WL, Mao Y, Wu H (2017) Cryo-EM structure of the DNA-PK holoenzyme. *Proceedings of the National Academy of Sciences* 114: 7367-7372
- Sheikh F, Hawwari A, Alhissi S, Al Gazlan S, Al Dhekri H, Rehan Khaliq AM, Borrero E, El-Baik L, Arnaout R, Al-Mousa H *et al* (2017) Loss of NHEJ1 Protein Due to a Novel Splice

Site Mutation in a Family Presenting with Combined Immunodeficiency, Microcephaly, and Growth Retardation and Literature Review. *J Clin Immunol* 37: 575-581

Shen HM, Wuerffel R, Cantillo JF, Priyadarshi S, Lei X, Liang J, Wu YL, Kenter AL (2021) Loop extrusion promotes an alternate pathway for isotype switching. *Cell Reports* 37: 110059

Shiloh Y, Ziv Y (2013) The ATM protein kinase: regulating the cellular response to genotoxic stress, and more. *Nat Rev Mol Cell Biol* 14: 197-210

Shinkai Y, Rathbun G, Lam KP, Oltz EM, Stewart V, Mendelsohn M, Charron J, Datta M, Young F, Stall AM *et al* (1992) RAG-2-deficient mice lack mature lymphocytes owing to inability to initiate V(D)J rearrangement. *Cell* 68: 855-867

Shirodkar P, Fenton AL, Meng L, Koch CA (2013) Identification and functional characterization of a Ku-binding motif in aprataxin polynucleotide kinase/phosphatase-like factor (APLF). *J Biol Chem* 288: 19604-19613

Singh RK, Kumar S, Prasad DN, Bhardwaj TR (2018) Therapeutic journey of nitrogen mustard as alkylating anticancer agents: Historic to future perspectives. *Eur J Med Chem* 151: 401-433

Slavoff SA, Heo J, Budnik BA, Hanakahi LA, Saghatelian A (2014) A human short open reading frame (sORF)-encoded polypeptide that stimulates DNA end joining. *J Biol Chem* 289: 10950-10957

Soulas-Spraul P, Le Guyader G, Rivera-Munoz P, Abramowski V, Olivier-Martin C, Goujet-Zalc C, Charneau P, de Villartay JP (2007) Role for DNA repair factor XRCC4 in immunoglobulin class switch recombination. *J Exp Med* 204: 1717-1727

Srinivas US, Tan BWQ, Vellayappan BA, Jeyasekharan AD (2019) ROS and the DNA damage response in cancer. *Redox Biol* 25: 101084

Stavnezer J, Schrader CE (2014) IgH chain class switch recombination: mechanism and regulation. *J Immunol* 193: 5370-5378

Stewart GS, Panier S, Townsend K, Al-Hakim AK, Kolas NK, Miller ES, Nakada S, Ylanko J, Olivarius S, Mendez M *et al* (2009) The RIDDLE syndrome protein mediates a ubiquitin-dependent signaling cascade at sites of DNA damage. *Cell* 136: 420-434

Stewart GS, Stankovic T, Byrd PJ, Wechsler T, Miller ES, Huissoon A, Drayson MT, West SC, Elledge SJ, Taylor AM (2007) RIDDLE immunodeficiency syndrome is linked to defects in 53BP1-mediated DNA damage signaling. *Proc Natl Acad Sci U S A* 104: 16910-16915

Stucki M, Clapperton JA, Mohammad D, Yaffe MB, Smerdon SJ, Jackson SP (2005) MDC1 directly binds phosphorylated histone H2AX to regulate cellular responses to DNA double-strand breaks. *Cell* 123: 1213-1226

Su SS, Modrich P (1986) Escherichia coli mutS-encoded protein binds to mismatched DNA base pairs. *Proc Natl Acad Sci U S A* 83: 5057-5061

Sung-Lim Y, Sung-Keun L (2017) Ultraviolet radiation: DNA damage, repair, and human disorders. *Mol Cell Toxicol* 13: 21-28

- Sutton BJ, Davies AM, Bax HJ, Karagiannis SN (2019) IgE Antibodies: From Structure to Function and Clinical Translation. *Antibodies (Basel)* 8
- Taccioli GE, Amatucci AG, Beamish HJ, Gell D, Xiang XH, Torres Arzayus MI, Priestley A, Jackson SP, Marshak Rothstein A, Jeggo PA *et al* (1998) Targeted disruption of the catalytic subunit of the DNA-PK gene in mice confers severe combined immunodeficiency and radiosensitivity. *Immunity* 9: 355-366
- Tanaka M, Takahara M, Nukina K, Hayashi A, Sakai W, Sugasawa K, Shiomi Y, Nishitani H (2017) Mismatch repair proteins recruited to ultraviolet light-damaged sites lead to degradation of licensing factor Cdt1 in the G1 phase. *Cell Cycle* 16: 673-684
- Tang M, Li S, Chen J (2021) Ubiquitylation in DNA double-strand break repair. *DNA Repair (Amst)* 103: 103129
- Taskiran EZ, Sonmez HE, Kosukcu C, Tavukcuoglu E, Yazici G, Esendagli G, Batu ED, Kiper POS, Bilginer Y, Alikasifoglu M *et al* (2019) A Novel Missense LIG4 Mutation in a Patient With a Phenotype Mimicking Behcet's Disease. *J Clin Immunol* 39: 99-105
- Tauchi H, Matsuura S, Kobayashi J, Sakamoto S, Komatsu K (2002) Nijmegen breakage syndrome gene, NBS1, and molecular links to factors for genome stability. *Oncogene* 21: 8967-8980
- Taylor AM, Groom A, Byrd PJ (2004) Ataxia-telangiectasia-like disorder (ATLD)-its clinical presentation and molecular basis. *DNA Repair (Amst)* 3: 1219-1225
- Thompson PS, Cortez D (2020) New insights into abasic site repair and tolerance. *DNA repair* 90: 102866-102866
- Tomida J, Takata KI, Bhetawal S, Person MD, Chao HP, Tang DG, Wood RD (2018) FAM35A associates with REV7 and modulates DNA damage responses of normal and BRCA1-defective cells. *Embo j* 37
- Tough DF, Sprent J (1994) Turnover of naive- and memory-phenotype T cells. *J Exp Med* 179: 1127-1135
- Tough DF, Sprent J (1995) Life span of naive and memory T cells. *Stem Cells* 13: 242-249
- Triest BV, Damstrup L, Falkenius J, Budach V, Troost E, Samuels M, Goddemeier T, Geertsen PF (2017) A phase Ia/Ib trial of the DNA-dependent protein kinase inhibitor (DNA-PKi) M3814 in combination with radiotherapy in patients with advanced solid tumors. *Journal of Clinical Oncology* 35: e14048-e14048
- Tsai CJ, Kim SA, Chu G (2007) Cernunnos/XLF promotes the ligation of mismatched and noncohesive DNA ends. *Proc Natl Acad Sci U S A* 104: 7851-7856
- Tsutsui H, Kinugawa S, Matsushima S (2011) Oxidative stress and heart failure. *Am J Physiol Heart Circ Physiol* 301: H2181-2190
- Tubbs A, Nussenzweig A (2017) Endogenous DNA Damage as a Source of Genomic Instability in Cancer. *Cell* 168: 644-656

Uchisaka N, Takahashi N, Sato M, Kikuchi A, Mochizuki S, Imai K, Nonoyama S, Ohara O, Watanabe F, Mizutani S *et al* (2009) Two brothers with ataxia-telangiectasia-like disorder with lung adenocarcinoma. *J Pediatr* 155: 435-438

UN (2021) Chemical Weapons. <https://www.un.org/disarmament/wmd/chemical/>

van der Burg M, Ijspeert H, Verkaik NS, Turul T, Wiegant WW, Morotomi-Yano K, Mari PO, Tezcan I, Chen DJ, Zdzienicka MZ *et al* (2009) A DNA-PKcs mutation in a radiosensitive T-B-SCID patient inhibits Artemis activation and nonhomologous end-joining. *J Clin Invest* 119: 91-98

van der Burg M, van Veelen LR, Verkaik NS, Wiegant WW, Hartwig NG, Barendregt BH, Brugmans L, Raams A, Jaspers NG, Zdzienicka MZ *et al* (2006) A new type of radiosensitive T-B-NK⁺ severe combined immunodeficiency caused by a LIG4 mutation. *J Clin Invest* 116: 137-145

van Kan M, Burns KE, Helsby NA (2021) A systematic review of inter-individual differences in the DNA repair processes involved in melphalan monoadduct repair in relation to treatment outcomes. *Cancer Chemotherapy and Pharmacology*

Vera G, Rivera-Munoz P, Abramowski V, Malivert L, Lim A, Bole-Feysot C, Martin C, Florkin B, Latour S, Revy P *et al* (2013) Cernunnos deficiency reduces thymocyte life span and alters the T cell repertoire in mice and humans. *Mol Cell Biol* 33: 701-711

Vidarsson G, Dekkers G, Rispens T (2014) IgG subclasses and allotypes: from structure to effector functions. *Front Immunol* 5: 520

Vietri MT, Molinari AM, Caliendo G, De Paola ML, Giovanna D, Gambardella AL, Petronella P, Cioffi M (2013) Double heterozygosity in the BRCA1 and BRCA2 genes in Italian family. *Clin Chem Lab Med* 51: 2319-2324

Villa A, Sobacchi C, Notarangelo LD, Bozzi F, Abinun M, Abrahamsen TG, Arkwright PD, Baniyash M, Brooks EG, Conley ME *et al* (2001) V(D)J recombination defects in lymphocytes due to RAG mutations: severe immunodeficiency with a spectrum of clinical presentations. *Blood* 97: 81-88

Visani G, Loscocco F, Bagaloni I, Ruzzo A, Fuligni F, Graziano F, Magnani M, Isidori A (2020) XRCC1 399GG genotype predicts significantly longer overall survival in resistant lymphoma patients treated with Benda-EAM and ASCT. *Bone Marrow Transplantation* 55: 818-820

Walker JR, Corpina RA, Goldberg J (2001) Structure of the Ku heterodimer bound to DNA and its implications for double-strand break repair. *Nature* 412: 607-614

Walters R, Kalb R, Gatei M, Kijas AW, Stumm M, Sobeck A, Wieland B, Varon R, Lerenthal Y, Lavin MF *et al* (2009) Human RAD50 deficiency in a Nijmegen breakage syndrome-like disorder. *Am J Hum Genet* 84: 605-616

Wang J, Aroumougame A, Lobrich M, Li Y, Chen D, Chen J, Gong Z (2014) PTIP associates with Artemis to dictate DNA repair pathway choice. *Genes Dev* 28: 2693-2698

- Wang K, Wei G, Liu D (2012) CD19: a biomarker for B cell development, lymphoma diagnosis and therapy. *Exp Hematol Oncol* 1: 36
- Wang L, Wuerffel R, Feldman S, Khamlichi AA, Kenter AL (2009) S region sequence, RNA polymerase II, and histone modifications create chromatin accessibility during class switch recombination. *J Exp Med* 206: 1817-1830
- Wang M, Wei PC, Lim CK, Gallina IS, Marshall S, Marchetto MC, Alt FW, Gage FH (2020a) Increased Neural Progenitor Proliferation in a hiPSC Model of Autism Induces Replication Stress-Associated Genome Instability. *Cell Stem Cell* 26: 221-233 e226
- Wang XS, Lee BJ, Zha S (2020b) The recent advances in non-homologous end-joining through the lens of lymphocyte development. *DNA Repair (Amst)* 94: 102874
- Wang Y, Liu J, Burrows PD, Wang J-Y (2020c) B Cell Development and Maturation. In: *B Cells in Immunity and Tolerance*, Wang J.-Y. (ed.) pp. 1-22. Springer Singapore: Singapore
- Ward IM, Reina-San-Martin B, Oлару A, Minn K, Tamada K, Lau JS, Cascalho M, Chen L, Nussenzweig A, Livak F *et al* (2004) 53BP1 is required for class switch recombination. *J Cell Biol* 165: 459-464
- Weemaes C, Hustinx T, Van Munster P, Bakkeren J, Taalman R (1981) A new chromosomal instability disorder: the Nijmegen breakage syndrome. *Acta Paediatr Scand* 70: 557-564
- Wei PC, Chang AN, Kao J, Du Z, Meyers RM, Alt FW, Schwer B (2016) Long Neural Genes Harbor Recurrent DNA Break Clusters in Neural Stem/Progenitor Cells. *Cell* 164: 644-655
- Wilson A, Held W, MacDonald HR (1994) Two waves of recombinase gene expression in developing thymocytes. *The Journal of experimental medicine* 179: 1355-1360
- Woodbine L, Neal JA, Sasi NK, Shimada M, Deem K, Coleman H, Dobyns WB, Ogi T, Meek K, Davies EG *et al* (2013) PRKDC mutations in a SCID patient with profound neurological abnormalities. *J Clin Invest* 123: 2969-2980
- Woods D, Turchi JJ (2013) Chemotherapy induced DNA damage response: convergence of drugs and pathways. *Cancer Biol Ther* 14: 379-389
- Xing M, Bjoras M, Daniel JA, Alt FW, Oksenysh V (2017) Synthetic lethality between murine DNA repair factors XLF and DNA-PKcs is rescued by inactivation of Ku70. *DNA Repair (Amst)* 57: 133-138
- Xing M, Oksenysh V (2019) Genetic interaction between DNA repair factors PAXX, XLF, XRCC4 and DNA-PKcs in human cells. *FEBS Open Bio* 9: 1315-1326
- Xing M, Yang M, Huo W, Feng F, Wei L, Jiang W, Ning S, Yan Z, Li W, Wang Q *et al* (2015) Interactome analysis identifies a new paralogue of XRCC4 in non-homologous end joining DNA repair pathway. *Nat Commun* 6: 6233
- Xu W, Edmondson DG, Evrard YA, Wakamiya M, Behringer RR, Roth SY (2000) Loss of Gcn5l2 leads to increased apoptosis and mesodermal defects during mouse development. *Nature Genetics* 26: 229-232

- Xu Y, Ashley T, Brainerd EE, Bronson RT, Meyn MS, Baltimore D (1996) Targeted disruption of ATM leads to growth retardation, chromosomal fragmentation during meiosis, immune defects, and thymic lymphoma. *Genes Dev* 10: 2411-2422
- Xu Y, Zhou H, Post G, Zan H, Casali P (2021) Rad52 mediates class-switch DNA recombination to IgD. *bioRxiv*: 2021.2006.2028.450246
- Xu Z, Zan H, Pone EJ, Mai T, Casali P (2012) Immunoglobulin class-switch DNA recombination: induction, targeting and beyond. *Nat Rev Immunol* 12: 517-531
- Yan CT, Boboila C, Souza EK, Franco S, Hickernell TR, Murphy M, Gumaste S, Geyer M, Zarrin AA, Manis JP *et al* (2007) IgH class switching and translocations use a robust non-classical end-joining pathway. *Nature* 449: 478-482
- Yang D, Sun Y, Chen J, Zhang Y, Fan S, Huang M, Xie X, Cai Y, Shang Y, Gui T *et al* (2020) REV7 is required for processing AID initiated DNA lesions in activated B cells. *Nature Communications* 11: 2812
- Yannoutsos N, Wilson P, Yu W, Chen HT, Nussenzweig A, Petrie H, Nussenzweig MC (2001) The role of recombination activating gene (RAG) reinduction in thymocyte development in vivo. *The Journal of experimental medicine* 194: 471-480
- Yano K, Morotomi-Yano K, Wang SY, Uematsu N, Lee KJ, Asaithamby A, Weterings E, Chen DJ (2008) Ku recruits XLF to DNA double-strand breaks. *EMBO Rep* 9: 91-96
- Yap TA, Plummer R, Azad NS, Helleday T (2019) The DNA Damaging Revolution: PARP Inhibitors and Beyond. *Am Soc Clin Oncol Educ Book* 39: 185-195
- Yatim KM, Lakkis FG (2015) A brief journey through the immune system. *Clin J Am Soc Nephrol* 10: 1274-1281
- Yi C, He C (2013) DNA repair by reversal of DNA damage. *Cold Spring Harb Perspect Biol* 5: a012575
- Yu J, Qin B, Lou Z (2020) Ubiquitin and ubiquitin-like molecules in DNA double strand break repair. *Cell Biosci* 10: 13
- Yu K, Lieber MR (2019) Current insights into the mechanism of mammalian immunoglobulin class switch recombination. *Crit Rev Biochem Mol Biol* 54: 333-351
- Yui MA, Feng N, Rothenberg EV (2010) Fine-scale staging of T cell lineage commitment in adult mouse thymus. *Journal of immunology (Baltimore, Md : 1950)* 185: 284-293
- Zahid S, Seif El Dahan M, Iehl F, Fernandez-Varela P, Le Du M-H, Ropars V, Charbonnier JB (2021) The Multifaceted Roles of Ku70/80. *International journal of molecular sciences* 22: 4134
- Zha S, Alt FW, Cheng HL, Brush JW, Li G (2007) Defective DNA repair and increased genomic instability in Cernunnos-XLF-deficient murine ES cells. *Proc Natl Acad Sci U S A* 104: 4518-4523

Zha S, Guo C, Boboila C, Oksenyich V, Cheng HL, Zhang Y, Wesemann DR, Yuen G, Patel H, Goff PH *et al* (2011) ATM damage response and XLF repair factor are functionally redundant in joining DNA breaks. *Nature* 469: 250-254

Zha S, Sekiguchi J, Brush JW, Bassing CH, Alt FW (2008) Complementary functions of ATM and H2AX in development and suppression of genomic instability. *Proc Natl Acad Sci U S A* 105: 9302-9306

Zhang X, Zhang Y, Ba Z, Kyritsis N, Casellas R, Alt FW (2019a) Fundamental roles of chromatin loop extrusion in antibody class switching. *Nature* 575: 385-389

Zhang Y, Zhang X, Ba Z, Liang Z, Dring EW, Hu H, Lou J, Kyritsis N, Zurita J, Shamim MS *et al* (2019b) The fundamental role of chromatin loop extrusion in physiological V(D)J recombination. *Nature* 573: 600-604

Zhang Y, Zhang X, Dai HQ, Hu H, Alt FW (2022) The role of chromatin loop extrusion in antibody diversification. *Nat Rev Immunol*

Zhao B, Watanabe G, Morten MJ, Reid DA, Rothenberg E, Lieber MR (2019) The essential elements for the noncovalent association of two DNA ends during NHEJ synapsis. *Nat Commun* 10: 3588

Zhao L, Bao C, Shang Y, He X, Ma C, Lei X, Mi D, Sun Y (2020) The Determinant of DNA Repair Pathway Choices in Ionising Radiation-Induced DNA Double-Strand Breaks. *Biomed Res Int* 2020: 4834965

Zhao X, Wei C, Li J, Xing P, Li J, Zheng S, Chen X (2017) Cell cycle-dependent control of homologous recombination. *Acta Biochim Biophys Sin (Shanghai)* 49: 655-668

Zhovmer A, Oksenyich V, Coin F (2010) Two sides of the same coin: TFIIH complexes in transcription and DNA repair. *ScientificWorldJournal* 10: 633-643

Zhu C, Bogue MA, Lim D-S, Hasty P, Roth DB (1996a) Ku86-Deficient Mice Exhibit Severe Combined Immunodeficiency and Defective Processing of V(D)J Recombination Intermediates. *Cell* 86: 379-389

Zhu C, Bogue MA, Lim DS, Hasty P, Roth DB (1996b) Ku86-deficient mice exhibit severe combined immunodeficiency and defective processing of V(D)J recombination intermediates. *Cell* 86: 379-389



Zhu J (2018) T Helper Cell Differentiation, Heterogeneity, and Plasticity. *Cold Spring Harbor perspectives in biology* 10: a030338

7. PAPERS I-III

PAPER I

Article

Generation of a Mouse Model Lacking the Non-Homologous End-Joining Factor Mri/Cyren

Sergio Castañeda-Zegarra ^{1,2,†} , Camilla Huse ^{1,2,†}, Øystein Røsand ^{1,2,†}, Antonio Sarno ^{1,2}, Mengtan Xing ^{1,2}, Raquel Gago-Fuentes ^{1,2}, Qindong Zhang ^{1,2}, Amin Alirezaylavasani ^{1,2}, Julia Werner ^{1,2,3}, Ping Ji ¹, Nina-Beate Liabakk ¹, Wei Wang ¹, Magnar Bjorås ^{1,2} and Valentyn Oksenyich ^{1,2,4,*} 

¹ Department of Clinical and Molecular Medicine (IKOM), Norwegian University of Science and Technology, 7491 Trondheim, Norway; sergio.m.c.zegarra@ntnu.no (S.C.-Z.); camilhus@stud.ntnu.no (C.H.); oystein.rosand@ntnu.no (Ø.R.); antonio.sarno@ntnu.no (A.S.); mengtan.xing@ntnu.no (M.X.); raquel.gago-fuentes@ntnu.no (R.G.-F.); qindongz@stud.ntnu.no (Q.Z.); aminalir@stud.ntnu.no (A.A.); julia.werner@stud.uni-heidelberg.de (J.W.); ping.ji@ntnu.no (P.J.); nina.beate.liabakk@ntnu.no (N.-B.L.); wei.wang@ntnu.no (W.W.); magnar.bjoras@ntnu.no (M.B.)

² St. Olavs Hospital, Trondheim University Hospital, Clinic of Medicine, Postboks 3250, Sluppen, 7006 Trondheim, Norway

³ Molecular Biotechnology MS programme, Heidelberg University, 69120 Heidelberg, Germany

⁴ Department of Biosciences and Nutrition (BioNut), Karolinska Institutet, 14183 Huddinge, Sweden

* Correspondence: valentyn.oksenych@ntnu.no; Tel.: +47-913-43-084

† These authors contributed equally to this work.

Received: 7 November 2019; Accepted: 26 November 2019; Published: 28 November 2019



Abstract: Classical non-homologous end joining (NHEJ) is a molecular pathway that detects, processes, and ligates DNA double-strand breaks (DSBs) throughout the cell cycle. Mutations in several NHEJ genes result in neurological abnormalities and immunodeficiency both in humans and mice. The NHEJ pathway is required for V(D)J recombination in developing B and T lymphocytes, and for class switch recombination in mature B cells. The Ku heterodimer formed by Ku70 and Ku80 recognizes DSBs and facilitates the recruitment of accessory factors (e.g., DNA-PKcs, Artemis, Paxx and Mri/Cyren) and downstream core factor subunits X-ray repair cross-complementing group 4 (XRCC4), XRCC4-like factor (XLF), and DNA ligase 4 (Lig4). Accessory factors might be dispensable for the process, depending on the genetic background and DNA lesion type. To determine the physiological role of Mri in DNA repair and development, we introduced a frame-shift mutation in the Mri gene in mice. We then analyzed the development of *Mri*-deficient mice as well as wild type and immunodeficient controls. Mice lacking Mri possessed reduced levels of class switch recombination in B lymphocytes and slow proliferation of neuronal progenitors when compared to wild type littermates. Human cell lines lacking Mri were as sensitive to DSBs as the wild type controls. Overall, we concluded that Mri/Cyren is largely dispensable for DNA repair and mouse development.

Keywords: NHEJ; double-strand breaks; mouse model; lymphocyte; neurodevelopment

1. Introduction

Non-homologous end-joining (NHEJ) is a molecular pathway that recognizes, processes, and repairs DNA double-strand breaks (DSBs) throughout the cell cycle [1]. Core NHEJ factors Ku70 and Ku80 form heterodimer (Ku) that is rapidly associated with the DSB sites facilitating recruitment of downstream factors including core x-ray cross-complementing 4 (XRCC4) and DNA ligase 4 (Lig4). XRCC4-like factor (XLF) is also a core factor that binds XRCC4 and stimulates Lig4-dependent DNA ligation. A number of accessory NHEJ factors are required for specific DNA end processing and DNA

complex stabilization, in other words, DNA-dependent protein kinase, catalytic subunit (DNA-PKcs), nuclease Artemis and structural components, a paralogue of XRCC4 and XLF (PAXX), and modulator of retroviral infection (Mri) [2,3]. Mice lacking Ku70, Ku80, DNA-PKcs, or Artemis possess severe combined immunodeficient phenotype (SCID), while inactivation of both alleles of the *Xlf* gene results in 2–3-fold reduced B and T cell counts [1,4–7]. Mice lacking PAXX or Mri possess no or very modest phenotype due to functional redundancy with XLF [8–12]. In contrast, mice lacking either XRCC4 or Lig4 demonstrate p53- and Ku-dependent embryonic lethality, which correlates with massive neuronal apoptosis in the central nervous system [1,13–17]. Combined inactivation of *Xlf* and *Dna-pkcs* results in p53- and Ku70-dependent perinatal lethality in mice [10,18,19]. Moreover, deficiency or haploinsufficiency for *Trp53* rescues synthetic lethality between *Xlf* and *Paxx* [10]. XLF is also functionally redundant in mouse development with Mri [20], recombination activating gene 2, RAG2 [21], and a number of DNA damage response (DDR) factors including Ataxia telangiectasia mutated (ATM) [6], histone H2AX [6,22], mediator of DNA damage checkpoint protein 1 (MDC1) [10], and p53-binding factor (53BP1) [7,23].

Development of B and T lymphocytes depends on programmed DSBs induced by RAG during the V(D)J recombination and NHEJ pathway, which is used for error-prone DNA repair [1]. Moreover, mature B cells replace constant regions of immunoglobulins during the somatic recombination process known as class switch recombination (CSR), when DSBs are initiated by activation-induced cytidine deaminase (AID) and Uridine-*N*-glycosylase (UNG), and NHEJ is used for DNA repair [1,24,25]. Furthermore, the NHEJ process is required for neurodevelopment by preventing neuronal apoptosis [1,26].

Mri was initially described as an open reading frame at human chromosome 7 (C7orf49), a factor reversing the resistance to retroviral infection in cell lines [27]. *Mri* was found to enhance NHEJ [28] and possess an *N*-terminal Ku-binding motif (KBM) [29]. Later, *Mri*/Cyren was suggested to inhibit NHEJ at telomeres during the S and G2 phases of the cell cycle [30], and finally confirmed to be a bona fide NHEJ factor, which is functionally redundant with XLF in mouse development including the V(D)J recombination and development of the central nervous system [20]. However, it was not clear whether XLF and *Mri* functionally overlap during the early stages of neurodevelopment (e.g., supporting proliferation and self-renewal of neuronal stem cells). Moreover, due to the lack of a viable mouse model deficient for both XLF and *Mri*, the impact of *Mri* on B and T lymphocyte development *in vivo* is not fully understood.

Here, we introduced a frame-shift mutation to *exon 2* of the murine *Mri* gene. By interbreeding heterozygous parents, we obtained *Mri*^{-/-}, *Mri*^{+/-}, and *Mri*^{+/+} mice at nearly expected ratios. *Mri*-deficient mice possessed normal body size and number of B and T lymphocytes; however, we detected that stimulated primary mature *Mri*^{-/-} B cells had reduced levels of IgG1, and *Mri*^{-/-} neurospheres showed a reduced proliferation rate when compared to the *Mri*^{+/+} controls.

2. Materials and Methods

2.1. Mouse Models

All experiments involving mice were performed according to the protocols approved by the Animal Resources Care Facility of Norwegian University of Science and Technology (NTNU, Trondheim, Norway). *Ung*^{-/-} mice were described previously [31]. *Mri*^{+/-} mice were generated on request and described here for the first time.

2.2. Generation of *Mri*^{+/-} Mice

Mri-deficient (*M*^{-/-}) mice were generated through a CRISPR/Cas9 gene-editing approach in 2017 by Horizon Discovery (Saint Louis, MO, USA) upon request from the Oksnych group (IKOM, Faculty of Medicine and Health Science, NTNU, Trondheim, Norway). Single-guide RNA (sgRNA) GGG CTG TCA TCC AAG AGG GGA GG was designed to target *exon 2* of the *Mri* gene in C57BL/6 mice. The 14 bp deletion resulted in a premature stop codon (Figure 1A). Cas9 and sgRNAs were injected

into single-cell fertilized embryos, which were then transferred back into pseudopregnant females for gestation. Live-born pups were screened for indel mutation by DNA sequencing. Homozygous pups were used for back-crossing with wild type C57BL/6 mice. Heterozygous *Mri*^{+/-} mice were obtained from Horizon Discovery.

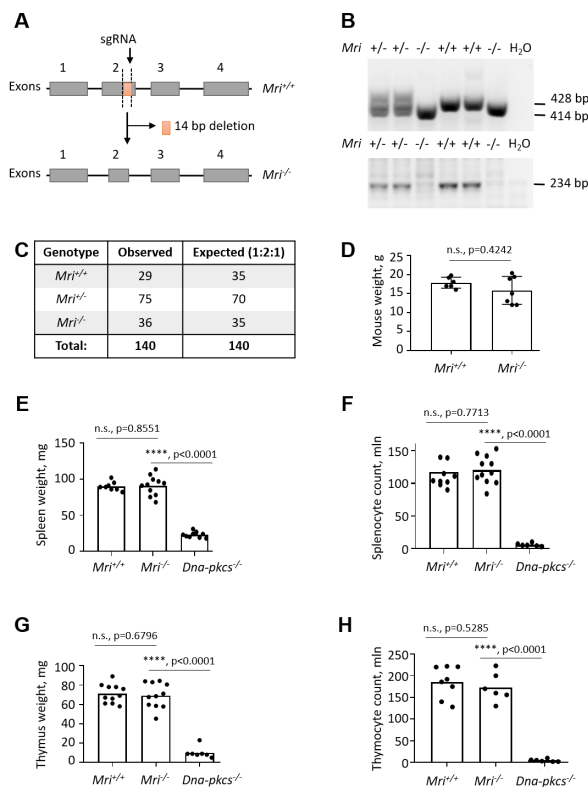


Figure 1. Generation of *Modulator of retrovirus infection*^{-/-} (*Mri*^{-/-}) mice. **(A)** Top. Schematic diagram of murine *Mri* locus indicating the frame-shift mutation in the *exon 2*, induced by the single guide RNA (sgRNA) and resulting in a 14 bp deletion. (Bottom) Resulting *Mri*^{-/-} locus lacking part of the *exon 2*. **(B)** Top. Polymerase chain reaction (PCR)-based genotyping strategy reveals the *Mri* WT allele (428 bp) and *Mri* null allele (414 bp). (Bottom) WT gene validation PCR revealed the *Mri* wild type allele (234 bp). **(C)** Analyses of 140 pups born from *Mri*^{+/-} parents revealed expected genetic distribution of *Mri*^{+/+} (29), *Mri*^{+/-} (75), and *Mri*^{-/-} (36) mice, which is close to the Mendelian distribution 1:2:1. **(D)** Body weight of six to eight week old *Mri*^{+/+} mice (n = 6) was not distinguishable from *Mri*^{-/-} mice (n = 7), $p = 0.4242$. **(E)** The weight of spleens isolated from *Mri*^{+/+} (n = 8) and *Mri*^{-/-} mice (n = 11) was not significantly different, $p = 0.8551$. Spleen size in immunodeficient *Dna-pkcs*^{-/-} mice (n = 10) was reduced when compared to the *Mri*^{+/+} and *Mri*^{-/-} mice, $p < 0.0001$. **(F)** Splenocyte count was not affected in the *Mri*^{-/-} mice (n = 11) when compared to the *Mri*^{+/+} (n = 10), $p = 0.7713$. A number of splenocytes in immunodeficient *Dna-pkcs*^{-/-} mice (n = 6) was significantly reduced when compared to *Mri*^{+/+} and *Mri*^{-/-} mice, $p < 0.0001$. **(G)** The weight of thymus from *Mri*^{+/+} (n = 11) and *Mri*^{-/-} (n = 11) mice was similar, $p = 0.6796$. Thymus size in immunodeficient *Dna-pkcs*^{-/-} mice (n = 7) was significantly reduced when compared to *Mri*^{+/+} and *Mri*^{-/-} mice, $p < 0.0001$. **(H)** The thymocyte count was nearly identical in *Mri*^{+/+} (n = 8) and *Mri*^{-/-} (n = 6) mice, $p = 0.5285$. A number of thymocytes in immunodeficient *Dna-pkcs*^{-/-} mice (n = 6) was significantly reduced when compared to *Mri*^{+/+} and *Mri*^{-/-} mice, $p < 0.0001$.

2.3. Mouse Genotyping

Two polymerase chain reactions (PCRs) were designed to determine the mouse genotypes. The first PCR was performed using TCAGGTCTGCCCTACTACTGA and GTGGTGGTGCTTCTCTGTGA primers, detecting both wild type (428 bp) and null (414 bp) alleles (Figure 1B). The second PCR performed with TCAGGTCTGCCCTACTACTGA and AGAGGGGAGGACCC primers was used to validate the presence of the WT allele (234 bp, Figure 1B). The PCRs were performed using 50 ng of genomic DNA extracted from murine tissues (e.g., ears, tails), in a final reaction volume of 25 μ L, using the Taq 2x Master Mix Kit (New England Biolabs[®] Inc., Ipswich, MA, USA; #M0270L). A 2.5% agarose gel was used to separate 428 bp and 414 bp PCR products during 18 h at 4 °C, 90 V; and 0.7% agarose gel was used to detect the 234 bp PCR product (75 min, room temperature, 124 V). Genomic DNA isolated from the *Mri*^{+/+} and *Mri*^{-/-} cells as well as samples with no genomic DNA were used as the PCR controls (Figure 1B).

2.4. Fluorescence-Activated Cell Sorting, Splenocyte, and Thymocyte Count

Fluorescence-activated cell sorting (FACS) analysis was performed as previously described [11,32]. Briefly, spleens and thymi were isolated from 2-month-old mice, and splenocytes and thymocytes were counted using Countess[™] Automated Cell Counter (Invitrogen, Carlsbad, CA, United States); the cell suspension was spun down and diluted with PBS to obtain a final cell concentration of 2.5×10^7 /mL. The samples of 2.5×10^6 splenocytes or thymocytes were blocked for 15 min at room temperature with Mouse BD fragment crystallizable (Fc) Block[™] (1:50 dilution) (BD Biosciences, Franklin Lakes, NJ, USA; #553142). The cells were then incubated with fluorochrome-conjugated antibodies (see below) and sorted.

2.5. Class Switch Recombination

Class switch recombination (CSR) from IgM to IgG1 was performed as previously described [11]. Naïve B lymphocytes were purified from spleens of 2-month-old mice using EasySep[™] mouse B cell enrichment kit (STEMCELL Technology, Vancouver, Canada; #19854), according to the manufacturers' instructions. For each CSR assay, 2×10^4 cells/200 μ L were used in duplicates. The cells were stimulated with LPS (lipopolysaccharides, 40 μ g/mL; Sigma Aldrich, St. Louis, MO, USA; #437627-5MG) and IL-4 (Interleukin 4, 20 ng/mL; PeproTech, Stockholm, Sweden; #214-14) for 96 h. Then, the cells were blocked with Fc receptor antibody (2.4G2) and normal mouse serum (Invitrogen, Carlsbad, CA, USA; #10410). The cells were washed in PermWash[™] (BD Biosciences, NJ, USA; #554723). Intracellular staining was done using fluorescently tagged anti-mouse antibodies (IgG1-APC) (BioLegend, San Diego, CA, USA; #406610) and the succeeding wash was performed in PermWash. The cells were resuspended in 300 μ L of CellFix (BD Biosciences, NJ, USA; #340181). Viable CD19⁺ B lymphocytes were analyzed for IgG1 expression using FlowJo[®] (Ashland, Oregon, USA) version 7.6 for Windows.

2.6. Double Strand Break Sensitivity Assay

The DSBs sensitivity assay was performed as previously described [10,32,33]. Human nearly-haploid HAP1 cells were generated by the Horizon Discovery Group (Waterbeach, Cambridge, UK, #HZGHC005061c001 and #HZGHC005061c004) and are commercially available. HAP1 cells were cultured according to the manufacturer's instructions. Doxorubicin (Selleckchem, Houston, TX, USA; #S1208), bleomycin (Selleckchem; #S1214), and etoposide (Sigma-Aldrich, St. Louis, MS, USA; #E1383) were used to induce DSBs, and PrestoBlue[™] Cell Viability Reagent (Thermo Fisher, Waltham, MA, USA; #A13262) was used to estimate cellular metabolism levels. Briefly, 2000 cells per well were seeded into 96-well plates in 100 μ L of Iscove Modified Dulbecco Media (IMDM) medium (day 0). On day 1, 50 μ L of the medium was replaced with 50 μ L of fresh medium containing doxorubicin, bleomycin, or etoposide, when indicated. Each experimental condition was performed in triplicates. On day 4, 11 μ L of 10 \times PrestoBlue reagent was added to the wells and incubated for 30 min at 37 °C. The

cellular viability was estimated according to manufacturer's instructions, using the excitation/emission wavelengths set at 544/590 nm.

2.7. Brain Isolation and Neural Stem Progenitor Cell Culture

The brain was isolated from postnatal day 1 mouse after the cerebellum was removed. The isolated brain was mechanically disrupted in the proliferation medium consisting of Dulbecco Modified Eagle Medium, Nutrient Mixture F12 (DMEM/F12; Thermo Fisher, Waltham, MA, USA; #11330-057), supplemented with penicillin/streptomycin (Thermo Fisher, Waltham, MA, USA; #15140122), B27 without vitamin A (Thermo Fischer Scientific, Waltham, MA, USA; #12587001), EGF (10 ng/mL; PeproTtech, Stockholm, Sweden; #AF-100-15), and bFGF (20 ng/mL; PeproTech; #100-18B). Neural stem progenitor cells (NSPC) form free-floating globular structures referred to as neurospheres. The neurospheres were formed during incubation at 37 °C, 5% CO₂ and 95% humidity in order to perform the proliferation and self-renewal assay [34].

2.8. Neural Stem Progenitor Cell Proliferation and Self-Renewal Assays

Early passage NSPCs (P3–P10) were used throughout all of the NSPC experiments. A PrestoBlue™ Cell Viability Assay was used to investigate the neurosphere proliferation rates, following the manufacturer's instructions during each incubation on days 1 to 7. The capacity of neural stem cells to maintain their multipotency *ex vivo* was assessed by determining the number and two-dimensional size of neurospheres [34]. Single NSPCs were plated onto 6-well suspension plates in the proliferation medium on day 0. During days 8 and 10 in culture, images of the entire wells were captured using an EVOS microscope. Only areas between 50 and 1500 pixels were included in the analyses.

2.9. Antibodies

The following antibodies were used for FACS. Rat anti-mouse anti-CD16/CD32 (Fc Block, BD Biosciences, San Jose, CA, USA; #553141, 1:50); anti-CD4-PE-Cy7 (Thermo Scientific, Waltham, MA, USA, #25-0042-81, 1:100); anti-CD8-PE-Cy5 (BD Biosciences, San Jose, CA, USA, #553034, 1:100); anti-CD19-PE-Cy7 (Biolegends, San Diego, CA, USA, #115520, 1:100); and hamster anti-mouse anti-CD3-APC (Biolegends, USA, #100312, 1:100).

3. Results

3.1. Generation of *Mri*^{-/-} Mice

To investigate the impact of *Mri* on mouse development, we generated a mouse model with 14 bp frame-shift deletion in *Mri* exon 2 on a C57BL/6 background (Figure 1A). Purified sgRNA and Cas9 RNA were introduced to fertilized oocytes, resulting in complete inactivation of the *Mri* gene. *Mri* status (WT, wild type, +/+; heterozygous, +/-; and null, -/-) was confirmed for every experiment by PCR screening (Figure 1B). *Mri*^{+/+}, *Mri*^{+/-}, and *Mri*^{-/-} mice were born from *Mri*^{+/-} parents at ratios close to 1:2:1 (Figure 1C). Thirty-day old *Mri*^{-/-} mice possessed an average body weight of 15.0 g, which was slightly lower, but not significantly different from the *Mri*^{+/+} controls, with a bodyweight of 17.5 g, on average (Figure 1D). The lifespan of *Mri*^{-/-} and *Mri*^{+/-} mice was monitored for up to 12 months, according to the local regulations. During this time frame, both *Mri*^{-/-} and *Mri*^{+/-} mice were fertile and had no cancer incidence, similar to the *Mri*^{+/+} controls.

3.2. *Mri*^{-/-} Mice Develop Normal Spleens and Thymi

The NHEJ is required for V(D)J recombination in developing B and T lymphocytes, and for CSR in mature B cells [1]. To determine specific functions of *Mri* in B and T cell development, we first analyzed spleens and thymi isolated from *Mri*-deficient and WT mice. The average weights of spleens (91 mg) and thymi (69 mg) as well as the average count of splenocytes (121 million) and thymocytes (173 million) was not affected in *Mri*^{-/-} mice when compared to *Mri*^{+/+} controls (90 mg;

71 mg; 118 million; 186 million, respectively). These numbers were significantly different from the immunodeficient controls, *Dna-pkcs*^{-/-} mice (23 mg; 10 mg; six million; five million, respectively) (Figure 1E–H). Moreover, the proportions of CD19⁺ B cells in spleens of six- to eight-week old *Mri*^{-/-} mice were on average 60%, which was similar to the proportion of CD19⁺ in *Mri*^{+/+} mice (55%, $p = 0.0668$), and significantly higher than the background levels detected in immunodeficient *Dna-pkcs*^{-/-} controls ($p < 0.0001$; Figure 2A). The average proportion of CD3⁺ T splenocytes in *Mri*^{-/-} mice (21%) was also similar to the one observed in the *Mri*^{+/+} controls (22%, $p = 0.8228$), and higher than in the *Dna-pkcs*^{-/-} controls (1%, $p < 0.0001$; Figure 2A). *Mri*^{+/+} and *Mri*^{-/-} mice had similar proportions of CD4⁺ T cells ($p = 0.8876$) and CD8⁺ T cells ($p = 0.7026$) in the spleens, while proportions of CD4⁺ and CD8⁺ T splenocytes in the *Dna-pkcs*^{-/-} controls were 4–5-fold reduced ($p < 0.0001$, Figure 2B). In the thymi of six- to eight-week old *Mri*^{+/+} and *Mri*^{-/-} mice, the proportions of CD4⁺, CD8⁺, and CD4⁺CD8⁺ T cells were similar ($p > 0.5589$), while only background levels were detected in the *Dna-pkcs*^{-/-} controls ($p < 0.0001$, Figure 2C).

3.3. Class Switch Recombination to IgG1 Is Reduced in *Mri*^{-/-} Mice

To determine whether *Mri* deficiency affects CSR, we isolated B cells from the spleens of *Mri*^{+/+} and *Mri*^{-/-} mice and stimulated the cells with LPS and IL-4. After 96 h, we detected that average IgG1 levels were 33% in *Mri*^{-/-} mice, which was significantly lower ($p = 0.0031$) than in the *Mri*^{+/+} controls (average 39%; Figure 2D). B lymphocytes isolated from *Ung*^{-/-} mice were used as the negative control and possessed on average only 2% of IgG1 at the end of the experiment (96 h), which was lower than in *Mri*^{+/+} or *Mri*^{-/-} mice ($p < 0.0001$).

3.4. Lack of *Mri* Results in the Reduced Proliferation Rate of Neuronal Stem Progenitor Cells

Previous studies have shown that single knockout of NHEJ DNA repair genes (e.g., *Xrcc4*, *Lig4*, *Ku70*) results in impaired nervous system development in mice [1,13,14]. To determine the impact of *Mri* on the developing nervous system, we used NSPC isolated from *Mri*^{+/+} and *Mri*^{-/-} mice at postnatal day 1. We performed four independent experiments using two cell lines from two mice of each genotype. The average proliferation rate of *Mri*^{-/-} neurospheres was approximately 35% lower than that in the WT controls, $p = 0.0043$ (Figure 3B).

3.5. Normal Self-Renewal Capacity of *Mri*-Deficient Neuronal Stem Progenitor Cells

To analyze the capacity of NSPCs to maintain the features of stem cells throughout cell divisions and numerous propagations (self-renewal capacity), we counted the number of neurospheres formed in cell culture. In four independent experiments, we plated 10,000 single NSPCs and cultured for eight days. In total, we counted 5123 neurospheres that originated from *Mri*^{+/+}, and 4608 from *Mri*^{-/-} mice. On average, there were 256 neurospheres in each of the 20 *Mri*^{+/+} samples analyzed, and 230 neurospheres in each of the 20 *Mri*^{-/-} samples ($p = 0.7254$, n.s., Figure 3C). In addition, images of the neurospheres were collected and the surface was calculated using *ImageJ* software. Inactivation of *Mri* did not affect the average diameter of neurospheres, which was 461 px² on average in *Mri*^{+/+} and 427 px² in *Mri*^{-/-} neurospheres, $p = 0.4915$ (Figure 3D). We concluded that *Mri* is dispensable for the self-renewal capacity of NSPC.

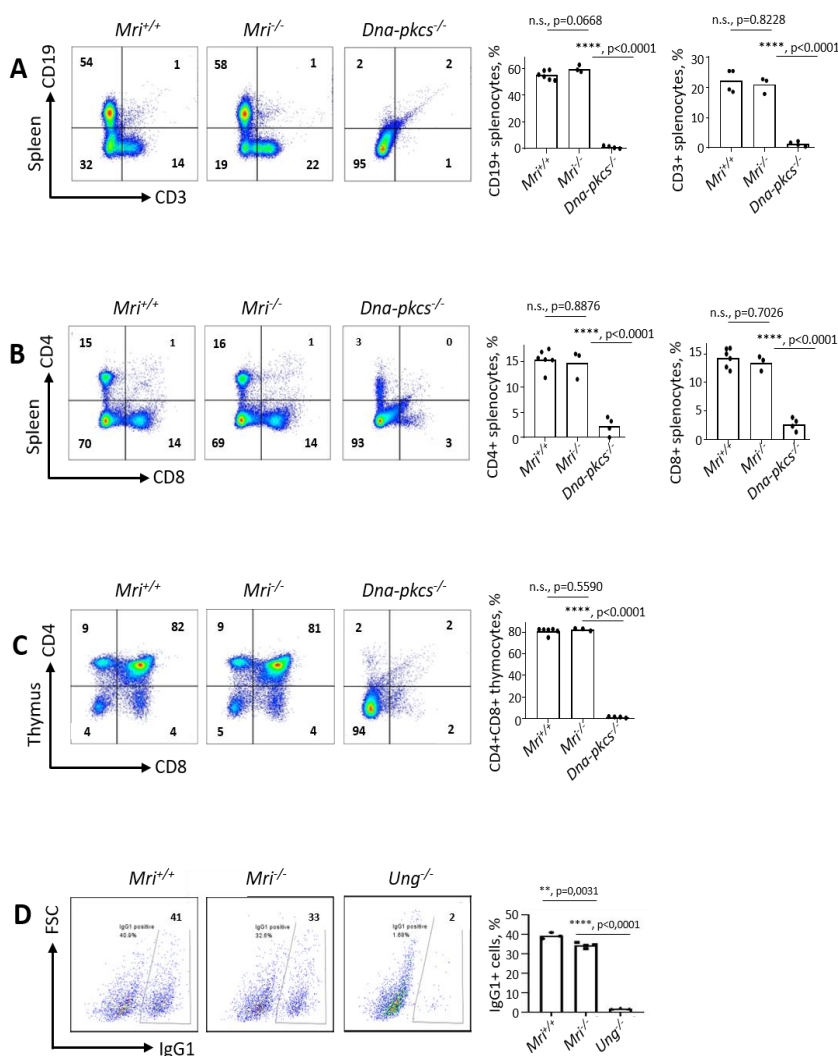


Figure 2. Lymphocyte development in *Mri*^{-/-} mice. **(A)** Proportions of T (CD3⁺) and B (CD19⁺) cells in the spleens of *Mri*^{+/+} (n = 6), *Mri*^{-/-} (n = 3), and *Dna-pkcs*^{-/-} (n = 4) mice. Proportions of T and B cells were similar in *Mri*^{+/+} and *Mri*^{-/-} mice, $p > 0.0667$, and were only background levels in immunodeficient *Dna-pkcs*^{-/-} mice, $p < 0.0001$. **(B)** Proportions of CD4⁺ and CD8⁺ T splenocytes in *Mri*^{+/+} (n = 6), *Mri*^{-/-} (n = 3), and *Dna-pkcs*^{-/-} (n = 4) mice. *Mri*^{-/-} mice possessed similar proportions of CD4⁺ T helper and CD8⁺ T cytotoxic cells when compared to *Mri*^{+/+} mice, $p = 0.8876$ and $p = 0.7026$, respectively. Only background levels of CD4⁺ and CD8⁺ T cells are present in immunodeficient *Dna-pkcs*^{-/-} spleens, $p < 0.0001$. **(C)** Proportions of CD4⁺, CD8⁺, and CD4⁺CD8⁺ thymocytes in *Mri*^{+/+} (n = 6), *Mri*^{-/-} (n = 3), and *Dna-pkcs*^{-/-} (n = 4) mice. Proportions of T cell types in *Mri*^{-/-} mice were similar to the ones detected in *Mri*^{+/+} mice, $p > 0.5589$, and higher than in *Dna-pkcs*^{-/-} mice, $p < 0.0001$. **(D)** CSR to IgG1 in primary B splenocytes isolated from the *Mri*^{-/-} mice (n = 4) was reduced when compared to the cells from the *Mri*^{+/+} mice (n = 3), $p = 0.0032$. CSR to IgG1 was significantly reduced in the *Ung*^{-/-} B cells (n = 3) when compared to the *Mri*^{+/+} and *Mri*^{-/-}, $p < 0.0001$.

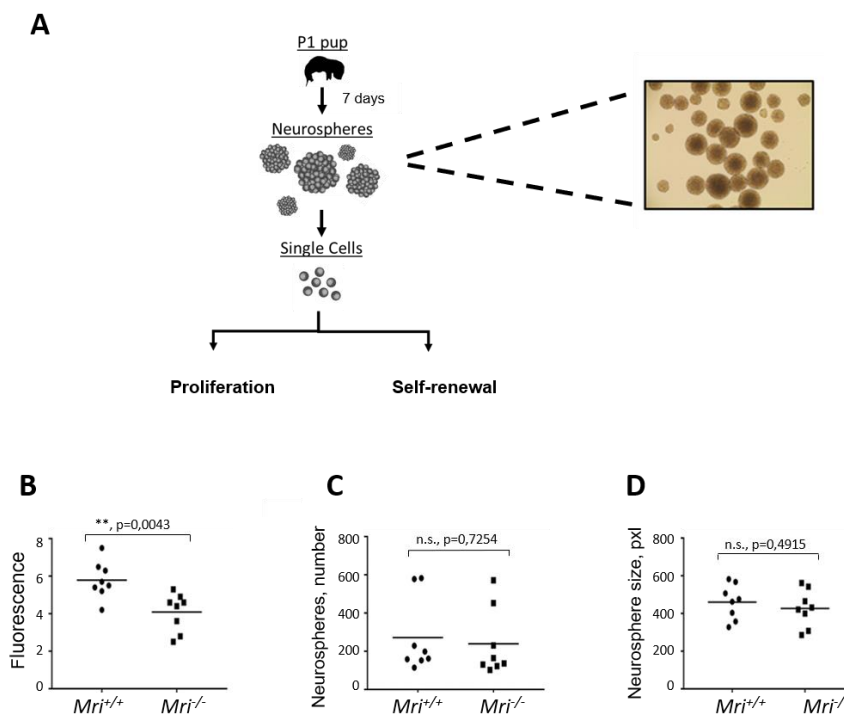


Figure 3. Characterization of neurogenesis in $Mri^{-/-}$ mice. For each experiment, four independent cell lines isolated from two mice were used ($n = 8$). (A) Neurosphere isolation diagram from $Mri^{+/+}$ and $Mri^{-/-}$ mice at postnatal day 1. (B) Neurosphere proliferation isolated from the $Mri^{-/-}$ mice was reduced when compared to the $Mri^{+/+}$ mice, $p = 0.0043$. (C) Number of neurospheres formed in cell culture for eight days. $Mri^{-/-}$ and $Mri^{+/+}$ neurospheres possessed similar self-renewal capacity, $p = 0.7254$. (D) Neurosphere size isolated from $Mri^{-/-}$ and $Mri^{+/+}$ mice were similar, $p = 0.4915$. The surface of neurospheres, pxl. Areas between 50 and 1500 pixels were included in the analyses. Four independent experiments using two cell lines of each genotype were performed in all experiments (A–C). p values were calculated using the unpaired t -test. The horizontal bars represent the average.

3.6. Human HAP1 Cells Lacking Mri Possess Normal Levels of Sensitivity to DNA Double-Strand Breaks

Deficiency for XRCC4, LIG4, XLF, or DNA-PKcs results in hypersensitivity to DSBs in human HAP1 cells [10,32,33]. To determine the effect of Mri on DSB sensitivity, we obtained two independent clones of MRI-deficient HAP1 cells as well as WT and XRCC4-deficient controls. We exposed the HAP1 cells to DSB-inducing agents bleomycin (0 to 0.4 μ M), doxorubicin (0 to 4 nM), and etoposide (0 to 160 nM), and evaluated the cell viability four days later (Figure 4). We observed no hypersensitivity of HAP1 cells lacking Mri when compared to WT controls. However, cells lacking XRCC4 were hypersensitive to all indicated compounds, bleomycin, doxorubicin, and etoposide ($p < 0.0001$, Figure 4).

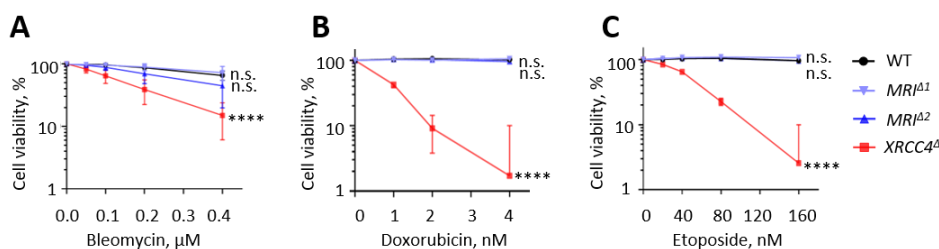


Figure 4. Sensitivity to DSBs in *Mri*-deficient HAP1 cells. Sensitization of WT, two independent *Mri*-deficient clones, *MRI*^{Δ1} and *MRI*^{Δ2}, and *XRCC4*^ΔHAP1 cells to bleomycin (A), doxorubicin (B), and etoposide (C) at indicated concentrations. Results are from the mean (SD) of three repeats. Cell viability (%) represents the relative proportion of the fluorescence normalized to untreated cells. Comparisons between every two groups were made using one-way ANOVA, GraphPad Prism 8. WT, *MRI*^{Δ1}, and *MRI*^{Δ2} vs. *XRCC4*^Δ, $p < 0.0001$ (****); WT vs. *MRI*^{Δ1}, $p = 0.9983$ (n.s.); WT vs. *MRI*^{Δ2}, $p = 0.1295$ (n.s.); *MRI*^{Δ1} vs. *MRI*^{Δ2}, $p = 0.1791$ (n.s).

4. Discussion

We have generated a new knockout mouse model with 14 bp deletion in *exon 2* of the *Mri* gene, *Mri*^{-/-}. While we were characterizing our mouse model, another group reported an independently-generated *Mri*-deficient mouse [20], which possessed a similar phenotype. Thus, our observations are confirmatory to the findings observed by the Sleckman group [20].

The mice lacking *Mri* were live-born at expected ratios and demonstrated normal growth and development of lymphoid organs. *Mri*^{-/-}, *Mri*^{+/-}, and *Mri*^{+/+} mice possessed similar sizes of spleens and thymi, a similar number of splenocytes and thymocytes, and proportions of B and T cells (Figure 1). Similar to *Mri*-deficient mice, *Paxx*^{-/-} mice did not have a detectable phenotype [8–12]. However, inactivation of other NHEJ factors resulted in a reduced number of B and T cells (*Xlf*^{-/-} mice, [4–7,18,21,23]), and block in B and T cell development (e.g., *Artemis*^{-/-} [35], *Dna-pkcs*^{-/-} [36], *Ku70*^{-/-} [37], *Ku80*^{-/-} [38]; or even embryonic lethality in *Xrcc4*^{-/-} [39] and *Lig4*^{-/-} [40]).

The CSR to IgG1 was reduced in primary B cells isolated from *Mri*^{-/-} mice when compared to WT controls (Figure 2), which suggests that *Mri* is involved in specific DNA repair-mediated event. Furthermore, we isolated neuronal stem progenitor cells from *Mri*^{-/-} brains and found that these cells proliferate slower when compared to *Mri*^{+/+} controls. Reduced proliferation rates of *Mri*-deficient neuronal stem progenitor cells could be explained, as one option, by lower expression or lack of factors functionally redundant with *Mri* in these cell types. Future studies would be required to address this option. Moreover, future studies may address questions such as neurological defects and cognitive functions in mice lacking *Mri* as well as whether the *Mri*-deficient mice are prone to infections.

In addition, we found that human nearly haploid HAP1 cell lines lacking *Mri* possessed no proliferation defect or hypersensitivity to DNA damaging agents such as etoposide, doxorubicin, and bleomycin (Figure 4). Previously, it was reported that murine embryonic fibroblasts (MEF) lacking *Mri* were hypersensitive to ionizing radiation when compared to WT controls, although the sensitivity was less obvious than in XLF-deficient MEFs [20]. The discrepancy between our and previously published data could be due to the usage of different cell types, the difference between species as well as distinct ways to induce DNA damages (e.g., chemicals vs. irradiation). Further studies involving various cell type models originated from different species, and using various DNA damaging strategies would deepen our understanding of the specific functions of *Mri* in DNA repair in mammalian cells. Overall, we concluded that the lack of *Mri* has a rather minor effect on murine and human cells.

Combined inactivation of *Mri* and *Xlf* [20], however, revealed an important role of *Mri* in mouse development, which was overlooked due to its functional redundancy with XLF. Synthetic lethality between *Mri* and *Xlf* complicated studies of genetic interaction between these factors in vivo. There are several potential ways to overcome this challenge. One option is to use conditional knockouts

of *Xlf* or *Mri* genes. Moreover, there might be another genetic-based approach. Inactivation of one or two alleles of *Trp53* partially rescued synthetic lethality between *Xlf* and *Dna-pkcs* [10,18,19] and *Xlf* and *Paxx* [10]. In addition, deficiency or haploinsufficiency for *Trp53* rescued embryonic lethality of *Lig4*^{-/-} and *Xrcc4*^{-/-} mice [13,14]. Inactivation of the *Atm* gene rescued embryonic lethality of *Lig4*^{-/-} mice [41]. Finally, inactivation of both alleles of *Ku80* rescued embryonic lethality of *Lig4*^{-/-} mice [17], and inactivation of *Ku70* rescued synthetic lethality between *Xlf* and *Dna-pkcs* [19]. Based on these data, one can speculate that inactivation of *Trp53*, *Atm*, *Ku70*, or *Ku80* will rescue synthetic lethality between *Xlf* and *Mri*. Moreover, given the critical roles of *Ku70* and *Ku80* in the initiation of classical NHEJ, one could propose that mice lacking all known NHEJ factors (e.g., *Ku70*^{-/-} *Ku80*^{-/-} *Dna-pkcs*^{-/-} *Artemis*^{-/-} *Xlf*^{-/-} *Paxx*^{-/-} *Mri*^{-/-} *Xrcc4*^{-/-} *Lig4*^{-/-}) will be viable, indistinguishable from *Ku*-deficient mice, and serve as a suitable *in vivo* model to investigate alternative end-joining, A-EJ.

5. Conclusions

A new *Mri*-deficient mouse model was generated. *Mri*-deficient mice possessed normal body size and number of B and T lymphocytes; however, *Mri* is required for an efficient class switch recombination process in mature B cells. *Mri*^{-/-} neurospheres showed a reduced proliferation rate, but similar self-renewal capacity when compared to the *Mri*^{+/+} controls.

Author Contributions: V.O. designed and performed experiments, contributed key reagents, and analyzed the data. A.S. performed the CSR assay using primary B cells. M.X. performed the DSBs sensitivity assay using human HAP1 cells. S.C.-Z., C.H., Ø.R., Q.Z., A.A., J.W., and N.-B.L. performed the lymphocyte analyses. Ø.R., W.W., and P.J. performed and analyzed the neurosphere-based experiments. R.G.-F. developed the *Mri*^{-/-} genotyping strategy. M.B. and V.O. interpreted the results. The paper was written by Ø.R., S.C.-Z., and V.O.; all authors read and approved the manuscript.

Funding: This work was supported by the Research Council of Norway Young Talent Investigator grant (#249774) to V.O. In addition, V.O.'s group was supported by the Liaison Committee for Education, Research, and Innovation in Central Norway (#13477); the Norwegian Cancer Society (#182355); FRIMEDBIO grants (#270491 and #291217), and The Outstanding Academic Fellow Program at NTNU (2017–2021). JW is supported by the Erasmus mobility program.

Acknowledgments: We gratefully acknowledge support by the Molecular Imaging Core Facility (CMIC) and Comparative Medicine Core Facility (CoMed) at the Faculty of Medicine and Health Sciences, NTNU (Trondheim).

Conflicts of Interest: The authors declare no conflicts of interest.

Abbreviations

ATM	Ataxia-telangiectasia mutated
CSR	Class switch recombination
DDR	DNA damage response
DNA-PKcs	DNA-dependent protein kinase
DSBs	DNA double-strand breaks
GFAP	Glial fibrillary acid protein
HAP1	A near-haploid human cell line derived from KBM-7 cell line
IL-4	Interleukin 4
Lig4	DNA ligase IV
LPS	Lipopolysaccharides
Mri	Modulator of retroviral infection
NHEJ	Non-homologous end-joining
NSPC	Neuronal stem progenitor cells
PAXX	Paralogue of XRCC4 and XLF
PCR	Polymerase chain reaction
XLF	XRCC4-like factor
XRCC4	X-ray repair cross-complementing protein 4

References

1. Kumar, V.; Alt, F.W.; Oksenysh, V. Functional overlaps between XLF and the ATM-dependent DNA double strand break response. *DNA Repair (Amst)* **2014**, *16*, 11–22. [[CrossRef](#)] [[PubMed](#)]
2. Pannunzio, N.R.; Watanabe, G.; Lieber, M.R. Nonhomologous DNA end-joining for repair of DNA double-strand breaks. *J. Biol. Chem.* **2018**, *293*, 10512–10523. [[CrossRef](#)] [[PubMed](#)]
3. Scully, R.; Panday, A.; Elango, R.; Willis, N.A. DNA double-strand break repair-pathway choice in somatic mammalian cells. *Nat. Rev. Mol. Cell Biol.* **2019**. [[CrossRef](#)] [[PubMed](#)]
4. Li, G.; Alt, F.W.; Cheng, H.L.; Brush, J.W.; Goff, P.H.; Murphy, M.M.; Franco, S.; Zhang, Y.; Zha, S. Lymphocyte-specific compensation for XLF/cernunnos end-joining functions in V(D)J recombination. *Mol. Cell* **2008**, *31*, 631–640. [[CrossRef](#)]
5. Vera, G.; Rivera-Munoz, P.; Abramowski, V.; Malivert, L.; Lim, A.; Bole-Feysot, C.; Martin, C.; Florin, B.; Latour, S.; Revy, P.; et al. Cernunnos deficiency reduces thymocyte life span and alters the T cell repertoire in mice and humans. *Mol. Cell Biol.* **2013**, *33*, 701–711. [[CrossRef](#)]
6. Zha, S.; Guo, C.; Boboila, C.; Oksenysh, V.; Cheng, H.L.; Zhang, Y.; Wesemann, D.R.; Yuen, G.; Patel, H.; Goff, P.H.; et al. ATM damage response and XLF repair factor are functionally redundant in joining DNA breaks. *Nature* **2011**, *469*, 250–254. [[CrossRef](#)]
7. Oksenysh, V.; Alt, F.W.; Kumar, V.; Schwer, B.; Wesemann, D.R.; Hansen, E.; Patel, H.; Su, A.; Guo, C. Functional redundancy between repair factor XLF and damage response mediator 53BP1 in V(D)J recombination and DNA repair. *Proc. Natl. Acad. Sci. USA* **2012**, *109*, 2455–2460. [[CrossRef](#)]
8. Abramowski, V.; Etienne, O.; Elsaid, R.; Yang, J.; Berland, A.; Kermasson, L.; Roch, B.; Musilli, S.; Moussu, J.P.; Lipson-Ruffert, K.; et al. PAXX and Xlf interplay revealed by impaired CNS development and immunodeficiency of double KO mice. *Cell Death Differ.* **2018**, *25*, 444–452. [[CrossRef](#)]
9. Balmus, G.; Barros, A.C.; Wijnhoven, P.W.; Lescale, C.; Hasse, H.L.; Boroviak, K.; le Sage, C.; Doe, B.; Speak, A.O.; Galli, A.; et al. Synthetic lethality between PAXX and XLF in mammalian development. *Genes Dev.* **2016**, *30*, 2152–2157. [[CrossRef](#)]
10. Castaneda-Zegarra, S.; Xing, M.; Gago-Fuentes, R.; Saeterstad, S.; Oksenysh, V. Synthetic lethality between DNA repair factors Xlf and Paxx is rescued by inactivation of Trp53. *DNA Repair (Amst)* **2019**, *73*, 164–169. [[CrossRef](#)]
11. Gago-Fuentes, R.; Xing, M.; Saeterstad, S.; Sarno, A.; Dewan, A.; Beck, C.; Bradamante, S.; BJORAS, M.; Oksenysh, V. Normal development of mice lacking PAXX, the paralogue of XRCC4 and XLF. *FEBS Open Bio* **2018**, *8*, 426–434. [[CrossRef](#)]
12. Liu, X.; Shao, Z.; Jiang, W.; Lee, B.J.; Zha, S. PAXX promotes KU accumulation at DNA breaks and is essential for end-joining in XLF-deficient mice. *Nat. Commun.* **2017**, *8*, 13816. [[CrossRef](#)]
13. Frank, K.M.; Sharpless, N.E.; Gao, Y.; Sekiguchi, J.M.; Ferguson, D.O.; Zhu, C.; Manis, J.P.; Horner, J.; DePinho, R.A.; Alt, F.W. DNA ligase IV deficiency in mice leads to defective neurogenesis and embryonic lethality via the p53 pathway. *Mol. Cell* **2000**, *5*, 993–1002. [[CrossRef](#)]
14. Gao, Y.; Ferguson, D.O.; Xie, W.; Manis, J.P.; Sekiguchi, J.; Frank, K.M.; Chaudhuri, J.; Horner, J.; DePinho, R.A.; Alt, F.W. Interplay of p53 and DNA-repair protein XRCC4 in tumorigenesis, genomic stability and development. *Nature* **2000**, *404*, 897–900. [[CrossRef](#)] [[PubMed](#)]
15. Boboila, C.; Jankovic, M.; Yan, C.T.; Wang, J.H.; Wesemann, D.R.; Zhang, T.; Fazeli, A.; Feldman, L.; Nussenzweig, A.; Nussenzweig, M.; et al. Alternative end-joining catalyzes robust IgH locus deletions and translocations in the combined absence of ligase 4 and Ku70. *Proc. Natl. Acad. Sci. USA* **2010**, *107*, 3034–3039. [[CrossRef](#)]
16. Boboila, C.; Yan, C.; Wesemann, D.R.; Jankovic, M.; Wang, J.H.; Manis, J.; Nussenzweig, A.; Nussenzweig, M.; Alt, F.W. Alternative end-joining catalyzes class switch recombination in the absence of both Ku70 and DNA ligase 4. *J. Exp. Med.* **2010**, *207*, 417–427. [[CrossRef](#)]
17. Karanjawala, Z.E.; Adachi, N.; Irvine, R.A.; Oh, E.K.; Shibata, D.; Schwarz, K.; Hsieh, C.L.; Lieber, M.R. The embryonic lethality in DNA ligase IV-deficient mice is rescued by deletion of Ku: Implications for unifying the heterogeneous phenotypes of NHEJ mutants. *DNA Repair (Amst)* **2002**, *1*, 1017–1026. [[CrossRef](#)]
18. Oksenysh, V.; Kumar, V.; Liu, X.; Guo, C.; Schwer, B.; Zha, S.; Alt, F.W. Functional redundancy between the XLF and DNA-PKcs DNA repair factors in V(D)J recombination and nonhomologous DNA end joining. *Proc. Natl. Acad. Sci. USA* **2013**, *110*, 2234–2239. [[CrossRef](#)]

19. Xing, M.; Bjoras, M.; Daniel, J.A.; Alt, F.W.; Oksenysh, V. Synthetic lethality between murine DNA repair factors XLF and DNA-PKcs is rescued by inactivation of Ku70. *DNA Repair (Amst)* **2017**, *57*, 133–138. [[CrossRef](#)]
20. Hung, P.J.; Johnson, B.; Chen, B.R.; Byrum, A.K.; Bredemeyer, A.L.; Yewdell, W.T.; Johnson, T.E.; Lee, B.J.; Deivasigamani, S.; Hindi, I.; et al. MRI Is a DNA Damage Response Adaptor during Classical Non-homologous End Joining. *Mol. Cell* **2018**, *71*, 332–342.e8. [[CrossRef](#)]
21. Lescale, C.; Abramowski, V.; Bedora-Faure, M.; Murigneux, V.; Vera, G.; Roth, D.B.; Revy, P.; de Villartay, J.P.; Deriano, L. RAG2 and XLF/Cernunnos interplay reveals a novel role for the RAG complex in DNA repair. *Nat. Commun.* **2016**, *7*, 10529. [[CrossRef](#)]
22. Chen, B.R.; Quinet, A.; Byrum, A.K.; Jackson, J.; Berti, M.; Thangavel, S.; Bredemeyer, A.L.; Hindi, I.; Mosammaparast, N.; Tyler, J.K.; et al. XLF and H2AX function in series to promote replication fork stability. *J. Cell Biol.* **2019**, *218*, 2113–2123. [[CrossRef](#)]
23. Liu, X.; Jiang, W.; Dubois, R.L.; Yamamoto, K.; Wolner, Z.; Zha, S. Overlapping functions between XLF repair protein and 53BP1 DNA damage response factor in end joining and lymphocyte development. *Proc. Natl. Acad. Sci. USA* **2012**, *109*, 3903–3908. [[CrossRef](#)] [[PubMed](#)]
24. Alt, F.W.; Zhang, Y.; Meng, F.L.; Guo, C.; Schwer, B. Mechanisms of programmed DNA lesions and genomic instability in the immune system. *Cell* **2013**, *152*, 417–429. [[CrossRef](#)]
25. Yeap, L.S.; Meng, F.L. Cis- and trans-factors affecting AID targeting and mutagenic outcomes in antibody diversification. *Adv. Immunol.* **2019**, *141*, 51–103. [[CrossRef](#)]
26. Alt, F.W.; Schwer, B. DNA double-strand breaks as drivers of neural genomic change, function, and disease. *DNA Repair (Amst)* **2018**, *71*, 158–163. [[CrossRef](#)]
27. Agarwal, S.; Harada, J.; Schreifels, J.; Lech, P.; Nikolai, B.; Yamaguchi, T.; Chanda, S.K.; Somia, N.V. Isolation, characterization, and genetic complementation of a cellular mutant resistant to retroviral infection. *Proc. Natl. Acad. Sci. USA* **2006**, *103*, 15933–15938. [[CrossRef](#)]
28. Slavoff, S.A.; Heo, J.; Budnik, B.A.; Hanakahi, L.A.; Saghatelian, A. A human short open reading frame (sORF)-encoded polypeptide that stimulates DNA end joining. *J. Biol. Chem.* **2014**, *289*, 10950–10957. [[CrossRef](#)]
29. Grundy, G.J.; Rulten, S.L.; Arribas-Bosacoma, R.; Davidson, K.; Kozik, Z.; Oliver, A.W.; Pearl, L.H.; Caldecott, K.W. The Ku-binding motif is a conserved module for recruitment and stimulation of non-homologous end-joining proteins. *Nat. Commun.* **2016**, *7*, 11242. [[CrossRef](#)]
30. Arnoult, N.; Correia, A.; Ma, J.; Merlo, A.; Garcia-Gomez, S.; Maric, M.; Tognetti, M.; Benner, C.W.; Boulton, S.J.; Saghatelian, A.; et al. Regulation of DNA repair pathway choice in S and G2 phases by the NHEJ inhibitor CYREN. *Nature* **2017**, *549*, 548–552. [[CrossRef](#)]
31. Nilsen, H.; Rosewell, I.; Robins, P.; Skjelbred, C.F.; Andersen, S.; Slupphaug, G.; Daly, G.; Krokan, H.E.; Lindahl, T.; Barnes, D.E. Uracil-DNA glycosylase (UNG)-deficient mice reveal a primary role of the enzyme during DNA replication. *Mol. Cell* **2000**, *5*, 1059–1065. [[CrossRef](#)]
32. Dewan, A.; Xing, M.; Lundbaek, M.B.; Gago-Fuentes, R.; Beck, C.; Aas, P.A.; Liabakk, N.B.; Saeterstad, S.; Chau, K.T.P.; Kavli, B.M.; et al. Robust DNA repair in PAXX-deficient mammalian cells. *FEBS Open Bio* **2018**, *8*, 442–448. [[CrossRef](#)]
33. Xing, M.; Oksenysh, V. Genetic interaction between DNA repair factors PAXX, XLF, XRCC4 and DNA-PKcs in human cells. *FEBS Open Bio* **2019**. [[CrossRef](#)]
34. Wang, W.; Osenbroch, P.; Skinnis, R.; Esbensen, Y.; Bjoras, M.; Eide, L. Mitochondrial DNA integrity is essential for mitochondrial maturation during differentiation of neural stem cells. *Stem Cells* **2010**, *28*, 2195–2204. [[CrossRef](#)]
35. Rooney, S.; Sekiguchi, J.; Zhu, C.; Cheng, H.L.; Manis, J.; Whitlow, S.; DeVido, J.; Foy, D.; Chaudhuri, J.; Lombard, D.; et al. Leaky Scid phenotype associated with defective V(D)J coding end processing in Artemis-deficient mice. *Mol. Cell* **2002**, *10*, 1379–1390. [[CrossRef](#)]
36. Gao, Y.; Chaudhuri, J.; Zhu, C.; Davidson, L.; Weaver, D.T.; Alt, F.W. A targeted DNA-PKcs-null mutation reveals DNA-PK-independent functions for KU in V(D)J recombination. *Immunity* **1998**, *9*, 367–376. [[CrossRef](#)]
37. Gu, Y.; Seidl, K.J.; Rathbun, G.A.; Zhu, C.; Manis, J.P.; van der Stoep, N.; Davidson, L.; Cheng, H.L.; Sekiguchi, J.M.; Frank, K.; et al. Growth retardation and leaky SCID phenotype of Ku70-deficient mice. *Immunity* **1997**, *7*, 653–665. [[CrossRef](#)]

38. Nussenzweig, A.; Chen, C.; da Costa Soares, V.; Sanchez, M.; Sokol, K.; Nussenzweig, M.C.; Li, G.C. Requirement for Ku80 in growth and immunoglobulin V(D)J recombination. *Nature* **1996**, *382*, 551–555. [[CrossRef](#)]
39. Gao, Y.; Sun, Y.; Frank, K.M.; Dikkes, P.; Fujiwara, Y.; Seidl, K.J.; Sekiguchi, J.M.; Rathbun, G.A.; Swat, W.; Wang, J.; et al. A critical role for DNA end-joining proteins in both lymphogenesis and neurogenesis. *Cell* **1998**, *95*, 891–902. [[CrossRef](#)]
40. Frank, K.M.; Sekiguchi, J.M.; Seidl, K.J.; Swat, W.; Rathbun, G.A.; Cheng, H.L.; Davidson, L.; Kangaloo, L.; Alt, F.W. Late embryonic lethality and impaired V(D)J recombination in mice lacking DNA ligase IV. *Nature* **1998**, *396*, 173–177. [[CrossRef](#)]
41. Sekiguchi, J.; Ferguson, D.O.; Chen, H.T.; Yang, E.M.; Earle, J.; Frank, K.; Whitlow, S.; Gu, Y.; Xu, Y.; Nussenzweig, A.; et al. Genetic interactions between ATM and the nonhomologous end-joining factors in genomic stability and development. *Proc. Natl. Acad. Sci. USA* **2001**, *98*, 3243–3248. [[CrossRef](#)] [[PubMed](#)]



© 2019 by the authors. Licensee MDPI, Basel, Switzerland. This article is an open access article distributed under the terms and conditions of the Creative Commons Attribution (CC BY) license (<http://creativecommons.org/licenses/by/4.0/>).

PAPER II

Article

Mediator of DNA Damage Checkpoint Protein 1 Facilitates V(D)J Recombination in Cells Lacking DNA Repair Factor XLF

Carole Beck^{1,2}, Sergio Castañeda-Zegarra^{1,2} , Camilla Huse^{1,2}, Mengtan Xing^{1,2} and Valentyn Oksenyich^{1,2,3,*} 

¹ Department of Clinical and Molecular Medicine (IKOM), Norwegian University of Science and Technology (NTNU), 7491 Trondheim, Norway; carole.beck@ntnu.no (C.B.); sergio.m.c.zegarra@ntnu.no (S.C.-Z.); camilla.huse@rr-research.no (C.H.); mengtan.xing@ous-research.no (M.X.)

² St. Olavs Hospital, Trondheim University Hospital, Clinic of Medicine, Postboks 3250 Sluppen, 7006 Trondheim, Norway

³ Department of Biosciences and Nutrition (BioNuT), Karolinska Institutet, 14183 Huddinge, Sweden

* Correspondence: valentyn.oksenych@ntnu.no

Received: 27 November 2019; Accepted: 24 December 2019; Published: 30 December 2019



Abstract: DNA double-strand breaks (DSBs) trigger the Ataxia telangiectasia mutated (ATM)-dependent DNA damage response (DDR), which consists of histone H2AX, MDC1, RNF168, 53BP1, PTIP, RIF1, Rev7, and Shieldin. Early stages of B and T lymphocyte development are dependent on recombination activating gene (RAG)-induced DSBs that form the basis for further V(D)J recombination. Non-homologous end joining (NHEJ) pathway factors recognize, process, and ligate DSBs. Based on numerous loss-of-function studies, DDR factors were thought to be dispensable for the V(D)J recombination. In particular, mice lacking Mediator of DNA Damage Checkpoint Protein 1 (MDC1) possessed nearly wild-type levels of mature B and T lymphocytes in the spleen, thymus, and bone marrow. NHEJ factor XRCC4-like factor (XLF)/Cernunnos is functionally redundant with ATM, histone H2AX, and p53-binding protein 1 (53BP1) during the lymphocyte development in mice. Here, we genetically inactivated *MDC1*, *XLF*, or both *MDC1* and *XLF* in murine vAbl pro-B cell lines and, using chromosomally integrated substrates, demonstrated that MDC1 stimulates the V(D)J recombination in cells lacking XLF. Moreover, combined inactivation of *MDC1* and *XLF* in mice resulted in synthetic lethality. Together, these findings suggest that MDC1 and XLF are functionally redundant during the mouse development, in general, and the V(D)J recombination, in particular.

Keywords: V(D)J recombination; vAbl cells; B lymphocytes; mouse genetics; genetic interaction

1. Introduction

In mammalian cells, DNA double-strand breaks (DSBs) activate the DNA damage response signaling (DDR). During DDR, Ataxia telangiectasia mutated (ATM) protein kinase phosphorylates multiple substrates, including histone H2AX and the scaffold proteins, mediator of DNA damage checkpoint protein 1 (MDC1) and p53-binding protein 1 (53BP1) [1]. The E3 ubiquitin ligases, really interesting new gene (RING) finger (RNF) 8 and RNF168, function downstream of the ATM to enhance 53BP1 binding, which, in turn, facilitates the recruitment of DDR effectors, Pax transactivation domain-interacting protein (PTIP), and Rap1-interacting factor 1 (RIF1) [1]. Moreover, methylated [2–4] and acetylated [5] histones may facilitate the DDR. In particular, histone H4 lysine 20 di-methylation (H4K20me2) [3] and histone H3 lysine 79 mono- and di-methylation (H3K79me1/2) [4] were thought to facilitate recruitment of 53BP1 to the sites of damaged DNA. Homologous recombination (HR), classical non-homologous end joining (NHEJ), and alternative end joining (A-EJ) are cellular pathways

that recognize and repair DSBs. NHEJ is initiated by the recruitment of the core Ku70/Ku80 (Ku) sensor to the DSB sites. Ku facilitates the recruitment of downstream factors, including the DNA-dependent protein kinase, catalytic subunit (DNA-PKcs), and the NHEJ core factors DNA ligase 4 (Lig4) and X-ray repair cross-complementing protein 4 (XRCC4). A number of NHEJ proteins, including accessory factors, stabilize the DNA repair complex and process DNA overhangs to facilitate ligation [1]. Among them, nuclease Artemis [6], XRCC4-like factor (XLF, or Cernunnos) [7,8], a paralogue of XRCC4 and XLF (PAXX) [9–11], and modulator of retrovirus infection (Mri) [12,13].

During the B and T lymphocyte development, both DDR and NHEJ pathways function in response to the recombination activating gene (RAG)-induced DSBs in the process known as the variable (V), diversity (D) and joining (J) gene segments recombination (V(D)J recombination). RAG is the nuclease that generates DSBs adjacent to the V, D, and J gene segments of immunoglobulin and T cell receptor genes. NHEJ is the only known process to recognize and efficiently repair RAG-induced DSBs [1,14]. V(D)J recombination is ablated in mice lacking core NHEJ factors, Ku70 [15] and Ku80 [16]. Inactivation of *XRCC4* or *Lig4* resulted in embryonic lethality in mice, while conditional inactivation or knocking down of *XRCC4* or *Lig4* in lymphocytes blocked the V(D)J recombination and NHEJ [1,17,18]. Accessory NHEJ factors DNA-dependent protein kinase, catalytic subunit (DNA-PKcs) and Artemis are required for the V(D)J recombination-associated DNA repair. Artemis is a nuclease that processes RAG-induced hairpin-sealed DNA ends, and DNA-PKcs is required to both structurally stabilize and phosphorylate Artemis [6,19–23]. On the contrary, germline inactivation of *XLF* [24,25], *PAXX* [26–29], or *Mri* [12,13] had no or modest impact on the DNA repair and lymphocyte development in general, and the V(D)J recombination in particular. Combined inactivation of *XLF* and *PAXX* resulted in the V(D)J recombination defect in cells [30–32] and synthetic lethality in mice [26,28,29,33]. Moreover, *XLF* is functionally redundant with DNA-PKcs [33–35], *Mri* [12,13], and RAG2 [36].

DDR factors were thought to be dispensable for the V(D)J recombination, because germline inactivation of *ATM* [37], *H2AX* [38,39], *MDC1* [40], or *53BP1* [41] resulted in modest or no effect on early stages of B and T lymphocyte development. Strikingly, combined inactivation of *XLF* and *ATM* [42], or *XLF* and *53BP1* [43,44], resulted in live-born mice with nearly no mature B and T lymphocytes due to the impaired V(D)J recombination. Additional ATM-dependent DDR factors, including *MDC1*, may be involved in the V(D)J recombination, and their functions might be revealed in the *XLF*-deficient background [1,42–44].

XLF is the NHEJ factor. Mutations in the *XLF* gene in humans result in combined immunodeficiency [8,45], and inactivation of the *XLF* gene in mice results in a modest reduction of B and T lymphocytes count [24,25]. *XLF* shares a structure with *XRCC4*, and binds *XRCC4* to stimulate the *Lig4* activity [7]. *XLF* has a yeast homolog *Nej1* that also stimulates the DNA repair in yeast [46]. Moreover, the lack of *XLF* results in increased levels of medulloblastoma in *Trp53*-deficient mice [24]. Together, these observations place *XLF* to the group of “core” NHEJ factors. *MDC1* is a DNA damage response protein acting downstream of *ATM* and upstream of *53BP1* [47]. Like *XLF*, the *MDC1* has no enzymatic activity and likely stabilizes the DNA repair complex and facilitates the recruitment of other DNA repair factors. Both *MDC1* and *XLF* can be phosphorylated by *ATM* and likely by DNA-PKcs to regulate their functions in DNA repair [1]. Moreover, both *XLF* and *MDC1* were proposed to tether the DNA at the DSB sites before the DNA ligation [1,48].

Here, we generated *MDC1*^{-/-}*XLF*^{-/-} double-knockout cell lines and demonstrated that *MDC1* is stimulating the V(D)J recombination in cells lacking *XLF*. Moreover, we demonstrated that combined inactivation of *MDC1* and *XLF* resulted in synthetic lethality in mice.

2. Materials and Methods

2.1. Generation of Abelson Murine Leukemia Virus-Transformed (vAbl) Cell Lines

Eμ-Bcl2⁺ and *XLF*^{-/-}*Eμ-Bcl2*⁺ vAbl cells were published earlier [34,42,43]. Five independent clones of *MDC1*^{-/-}*Eμ-Bcl2*⁺ were generated using two three-week-old mice following the procedure described

previously [34,42,43,49,50]. Additionally, the *XLF* gene was inactivated in $E\mu$ -*Bcl2*⁺ vAbl cells to obtain *XLF*^{-/-} $E\mu$ -*Bcl2*⁺ cell lines, and in *MDC1*^{-/-} $E\mu$ -*Bcl2*⁺ to generate *MDC1*^{-/-}*XLF*^{-/-} $E\mu$ -*Bcl2*⁺ vAbl lines, using the clustered regularly interspaced short palindromic repeats (CRISPR)/CRISPR-associated protein 9 (Cas9) gene-editing approach as described earlier [51]. Briefly, oligonucleotides corresponding to single guide RNAs (sgRNAs) were cloned into the plasmid vector LentiCRISPR v2 (Addgene plasmid #52961, Addgene, Watertown, MA, USA) [52]. The following sgRNAs were used to target *exon 3* of the *XLF* gene: sgRNA1_FWD: 5'-CTTAGCATACACCAACTTC-3'; sgRNA1_REV: 5'-GAAGTTGGTGTATGCTAAG-3'; sgRNA2_FWD: 5'-CCACCAACAGGTACTCATA-3'; sgRNA2_REV: 5'-TATGAGTACCTGTTGGTGG-3'. Parental vAbl cells were transduced with lentiviral vectors containing corresponding sgRNA sequences, and up to 200 clones were screened by western blot. The cells lacking the *XLF* signal were used to validate the deletion of the *exon 3* by DNA sequencing (available upon request). Two *XLF*^{-/-} clones and four *MDC1*^{-/-}*XLF*^{-/-} clones were used for experiments. Mock-treated and parental vAbl cells were used as DNA repair-proficient controls.

2.2. Antibodies

The following antibodies were used for western blot: rabbit polyclonal anti-*XLF* (Bethyl, Montgomery, TX, USA; A300-730A, dilution 1:2000), swine polyclonal anti-rabbit immunoglobulin-horseradish peroxidase-conjugated (Ig-HRP; Dako antibodies, Dako, Glostrup, Denmark; #P0399, dilution 1:5000), mouse monoclonal anti- β -actin (Abcam, Cambridge, UK; ab8226, dilution 1:2000), rabbit polyclonal anti-mouse Ig-HRP (Dako antibodies, Dako, Glostrup, Denmark; #P0260, dilution 1:5000), and goat polyclonal anti-mouse Ig-HRP (Dako antibodies, Dako, Glostrup, Denmark; #P0447, dilution 1:5000).

2.3. Variable (V), Diversity (D) and Joining (J) Gene Segments Recombination (V(D)J Recombination) Assays Based on Chromosomally Integrated pMX Cassettes

V(D)J recombination assays were performed using chromosomally-integrated *pMX inversion* (*pMX-INV*) and *pMX deletion* (*pMX-DEL*) substrates, as previously described [34,42,43,49,50]. In the *pMX-INV* cassette, the *green fluorescent protein* (*GFP*) gene is placed in the reversed orientation and the *GFP* protein is not expressed. Upon the RAG-induced V(D)J recombination, the *GFP* gene is placed in the sense orientation leading to the *GFP* protein expression. The *GFP* protein is then detected by flow cytometry to estimate the V(D)J recombination efficiency in indicated vAbl cells [42,49,50]. For the Southern blot-based experiments, we used chromosomally-integrated *pMX-DEL* cassettes. During the V(D)J recombination, the *pMX-DEL*^{CJ} cassette results in an intermediate product with hairpin-sealed coding ends that require Artemis nuclease activity to open the hairpins prior DNA ligase 4-dependent DNA ligation, leading to coding joints (CJ). On the contrary, the *pMX-DEL*^{SJ} cassette results in the RAG-dependent generation of blunt signal ends (SE) that can be directly ligated by DNA ligase 4 and do not require Artemis nuclease activity, leading to signal joints (SJ) [34,42,43,49,50].

2.4. Mice

All experiments involving mice were performed according to the protocols approved by the Norges teknisk-naturvitenskapelige universitet (NTNU), FOTS#8319. *MDC1*^{+/-} [40], *XLF*^{+/ Δ} [24], and $E\mu$ -*Bcl2*⁺ [53] mice were described previously. The $E\mu$ -*Bcl2*⁺ transgenic mice were used to generate vAbl pre-B cells and increase cell survival during the experimental procedures [49].

2.5. Proliferation Assay

Fifty thousand vAbl cells were plated in 2 mL of Roswell Park Memorial Institute (RPMI) medium in triplicates into 6-well plates. Similarly, fifty thousand human haploid 1 (HAP1) cells were plated in Iscove's Modified Dulbecco's Medium (IMDM; Thermo Fisher, Waltham, MA, USA; 21980065) and supplemented with 10% fetal bovine serum, FBS (Sigma, St. Louis, MO, USA; F7524), and 1% penicillin-streptomycin (Thermo Fisher, Waltham, MA, USA; 15140122) at 37 °C with 5% CO₂, according to the manufacturer's instructions. *MDC1* ^{Δ} HAP1 cells are nearly haploid human cells that were

custom-generated by request and provided by Horizon Discovery (Waterbeach, Cambridge, UK; HZGHC005077c003). The HAP1 cells are human, nearly haploid cell lines derived from the chronic myelogenous leukemia (CML) cell line (KMB-7). The HAP1 model has been recently used to develop knockout human cells (e.g., References [13,33,51,54]).

Both vAbl and HAP1 cells were counted every 24 h using a Countess™ Automated Cell Counter (Invitrogen, Carlsbad, CA, USA) with Trypan blue staining (Invitrogen, Carlsbad, CA, USA) and bright-field detection. Statistical analyses were performed using GraphPad Prism 8 (La Jolla, CA, USA), one-way analysis of variance (ANOVA), and *t*-test.

3. Results

3.1. Robust V(D)J Recombination in Progenitor-B Cells Lacking Mediator of DNA Damage Checkpoint Protein 1 (MDC1)

Mice lacking MDC1 possess nearly wild-type levels of B and T lymphocytes [40]. Combined inactivation of *MDC1* and *Artemis* suggests that MDC1 protects or stabilizes RAG-induced DSBs before ligation. In particular, the vAbl cells lacking MDC1 and *Artemis* possess ATM-dependent degradation of free DNA ends during the attempted V(D)J recombination [55]. To further determine the impact of MDC1 on the V(D)J recombination, we inter-crossed *MDC1*^{+/-}*Eμ-Bcl2*⁺ mice and isolated the cells from the bone marrow of three-week-old *MDC1*^{-/-}*Eμ-Bcl2*⁺ animals. We then established Abelson murine leukemia virus kinase-transformed pro-B cells (vAbl) and chromosomally-integrated either *pMX-INV* or *pMX-DEL* V(D)J recombination cassettes, as described previously [18,34,42,43,49]. Similar to wild type (WT) controls, two independently generated MDC1-deficient vAbl cell lines possessed robust coding-end (CE) and signal end (SE) joining (Supplementary Figure S1). We concluded that MDC1 is dispensable for the V(D)J recombination in WT vAbl progenitor B cells.

3.2. Synthetic Lethality Between Mediator of DNA Damage Checkpoint Protein 1 (MDC1) and XRCC4-Like Factor (XLF) in Mouse

To further investigate the role of MDC1 during the V(D)J recombination, we first attempted to generate the *MDC1*^{-/-}*XLF*^{-/-} double knockout mice. Individual inactivation of *MDC1* or *XLF* results in live-born mice that possess modest levels of DNA repair defects [24,25,34,40,42–44]. First, we obtained *MDC1*^{+/-}*XLF*^{-/-} mice, starting with available heterozygous *MDC1*^{+/-} [40] and *XLF*^{+/-} [24] animals. By inter-crossing *MDC1*^{+/-}*XLF*^{-/-} mice, we obtained and genotyped 104 pups, including 34 *MDC1*^{+/+}*XLF*^{-/-} and 70 *MDC1*^{+/-}*XLF*^{-/-} (Table 1). Strikingly, we detected no *MDC1*^{-/-}*XLF*^{-/-} double knockout pups, and the final genotype distribution was 34:70:0 (1:2:0) (Table 1). We concluded that combined inactivation of *MDC1* and *XLF* results in embryonic lethality.

Table 1. Synthetic lethality between Mediator of DNA Damage Checkpoint Protein 1 (*MDC1*) and XRCC4-like factor (*XLF*).

Genotypes	Live Born	Expected (1:2:1)	Expected * (1:2:0)
<i>MDC1</i> ^{+/+} <i>XLF</i> ^{-/-}	34	26	35
<i>MDC1</i> ^{+/-} <i>XLF</i> ^{-/-}	70	52	69
<i>MDC1</i> ^{-/-} <i>XLF</i> ^{-/-}	0	26	0
Total	104	104	104

* Corrected expected distribution, which does not include the probability of *MDC1*^{-/-}*XLF*^{-/-} mice.

3.3. Generation of *XLF*^{-/-} Knockout and *MDC1*^{-/-}*XLF*^{-/-} Double Knockout vAbl Cell Lines

To obtain double knockout *MDC1*^{-/-}*XLF*^{-/-} and control *XLF*^{-/-} vAbl cells, we inactivated the *XLF* gene in *MDC1*^{-/-} and WT vAbl cells using the CRISPR/Cas9 gene-editing approach (see the Materials and Methods Section). Briefly, we targeted *exon 3* of the *XLF* gene (Figure 1A) and verified gene inactivation by western blot (Figure 1B) and DNA sequencing (available upon request). The proliferation

of WT, $XLF^{-/-}$, and $MDC1^{-/-}$ vAbl cells were of similar rates during the 72 h, $p > 0.05$ (Figure 1C). On the contrary, $MDC1^{-/-} XLF^{-/-}$ double knockout vAbl cell lines possessed reduced proliferation rates (****, $p < 0.0001$) at 48 and 72 h of the experiment (Figure 1C). Inactivation of the $MDC1$ gene in human HAP1 cells resulted in proliferation rates similar to WT cells at 24–72 h, and reduced proliferation rates at 96 and 120 h (Figure 1D).

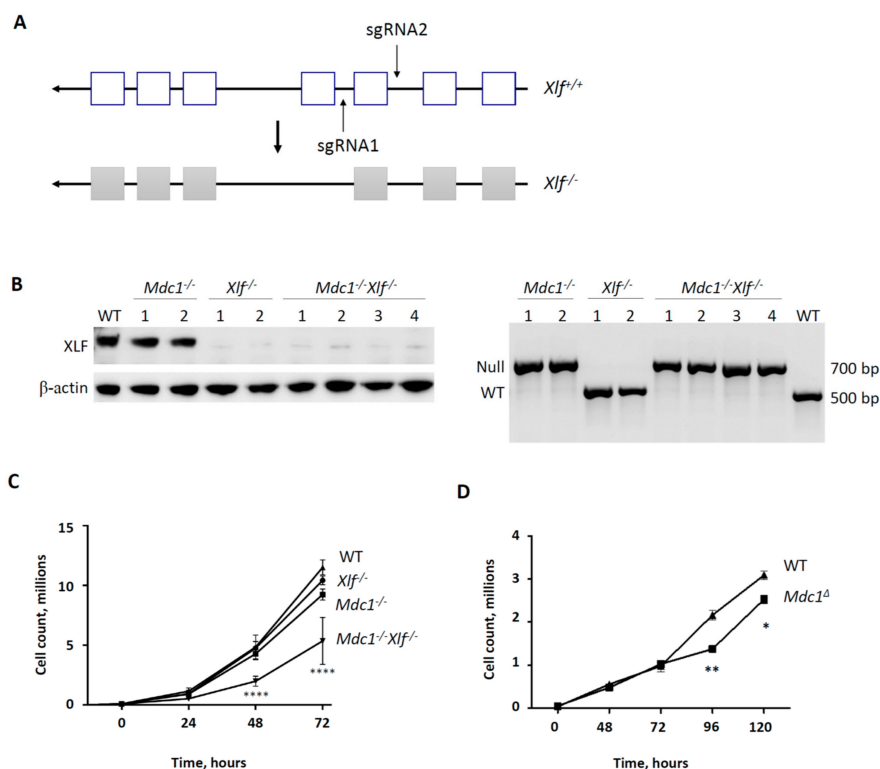


Figure 1. Generation of $MDC1^{-/-} XLF^{-/-}$ vAbl cells. (A) Clustered regularly interspaced short palindromic repeats (CRISPR)/CRISPR-associated protein 9 (Cas9)-mediated inactivation of the *XLF* gene targeting *exon 3* in Abelson murine leukemia virus-transformed (vAbl) progenitor-B cell lines. (B) Western blot detecting XRCC4-like factor (XLF) protein in wild type (WT) and Mediator of DNA Damage Checkpoint Protein 1-deficient ($MDC1^{-/-}$) vAbl cells. No signal corresponding to XLF was detected in $XLF^{-/-}$ and $MDC1^{-/-} XLF^{-/-}$ vAbl cells. Antibody against beta-actin was used to detect beta-actin, a loading control (left). Polymerase chain reaction (PCR) followed by agarose gel electrophoresis detecting *MDC1* null and WT alleles (right). The 500 base pairs (bp) band corresponds to the WT allele, and the 700 bp band corresponds to the *MDC1* null allele (right). (C) The proliferation of vAbl cells lacking either XLF or MDC1, both $MDC1/XLF$, and WT controls. WT, $XLF^{-/-}$, and $MDC1^{-/-}$ cells proliferate with a similar rate (n.s., $p > 0.05$). $MDC1^{-/-} XLF^{-/-}$ cells proliferate slower than WT, $XLF^{-/-}$ and $MDC1^{-/-}$ vAbl cells (****, $p < 0.0001$). Data represent the mean \pm standard deviation (SD) of three independent experiments using 1 WT control, 2 $MDC1^{-/-}$, 2 $XLF^{-/-}$, and 2 $MDC1^{-/-} XLF^{-/-}$ clones. (D) The proliferation of haploid 1 (HAP1) cells lacking MDC1, and wild type (WT) controls. $MDC1^{\Delta}$ HAP1 cells possess reduced proliferation rates when compared to WT at 96 and 120 hours (h) of the experiment (*, $p < 0.05$; **, $p < 0.01$). Data represent the mean \pm standard deviation (SD) of three independent experiments using WT parental control and $MDC1^{\Delta}$ clones.

3.4. Reduced V(D)J Recombination Efficiency in *vAbl* Pro-B Cells Lacking both MDC1 and XLF

To determine the impact of MDC1 on V(D)J recombination, we chromosomally-integrated the cassette-carrying *GFP* gene in reverse orientation and flanked by DNA sequences recognized by RAG (*pMX-INV*) [49,50] (Figure 2A). To induce the RAG expression, we exposed the cells to the *vAbl* kinase inhibitor STI571 (Gleevec). Upon a successful V(D)J recombination event, the cells expressing GFP were detectable by flow cytometry [42,49,50]. The cells lacking MDC1 possessed relatively high levels of V(D)J recombination reflected by GFP expression (29%), which was in the range of WT and *XLF*^{-/-} cell lines (34% and 37%, respectively) (Figure 2B–D). Strikingly, combined inactivation of *MDC1* and *XLF* resulted in a significantly reduced proportion of GFP-expressing *vAbl* cells when compared to WT and single knockout controls (average levels of 20%; ****, *p* < 0.0001). Double knockout *DNA-PKcs*^{-/-} *XLF*^{-/-} *vAbl* cells were used as a negative control to establish background levels of the experiments (0% of GFP-positive cells) [34]. We concluded that MDC1 is stimulating the V(D)J recombination in *XLF*-deficient cells, due to functional complementarity between MDC1 and *XLF* in this process.

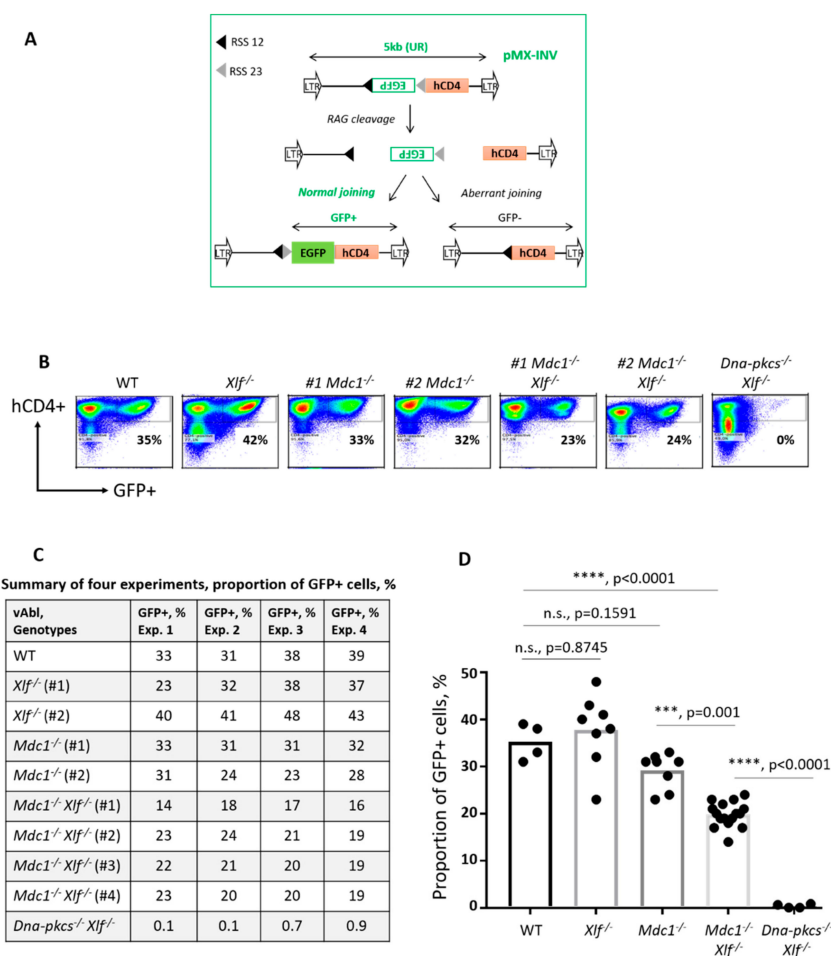


Figure 2. Mediator of DNA Damage Checkpoint Protein 1 (MDC1) stimulates the *variable* (V), *diversity* (D) and *joining* (J) gene segments recombination (V(D)J recombination) in the cells lacking XRCC4-like factor (XLF). (A) Schematic representation of the green fluorescent protein (GFP) expression-based

V(D)J recombination reporter. Upon treatment with STI571, the recombination activating gene (RAG) induces DNA double-strand breaks (DSBs) at dedicated sites flanking the *GFP* gene in reverse orientation. After inversion and DSB repair, the *GFP* gene is placed in the sense orientation, and the GFP protein is expressed and detected by flow cytometry. (B) Examples of flow cytometry-based quantification of GFP-positive vAbl cells (WT, *XLF*^{-/-}, *MDC1*^{-/-}, *MDC1*^{-/-}*XLF*^{-/-}, and *DNA-PKcs*^{-/-}*XLF*^{-/-}) following exposure to STI571 for 96 hours (h). The human cluster of differentiation 4 (hCD4) was used as a surface marker of the chromosomally integrated V(D)J recombination cassette. At day 0, vAbl cells were sorted based on the hCD4 expression, and hCD4-positive cells were used for the experiments. (C) Proportions of the GFP-positive vAbl cells of indicated genotypes in the V(D)J recombination experiments using chromosomally integrated cassettes. Data represent the mean ± standard deviation (SD) of four independent experiments using one WT, two *XLF*^{-/-}, two *MDC1*^{-/-}, and four *MDC1*^{-/-}*XLF*^{-/-} lines, used in all the experiments. *DNA-PKcs*^{-/-}*XLF*^{-/-} vAbl cells were used as a non-homologous end joining (NHEJ)-deficient negative control, to establish background levels of GFP expression. (D) Statistical analyses of V(D)J recombination efficiency in vAbl cells. WT versus *XLF*^{-/-} (n.s., $p = 0.8745$); WT versus *MDC1*^{-/-} (n.s., $p = 0.1591$), WT versus *MDC1*^{-/-}*XLF*^{-/-} (****, $p < 0.0001$); WT versus *DNA-PKcs*^{-/-}*XLF*^{-/-} (****, $p < 0.0001$); *XLF*^{-/-} versus *MDC1*^{-/-}*XLF*^{-/-} (****, $p < 0.0001$); *XLF*^{-/-} versus *DNA-PKcs*^{-/-}*XLF*^{-/-} (****, $p < 0.0001$); *MDC1*^{-/-} versus *MDC1*^{-/-}*XLF*^{-/-} (****, $p = 0.0001$); *MDC1*^{-/-} versus *DNA-PKcs*^{-/-}*XLF*^{-/-} (****, $p < 0.0001$); *MDC1*^{-/-}*XLF*^{-/-} versus *DNA-PKcs*^{-/-}*XLF*^{-/-} (****, $p < 0.0001$).

4. Discussion

Inactivation of *RAG* and most of the known NHEJ factor genes in mice leads to immunodeficiency [12,56]. Recently, we and others found that single inactivation of *XLF*, *PAXX*, or *Mri* genes results in mice with the nearly normal immune system, due to the overlapping functions between *XLF* and *PAXX* [26–29,33], as well as *XLF* and *Mri* [12,13] (Table 2). The ATM-dependent DDR pathway was initially thought to be dispensable for the V(D)J recombination, although more recent studies using combined genetic inactivation of *XLF* and *ATM* [42], as well as *DNA-PKcs* and *ATM* [21,57], revealed that ATM is indeed involved in the early stages of B and T lymphocyte development and its function is partially compensated by *XLF* and *DNA-PKcs*. Later, we and others found that ATM substrates, *H2AX* and *53BP1*, are also required for B and T lymphocyte development due to their functions in V(D)J recombination [42–44] (Table 2). Here, we show that another ATM substrate, *MDC1*, is involved in the V(D)J recombination and its function is compensated in WT cells by *XLF*. Combined inactivation of *ATM* and *XLF*, or *53BP1* and *XLF*, resulted in immunodeficient mice of smaller sizes than single knockouts or wild-type controls, with abrogated NHEJ, resembling *Ku70*^{-/-} or *Ku80*^{-/-} knockouts [1,42–44]. Differently, combined inactivation of *DNA-PKcs* and *XLF* [34,35], *H2AX* and *XLF* [42], or *MDC1* and *XLF* ([33]; and this study) resulted in embryonic lethality in mice, challenging genetic interaction studies in vivo (Table 2). One option to overcome this obstacle is to develop conditional knockouts allowing inactivation of *DNA-PKcs*, *XLF*, or *MDC1* in developing B and T lymphocytes in adult mice. An alternative option is to develop more complex mouse models using, for example, *p53*^{-/-} or *p53*^{+/-} backgrounds, allowing for the rescue of embryonic lethality (e.g., References [33,35]).

Knocking out genes of interest in cell lines may complement and sometimes substitute in vivo experiments using transgenic mice. In particular, vAbl cell lines can be modified using the CRISPR/Cas9 gene-editing approach and serve as a model system to elucidate the specific roles of a particular gene (e.g., References [30–32,50]). Moreover, human, nearly haploid HAP1 cells derived from the KMB-7 cell lines have been recently used to develop genetically-modified cells (e.g., References [13,33,51,54]).

It becomes more accepted that the DDR pathway contributes to the V(D)J recombination in developing B and T lymphocytes [1,34,42–44]. However, the mechanistic aspects underlying the specific roles of the DDR factors in this process remain unclear. One can speculate that DDR factors share the functions with *XLF*, e.g., by stabilizing the DNA repair complex or supporting timely recruitment and dissociation of the NHEJ factors. The DDR pathway may also contribute to distinct but complementary *XLF* aspects of the DNA repair, e.g., by recruiting the downstream enzymes,

supporting the DNA damage-induced post-translational modifications of DNA repair factors and histones, or protecting the free DNA ends from the nuclease-dependent processing before the DNA ligation step [1,34,42–44,55]. In particular, the role of MDC1 during the V(D)J recombination might be to stabilize the DNA repair complex, to protect the free DNA ends, to ensure efficient recruitment of downstream DDR factors, such as 53BP1, PTIP, RIF1, Shieldin, etc. [1,42–44,47,55,58], or to exit from the G1 phase of the cell cycle following the RAG-induced DSB [59]. Further research is required to identify specific roles of MDC1 and XLF in DNA repair.

Table 2. Impact of NHEJ-deficiency on V(D)J recombination in mice.

Genotypes	V(D)J Recombination	Mice
Single Knockouts		
<i>DNA-PKcs</i> ^{-/-} [23]	No	Alive
<i>PAXX</i> ^{-/-} [9–11,27]	Normal	Alive
<i>Mri</i> ^{-/-} [12,13]	Normal	Alive
<i>XLF</i> ^{-/-} [24,25]	Normal	Alive
<i>ATM</i> ^{-/-} [37]	Normal	Alive
<i>H2AX</i> ^{-/-} [38,39]	Reduced	Alive
<i>MDC1</i> ^{-/-} [40]	Normal	Alive
<i>53BP1</i> ^{-/-} [41]	Normal	Alive
<i>RAG2</i> ^{ΔΔ} [60]	Reduced	Alive
Double Knockouts		
<i>XLF</i> ^{-/-} <i>DNA-PKcs</i> ^{-/-} [34,35]	No	Embryonic lethality
<i>XLF</i> ^{-/-} <i>PAXX</i> ^{-/-} [26,28,29,33]	No	Embryonic lethality
<i>XLF</i> ^{-/-} <i>Mri</i> ^{-/-} [12]	No	Embryonic lethality
<i>XLF</i> ^{-/-} <i>ATM</i> ^{-/-} [42]	Very low	Alive, small
<i>XLF</i> ^{-/-} <i>H2AX</i> ^{-/-} [42]	Reduced	Embryonic lethality
<i>XLF</i> ^{-/-} <i>MDC1</i> ^{-/-} [*]	Reduced	Embryonic lethality
<i>XLF</i> ^{-/-} <i>53BP1</i> ^{-/-} [43,44]	Very low	Alive, small
<i>XLF</i> ^{-/-} <i>RAG2</i> ^{ΔΔ} [36]	Very low	Alive

References are cited. This study [*].

The proliferation rate of vAbl cells lacking both XLF and MDC1 was reduced when compared to single-deficient and WT controls (Figure 1) at 72 h. Moreover, proliferation rates of MDC1-deficient cells were also reduced when compared to WT, although not significant. Furthermore, the lack of MDC1 alone resulted in significantly reduced proliferation rates of human HAP1 cells at 96 and 120 h (Figure 1). These observations may suggest that, first, the lack of MDC1 is compensated by the presence of XLF in murine cells, and second, that the MDC1 is required for efficient DNA repair and proliferation of human cells, likely by supporting the cell cycle progression and DNA damage tolerance [47,59].

5. Conclusions

Multiple DDR factors are involved in the V(D)J recombination. Due to the functional redundancy between the DDR and NHEJ pathways, complex genetic in vivo and in vitro models will be appropriate to uncover specific functions of DDR factors in B and T lymphocyte development and further elucidate mechanisms underlying their roles.

Supplementary Materials: The following are available online at <http://www.mdpi.com/2218-273X/10/1/60/s1>, Figure S1: Robust V(D)J recombination in vAbl cells lacking MDC1.

Author Contributions: All the authors designed, performed, and analyzed the experiments. The manuscript was written by V.O. All of the authors read and approved the final version of the manuscript. All authors have read and agreed to the published version of the manuscript.

Funding: This work was supported by the Research Council of Norway Young Talent Investigator grant (#249774) to V.O. In addition, Oksenysh group was supported by the Liaison Committee for education, research,

and innovation in Central Norway (#13477; #38881), the Norwegian Cancer Society (#182355), FRIMEDBIO grants (#270491 and #291217), and The Outstanding Academic Fellow Program at NTNU (2017–2021).

Conflicts of Interest: The authors declare no conflict of interest.

References

1. Kumar, V.; Alt, F.W.; Oksenyich, V. Functional overlaps between XLF and the ATM-dependent DNA double strand break response. *DNA Repair* **2014**, *16*, 11–22. [[CrossRef](#)] [[PubMed](#)]
2. Oksenyich, V.; Zhovmer, A.; Ziani, S.; Mari, P.O.; Eberova, J.; Nardo, T.; Stefanini, M.; Giglia-Mari, G.; Egly, J.M.; Coin, F. Histone methyltransferase DOT1L drives recovery of gene expression after a genotoxic attack. *PLoS Genet.* **2013**, *9*, e1003611. [[CrossRef](#)] [[PubMed](#)]
3. Botuyan, M.V.; Lee, J.; Ward, I.M.; Kim, J.E.; Thompson, J.R.; Chen, J.; Mer, G. Structural basis for the methylation state-specific recognition of histone H4-K20 by 53BP1 and Crb2 in DNA repair. *Cell* **2006**, *127*, 1361–1373. [[CrossRef](#)] [[PubMed](#)]
4. Huyen, Y.; Zgheib, O.; Ditullio, R.A., Jr.; Gorgoulis, V.G.; Zacharatos, P.; Petty, T.J.; Sheston, E.A.; Mellert, H.S.; Stavridi, E.S.; Halazonetis, T.D. Methylated lysine 79 of histone H3 targets 53BP1 to DNA double-strand breaks. *Nature* **2004**, *432*, 406–411. [[CrossRef](#)] [[PubMed](#)]
5. Lee, H.S.; Park, J.H.; Kim, S.J.; Kwon, S.J.; Kwon, J. A cooperative activation loop among SWI/SNF, gamma-H2AX and H3 acetylation for DNA double-strand break repair. *EMBO J.* **2010**, *29*, 1434–1445. [[CrossRef](#)] [[PubMed](#)]
6. Ma, Y.; Pannicke, U.; Schwarz, K.; Lieber, M.R. Hairpin opening and overhang processing by an Artemis/DNA-dependent protein kinase complex in nonhomologous end joining and V(D)J recombination. *Cell* **2002**, *108*, 781–794. [[CrossRef](#)]
7. Ahnesorg, P.; Smith, P.; Jackson, S.P. XLF interacts with the XRCC4-DNA ligase IV complex to promote DNA nonhomologous end-joining. *Cell* **2006**, *124*, 301–313. [[CrossRef](#)]
8. Buck, D.; Malivert, L.; de Chasseval, R.; Barraud, A.; Fondaneche, M.C.; Sanal, O.; Plebani, A.; Stephan, J.L.; Hufnagel, M.; le Deist, F.; et al. Cernunnos, a novel nonhomologous end-joining factor, is mutated in human immunodeficiency with microcephaly. *Cell* **2006**, *124*, 287–299. [[CrossRef](#)]
9. Craxton, A.; Somers, J.; Munnur, D.; Jukes-Jones, R.; Cain, K.; Malewicz, M. XLS (c9orf142) is a new component of mammalian DNA double-stranded break repair. *Cell Death Differ.* **2015**, *22*, 890–897. [[CrossRef](#)]
10. Ochi, T.; Blackford, A.N.; Coates, J.; Jhujh, S.; Mehmood, S.; Tamura, N.; Travers, J.; Wu, Q.; Draviam, V.M.; Robinson, C.V.; et al. DNA repair. PAXX, a paralog of XRCC4 and XLF, interacts with Ku to promote DNA double-strand break repair. *Science* **2015**, *347*, 185–188. [[CrossRef](#)]
11. Xing, M.; Yang, M.; Huo, W.; Feng, F.; Wei, L.; Jiang, W.; Ning, S.; Yan, Z.; Li, W.; Wang, Q.; et al. Interactome analysis identifies a new paralogue of XRCC4 in non-homologous end joining DNA repair pathway. *Nat. Commun.* **2015**, *6*, 6233. [[CrossRef](#)] [[PubMed](#)]
12. Hung, P.J.; Johnson, B.; Chen, B.R.; Byrum, A.K.; Bredemeyer, A.L.; Yewdell, W.T.; Johnson, T.E.; Lee, B.J.; Deivasigamani, S.; Hindi, I.; et al. MRI Is a DNA Damage Response Adaptor during Classical Non-homologous End Joining. *Mol. Cell* **2018**, *71*, 332–342.e8. [[CrossRef](#)]
13. Castaneda-Zegarra, S.; Huse, C.; Røsand, Ø.; Sarno, A.; Xing, M.; Gago-Fuentes, R.; Zhang, Q.; Alirezaylavasani, A.; Werner, J.; Ji, P.; et al. Generation of a Mouse Model Lacking the Non-Homologous End-Joining Factor Mri/Cyren. *Biomolecules* **2019**, *9*, 798. [[CrossRef](#)] [[PubMed](#)]
14. Alt, F.W.; Zhang, Y.; Meng, F.L.; Guo, C.; Schwer, B. Mechanisms of programmed DNA lesions and genomic instability in the immune system. *Cell* **2013**, *152*, 417–429. [[CrossRef](#)] [[PubMed](#)]
15. Gu, Y.; Seidl, K.J.; Rathbun, G.A.; Zhu, C.; Manis, J.P.; van der Stoep, N.; Davidson, L.; Cheng, H.L.; Sekiguchi, J.M.; Frank, K.; et al. Growth retardation and leaky SCID phenotype of Ku70-deficient mice. *Immunity* **1997**, *7*, 653–665. [[CrossRef](#)]
16. Nussenzweig, A.; Chen, C.; da Costa Soares, V.; Sanchez, M.; Sokol, K.; Nussenzweig, M.C.; Li, G.C. Requirement for Ku80 in growth and immunoglobulin V(D)J recombination. *Nature* **1996**, *382*, 551–555. [[CrossRef](#)] [[PubMed](#)]
17. Yan, C.T.; Kaushal, D.; Murphy, M.; Zhang, Y.; Datta, A.; Chen, C.; Monroe, B.; Mostoslavsky, G.; Coakley, K.; Gao, Y.; et al. XRCC4 suppresses medulloblastomas with recurrent translocations in p53-deficient mice. *Proc. Natl. Acad. Sci. USA* **2006**, *103*, 7378–7383. [[CrossRef](#)]

18. Boboila, C.; Oksenysh, V.; Gostissa, M.; Wang, J.H.; Zha, S.; Zhang, Y.; Chai, H.; Lee, C.S.; Jankovic, M.; Saez, L.M.; et al. Robust chromosomal DNA repair via alternative end-joining in the absence of X-ray repair cross-complementing protein 1 (XRCC1). *Proc. Natl. Acad. Sci. USA* **2012**, *109*, 2473–2478. [[CrossRef](#)]
19. Bosma, G.C.; Custer, R.P.; Bosma, M.J. A severe combined immunodeficiency mutation in the mouse. *Nature* **1983**, *301*, 527–530. [[CrossRef](#)]
20. Rooney, S.; Sekiguchi, J.; Zhu, C.; Cheng, H.L.; Manis, J.; Whitlow, S.; DeVido, J.; Foy, D.; Chaudhuri, J.; Lombard, D.; et al. Leaky Scid phenotype associated with defective V(D)J coding end processing in Artemis-deficient mice. *Mol. Cell* **2002**, *10*, 1379–1390. [[CrossRef](#)]
21. Zha, S.; Jiang, W.; Fujiwara, Y.; Patel, H.; Goff, P.H.; Brush, J.W.; Dubois, R.L.; Alt, F.W. Ataxia telangiectasia-mutated protein and DNA-dependent protein kinase have complementary V(D)J recombination functions. *Proc. Natl. Acad. Sci. USA* **2011**, *108*, 2028–2033. [[CrossRef](#)] [[PubMed](#)]
22. Jiang, W.; Crowe, J.L.; Liu, X.; Nakajima, S.; Wang, Y.; Li, C.; Lee, B.J.; Dubois, R.L.; Liu, C.; Yu, X.; et al. Differential phosphorylation of DNA-PKcs regulates the interplay between end-processing and end-ligation during nonhomologous end-joining. *Mol. Cell* **2015**, *58*, 172–185. [[CrossRef](#)] [[PubMed](#)]
23. Gao, Y.; Chaudhuri, J.; Zhu, C.; Davidson, L.; Weaver, D.T.; Alt, F.W. A targeted DNA-PKcs-null mutation reveals DNA-PK-independent functions for KU in V(D)J recombination. *Immunity* **1998**, *9*, 367–376. [[CrossRef](#)]
24. Li, G.; Alt, F.W.; Cheng, H.L.; Brush, J.W.; Goff, P.H.; Murphy, M.M.; Franco, S.; Zhang, Y.; Zha, S. Lymphocyte-specific compensation for XLF/cernunnos end-joining functions in V(D)J recombination. *Mol. Cell* **2008**, *31*, 631–640. [[CrossRef](#)]
25. Vera, G.; Rivera-Munoz, P.; Abramowski, V.; Malivert, L.; Lim, A.; Bole-Feysot, C.; Martin, C.; Florin, B.; Latour, S.; Revy, P.; et al. Cernunnos deficiency reduces thymocyte life span and alters the T cell repertoire in mice and humans. *Mol. Cell Biol.* **2013**, *33*, 701–711. [[CrossRef](#)]
26. Balmus, G.; Barros, A.C.; Wijnhoven, P.W.; Lescale, C.; Hasse, H.L.; Boroviak, K.; le Sage, C.; Doe, B.; Speak, A.O.; Galli, A.; et al. Synthetic lethality between PAXX and XLF in mammalian development. *Genes Dev.* **2016**, *30*, 2152–2157. [[CrossRef](#)]
27. Gago-Fuentes, R.; Xing, M.; Saeterstad, S.; Sarno, A.; Dewan, A.; Beck, C.; Bradamante, S.; Bjoras, M.; Oksenysh, V. Normal development of mice lacking PAXX, the paralogue of XRCC4 and XLF. *FEBS Open Bio* **2018**, *8*, 426–434. [[CrossRef](#)]
28. Liu, X.; Shao, Z.; Jiang, W.; Lee, B.J.; Zha, S. PAXX promotes KU accumulation at DNA breaks and is essential for end-joining in XLF-deficient mice. *Nat. Commun.* **2017**, *8*, 13816. [[CrossRef](#)]
29. Abramowski, V.; Etienne, O.; Elsaid, R.; Yang, J.; Berland, A.; Kermasson, L.; Roch, B.; Musilli, S.; Moussu, J.P.; Lipson-Ruffert, K.; et al. PAXX and Xlf interplay revealed by impaired CNS development and immunodeficiency of double KO mice. *Cell Death Differ.* **2018**, *25*, 444–452. [[CrossRef](#)]
30. Kumar, V.; Alt, F.W.; Frock, R.L. PAXX and XLF DNA repair factors are functionally redundant in joining DNA breaks in a G1-arrested progenitor B-cell line. *Proc. Natl. Acad. Sci. USA* **2016**, *113*, 10619–10624. [[CrossRef](#)]
31. Hung, P.J.; Chen, B.R.; George, R.; Liberman, C.; Morales, A.J.; Colon-Ortiz, P.; Tyler, J.K.; Sleckman, B.P.; Bredemeyer, A.L. Deficiency of XLF and PAXX prevents DNA double-strand break repair by non-homologous end joining in lymphocytes. *Cell Cycle* **2017**, *16*, 286–295. [[CrossRef](#)]
32. Lescale, C.; Lenden Hasse, H.; Blackford, A.N.; Balmus, G.; Bianchi, J.J.; Yu, W.; Bacoccina, L.; Jarade, A.; Clouin, C.; Sivapalan, R.; et al. Specific Roles of XRCC4 Paralogs PAXX and XLF during V(D)J Recombination. *Cell Rep.* **2016**, *16*, 2967–2979. [[CrossRef](#)]
33. Castaneda-Zegarra, S.; Xing, M.; Gago-Fuentes, R.; Saeterstad, S.; Oksenysh, V. Synthetic lethality between DNA repair factors Xlf and Paxx is rescued by inactivation of Trp53. *DNA Repair* **2019**, *73*, 164–169. [[CrossRef](#)]
34. Oksenysh, V.; Kumar, V.; Liu, X.; Guo, C.; Schwer, B.; Zha, S.; Alt, F.W. Functional redundancy between the XLF and DNA-PKcs DNA repair factors in V(D)J recombination and nonhomologous DNA end joining. *Proc. Natl. Acad. Sci. USA* **2013**, *110*, 2234–2239. [[CrossRef](#)] [[PubMed](#)]
35. Xing, M.; Bjoras, M.; Daniel, J.A.; Alt, F.W.; Oksenysh, V. Synthetic lethality between murine DNA repair factors XLF and DNA-PKcs is rescued by inactivation of Ku70. *DNA Repair* **2017**, *57*, 133–138. [[CrossRef](#)] [[PubMed](#)]
36. Lescale, C.; Abramowski, V.; Bedora-Faure, M.; Murigneux, V.; Vera, G.; Roth, D.B.; Revy, P.; de Villartay, J.P.; Deriano, L. RAG2 and XLF/Cernunnos interplay reveals a novel role for the RAG complex in DNA repair. *Nat. Commun.* **2016**, *7*, 10529. [[CrossRef](#)]

37. Zha, S.; Sekiguchi, J.; Brush, J.W.; Bassing, C.H.; Alt, F.W. Complementary functions of ATM and H2AX in development and suppression of genomic instability. *Proc. Natl. Acad. Sci. USA* **2008**, *105*, 9302–9306. [[CrossRef](#)]
38. Bassing, C.H.; Chua, K.F.; Sekiguchi, J.; Suh, H.; Whitlow, S.R.; Fleming, J.C.; Monroe, B.C.; Ciccone, D.N.; Yan, C.; Vlasakova, K.; et al. Increased ionizing radiation sensitivity and genomic instability in the absence of histone H2AX. *Proc. Natl. Acad. Sci. USA* **2002**, *99*, 8173–8178. [[CrossRef](#)]
39. Bassing, C.H.; Suh, H.; Ferguson, D.O.; Chua, K.F.; Manis, J.; Eckersdorff, M.; Gleason, M.; Bronson, R.; Lee, C.; Alt, F.W. Histone H2AX: A dosage-dependent suppressor of oncogenic translocations and tumors. *Cell* **2003**, *114*, 359–370. [[CrossRef](#)]
40. Lou, Z.; Minter-Dykhouse, K.; Franco, S.; Gostissa, M.; Rivera, M.A.; Celeste, A.; Manis, J.P.; van Deursen, J.; Nussenzweig, A.; Paull, T.T.; et al. MDC1 maintains genomic stability by participating in the amplification of ATM-dependent DNA damage signals. *Mol. Cell* **2006**, *21*, 187–200. [[CrossRef](#)]
41. Manis, J.P.; Morales, J.C.; Xia, Z.; Kutok, J.L.; Alt, F.W.; Carpenter, P.B. 53BP1 links DNA damage-response pathways to immunoglobulin heavy chain class-switch recombination. *Nat. Immunol.* **2004**, *5*, 481–487. [[CrossRef](#)] [[PubMed](#)]
42. Zha, S.; Guo, C.; Boboila, C.; Oksenychn, V.; Cheng, H.L.; Zhang, Y.; Wesemann, D.R.; Yuen, G.; Patel, H.; Goff, P.H.; et al. ATM damage response and XLF repair factor are functionally redundant in joining DNA breaks. *Nature* **2011**, *469*, 250–254. [[CrossRef](#)]
43. Oksenychn, V.; Alt, F.W.; Kumar, V.; Schwer, B.; Wesemann, D.R.; Hansen, E.; Patel, H.; Su, A.; Guo, C. Functional redundancy between repair factor XLF and damage response mediator 53BP1 in V(D)J recombination and DNA repair. *Proc. Natl. Acad. Sci. USA* **2012**, *109*, 2455–2460. [[CrossRef](#)] [[PubMed](#)]
44. Liu, X.; Jiang, W.; Dubois, R.L.; Yamamoto, K.; Wolner, Z.; Zha, S. Overlapping functions between XLF repair protein and 53BP1 DNA damage response factor in end joining and lymphocyte development. *Proc. Natl. Acad. Sci. USA* **2012**, *109*, 3903–3908. [[CrossRef](#)] [[PubMed](#)]
45. Du, L.; Peng, R.; Bjorkman, A.; Filipe de Miranda, N.; Rosner, C.; Kotnis, A.; Berglund, M.; Liu, C.; Rosenquist, R.; Enblad, G.; et al. Cernunnos influences human immunoglobulin class switch recombination and may be associated with B cell lymphomagenesis. *J. Exp. Med.* **2012**, *209*, 291–305. [[CrossRef](#)] [[PubMed](#)]
46. Valencia, M.; Bentele, M.; Vaze, M.B.; Herrmann, G.; Kraus, E.; Lee, S.E.; Schar, P.; Haber, J.E. NEJ1 controls non-homologous end joining in *Saccharomyces cerevisiae*. *Nature* **2001**, *414*, 666–669. [[CrossRef](#)] [[PubMed](#)]
47. Salguero, I.; Belotserkovskaya, R.; Coates, J.; Sczaniecka-Clift, M.; Demir, M.; Jhujh, S.; Wilson, M.D.; Jackson, S.P. MDC1 PST-repeat region promotes histone H2AX-independent chromatin association and DNA damage tolerance. *Nat. Commun.* **2019**, *10*, 5191. [[CrossRef](#)] [[PubMed](#)]
48. Leimbacher, P.A.; Jones, S.E.; Shorrocks, A.K.; de Marco Zompit, M.; Day, M.; Blaauwendraad, J.; Bundschuh, D.; Bonham, S.; Fischer, R.; Fink, D.; et al. MDC1 Interacts with TOPBP1 to Maintain Chromosomal Stability during Mitosis. *Mol. Cell* **2019**, *74*, 571–583.e8. [[CrossRef](#)]
49. Bredemeyer, A.L.; Sharma, G.G.; Huang, C.Y.; Helmink, B.A.; Walker, L.M.; Khor, K.C.; Nuskey, B.; Sullivan, K.E.; Pandita, T.K.; Bassing, C.H.; et al. ATM stabilizes DNA double-strand-break complexes during V(D)J recombination. *Nature* **2006**, *442*, 466–470. [[CrossRef](#)]
50. Lenden Hasse, H.; Lescale, C.; Bianchi, J.J.; Yu, W.; Bedora-Faure, M.; Deriano, L. Generation and CRISPR/Cas9 editing of transformed progenitor B cells as a pseudo-physiological system to study DNA repair gene function in V(D)J recombination. *J. Immunol. Methods* **2017**, *451*, 71–77. [[CrossRef](#)]
51. Dewan, A.; Xing, M.; Lundbaek, M.B.; Gago-Fuentes, R.; Beck, C.; Aas, P.A.; Liabakk, N.B.; Saeterstad, S.; Chau, K.T.P.; Kavli, B.M.; et al. Robust DNA repair in PAXX-deficient mammalian cells. *FEBS Open Bio* **2018**, *8*, 442–448. [[CrossRef](#)] [[PubMed](#)]
52. Sanjana, N.E.; Shalem, O.; Zhang, F. Improved vectors and genome-wide libraries for CRISPR screening. *Nat. Methods* **2014**, *11*, 783–784. [[CrossRef](#)]
53. Strasser, A.; Harris, A.W.; Cory, S. bcl-2 transgene inhibits T cell death and perturbs thymic self-censorship. *Cell* **1991**, *67*, 889–899. [[CrossRef](#)]
54. Xing, M.; Oksenychn, V. Genetic interaction between DNA repair factors PAXX, XLF, XRCC4 and DNA-PKcs in human cells. *FEBS Open Bio* **2019**. [[CrossRef](#)] [[PubMed](#)]
55. Helmink, B.A.; Tubbs, A.T.; Dorsett, Y.; Bednarski, J.J.; Walker, L.M.; Feng, Z.; Sharma, G.G.; McKinnon, P.J.; Zhang, J.; Bassing, C.H.; et al. H2AX prevents CtIP-mediated DNA end resection and aberrant repair in G1-phase lymphocytes. *Nature* **2011**, *469*, 245–249. [[CrossRef](#)] [[PubMed](#)]

56. Kumar, V.; Alt, F.W.; Oksenyich, V. Reprint of “Functional overlaps between XLF and the ATM-dependent DNA double strand break response”. *DNA Repair* **2014**, *17*, 52–63. [[CrossRef](#)]
57. Gapud, E.J.; Dorsett, Y.; Yin, B.; Callen, E.; Bredemeyer, A.; Mahowald, G.K.; Omi, K.Q.; Walker, L.M.; Bednarski, J.J.; McKinnon, P.J.; et al. Ataxia telangiectasia mutated (Atm) and DNA-PKcs kinases have overlapping activities during chromosomal signal joint formation. *Proc. Natl. Acad. Sci. USA* **2011**, *108*, 2022–2027. [[CrossRef](#)] [[PubMed](#)]
58. Dev, H.; Chiang, T.W.; Lescale, C.; de Krijger, I.; Martin, A.G.; Pilger, D.; Coates, J.; Sczaniecka-Clift, M.; Wei, W.; Ostermaier, M.; et al. Shieldin complex promotes DNA end-joining and counters homologous recombination in BRCA1-null cells. *Nat. Cell Biol.* **2018**, *20*, 954–965. [[CrossRef](#)]
59. Innes, C.L.; Hesse, J.E.; Morales, A.J.; Helmink, B.A.; Schurman, S.H.; Sleckman, B.P.; Paules, R.S. DNA damage responses in murine Pre-B cells with genetic deficiencies in damage response genes. *Cell Cycle* **2020**, *19*, 67–83. [[CrossRef](#)]
60. Deriano, L.; Chaumeil, J.; Coussens, M.; Multani, A.; Chou, Y.; Alekseyenko, A.V.; Chang, S.; Skok, J.A.; Roth, D.B. The RAG2 C terminus suppresses genomic instability and lymphomagenesis. *Nature* **2011**, *471*, 119–123. [[CrossRef](#)]



© 2019 by the authors. Licensee MDPI, Basel, Switzerland. This article is an open access article distributed under the terms and conditions of the Creative Commons Attribution (CC BY) license (<http://creativecommons.org/licenses/by/4.0/>).

Mediator of DNA damage checkpoint protein 1 facilitates V(D)J recombination in cells lacking DNA repair factor XLF

Carole Beck ^{1,2}, Sergio Castañeda-Zegarra ^{1,2}, Camilla Huse ^{1,2}, Mengtan Xing ^{1,2}, Valentyn Oksenyich ^{1,2,3,*}

- ¹ Department of Clinical and Molecular Medicine (IKOM), Norwegian University of Science and technology, 7491 Trondheim, Norway; carole.beck@ntnu.no (C.B.); camilla.huse@rr-research.no (C.H.); sergio.m.c.zegarra@ntnu.no (S.CZ.); valentyn.oksenych@ntnu.no (V.O.)
 - ² St. Olavs Hospital, Trondheim University Hospital, Clinic of Medicine, Postboks 3250 Sluppen, 7006 Trondheim, Norway.
 - ³ Department of Biosciences and Nutrition (BioNuT), Karolinska Institutet, 14183 Huddinge, Sweden.
- * Correspondence: valentyn.oksenych@ntnu.no;

This material includes: Robust V(D)J recombination in vAbl cells lacking MDC1 (Figure S1).

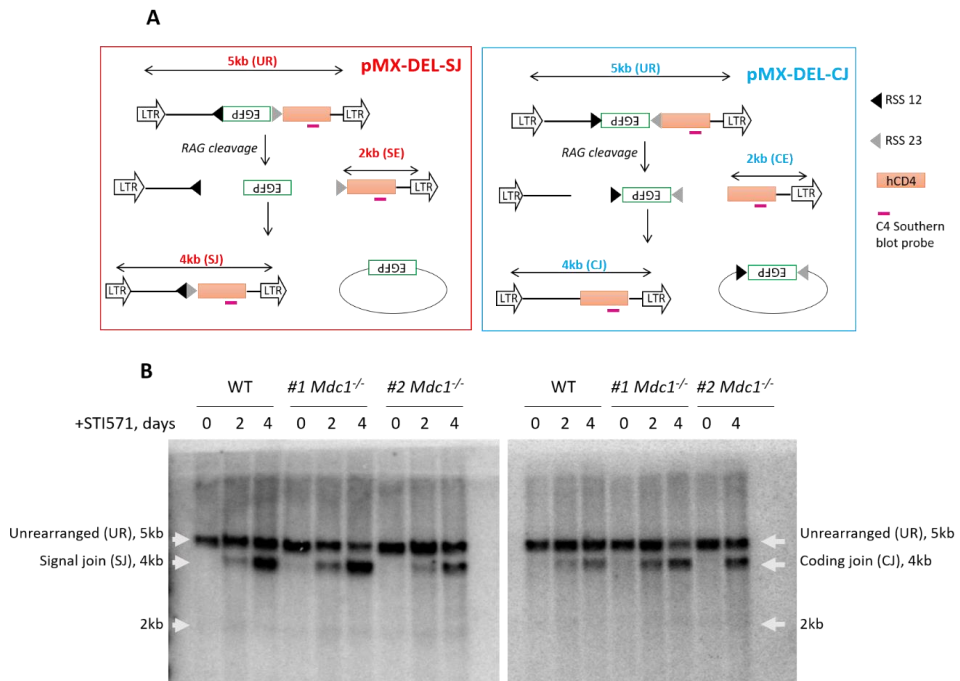


Figure S1. Robust V(D)J recombination in vAbl cells lacking MDC1. (A) Schematic representation of pMX-Del-SJ deletional V(D)J recombination cassette with blunt SJ DNA ends (left) and pMX-Del-CJ cassette with hairpin-sealed CJ DNA ends (right). (B) Southern blot representing original V(D)J recombination cassette (5kb), and product of deletional V(D)J recombination (4kb). Very weak to no signal is detected at 2kb (free DNA ends) suggesting either rapid DNA repair or degradation of unjoined DNA ends.

PAPER III

Leaky severe combined immunodeficiency in mice lacking non-homologous end joining factors XLF and MRI

Sergio Castañeda-Zegarra^{1,2,*}, Qindong Zhang^{1,3,*}, Amin Alirezaylavasani¹, Marion Fernandez-Berrocal¹, Rouan Yao¹, Valentyn Oksenyich^{1,4,5}

¹Department of Clinical and Molecular Medicine (IKOM), Norwegian University of Science and Technology, Trondheim, Norway

²Science for Life Laboratory, Department of Oncology-Pathology, Karolinska Institutet, Stockholm, Sweden

³Department of Cancer Immunology, Institute for Cancer Research, The Norwegian Radium Hospital, Oslo University Hospital, Oslo, Norway

⁴Department of Biosciences and Nutrition (BioNut), Karolinska Institutet, Huddinge, Sweden

⁵Institute of Clinical Medicine, UiT The Arctic University of Norway, Tromsø, Norway

*Equal contribution

Correspondence to: Valentyn Oksenyich, Sergio Castañeda-Zegarra; email: valentyn.oksenyich@uit.no, sergio.m.c.zegarra@ntnu.no

Keywords: NHEJ, cernunnos, cyren, pro-B cells, lymphocyte

Received: July 3, 2020

Accepted: September 21, 2020

Published: December 7, 2020

Copyright: © 2020 Castañeda-Zegarra et al. This is an open access article distributed under the terms of the [Creative Commons Attribution License](https://creativecommons.org/licenses/by/3.0/) (CC BY 3.0), which permits unrestricted use, distribution, and reproduction in any medium, provided the original author and source are credited.

ABSTRACT

Non-homologous end-joining (NHEJ) is a DNA repair pathway required to detect, process, and ligate DNA double-stranded breaks (DSBs) throughout the cell cycle. The NHEJ pathway is necessary for V(D)J recombination in developing B and T lymphocytes. During NHEJ, Ku70 and Ku80 form a heterodimer that recognizes DSBs and promotes recruitment and function of downstream factors PAXX, MRI, DNA-PKcs, Artemis, XLF, XRCC4, and LIG4. Mutations in several known NHEJ genes result in severe combined immunodeficiency (SCID). Inactivation of *Mri*, *Paxx* or *Xlf* in mice results in normal or mild phenotype, while combined inactivation of *Xlf/Mri*, *Xlf/Paxx*, or *Xlf/Dna-pkcs* leads to late embryonic lethality. Here, we describe three new mouse models. We demonstrate that deletion of *Trp53* rescues embryonic lethality in mice with combined deficiencies of *Xlf* and *Mri*. Furthermore, *Xlf^{-/-}Mri^{-/-}Trp53^{+/-}* and *Xlf^{-/-}Paxx^{-/-}Trp53^{+/-}* mice possess reduced body weight, severely reduced mature lymphocyte counts, and accumulation of progenitor B cells. We also report that combined inactivation of *Mri/Paxx* results in live-born mice with modest phenotype, and combined inactivation of *Mri/Dna-pkcs* results in embryonic lethality. Therefore, we conclude that XLF is functionally redundant with MRI and PAXX during lymphocyte development *in vivo*. Moreover, *Mri* genetically interacts with *Dna-pkcs* and *Paxx*.

INTRODUCTION

Non-homologous end-joining (NHEJ) is a DNA repair pathway that recognizes, processes and ligates DNA double-stranded breaks (DSB) throughout the cell cycle. NHEJ is required for lymphocyte development; in particular, to repair DSBs induced by the recombination activating genes (RAG) 1 and 2 in developing B and T

lymphocytes, and by activation-induced cytidine deaminase (AID) in mature B cells [1]. NHEJ is initiated when Ku70 and Ku80 (Ku) are recruited to the DSB sites. Ku, together with DNA-dependent protein kinase, catalytic subunit (DNA-PKcs), forms the DNA-PK holoenzyme [2]. Subsequently, the nuclease Artemis is recruited to the DSB sites to process DNA hairpins and overhangs [3]. Finally, DNA ligase IV (LIG4), X-

ray repair cross-complementing protein 4 (XRCC4) and XRCC4-like factor (XLF) mediate DNA end ligation. The NHEJ complex is stabilized by a paralogue of XRCC4 and XLF (PAXX) and a modulator of retroviral infection (MRI/CYREN) [4, 5].

Inactivation of *Ku70*, *Ku80*, *Dna-pkcs* or *Artemis* results in severe combined immunodeficiency (SCID) characterized by lack of mature B and T lymphocytes [2, 3, 6–8]. Deletion of both alleles of *Xrcc4* [9] or *Lig4* [10] results in late embryonic lethality in mice, which correlates with increased apoptosis in the central nervous system (CNS). Inactivation of *Xlf* (*Cernunnos*) only results in modest immunodeficiency in mice [11–13], while mice lacking *Paxx* [14–17] or *Mri* [5, 18] display no overt phenotype.

The mild phenotype observed in mice lacking XLF could be explained by functional redundancy between XLF and multiple DNA repair factors, including *Ataxia telangiectasia* mutated (ATM), histone H2AX [19], Mediator of DNA Damage Checkpoint 1 (MDC1) [20, 21], p53-binding protein 1 (53BP1) [17, 22], RAG2 [23], DNA-PKcs [20, 24, 25], PAXX [4, 14, 15, 20, 26–28] and MRI [5]. However, combined inactivation of *Xlf* and *Paxx* [4, 14, 15, 20], as well as *Xlf* and *Mri* [5], results in late embryonic lethality in mice, presenting a challenge to the study of B and T lymphocyte development *in vivo*. It has also been shown that both embryonic lethality and increased levels of CNS neuronal apoptosis in mice with deficiency in *Lig4* [9, 10, 29, 30], *Xrcc4* [9, 31], *Xlf* and *Paxx* [20], or *Xlf* and *Dna-pkcs* [24, 25] is p53-dependent.

In this study, we rescue synthetic lethality from *Xlf* and *Mri* by inactivating one or two alleles of *Trp53*. We also show that both *Xlf^{-/-}Mri^{-/-}Trp53^{+/-}* and *Xlf^{-/-}Paxx^{-/-}Trp53^{+/-}* mice possess a leaky SCID phenotype with severely reduced mature B and T lymphocyte counts in the spleen, low mature T cell counts in the thymus, and accumulated progenitor B cells in the bone marrow. Finally, we demonstrate that MRI is functionally redundant with DNA-PKcs and PAXX.

RESULTS

Inactivation of *Trp53* gene rescued embryonic lethality in mice lacking XLF and MRI

Combined inactivation of *Xlf* and *Mri* has previously been shown to result in synthetic lethality in mice [5]. To generate XLF/MRI deficient mice with altered expression of *Trp53*, we intercrossed an *Mri^{-/-}* strain [18] with an *Xlf^{-/-}Trp53^{+/-}* [20] strain. Next, we selected and intercrossed triple heterozygous (*Xlf^{+/-}Mri^{+/-}Trp53^{+/-}*), and later, *Xlf^{-/-}Mri^{+/-}Trp53^{+/-}* mice. With PCR

screening, we identified *Xlf^{-/-}Mri^{-/-}Trp53^{+/-}* (n=11), *Xlf^{-/-}Mri^{-/-}Trp53^{-/-}* (n=2), and *Xlf^{-/-}Mri^{-/-}Trp53^{+/+}* (n=1) (Figure 1A) among the resulting offspring. Mice lacking both XLF and MRI possessed reduced weight (12 g on average, $p<0.0001$) when compared with gender- and age-matched WT (19 g), *Xlf^{-/-}* (19 g) and *Mri^{-/-}* (20 g) controls (Figure 1B and 1C). In addition, *Xlf^{-/-}Mri^{-/-}Trp53^{+/-}* and *Xlf^{-/-}Mri^{-/-}Trp53^{-/-}* mice were viable up to 63 days and died for unknown reasons. We used *Xlf^{-/-}Mri^{-/-}Trp53^{+/-}* mice to further characterize the development of B and T lymphocytes *in vivo*.

Leaky SCID in *Xlf^{-/-}Mri^{-/-}Trp53^{+/-}* mice

To determine the roles of XLF and MRI in lymphocyte development *in vivo*, we isolated the thymus, spleen, and femur from *Xlf^{-/-}Mri^{-/-}Trp53^{+/-}* mice, as well as from *Xlf^{-/-}*, *Mri^{-/-}*, *Trp53^{+/-}* and WT controls. Combined deficiency for XLF and MRI resulted in a 3-fold reduction in thymus size (32 mg on average, $p<0.0001$) and a 9-fold reduction in thymocyte count (1.9×10^7 , $p<0.0001$) when compared to single deficient or WT controls (Figure 1D). Similarly, both average spleen weight (22 mg, $p<0.0001$) and splenocyte count (2.0×10^7 , $p<0.0001$) in *Xlf^{-/-}Mri^{-/-}Trp53^{+/-}* mice decreased approximately 4–5 fold when compared with WT and single deficient controls (Figure 1E). The reduced number of splenocytes in XLF/MRI double-deficient mice could be explained by decreased populations of B and T lymphocytes observed in the *Xlf^{-/-}Mri^{-/-}Trp53^{+/-}* mice (Figure 1F–1H and Supplementary Tables 1–4). Specifically, CD3⁺ T cells were reduced 6-fold ($p<0.0001$), while CD19⁺ B cells were reduced 50-fold ($p<0.0001$) when compared with single deficient and WT controls (Figure 1F–1H). Likewise, counts of CD4⁺ and CD8⁺ T cells in the spleen (Supplementary Tables 3 and 4), were all dramatically reduced when compared with single deficient and WT controls (about 4-fold, $p<0.0001$; Figure 1F, 1H) as well as counts of CD4⁺, CD8⁺ and CD4⁺CD8⁺ T cells in the thymus (Figure 1F, 1I and Supplementary Tables 5–7). From these observations, we conclude that XLF and MRI are functionally redundant during B and T lymphocytes development in mice.

Leaky SCID in mice lacking XLF and PAXX

Combined inactivation of XLF and PAXX has been shown to result in embryonic lethality in mice [4, 14, 15, 20]. To determine the impact of XLF and PAXX on B and T cell development *in vivo*, we rescued the synthetic lethality by inactivating one allele of *Trp53*, as described previously [20]. We did not detect any direct influence of altered *Trp53* genotype on lymphocyte development (Supplementary Tables 1–9). The resulting *Xlf^{-/-}Paxx^{-/-}Trp53^{+/-}* and *Xlf^{-/-}Paxx^{-/-}Trp53^{-/-}* mice possess

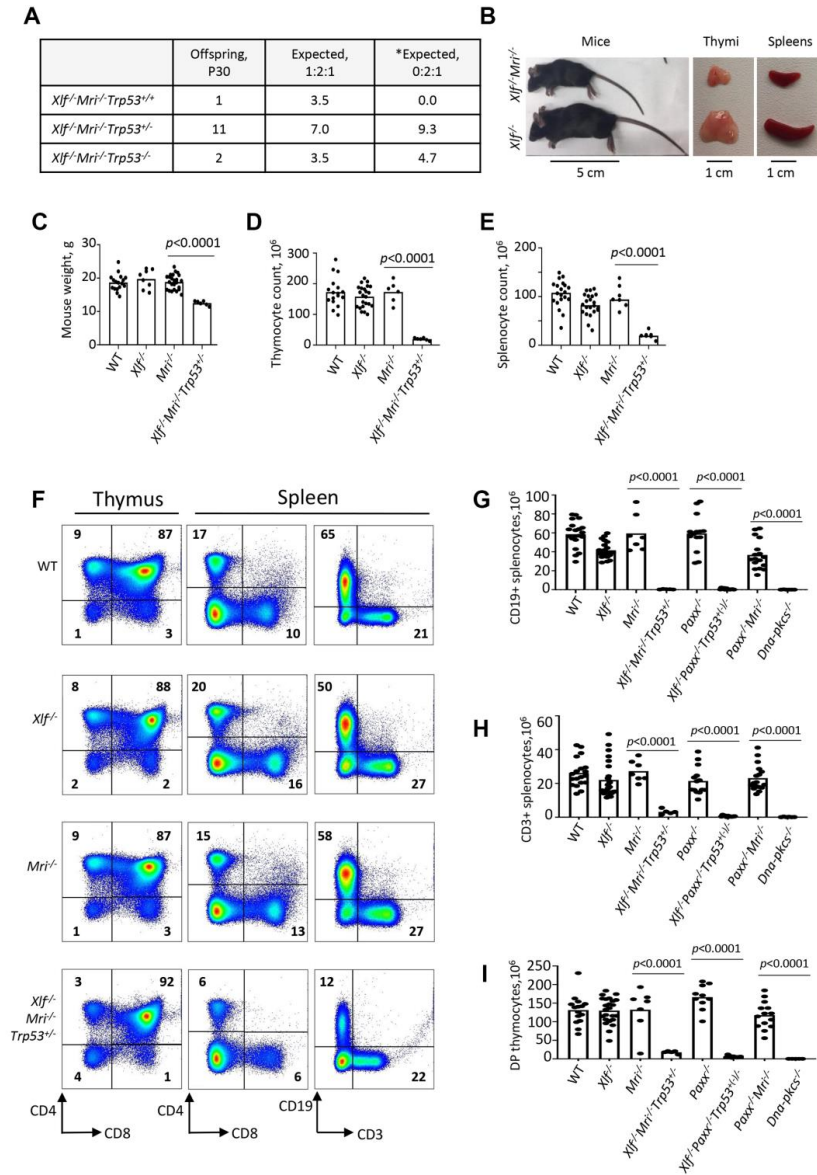


Figure 1. Development of B and T lymphocytes in *Xlf^{-/-}Mri^{-/-}Trp53^{+/-}* mice. (A) Number of thirty-day-old mice (P30) of indicated genotypes. *Expected distribution assuming lethality. (B) Comparison of body size, thymi and spleens of XLF/MRI-deficient and XLF-deficient mice of the same age. (C) Weights of WT, *Xlf^{-/-}*, *Mri^{-/-}*, *Xlf^{-/-}Mri^{-/-}Trp53^{+/-}* mice. (D, E) Number ($\times 10^6$) of thymocytes (D) and splenocytes (E) in WT, *Xlf^{-/-}*, *Mri^{-/-}*, *Xlf^{-/-}Mri^{-/-}Trp53^{+/-}* mice. (F) Flow cytometric analysis of thymic and splenic T cell subsets and splenic B cells. (G, H, I) Number ($\times 10^6$) of splenic CD19+ B cells (G), splenic CD3+ T cells (H) and thymic CD4+CD8+ double positive (DP) T cells (I) in WT, *Xlf^{-/-}*, *Mri^{-/-}*, *Xlf^{-/-}Mri^{-/-}Trp53^{+/-}*, *Paxx^{-/-}*, *Xlf^{-/-}Paxx^{-/-}Trp53^{+/-}* and *Paxx^{-/-}Mri^{-/-}* mice. *Dna-pkcs^{-/-}* mice were used as an immunodeficient control. Comparisons between every two groups were made using one-way ANOVA, GraphPad Prism 8.0.1. *Xlf^{-/-}Paxx^{-/-}Trp53^{+/-}* is a combination of *Xlf^{-/-}Paxx^{-/-}Trp53^{+/-}* and *Xlf^{-/-}Paxx^{-/-}Trp53^{-/-}*. Not shown in the graph for (G): WT vs *Paxx^{-/-}Mri^{-/-}*, $p < 0.0001$ (****), *Paxx^{-/-}* vs *Paxx^{-/-}Mri^{-/-}*, $p < 0.0001$ (****), *Mri^{-/-}* vs *Paxx^{-/-}Mri^{-/-}*, $p < 0.0025$ (**), *Xlf^{-/-}* vs *Paxx^{-/-}Mri^{-/-}*, $p = 0.9270$ (n.s), *Xlf^{-/-}Mri^{-/-}Trp53^{+/-}* vs *Paxx^{-/-}Mri^{-/-}*, $p < 0.0001$ (****), and *Xlf^{-/-}Paxx^{-/-}Trp53^{+/-}* vs *Paxx^{-/-}Mri^{-/-}*, $p < 0.0001$ (****).

30- to 40-fold reduced thymocyte count (4.0×10^6 , $p < 0.0001$) when compared to WT (1.3×10^8), $Xlf^{-/-}$ (1.4×10^8) and $Paxx^{-/-}$ (1.7×10^8) mice. This is reflected in decreased levels of double-positive CD4+CD8+ cells, as well as decreased levels of single-positive CD4+ and CD8+ T cells (Figure 1, Supplementary Figure 1, and Supplementary Tables 5–7). Spleen development was dramatically affected in mice lacking XLF and PAXX compared to WT and single-deficient controls, due to the lack of B cells and decreased T cell count (Figure 1, Supplementary Figure 1, and Supplementary Tables 1–4). When compared with the WT and single knockout controls, $Xlf^{-/-}Paxx^{-/-}Trp53^{+/+}$ and $Xlf^{-/-}Paxx^{-/-}Trp53^{-/-}$ mice had a 100- to 600-fold reduction in CD19+ B splenocyte count (0.7×10^6 , $p < 0.0001$) and a 50- to 90-fold reduction in CD3+ splenocyte count (to 0.5×10^6) (Figure 1F–1H and Supplementary Figure 1). From these results, we concluded that XLF and PAXX are functionally redundant during the B and T lymphocyte development *in vivo*.

Early B cell development is abrogated in mice lacking XLF and MRI, or XLF and PAXX

Reduced counts and proportions of mature B lymphocytes in $Xlf^{-/-}Mri^{-/-}Trp53^{+/+}$ mice suggest a blockage in B cell development in the bone marrow. To

investigate this further, we isolated the bone marrow cells from femora of mice lacking XLF, MRI or both XLF/MRI, and analyzed the proportions of B220+CD43+IgM- progenitor B cells and B220+CD43-IgM+ immature and mature B cells. We detected only background levels of B220+CD43-IgM+ B cells in bone marrows isolated from $Xlf^{-/-}Mri^{-/-}Trp53^{+/+}$ mice (Figure 2A, 2B and Supplementary Table 8). However, these mice exhibited a 2- to 3-fold higher proportion of pro-B cells when compared with WT, $Xlf^{-/-}$ and $Mri^{-/-}$ controls (Figure 2A, 2C and Supplementary Table 9). Similarly, $Xlf^{-/-}Paxx^{-/-}Trp53^{+/+}$ and $Xlf^{-/-}Paxx^{-/-}Trp53^{-/-}$ mice also possess background levels of IgM+ B cells ($p < 0.0001$; Figure 2A, 2B and Supplementary Table 8) while having 3- to 4-fold higher proportion of pro-B cells when compared with WT, $Xlf^{-/-}$ and $Paxx^{-/-}$ controls ($p < 0.0001$; Figure 2A, 2C and Supplementary Table 9). Therefore, we conclude that B cell development is blocked at the pro-B cell stage of $Xlf^{-/-}Mri^{-/-}Trp53^{+/+}$ and $Xlf^{-/-}Paxx^{-/-}Trp53^{+/+}$ mice.

$Paxx^{-/-}Mri^{-/-}$ mice possess a modest phenotype

Both PAXX and MRI are NHEJ factors that are functionally redundant with XLF in mice. Combined inactivation of *Paxx* and *Xlf* [4, 14, 15, 20], or *Mri* and *Xlf* [5]; this study) results in synthetic lethality in mice,

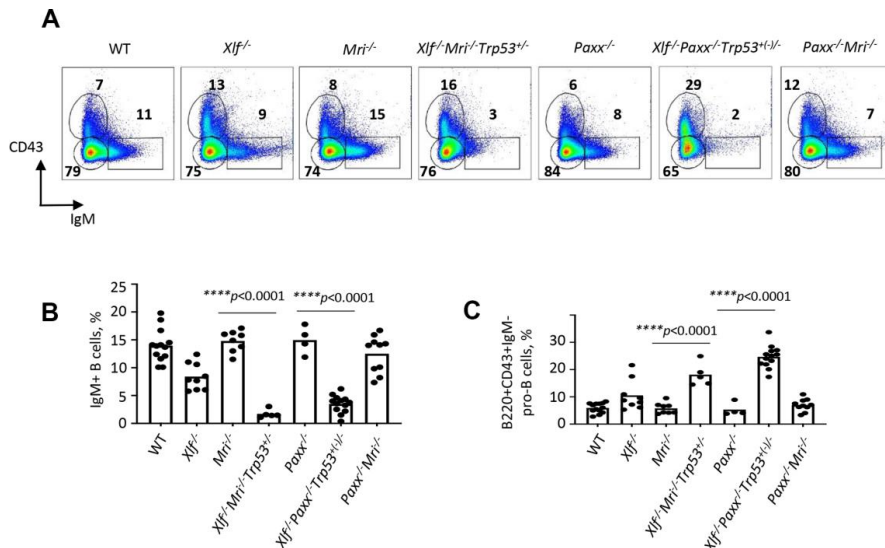


Figure 2. Development of B cells is abrogated in bone marrow of $Xlf^{-/-}Mri^{-/-}Trp53^{+/+}$ and $Xlf^{-/-}Paxx^{-/-}Trp53^{+/+}$ mice. (A) Flow cytometric analysis of developing B cells. Upper left boxes mark B220+CD43+IgM- progenitor B cell populations, and lower right boxes mark the B220+CD43-IgM+ B cells. (B, C) Frequencies (%) of B220+CD43-IgM+ B cells (B) and B220+CD43+IgM- progenitor B cells (C) in WT, $Xlf^{-/-}$, $Mri^{-/-}$, $Xlf^{-/-}Mri^{-/-}Trp53^{+/+}$, $Paxx^{-/-}$, $Xlf^{-/-}Paxx^{-/-}Trp53^{+/+}$, and $Paxx^{-/-}Mri^{-/-}$ mice. Comparisons between groups were made using one-way ANOVA, GraphPad Prism 8.0.1. $Xlf^{-/-}Paxx^{-/-}Trp53^{+/+}$ is a combination of $Xlf^{-/-}Paxx^{-/-}Trp53^{+/+}$ and $Xlf^{-/-}Paxx^{-/-}Trp53^{-/-}$.

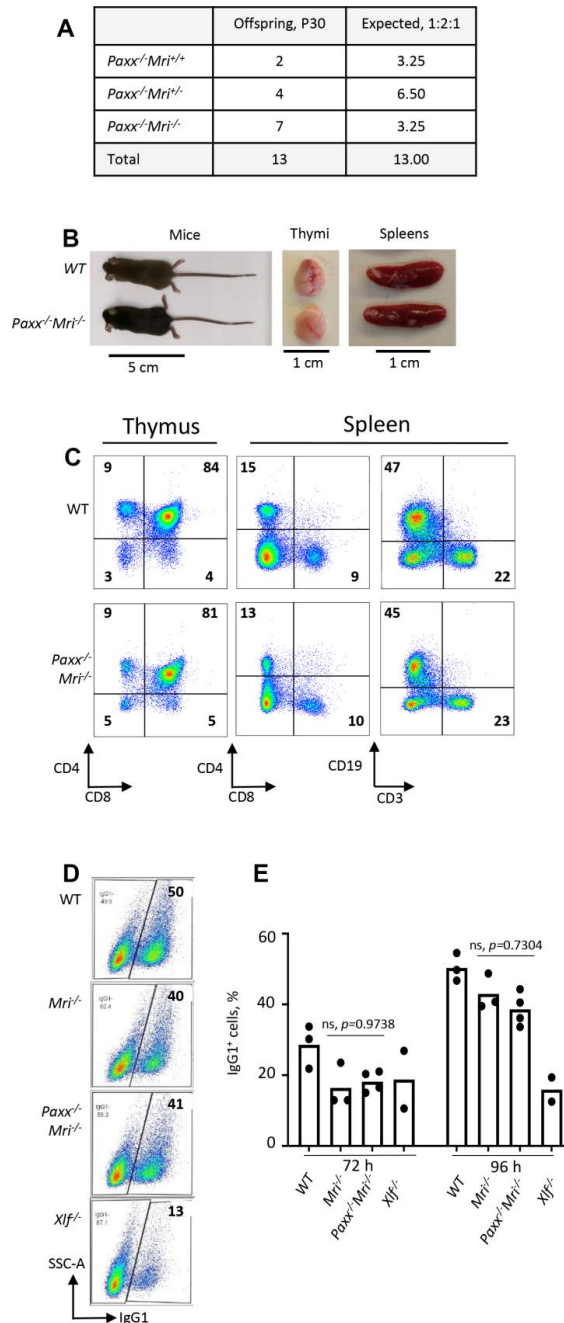


Figure 3. Development of B and T cells in *Paxx^{-/-}Mri^{-/-}* mice. (A) Number of thirty-day-old mice (P30) of indicated genotypes. Parents were *Paxx^{+/+}Mri^{+/+}* and *Paxx^{-/-}Mri^{+/+}*. **(B)** Example of thirty-day-old *Paxx^{-/-}Mri^{-/-}* and WT male littermates with their respective thymi and spleens. **(C)** Example of flow cytometry analyzes of B and T cells in *Paxx^{-/-}Mri^{-/-}* and WT mice. **(D, E)** Class switching analyzes of *in vitro* activated naïve B cells of indicated genotypes.

as well as in abrogated V(D)J recombination in vAbl pre-B cells [4, 5, 14, 15, 27]. To determine if *Paxx* genetically interacts with *Mri*, we intercrossed mice that are heterozygous or null for both genes (such as *Paxx*^{-/-}*Mri*^{+/-} and *Paxx*^{+/-}*Mri*^{+/-}). We found that resulting *Paxx*^{-/-}*Mri*^{-/-} mice are live-born, fertile, and are similar in size to WT littermates (17 g, $p > 0.9999$) (Figure 3A and 3B). Specifically, we observe that *Paxx*^{-/-}*Mri*^{-/-} mice have normal thymocyte and splenocyte counts. Furthermore, *Paxx*^{-/-}*Mri*^{-/-} mice underwent normal T cell development that was indistinguishable from the WT, *Paxx*^{-/-}, and *Mri*^{-/-} controls (Figures 1H, I and 3C). However, *Paxx*^{-/-}*Mri*^{-/-} mice had reduced CD19+ B cell counts (Figure 1G) when were compared to WT, *Paxx*^{-/-} and *Mri*^{-/-} controls ($p < 0.0025$). Moreover, CD19+ B cell counts were similar in *Paxx*^{-/-}*Mri*^{-/-} and *Xlf*^{-/-} mice ($p > 0.9270$), suggesting that combined depletion of PAXX and MRI has modest phenotype similar to the one in XLF-deficient mice. CSR to IgG1 was performed in order to determine if DNA repair-dependent immunoglobulin production is affected in mature B cells lacking PAXX and MRI [16, 18]. *Paxx* inactivation did not affect Ig switch to IgG1 in MRI-deficient B cells (Figure 3D and 3E). The quantity of IgG1+ cells after CSR stimulation was similar between *Paxx*^{-/-}*Mri*^{-/-} and *Mri*^{-/-} naïve B cells ($p > 0.73$). From this, we can conclude that there is a genetic interaction between *Paxx* and *Mri* *in vivo*, and it is only detected in B cells.

Synthetic lethality between *Mri* and *Dna-pkcs* in mice

Both MRI and DNA-PKcs are functionally redundant with XLF in mouse development [5, 24]. Combined inactivation of *Paxx* and *Mri* (this study), or *Paxx* and *Dna-pkcs* [20] genes results in live-born mice that are indistinguishable from single deficient controls. To determine if *Mri* genetically interacts with *Dna-pkcs*, we crossed *Mri*^{+/-} and *Dna-pkcs*^{+/-} mouse strains, then intercrossed the double-heterozygous *Mri*^{+/-}*Dna-pkcs*^{+/-}, and then *Mri*^{-/-}*Dna-pkcs*^{+/-} mice (Figure 4A). We identified 12 *Mri*^{-/-}*Dna-pkcs*^{+/+} and 12 *Mri*^{-/-}*Dna-pkcs*^{+/-}, but no *Mri*^{-/-}*Dna-pkcs*^{-/-} mice (out of 6 expected). To determine if double-deficient *Mri*^{-/-}*Dna-pkcs*^{-/-} embryos are present at day E14.5, we intercrossed *Mri*^{-/-}*Dna-pkcs*^{+/-} mice, extracted and genotyped the embryos (Figure 4B). We identified two *Mri*^{-/-}*Dna-pkcs*^{-/-} mice at E14.5 (63mg), which were about 40% lighter than *Mri*^{-/-} littermates (108mg) (Figure 4C and 4D). A Chi-Square test (χ^2) was performed to determine if the embryonic distribution data fits the mendelian ratio of 1:2:1 that is expected from *Mri*^{-/-}*Dna-pkcs*^{+/-} parents. With DF=2 and $\chi^2=1.8$, the corresponding p-value lies within the range $0.25 < p < 0.5$. This affirms that our data fit the expected 1:2:1 distribution and suggests that *Mri*^{-/-}*Dna-pkcs*^{-/-} is synthetic lethal. Therefore, we can conclude that there is genetic interaction between *Mri* and *Dna-pkcs* *in vivo*.

DISCUSSION

Recent findings by our and other research groups suggest that MRI forms heterogeneous complexes involving PAXX or XLF, which function during DNA DSB repair by NHEJ [5]. Furthermore, genetic inactivation of *Xlf* [11], *Paxx* [4, 14–16], or *Mri* [5, 18] in mice leads to development of modest or no detectable phenotype. However, combined inactivation of *Xlf* and *Mri* [5] or *Xlf* and *Paxx* [4, 14, 15] results in embryonic lethality, which correlates with increased levels of neuronal apoptosis in the CNS (Figure 5). Here, we show that synthetic lethality produced by combined inactivation of *Xlf* and *Mri* can be rescued by altered *Trp53* expression, similar to our previous *Xlf*^{-/-}*Paxx*^{-/-}*Trp53*^{+/-} [20] mouse model. Furthermore, we have developed and presented here *Paxx*^{-/-}*Mri*^{-/-} and *Mri*^{-/-}*Dna-pkcs*^{-/-} double deficient models.

Our findings have demonstrated that mice lacking XLF, MRI and p53, although live-born, possess a leaky SCID phenotype. *Xlf*^{-/-}*Mri*^{-/-}*Trp53*^{+/-} mice have a clear fraction of mature B cells in the spleens (CD19+) and bone marrow (B220+CD43-IgM+) (Figures 1 and 2), as well as clear fractions of double- and single-positive T cells in the thymus (CD4+CD8+, CD4+, CD8+) and single-positive T cells in the spleen (CD4+ and CD8+) (Figure 1). However, the cell fractions from these mice are noticeably smaller than those of WT or single-deficient mice. Strikingly, we were able to identify one *Xlf*^{-/-}*Mri*^{-/-}*Trp53*^{+/+} mouse at day P30 post-birth. This mouse resembled *Xlf*^{-/-}*Mri*^{-/-}*Trp53*^{+/-} mice of similar age with respect of B and T cell development (Supplementary Table 10), although this mouse was generally sicker than its littermates and had to be euthanized. Similarly, one live-born *Xlf*^{-/-}*Paxx*^{-/-} mouse was reported by Balmus et al. 2016 [15], indicating that, exceptionally, embryonic lethality in NHEJ ligation-deficient mice can be overcome, likely due to activity of alternative end-joining. Previously, in 2018, Hung et al. [5] reported that combined inactivation of *Xlf* and *Mri* in vAbl pre-B cells results in a severe block in V(D)J recombination and accumulation of unrepaired DSBs *in vitro*, although it was unclear whether this combined inactivation would lead to a deficiency in B lymphocytes when translated to a mouse model [5]. Similarly, double deficient vAbl pre-B cells lacking *Xlf* and *Paxx* are also unable to sustain V(D)J recombination. Importantly, the lack of a progenitor T cell model system left the question of T cell development in *Xlf*^{-/-}*Mri*^{-/-} and *Xlf*^{-/-}*Paxx*^{-/-} mice completely unexplored.

Previously, we showed that mice lacking XLF, PAXX and p53 were live-born and had nearly no B and T cells, reduced size of spleen and hardly detectable thymus [20] (Figure 5). Consistent with this model, a conditional

knockout mouse model, which results in double-deficiency of XLF/PAXX in early hematopoietic progenitor cells, was also able to overcome the embryonic lethality of *Xlf^{-/-}Paxx^{-/-}* mice [33]. With this model, impairment of V(D)J recombination in *Xlf^{-/-}Paxx^{-/-}* cells, as well as the resulting depletion of mature B cells and lack of a visible thymus could also be observed *in vivo* [33]. Our new data provide evidence that *Xlf^{-/-}Paxx^{-/-}Trp53^{+/-}* and *Xlf^{-/-}Paxx^{-/-}Trp53^{-/-}* mice possess a very small number of mature B cells in the spleen and bone marrow, as well as very minor fractions of single positive T cells in thymus and spleen (Figures 2, 5 and Supplementary Figure 1). Therefore, both mature B and T cells are present in mice lacking XLF/PAXX and XLF/MRI. This can be explained by incomplete blockage in NHEJ and V(D)J recombination, in which the process is dramatically reduced but still possible. We also detected more mature T cells than B cells in these double-deficient mice. Potential explanations include longer lifespan of T cells, which accumulate over time following low efficiency of V(D)J recombination, while B cells are eliminated faster from the pool due to the

different physiology [34, 35]. It is also possible that the T cells we detected are a resultant subpopulation that is descendent from the few cells that were able to bypass V(D)J recombination [12]. In this case, the repertoire of T cells based on T cell receptor in mice lacking XLF/PAXX and XLF/MRI would be significantly lower than in control mice, even if normalized to the total cell count. Due to the small presence of mature B and T cells in *Xlf^{-/-}Mri^{-/-}Trp53^{+/-}*, *Xlf^{-/-}Paxx^{-/-}Trp53^{+/-}* and *Xlf^{-/-}Paxx^{-/-}Trp53^{-/-}* mice, we categorize the observed immunodeficient phenotypes as “leaky SCID”. Previously, leaky SCID has been described in mice lacking other NHEJ factors, such as *Ku70^{-/-}* [6], *Artemis^{-/-}* [3], *Lig4^{-/-}Trp53^{-/-}* [10, 30], *Xrcc4^{-/-}Trp53^{-/-}* [9, 31], *Xlf^{-/-}Atm^{-/-}* [19] and *Xlf^{-/-}Rag2^{olo}* [23].

In addition to XLF/MRI and XLF/PAXX deficient mice, inactivation of one or two alleles of *Trp53* also rescues the embryonic lethality of *Xrcc4^{-/-}* [9, 31], *Lig4^{-/-}* [10, 30] and *Xlf^{-/-}Dna-pkcs^{-/-}* [20] mice. We propose a model (Figure 5), when single deficiency for DNA-PKcs, PAXX or MRI results in no or modest

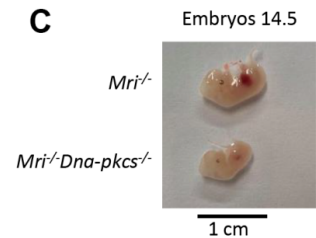
A

	Offspring, P30	Expected, 1:2:1	*Expected, 1:2:0
<i>Mri^{-/-}Dna-pkcs^{+/+}</i>	12	6	8
<i>Mri^{-/-}Dna-pkcs^{+/-}</i>	12	12	16
<i>Mri^{-/-}Dna-pkcs^{-/-}</i>	0	6	0

B

	Offspring, E14.5	Expected, 1:2:1	*Expected, 1:2:0
<i>Mri^{-/-}Dna-pkcs^{+/+}</i>	1	2.5	3.3
<i>Mri^{-/-}Dna-pkcs^{+/-}</i>	7	5.0	6.7
<i>Mri^{-/-}Dna-pkcs^{-/-}</i>	2	2.5	0.0

C



D

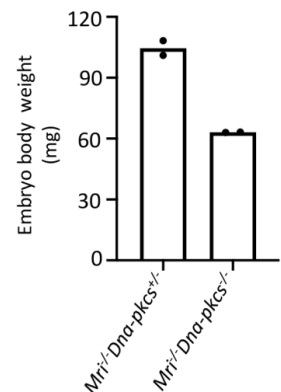


Figure 4. Genetic interaction between *Mri* and *Dna-pkcs* *in vivo*. (A) No live-born *Mri^{-/-}Dna-pkcs^{-/-}* mice were detected. (B, C) *Mri^{-/-}Dna-pkcs^{-/-}* embryos were detected at day E14.5. (D) Body weight in milligrams (mg) from two E14.5 *Mri^{-/-}Dna-pkcs^{+/+}* and *Mri^{-/-}Dna-pkcs^{-/-}* embryos from the same litter. The mendelian ratio 1:2:1 in embryos was verified by the Chi-Square test (χ^2). The χ^2 was 1.8 and its corresponding probability was between 25 and 50%. *Expected distribution assuming lethality.

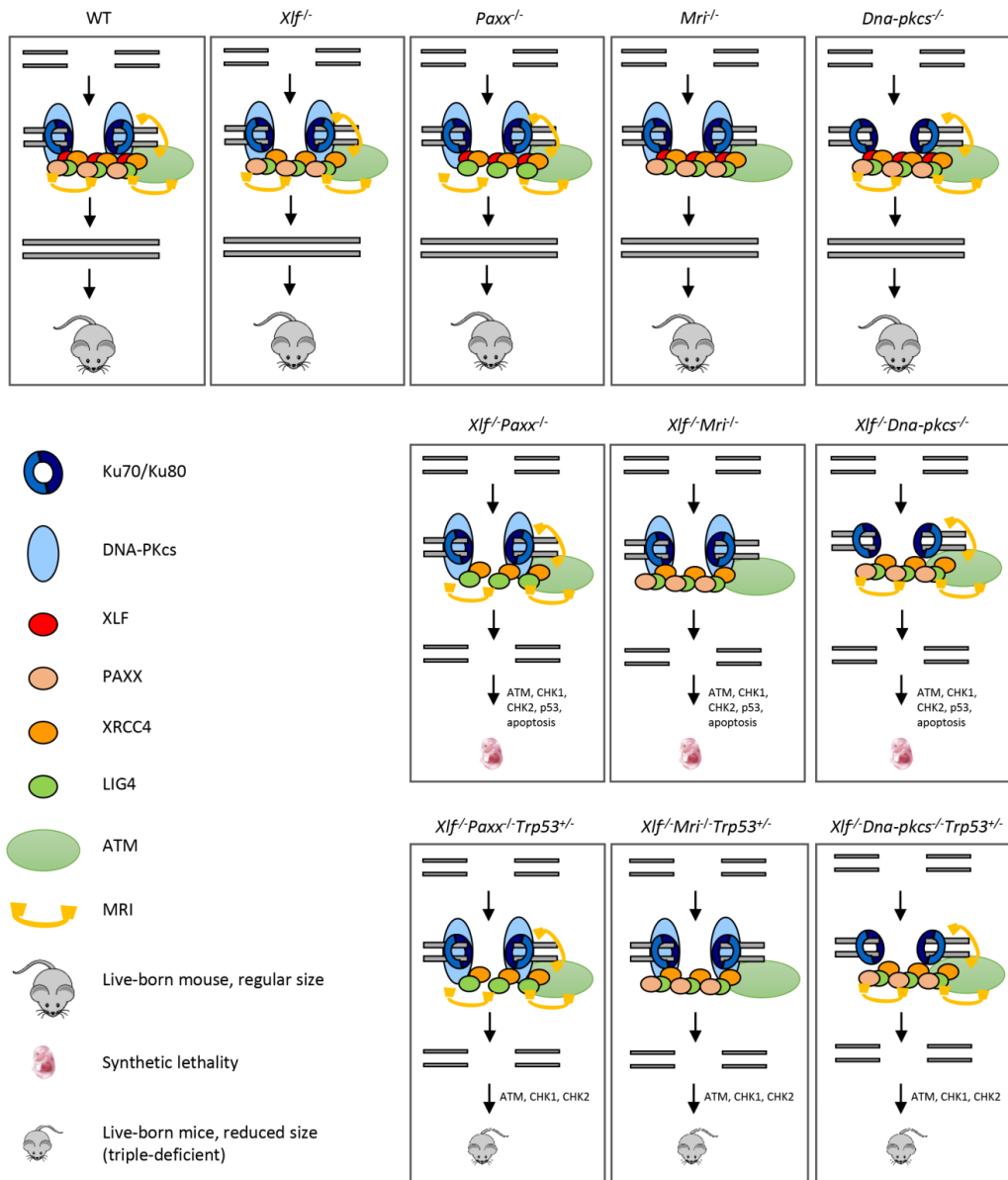


Figure 5. Mutations in NHEJ genes result in distinct phenotypes. Suggested models. Inactivation of *Paxx* or *Mri* results in live-born mice with nearly no DNA repair defects. Inactivation of *Xlf* or *Dna-pkcs* results in live-born mice with increased levels of genomic instability due to reduced NHEJ activity. Combined inactivation of *Xlf/Paxx*, *Xlf/Mri* or *Xlf/Dna-pkcs* leads to embryonic lethality in mice that correlate with high levels of genomic instability and nearly no NHEJ. Accumulated DSBs activate the ATM-dependent DNA damage response (DDR) pathway; ATM phosphorylates CHK checkpoint proteins that further trigger cell cycle arrest and apoptosis. Alternative end-joining is blocked by presence of Ku70/Ku80. Inactivation of one or two alleles of *Trp53* rescues embryonic lethality of *Xlf/Paxx*, *Xlf/Mri* and *Xlf/Dna-pkcs* mice. While in these mice the levels of DSBs are increased and ATM-dependent DDR response is activated, lack of p53 prevents massive apoptosis and thus results in alive mice. Sizes of the triple-deficient mice are reduced, as one option, due to DNA damage-dependent cell cycle arrest in multiple cells of the body. The embryonic lethality in mice lacking *Xlf/Paxx* and *Xlf/Mri* is likely to be rescued by inactivation of *Ku70* or *Ku80*.

phenotypes, and DSBs are efficiently repaired. Combined inactivation of *Xlf/Dna-pkcs*, *Xlf/Paxx* and *Xlf/Mri* results in inefficient DSB ligation, accumulation of DNA breaks, activation of ATM-dependent DDR, checkpoint protein CHK2, stabilization of p53 and massive apoptosis. This results in embryonic lethality in mice. Furthermore, inactivation of *Trp53* results in *Xlf/Dna-pkcs/Trp53*, *Xlf/Paxx/Trp53* and *Xlf/Mri/Trp53* triple-deficient mice. While DNA breaks in these mice are not repaired, ATM-dependent DDR response and activation of CHK proteins takes place. However, without p53, apoptosis is not activated, allowing survival of mice (Figure 5). Moreover, we propose that inactivation of *Atm* will also rescue embryonic lethality of *Xlf/Paxx* and *Xlf/Mri* mice due to the mechanisms proposed above. However, inactivation of *Atm* will not rescue embryonic lethality of *Xlf/Dna-pkcs* mice, due to synthetic lethality between *Atm* and *Dna-pkcs*.

It is important to note that altered *Trp53* expression is not always sufficient to rescue embryonic lethality in mice; for example, PLK1-interacting checkpoint helicase (PICH)-deficient mice possess developmental defects in the presence or absence of p53 [36], and ATR mutants (Seckel syndrome) are not completely rescued from embryonic lethality with the inactivation of *Trp53* [37]. Embryonic lethality of XLF/PAXX and XLF/MRI double-deficient mice can be explained by the presence of Ku70/Ku80 heterodimer at the DSBs sites, which blocks DNA repair by alternative end-joining pathway(s), leading to massive apoptosis and cell cycle arrest [38]. Previously, it was shown that embryonic lethality of LIG4-deficient [39] and XLF/DNA-PKcs double-deficient mice [25] could be rescued by inactivating *Ku70* or *Ku80* genes. Similarly, we propose that inactivation of either *Ku70* or *Ku80* gene will rescue the embryonic lethality of XLF/PAXX and XLF/MRI double-deficient mice and will result in mice indistinguishable from Ku70- or Ku80-deficient controls (Figure 5).

Recent studies have shown that *Xlf* genetically interacts with *Rag2* [23] and DDR factors, such as *Atm*, *53bp1*, *H2ax*, and *Mdc1* [17, 19–22, 38]. *Xlf^{-/-}Rag2^{c/c}* mice almost completely lack mature B cells and have significantly fewer mature T cells than single deficient controls [23]. *Xlf^{-/-}Atm^{-/-}* and *Xlf^{-/-}53bp1^{-/-}* mice are live-born and exhibit reduced body weight, increased genomic instability, and severe lymphocytopenia as a result of V(D)J recombination impairment in developing B and T cells [1, 17, 19, 22]. *Xlf^{-/-}H2ax^{-/-}* and *Xlf^{-/-}Mdc1^{-/-}*, on the other hand, are embryonic lethal [19–21]. There are several possible explanations for the functional redundancy observed between DNA repair genes. For instance, the two factors could have identical

(e.g., if both proteins are involved in ligation or DNA end tethering) or complementary (e.g., if one protein stimulates ligation while the other is required for DNA end tethering) functions. To date, XLF has been shown to genetically interact with multiple DNA repair factors [1, 4, 5, 14, 15, 19, 20, 24, 25], and this list is likely to grow [38, 40]. However, no clear genetic interaction has been shown between *Xlf* and *Artemis* or *Xrcc4* in the context of mouse development and V(D)J recombination [24], meaning that it remains difficult to predict genetic interactions without developing and characterizing genetic models.

We found that mice with combined inactivation of *Paxx* and *Mri* (*Paxx^{-/-}Mri^{-/-}*) are live-born, fertile, and undergo almost normal B and T cell development (Figure 3), where only the number of splenic B cells is affected, giving rise to a modest phenotype. Moreover, inactivation of *Paxx* did not affect the CSR efficiency in *in vitro* stimulated MRI-deficient B cells (Figure 3), thereby confirming our observations *in vitro*. It has been also shown that combined inactivation of *Paxx* and *Mri* genes in vAbl pre-B cells lead to similar V(D)J recombination efficiency to single-deficient *Mri^{-/-}*, *Paxx^{-/-}* and WT controls [5]. Thus, we conclude that there is a genetic interaction between *Paxx* and *Mri*, which results in a modest phenotype.

Lastly, we found that combined inactivation of *Mri* and *Dna-pkcs* (*Mri^{-/-}Dna-pkcs^{-/-}*) leads to embryonic lethality, and that E14.5 *Mri^{-/-}Dna-pkcs^{-/-}* murine embryos were about 40% smaller than single-deficient siblings (Figure 4). DNA-PKcs is associated with the N-terminus of the MRI and Ku heterodimer in the process of recognizing DSBs [5], which may account for genetic interaction between *Mri* and *Dna-pkcs*. Thus, inactivation of *Trp53*, *Ku70* or *Ku80* may be a viable method to rescue synthetic lethality from *Mri^{-/-}Dna-pkcs^{-/-}* mice.

In conclusion, we have developed and described several complex genetic mouse models (Figure 5). *Xlf^{-/-}Mri^{-/-}Trp53^{+/-}* and *Xlf^{-/-}Paxx^{-/-}Trp53^{+/-}* mice possessed severely impaired B and T lymphocyte development, leaky SCID; *Paxx^{-/-}Mri^{-/-}* mice develop a modest B cell phenotype; and *Mri^{-/-}Dna-pkcs^{-/-}* mice are embryonic lethal.

MATERIALS AND METHODS

Mice

All experiments involving mice were performed according to the protocols approved by the Comparative Medicine Core Facility (CoMed) at the Norwegian University of Science and Technology (NTNU),

Trondheim, Norway). *Xlf*^{+/-} [11] and *Dna-pkcs*^{+/-} [2] mice were imported from the laboratory of Professor Frederick W. Alt at Harvard Medical School. *Trp53*^{+/-} mice [32] were imported from Jackson Laboratories. *Paxx*^{+/-} [16] and *Mri*^{+/-} [18] mice were generated by the Oksenyich group and described previously.

Lymphocyte development

Lymphocyte populations were analyzed by flow cytometry [16, 18, 19, 22]. In summary, cells were isolated from the spleen, thymus, and femur of 5-7-week-old mice and treated with red blood cell lysis buffer Hybri-Max™ (Sigma Aldrich, St. Louis, MO, USA; #R7757). The cells were resuspended in PBS (Thermo Scientific, Basingstoke, UK; #BR0014G) containing 5% Fetal bovine serum, FCS (Sigma Life Science, St. Louis, Missouri, United States; #F7524), and counted using a Countess™ II Automated Cell Counter (Invitrogen, Carlsbad, CA, United States; #A27977). Then, the cell suspension was diluted with PBS to get a final cell concentration of 2.5 x 10⁷ cells/mL. Finally, surface markers were labeled with fluorochrome-conjugated antibodies and the cell populations were analyzed using flow cytometry.

Class switch recombination (CSR)

Spleens were isolated from 5-7-week-old mice and stored in cold PBS. Splenocytes were obtained by mincing the spleens, and naïve B cells were negatively selected using an EasySep Isolation kit (Stemcell™, Cambridge, UK; #19854). Lipopolysaccharide (LPS; 40 µg/mL; Sigma Aldrich, St. Louis, MO, USA; #437627-5MG) and interleukin 4 (IL-4; 20 ng/mL; PeproTech, Stockholm, Sweden; #214-14) were used to induce CSR to IgG1. Expression of IgG1 was analyzed by flow cytometry.

Antibodies

The following antibodies were used for flow cytometric analysis: rat anti-CD4-PE-Cy7 (BD Pharmingen™, Allschwil, Switzerland, #552775; 1:100); rat anti-CD8-PE-Cy5 (BD Pharmingen™, Allschwil, Switzerland, #553034; 1:100); anti-CD19-PE-Cy7 (Biolegend, San Diego, CA, USA, #115520; 1:100); hamster anti-mouse anti-CD3-FITC (BD Pharmingen™, Allschwil, Switzerland, #561827; 1:100); rat anti-mouse anti-CD43-FITC (BD Pharmingen™, Allschwil, Switzerland, #561856; 1:100); rat anti-mouse anti-CD45R/B220-APC (BD Pharmingen™, Allschwil, Switzerland; #553092; 1:100); rat anti-mouse anti-IgM-PE-Cy7 (BD Pharmingen™, Allschwil, Switzerland, #552867; 1:100); rat anti-mouse IgG1-APC (BD Pharmingen™, Allschwil, Switzerland; #550874; 1:100). A LIVE/DEAD™ fixable violet dead cell stain

kit (ThermoFisher Scientific, Waltham, MA, USA; #L34955; 1:1000) was used to identify dead cells.

Statistics

Statistical analyses were performed using one-way ANOVA, GraphPad Prism 8.0.1.244 (San Diego, CA, USA). In all statistical tests, $p < 0.05$ were taken to be significant (* $p < 0.05$; ** $p < 0.01$; *** $p < 0.001$; **** $p < 0.0001$).

AUTHOR CONTRIBUTIONS

VO, SCZ, QZ, AL and MFB designed the study, analyzed and interpreted the results. SCZ, QZ, AL and MFB performed most of the experiments. VO wrote the paper with the help of SCZ and RY. All the authors contributed to writing of the final manuscript.

CONFLICTS OF INTEREST

The authors declare no conflicts of interest.

FUNDING

This work was supported by the Research Council of Norway Young Talent Investigator grant (#249774) to V.O. In addition, VO group was supported by the Liaison Committee for Education, Research, and Innovation in Central Norway (#13477; #38811); the Norwegian Cancer Society (#182355); the Research Council of Norway FRIMEDBIO grants (#270491 and #291217), and The Outstanding Academic Fellow Program at NTNU (2017–2021). Karolinska Institutet Stiftelser och Fonder (#2020-02155).

REFERENCES

1. Kumar V, Alt FW, Oksenyich V. Functional overlaps between XLF and the ATM-dependent DNA double strand break response. *DNA Repair (Amst)*. 2014; 16:11–22. <https://doi.org/10.1016/j.dnarep.2014.01.010> PMID:24674624
2. Gao Y, Chaudhuri J, Zhu C, Davidson L, Weaver DT, Alt FW. A targeted DNA-PKcs-null mutation reveals DNA-PK-independent functions for KU in V(D)J recombination. *Immunity*. 1998; 9:367–76. [https://doi.org/10.1016/s1074-7613\(00\)80619-6](https://doi.org/10.1016/s1074-7613(00)80619-6) PMID:9768756
3. Rooney S, Sekiguchi J, Zhu C, Cheng HL, Manis J, Whitlow S, DeVido J, Foy D, Chaudhuri J, Lombard D, Alt FW. Leaky scid phenotype associated with defective V(D)J coding end processing in artemis-deficient mice. *Mol Cell*. 2002; 10:1379–90.

[https://doi.org/10.1016/s1097-2765\(02\)00755-4](https://doi.org/10.1016/s1097-2765(02)00755-4)
PMID:12504013

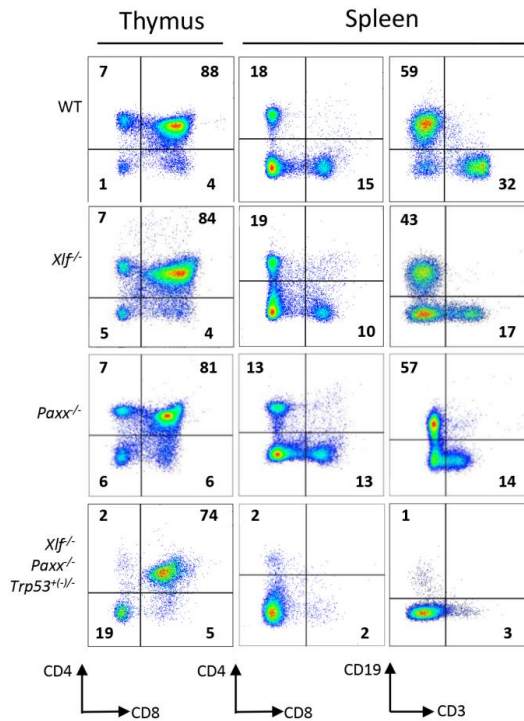
4. Liu X, Shao Z, Jiang W, Lee BJ, Zha S. PAXX promotes KU accumulation at DNA breaks and is essential for end-joining in XLF-deficient mice. *Nat Commun.* 2017; 8:13816.
<https://doi.org/10.1038/ncomms13816>
PMID:28051062
5. Hung PJ, Johnson B, Chen BR, Byrum AK, Bredemeyer AL, Yewdell WT, Johnson TE, Lee BJ, Deivasigamani S, Hindi I, Amatya P, Gross ML, Paull TT, et al. MRI is a DNA damage response adaptor during classical non-homologous end joining. *Mol Cell.* 2018; 71:332–42.e8.
<https://doi.org/10.1016/j.molcel.2018.06.018>
PMID:30017584
6. Gu Y, Seidl KJ, Rathbun GA, Zhu C, Manis JP, van der Stoep N, Davidson L, Cheng HL, Sekiguchi JM, Frank K, Stanhope-Baker P, Schlissel MS, Roth DB, Alt FW. Growth retardation and leaky SCID phenotype of Ku70-deficient mice. *Immunity.* 1997; 7:653–65.
[https://doi.org/10.1016/s1074-7613\(00\)80386-6](https://doi.org/10.1016/s1074-7613(00)80386-6)
PMID:9390689
7. Nussenzweig A, Chen C, da Costa Soares V, Sanchez M, Sokol K, Nussenzweig MC, Li GC. Requirement for Ku80 in growth and immunoglobulin V(D)J recombination. *Nature.* 1996; 382:551–55.
<https://doi.org/10.1038/382551a0> PMID:8700231
8. Ma Y, Pannicke U, Schwarz K, Lieber MR. Hairpin opening and overhang processing by an artemis/DNA-dependent protein kinase complex in nonhomologous end joining and V(D)J recombination. *Cell.* 2002; 108:781–94.
[https://doi.org/10.1016/s0092-8674\(02\)00671-2](https://doi.org/10.1016/s0092-8674(02)00671-2)
PMID:11955432
9. Gao Y, Sun Y, Frank KM, Dikkes P, Fujiwara Y, Seidl KJ, Sekiguchi JM, Rathbun GA, Swat W, Wang J, Bronson RT, Malynn BA, Bryans M, et al. A critical role for DNA end-joining proteins in both lymphogenesis and neurogenesis. *Cell.* 1998; 95:891–902.
[https://doi.org/10.1016/s0092-8674\(00\)81714-6](https://doi.org/10.1016/s0092-8674(00)81714-6)
PMID:9875844
10. Frank KM, Sekiguchi JM, Seidl KJ, Swat W, Rathbun GA, Cheng HL, Davidson L, Kangaloo L, Alt FW. Late embryonic lethality and impaired V(D)J recombination in mice lacking DNA ligase IV. *Nature.* 1998; 396:173–77.
<https://doi.org/10.1038/24172>
PMID:9823897
11. Li G, Alt FW, Cheng HL, Brush JW, Goff PH, Murphy MM, Franco S, Zhang Y, Zha S. Lymphocyte-specific compensation for XLF/cernunnos end-joining functions in V(D)J recombination. *Mol Cell.* 2008; 31:631–40.
<https://doi.org/10.1016/j.molcel.2008.07.017>
PMID:18775323
12. Vera G, Rivera-Munoz P, Abramowski V, Malivert L, Lim A, Bole-Feysot C, Martin C, Florkin B, Latour S, Revy P, de Villartay JP. Cernunnos deficiency reduces thymocyte life span and alters the T cell repertoire in mice and humans. *Mol Cell Biol.* 2013; 33:701–11.
<https://doi.org/10.1128/MCB.01057-12>
PMID:23207905
13. Roch B, Abramowski V, Chaumeil J, de Villartay JP. Cernunnos/Xlf deficiency results in suboptimal V(D)J recombination and impaired lymphoid development in mice. *Front Immunol.* 2019; 10:443.
<https://doi.org/10.3389/fimmu.2019.00443>
PMID:30923523
14. Abramowski V, Etienne O, Elsaid R, Yang J, Berland A, Kermasson L, Roch B, Musilli S, Moussu JP, Lipson-Ruffert K, Revy P, Cumano A, Boussin FD, de Villartay JP. PAXX and Xlf interplay revealed by impaired CNS development and immunodeficiency of double KO mice. *Cell Death Differ.* 2018; 25:444–52.
<https://doi.org/10.1038/cdd.2017.184>
PMID:29077092
15. Balmus G, Barros AC, Wijnhoven PW, Lescale C, Hasse HL, Boroviak K, le Sage C, Doe B, Speak AO, Galli A, Jacobsen M, Deriano L, Adams DJ, et al. Synthetic lethality between PAXX and XLF in mammalian development. *Genes Dev.* 2016; 30:2152–57.
<https://doi.org/10.1101/gad.290510.116>
PMID:27798842
16. Gago-Fuentes R, Xing M, Sæterstad S, Sarno A, Dewan A, Beck C, Bradamante S, Bjørås M, Oksenysh V. Normal development of mice lacking PAXX, the paralogue of XRCC4 and XLF. *FEBS Open Bio.* 2018; 8:426–34.
<https://doi.org/10.1002/2211-5463.12381>
PMID:29511619
17. Liu X, Jiang W, Dubois RL, Yamamoto K, Wolner Z, Zha S. Overlapping functions between XLF repair protein and 53BP1 DNA damage response factor in end joining and lymphocyte development. *Proc Natl Acad Sci USA.* 2012; 109:3903–08.
<https://doi.org/10.1073/pnas.1120160109>
PMID:22355127
18. Castañeda-Zegarra S, Huse C, Røsand Ø, Sarno A, Xing M, Gago-Fuentes R, Zhang Q, Alirezaylavasani A, Werner J, Ji P, Liabakk NB, Wang W, Bjørås M, Oksenysh V. Generation of a mouse model lacking the non-homologous end-joining factor mri/cyren. *Biomolecules.* 2019; 9:798.
<https://doi.org/10.3390/biom9120798>
PMID:31795137

19. Zha S, Guo C, Boboila C, Oksenykh V, Cheng HL, Zhang Y, Wesemann DR, Yuen G, Patel H, Goff PH, Dubois RL, Alt FW. ATM damage response and XLF repair factor are functionally redundant in joining DNA breaks. *Nature*. 2011; 469:250–54.
<https://doi.org/10.1038/nature09604>
PMID:21160472
20. Castañeda-Zegarra S, Xing M, Gago-Fuentes R, Sæterstad S, Oksenykh V. Synthetic lethality between DNA repair factors Xlf and Paxx is rescued by inactivation of Trp53. *DNA Repair (Amst)*. 2019; 73:164–69.
<https://doi.org/10.1016/j.dnarep.2018.12.002>
PMID:30579708
21. Beck C, Castañeda-Zegarra S, Huse C, Xing M, Oksenykh V. Mediator of DNA damage checkpoint protein 1 facilitates V(D)J recombination in cells lacking DNA repair factor XLF. *Biomolecules*. 2019; 10:60.
<https://doi.org/10.3390/biom10010060>
PMID:31905950
22. Oksenykh V, Alt FW, Kumar V, Schwer B, Wesemann DR, Hansen E, Patel H, Su A, Guo C. Functional redundancy between repair factor XLF and damage response mediator 53BP1 in V(D)J recombination and DNA repair. *Proc Natl Acad Sci U S A*. 2012; 109:2455–60.
<https://doi.org/10.1073/pnas.1121458109>
PMID:22308489
23. Lescale C, Abramowski V, Bedora-Faure M, Murigneux V, Vera G, Roth DB, Revy P, de Villartay JP, Deriano L. RAG2 and XLF/cernunnos interplay reveals a novel role for the RAG complex in DNA repair. *Nat Commun*. 2016; 7:10529.
<https://doi.org/10.1038/ncomms10529>
PMID:26833222
24. Oksenykh V, Kumar V, Liu X, Guo C, Schwer B, Zha S, Alt FW. Functional redundancy between the XLF and DNA-PKcs DNA repair factors in V(D)J recombination and nonhomologous DNA end joining. *Proc Natl Acad Sci U S A*. 2013; 110:2234–9.
<https://doi.org/10.1073/pnas.1222573110>
PMID:23345432
25. Xing M, Bjørås M, Daniel JA, Alt FW, Oksenykh V. Synthetic lethality between murine DNA repair factors XLF and DNA-PKcs is rescued by inactivation of Ku70. *DNA Repair (Amst)*. 2017; 57:133–38.
<https://doi.org/10.1016/j.dnarep.2017.07.008>
PMID:28759779
26. Lescale C, Lenden Hasse H, Blackford AN, Balmus G, Bianchi JJ, Yu W, Bacoccina L, Jarade A, Clouin C, Sivapalan R, Reina-San-Martin B, Jackson SP, Deriano L. Specific roles of XRCC4 paralogs PAXX and XLF during V(D)J recombination. *Cell Rep*. 2016; 16:2967–79.
<https://doi.org/10.1016/j.celrep.2016.08.069>
PMID:27601299
27. Kumar V, Alt FW, Frock RL. PAXX and XLF DNA repair factors are functionally redundant in joining DNA breaks in a G1-arrested progenitor b-cell line. *Proc Natl Acad Sci USA*. 2016; 113:10619–24.
<https://doi.org/10.1073/pnas.1611882113>
PMID:27601633
28. Hung PJ, Chen BR, George R, Liberman C, Morales AJ, Colon-Ortiz P, Tyler JK, Sleckman BP, Bredemeyer AL. Deficiency of XLF and PAXX prevents DNA double-strand break repair by non-homologous end joining in lymphocytes. *Cell Cycle*. 2017; 16:286–95.
<https://doi.org/10.1080/15384101.2016.1253640>
PMID:27830975
29. Barnes DE, Stamp G, Rosewell I, Denzel A, Lindahl T. Targeted disruption of the gene encoding DNA ligase IV leads to lethality in embryonic mice. *Curr Biol*. 1998; 8:1395–98.
[https://doi.org/10.1016/s0960-9822\(98\)00021-9](https://doi.org/10.1016/s0960-9822(98)00021-9)
PMID:9889105
30. Frank KM, Sharpless NE, Gao Y, Sekiguchi JM, Ferguson DO, Zhu C, Manis JP, Horner J, DePinho RA, Alt FW. DNA ligase IV deficiency in mice leads to defective neurogenesis and embryonic lethality via the p53 pathway. *Mol Cell*. 2000; 5:993–1002.
[https://doi.org/10.1016/s1097-2765\(00\)80264-6](https://doi.org/10.1016/s1097-2765(00)80264-6)
PMID:10911993
31. Gao Y, Ferguson DO, Xie W, Manis JP, Sekiguchi J, Frank KM, Chaudhuri J, Horner J, DePinho RA, Alt FW. Interplay of p53 and DNA-repair protein XRCC4 in tumorigenesis, genomic stability and development. *Nature*. 2000; 404:897–900.
<https://doi.org/10.1038/35009138>
PMID:10786799
32. Jacks T, Remington L, Williams BO, Schmitt EM, Halachmi S, Bronson RT, Weinberg RA. Tumor spectrum analysis in p53-mutant mice. *Curr Biol*. 1994; 4:1–7.
[https://doi.org/10.1016/s0960-9822\(00\)00002-6](https://doi.org/10.1016/s0960-9822(00)00002-6)
PMID:7922305
33. Musilli S, Abramowski V, Roch B, de Villartay JP. An in vivo study of the impact of deficiency in the DNA repair proteins PAXX and XLF on development and maturation of the hemolymphoid system. *J Biol Chem*. 2020; 295:2398–406.
<https://doi.org/10.1074/jbc.AC119.010924>
PMID:31915249
34. Di Rosa F, Ramaswamy S, Ridge JP, Matzinger P. On the lifespan of virgin T lymphocytes. *J Immunol*. 1999; 163:1253–57.
PMID:10415021

35. Fulcher DA, Basten A. B cell life span: a review. *Immunol Cell Biol.* 1997; 75:446–55. <https://doi.org/10.1038/icb.1997.69> PMID:[9429891](https://pubmed.ncbi.nlm.nih.gov/9429891/)
36. Albers E, Sbroggiò M, Pladevall-Morera D, Bizard AH, Avram A, Gonzalez P, Martin-Gonzalez J, Hickson ID, Lopez-Contreras AJ. Loss of PICH results in chromosomal instability, p53 activation, and embryonic lethality. *Cell Rep.* 2018; 24:3274–84. <https://doi.org/10.1016/j.celrep.2018.08.071> PMID:[30232008](https://pubmed.ncbi.nlm.nih.gov/30232008/)
37. Murga M, Bunting S, Montaña MF, Soria R, Mulero F, Cañamero M, Lee Y, McKinnon PJ, Nussenzweig A, Fernandez-Capetillo O. A mouse model of ATR-seckel shows embryonic replicative stress and accelerated aging. *Nat Genet.* 2009; 41:891–98. <https://doi.org/10.1038/ng.420> PMID:[19620979](https://pubmed.ncbi.nlm.nih.gov/19620979/)
38. Castañeda-Zegarra S, Fernandez-Berrocal M, Tkachov M, Yao R, Upfold NL, Oksenysh V. Genetic interaction between the non-homologous end-joining factors during B and T lymphocyte development: in vivo mouse models. *Scand J Immunol.* 2020; 92:e12936. <https://doi.org/10.1111/sji.12936> PMID:[32654175](https://pubmed.ncbi.nlm.nih.gov/32654175/)
39. Karanjawala ZE, Adachi N, Irvine RA, Oh EK, Shibata D, Schwarz K, Hsieh CL, Lieber MR. The embryonic lethality in DNA ligase IV-deficient mice is rescued by deletion of ku: implications for unifying the heterogeneous phenotypes of NHEJ mutants. *DNA Repair (Amst).* 2002; 1:1017–26. [https://doi.org/10.1016/s1568-7864\(02\)00151-9](https://doi.org/10.1016/s1568-7864(02)00151-9) PMID:[12531011](https://pubmed.ncbi.nlm.nih.gov/12531011/)
40. Wang XS, Lee BJ, Zha S. The recent advances in non-homologous end-joining through the lens of lymphocyte development. *DNA Repair (Amst).* 2020; 94:102874. <https://doi.org/10.1016/j.dnarep.2020.102874> PMID:[32623318](https://pubmed.ncbi.nlm.nih.gov/32623318/)

SUPPLEMENTARY MATERIALS

Supplementary Figure



Supplementary Figure 1. B and T cell development in *Xlf*^{-/-} *Paxx*^{-/-} *Trp53*^{+/-/-} mice. Examples of flow cytometric analysis of thymic and splenic T cell subsets and splenic CD19+ B cells. *Xlf*^{-/-} *Paxx*^{-/-} *Trp53*^{+/-/-} is a combination of *Xlf*^{-/-} *Paxx*^{-/-} *Trp53*^{-/-} and *Xlf*^{-/-} *Paxx*^{-/-} *Trp53*^{+/-}.

Supplementary Tables

Supplementary Table 1. Summary of splenic CD19+ B cells.

WT	<i>Xlf</i> ^{-/-}	<i>Mri</i> ^{-/-}	<i>Xlf</i> ^{-/-} <i>Mri</i> ^{-/-} <i>Trp53</i> ^{+/-}	<i>Paxx</i> ^{-/-}	<i>Xlf</i> ^{-/-} <i>Paxx</i> ^{-/-} <i>Trp53</i> ^{+(-)/-}		<i>Paxx</i> ^{-/-} <i>Mri</i> ^{-/-}	<i>Dna-pkcs</i> ^{-/-}
					<i>Trp53</i> ^{+/-}	<i>Trp53</i> ^{-/-}		
55.82	38.91	41.56	0.48	28.22	0.18	0.42	21.71	0.02
60.49	59.69	56.91	0.23	29.15	0.11	1.53	34.40	0.36
79.07	41.87	42.70	0.80	91.10	0.05	0.93	42.52	0.03
63.94	39.23	92.59	0.48	58.69	0.20		55.20	0.08
36.16	54.24	79.30	0.19	55.26	0.16		21.26	0.02
56.50	41.89	48.03		61.57	2.21		31.01	0.05
63.69	36.46	55.14		56.28	1.82		25.84	
42.85	37.87			39.59	0.58		15.51	
75.05	28.68			55.36	0.08		32.73	
67.60	39.08			61.29			58.43	
38.27	29.73			80.28			64.75	
79.47	47.11			61.29			36.96	
29.43	56.65			93.23			37.92	
52.58	44.10			61.86			63.63	
65.47	34.65						31.99	
62.80	30.79						22.31	
56.68	34.55						28.62	
57.03	50.48							
54.05	52.23							
75.79	36.41							

CD19+ splenocytes ($\times 10^6$) in WT, *Xlf*^{-/-}, *Mri*^{-/-}, *Xlf*^{-/-}*Mri*^{-/-}*Trp53*^{+/-}, *Paxx*^{-/-}, *Xlf*^{-/-}*Paxx*^{-/-}*Trp53*^{+(-)/-} and *Paxx*^{-/-}*Mri*^{-/-} mice. *Dna-pkcs*^{-/-} mice were used as an immunodeficient control. *Xlf*^{-/-}*Paxx*^{-/-}*Trp53*^{+(-)/-} is a combination of *Xlf*^{-/-}*Paxx*^{-/-}*Trp53*^{+/-} and *Xlf*^{-/-}*Paxx*^{-/-}*Trp53*^{-/-}.

Supplementary Table 2. Summary of splenic CD3+ T cells.

WT	<i>Xlf</i> ^{-/-}	<i>Mri</i> ^{-/-}	<i>Xlf</i> ^{-/-} <i>Mri</i> ^{-/-} <i>Trp53</i> ^{+/-}	<i>Paxx</i> ^{-/-}	<i>Xlf</i> ^{-/-} <i>Paxx</i> ^{-/-} <i>Trp53</i> ^{+(-)/-}		<i>Paxx</i> ^{-/-} <i>Mri</i> ^{-/-}	<i>Dna-pkcs</i> ^{-/-}
					<i>Trp53</i> ^{+/-}	<i>Trp53</i> ^{-/-}		
41.61	15.06	23.01	5.55	34.34	0.13	0.41	26.93	0.38
37.93	36.01	36.61	3.31	21.89	0.52	1.42	24.53	0.23
42.64	33.33	23.12	3.05	38.84	0.42	0.84	36.66	0.03
29.44	39.67	32.84	2.36	23.51	0.26		41.18	0.09
15.25	30.11	30.74	1.55	31.11	0.92		15.22	0.02
22.62	15.19	19.45		16.26	0.25		18.83	0.07
20.41	49.15	25.38		14.86	0.71		20.21	
18.50	24.24			10.45	0.38		13.65	
27.19	17.04			14.62			17.85	
24.49	14.83			16.18			25.19	
13.86	15.41			21.20			28.55	
28.79	11.67			16.18			20.70	
19.05	15.90			24.62			16.90	
23.72	12.10			16.34			32.74	
22.75	19.17						17.44	
20.53	23.05						19.22	
27.01	17.94						18.25	
25.60	14.10							
35.90	12.52							
	14.06							
	20.54							
	21.25							
	42.82							
	14.81							

CD3+ splenocytes ($\times 10^6$) in WT, *Xlf*^{-/-}, *Mri*^{-/-}, *Xlf*^{-/-}*Mri*^{-/-}*Trp53*^{+/-}, *Paxx*^{-/-}, *Xlf*^{-/-}*Paxx*^{-/-}*Trp53*^{+(-)/-} and *Paxx*^{-/-}*Mri*^{-/-} mice. *Dna-pkcs*^{-/-} mice were used as an immunodeficient control. *Xlf*^{-/-}*Paxx*^{-/-}*Trp53*^{+(-)/-} is a combination of *Xlf*^{-/-}*Paxx*^{-/-}*Trp53*^{+/-} and *Xlf*^{-/-}*Paxx*^{-/-}*Trp53*^{-/-}.

Supplementary Table 3. Summary of splenic CD4+ T cells.

WT	<i>Xlf</i> ^{-/-}	<i>Mri</i> ^{-/-}	<i>Xlf</i> ^{-/-} <i>Mri</i> ^{-/-} <i>Trp53</i> ^{+/-}	<i>Paxx</i> ^{-/-}	<i>Xlf</i> ^{-/-} <i>Paxx</i> ^{-/-} <i>Trp53</i> ^{+(-)/-}		<i>Paxx</i> ^{-/-} <i>Mri</i> ^{-/-}	<i>Dna-pkcs</i> ^{-/-}
					<i>Trp53</i> ^{+/-}	<i>Trp53</i> ^{-/-}		
19.51	5.46	10.36	1.14	12.17	0.03	0.49	8.3	0.08
17.39	11.43	15.61	1.66	9.96	0.01	0.34	12.54	0.05
18.17	18.99	13.88	1.09	24.65	0.49	0.56	17.64	0.09
9.23	15.66	19.32	0.96	15.97	0.59		18.51	
13.63	14.9	17.57		19.38	0.35		6.66	
12.38	6.88	13.25			0.37		8.13	
11.89	21.81	14.42			0.37		8.92	
9.844					0.27		5.51	
8.961							9.67	
9.96							15.61	
15.85							18.01	
19.29							10.36	
16.42								
12.85								

CD4+ splenocytes ($\times 10^6$) in WT, *Xlf*^{-/-}, *Mri*^{-/-}, *Xlf*^{-/-}*Mri*^{-/-}*Trp53*^{+/-}, *Paxx*^{-/-}, *Xlf*^{-/-}*Paxx*^{-/-}*Trp53*^{+(-)/-} and *Paxx*^{-/-}*Mri*^{-/-} mice. *Dna-pkcs*^{-/-} mice were used as an immunodeficient control. *Xlf*^{-/-}*Paxx*^{-/-}*Trp53*^{+(-)/-} is a combination of *Xlf*^{-/-}*Paxx*^{-/-}*Trp53*^{+/-} and *Xlf*^{-/-}*Paxx*^{-/-}*Trp53*^{-/-}.

Supplementary Table 4. Summary of splenic CD8+ T cells.

WT	<i>Xlf</i> ^{-/-}	<i>Mri</i> ^{-/-}	<i>Xlf</i> ^{-/-} <i>Mri</i> ^{-/-} <i>Trp53</i> ^{+/-}	<i>Paxx</i> ^{-/-}	<i>Xlf</i> ^{-/-} <i>Paxx</i> ^{-/-} <i>Trp53</i> ^{+(-)/-}		<i>Paxx</i> ^{-/-} <i>Mri</i> ^{-/-}	<i>Dna-pkcs</i> ^{-/-}
					<i>Trp53</i> ^{+/-}	<i>Trp53</i> ^{-/-}		
14.39	4.03	12.59	0.74	6.83	0.32	0.40	5.86	0.08
18.35	12.06	14.79	1.72	9.30	0.07	0.41	10.45	0.05
12.31	12.73	10.57	1.19	15.76	0.22	0.29	15.26	0.06
7.13	13.11	18.08	0.66	12.05	0.24		16.02	
9.70	9.67	15.62		14.11	0.02		5.60	
9.64	6.39	9.96			0.39		7.69	
7.96	14.92	12.09			0.20		7.16	
14.26							4.86	
12.96							7.28	
13.91							13.26	
11.62							14.87	
12.17							7.78	
10.88								
7.88								

CD8+ splenocytes ($\times 10^6$) in WT, *Xlf*^{-/-}, *Mri*^{-/-}, *Xlf*^{-/-}*Mri*^{-/-}*Trp53*^{+/-}, *Paxx*^{-/-}, *Xlf*^{-/-}*Paxx*^{-/-}*Trp53*^{+(-)/-} and *Paxx*^{-/-}*Mri*^{-/-} mice. *Dna-pkcs*^{-/-} mice were used as an immunodeficient control. *Xlf*^{-/-}*Paxx*^{-/-}*Trp53*^{+(-)/-} is a combination of *Xlf*^{-/-}*Paxx*^{-/-}*Trp53*^{+/-} and *Xlf*^{-/-}*Paxx*^{-/-}*Trp53*^{-/-}.

Supplementary Table 5. Summary of thymic CD4+ T cells.

WT	<i>Xlf</i> ^{-/-}	<i>Mri</i> ^{-/-}	<i>Xlf</i> ^{-/-} <i>Mri</i> ^{-/-} <i>Trp53</i> ^{+/-}	<i>Paxx</i> ^{-/-}	<i>Xlf</i> ^{-/-} <i>Paxx</i> ^{-/-} <i>Trp53</i> ^{+(-)/-}		<i>Paxx</i> ^{-/-} <i>Mri</i> ^{-/-}	<i>Dna-pkcs</i> ^{-/-}
					<i>Trp53</i> ^{+/-}	<i>Trp53</i> ^{-/-}		
9.88	8.45	8.63	1.32	6.01	0.66	0.13	5.53	0.02
9.06	3.41	10.16	0.48	8.77	0.07	0.06	8.40	0.001
10.48	11.88	6.74	0.89	12.88	0.07	0.19	4.31	0.01
16.33	7.05	7.95	0.65	11.10	0.11		6.77	0.02
7.50	6.67	15.23	0.50	9.80	0.40		6.85	
10.64	11.66	17.57			0.29		13.08	
7.12		15.94			0.19		9.52	
4.33		10.99			0.13		6.86	
2.55		15.88					12.67	
11.74		9.21					12.97	
13.15								
14.54								
14.41								
12.07								
11.39								
9.70								

CD4+ thymocytes (×10⁶) in WT, *Xlf*^{-/-}, *Mri*^{-/-}, *Xlf*^{-/-}*Mri*^{-/-}*Trp53*^{+/-}, *Paxx*^{-/-}, *Xlf*^{-/-}*Paxx*^{-/-}*Trp53*^{+(-)/-} and *Paxx*^{-/-}*Mri*^{-/-} mice. *Dna-pkcs*^{-/-} mice were used as an immunodeficient control. *Xlf*^{-/-}*Paxx*^{-/-}*Trp53*^{+(-)/-} is a combination of *Xlf*^{-/-}*Paxx*^{-/-}*Trp53*^{+/-} and *Xlf*^{-/-}*Paxx*^{-/-}*Trp53*^{-/-}.

Supplementary Table 6. Summary of thymic CD8+ T cells.

WT	<i>Xlf</i> ^{-/-}	<i>Mri</i> ^{-/-}	<i>Xlf</i> ^{-/-} <i>Mri</i> ^{-/-} <i>Trp53</i> ^{+/-}	<i>Paxx</i> ^{-/-}	<i>Xlf</i> ^{-/-} <i>Paxx</i> ^{-/-} <i>Trp53</i> ^{+(-)/-}		<i>Paxx</i> ^{-/-} <i>Mri</i> ^{-/-}	<i>Dna-pkcs</i> ^{-/-}
					<i>Trp53</i> ^{+/-}	<i>Trp53</i> ^{-/-}		
2.70	2.39	3.48	0.64	4.34	0.18	0.19	1.08	0.02
2.00	1.83	3.43	0.33	2.93	0.06	0.09	1.85	0.001
3.84	3.40	1.82	0.91	5.51	0.28	0.21	1.33	0.01
4.69	2.60	2.72	0.29	4.52	0.51		2.24	0.01
1.47	2.60	7.14	0.67	4.7	0.15		3.07	
2.11	3.59	6.40			0.23		6.2	
5.07		5.45			0.60		4.03	
3.26		4.28			0.49		3.16	
1.98							5.14	
3.91							5.11	
13.59								
11.68								
13.78								
3.47								
5.36								
4.90								
2.25								
4.56								

CD8+ thymocytes (×10⁶) in WT, *Xlf*^{-/-}, *Mri*^{-/-}, *Xlf*^{-/-}*Mri*^{-/-}*Trp53*^{+/-}, *Paxx*^{-/-}, *Xlf*^{-/-}*Paxx*^{-/-}*Trp53*^{+(-)/-} and *Paxx*^{-/-}*Mri*^{-/-} mice. *Dna-pkcs*^{-/-} mice were used as an immunodeficient control. *Xlf*^{-/-}*Paxx*^{-/-}*Trp53*^{+(-)/-} is a combination of *Xlf*^{-/-}*Paxx*^{-/-}*Trp53*^{+/-} and *Xlf*^{-/-}*Paxx*^{-/-}*Trp53*^{-/-}.

Supplementary Table 7. Summary of thymic CD4+CD8+ double positive T cells.

WT	<i>Xlf</i> ^{-/-}	<i>Mri</i> ^{-/-}	<i>Xlf</i> ^{-/-} <i>Mri</i> ^{-/-} <i>Trp53</i> ^{+/-}	<i>Paxx</i> ^{-/-}	<i>Xlf</i> ^{-/-} <i>Paxx</i> ^{-/-} <i>Trp53</i> ^{+(-)/-}		<i>Paxx</i> ^{-/-} <i>Mri</i> ^{-/-}	<i>Dna-pkcs</i> ^{-/-}
					<i>Trp53</i> ^{+/-}	<i>Trp53</i> ^{-/-}		
154.05	48.40	160.60	20.69	132.56	2.68	6.22	75.37	0.17
141.52	73.77	133.62	11.40	161.22	7.21	6.54	184.27	0.002
230.74	163.07	14.22	21.18	151.30	6.79	5.14	122.11	0.0002
147.74	95.47	165.78	17.78	208.39	3.39		105.44	0.001
138.62	115.71	154.74	17.71	202.99	3.72		88.37	0.002
98.78	115.77	193.15		161.06	4.43		168.00	
115.10	174.36	102.72		171.03	11.90		122.32	
66.71	144.88			100.87	5.18		87.20	
102.13	160.88			175.18			136.82	
162.51	105.29			197.59			153.47	
126.04	155.83						114.36	
79.43	90.46						136.39	
140.22	118.17						55.65	
146.71	183.46						96.22	
119.15	158.35							
	172.50							
	146.98							
	101.50							
	143.61							
	114.38							
	132.49							
	105.96							
	136.45							
	162.14							

CD4+CD8+ thymocytes ($\times 10^6$) in WT, *Xlf*^{-/-}, *Mri*^{-/-}, *Xlf*^{-/-}*Mri*^{-/-}*Trp53*^{+/-}, *Paxx*^{-/-}, *Xlf*^{-/-}*Paxx*^{-/-}*Trp53*^{+(-)/-} and *Paxx*^{-/-}*Mri*^{-/-} mice. *Dna-pkcs*^{-/-} mice were used as an immunodeficient control. *Xlf*^{-/-}*Paxx*^{-/-}*Trp53*^{+(-)/-} is a combination of *Xlf*^{-/-}*Paxx*^{-/-}*Trp53*^{+/-} and *Xlf*^{-/-}*Paxx*^{-/-}*Trp53*^{-/-}.

Supplementary Table 8. Summary of IgM+ B cells in bone marrow.

WT	<i>Xlf</i> ^{-/-}	<i>Mri</i> ^{-/-}	<i>Xlf</i> ^{-/-} <i>Mri</i> ^{-/-} <i>Trp53</i> ^{+/-}	<i>Paxx</i> ^{-/-}	<i>Xlf</i> ^{-/-} <i>Paxx</i> ^{-/-} <i>Trp53</i> ^{+(-)/-}		<i>Paxx</i> ^{-/-} <i>Mri</i> ^{-/-}
					<i>Trp53</i> ^{+/-}	<i>Trp53</i> ^{-/-}	
19.80	7.82	17.10	3.04	17.8	2.19	3.26	15.90
16.70	11.00	16.30	1.47	14.3	2.53	4.01	16.70
18.60	8.47	16.00	1.42	15.9	4.09	3.55	14.30
10.10	6.04	15.80	1.10	11.9	0.37		14.00
14.10	7.68	13.80	1.57		4.60		10.10
11.60	6.06	11.50			4.35		9.82
12.40	12.40	14.90			1.50		7.34
13.90	10.60	13.00			3.76		8.22
14.10	5.79				5.19		14.60
14.50					6.20		14.10
13.70							
10.10							
12.10							

Frequencies (%) of B220+CD43-IgM+ B cells in WT, *Xlf*^{-/-}, *Mri*^{-/-}, *Xlf*^{-/-}*Mri*^{-/-}*Trp53*^{+/-}, *Paxx*^{-/-}, *Xlf*^{-/-}*Paxx*^{-/-}*Trp53*^{+(-)/-} and *Paxx*^{-/-}*Mri*^{-/-} mice. *Xlf*^{-/-}*Paxx*^{-/-}*Trp53*^{+(-)/-} is a combination of *Xlf*^{-/-}*Paxx*^{-/-}*Trp53*^{+/-} and *Xlf*^{-/-}*Paxx*^{-/-}*Trp53*^{-/-}.

w

Supplementary Table 9. Summary of progenitor B cells in bone marrow.

WT	<i>Xlf</i> ^{-/-}	<i>Mri</i> ^{-/-}	<i>Xlf</i> ^{-/-} <i>Mri</i> ^{-/-} <i>Trp53</i> ^{+/-}	<i>Paxx</i> ^{-/-}	<i>Xlf</i> ^{-/-} <i>Paxx</i> ^{-/-} <i>Trp53</i> ^{+(-)/-}		<i>Paxx</i> ^{-/-} <i>Mri</i> ^{-/-}
					<i>Trp53</i> ^{+/-}	<i>Trp53</i> ^{-/-}	
6.00	21.6	3.74	24.90	8.92	33.70	20.10	7.53
7.47	8.73	4.31	14.50	4.40	28.40	24.00	7.04
3.38	17.5	9.53	17.20	4.07	23.20	25.60	8.64
6.96	10.9	7.03	14.90	3.81	21.90		10.9
5.02	9.61	6.73	19.00		26.80		9.00
5.49	7.99	6.58			27.10		6.28
2.75	5.31	4.17			25.10		6.76
4.25	7.16	4.28			17.30		6.20
7.58	6.08				22.20		3.32
7.47					25.50		4.06
5.03							
7.72							
8.29							

Frequencies (%) of B220+CD43-IgM- pro-B cells in WT, *Xlf*^{-/-}, *Mri*^{-/-}, *Xlf*^{-/-}*Mri*^{-/-}*Trp53*^{+/-}, *Paxx*^{-/-}, *Xlf*^{-/-}*Paxx*^{-/-}*Trp53*^{+(-)/-} and *Paxx*^{-/-}*Mri*^{-/-} mice. *Xlf*^{-/-}*Paxx*^{-/-}*Trp53*^{+(-)/-} is a combination of *Xlf*^{-/-}*Paxx*^{-/-}*Trp53*^{+/-} and *Xlf*^{-/-}*Paxx*^{-/-}*Trp53*^{-/-}.

Supplementary Table 10. Lymphocytic development in the *Xlf*^{-/-}*Mri*^{-/-}*Trp53*^{+/-} mouse.

Splenocytes (×10 ⁶)				Thymocytes (×10 ⁶)			Cell populations (%) in bone marrow	
CD19+ B cells	CD3+ T cells	CD4+ T cells	CD8+ T cells	CD4+ T cells	CD8+ T cells	CD4+CD8+ T cells	IgM+ B cells	Pro-B cells
0.11	0.80	0.53	0.41	0.42	0.41	15.70	2.71	19.40

Summary of splenic (×10⁶) B- and T cells; and T cell subpopulations in the thymus (×10⁶). Frequencies (%) in bone marrow of B220+CD43-IgM+ B cells and B220+CD43-IgM- pro-B cells.

ISBN 978-82-326-5493-2 (printed ver.)
ISBN 978-82-326-6461-0 (electronic ver.)
ISSN 1503-8181 (printed ver.)
ISSN 2703-8084 (online ver.)



NTNU

Norwegian University of
Science and Technology